Charles University in Prague

Faculty of Science

Synthesis and properties of conjugated metallo-supramolecular polymers

Ph.D. Thesis

RNDr. Pavla Štenclová

Supervisor: RNDr. Jan Svoboda, Ph.D.

Prague, 2015

Statement

I hereby declare that this submission is my own work and that, to the best of my knowledge and belief, it contains neither material previously published or written by another person nor material which to a substantial extent has been accepted for the award of any other degree or diploma of the University or other Institute of higher education, except for the already published results, which are included in the list of references.

Prague, ……..

Acknowledgment

At this place I would like to thank to my supervisor dr. Jan Svoboda for his support during the syntheses as well as during the writing and publishing the results. He is also greatly acknowledged for some advanced measurements of photoluminescence, for DFT calculations and other technical support.

Dr. Ivana Šloufová is greatly acknowledged for measurements of Raman and advanced infrared spectra and their interpretation.

Dr. Jiří Zedník is greatly acknowledged for the advanced measurements of NMR spectra, especially the multidimensional techniques.

The Grant Agency of the Charles University (project no. 64213) and the Czech Science Foundation (project no. P108/12/1143) are greatly acknowledged for financial support.

Many thanks belong to the colleagues of the Department of Physical and Macromolecular Chemistry for pleasant atmosphere and fruitful discussions.

Last but not least, prof. Jiří Vohlídal is especially appreciated for his endless enthusiasm and new ideas brought to the field of metallo-supramolecular polymers/dynamers.

Special thank belongs to my family and friends, who know barely nothing about chemistry but still supported me during my doubts that chemistry is the right way I should follow.

Abstract

More than twenty new bis(*tpy*)oligothiophenes (*tpy* stands for 2,2':6',2''-terpyridin-4'-yl) with unsubstituted as well as substituted (with methyl, hexyl, bromohexyl or 6-(4-methoxyphenoxy)hexyl groups) central blocks comprising one to four thiophene rings have been prepared as building blocks (unimers) for constitutional dynamic metallo-supramolecular polymers (MSPs) soluble in common organic solvents. In addition a series of ionic unimers soluble in alcohols and partially in water have been prepared by modification of bromohexyl unimers with trimethylamine or triethylphosphine.

Spectroscopic studies have shown that the steric hindrances prevail over the electronic effects of substituents as regards the impact on the delocalization of electrons along unimer chains. Unimers with high steric hindrances in the middle of the central oligothiophene block were found to behave nearly like the unimers with half central block.

Three stages of the assembly of MSPs from unimers and metal ions in solutions were characterized by the UV/vis and fluorescence spectroscopy, viscometry and size exclusion chromatography: (*i*) formation of dimers U-Mt^{2+}-U in the early stages of assembling, (*ii*) assembly to longer MSPs chains, and (*iii*) end-capping with surplus metal ions and partial decomposition of MSPs chains.

The observed changes in optical absorption spectra indicate a significantly increased extent of the delocalization of electrons upon binding the unimer molecules into polymer chains. On the other hand, a blue shift of luminescence emission in thin films of the most of MSPs compared to parent unimers indicates that the bulky *tpy*-Mt^{2+}-*tpy* linkages suppress efficient planarization of unimer units in thin films of MSPs. Fe-MSPs exhibit MLCT band giving them typical blue color and are non-emissive in contrast to Zn-MSPs.

Evidences from spectroscopic, viscometric and SEC techniques proved fast constitutional dynamic for Zn-MSPs while very slow for Fe-MSPs. Slow dynamic in Fe^{2+}/unimer systems allowed the molecular-mass characterization of these systems by SEC. Remarkable influence on stability of MSPs was found by experiments in different solvents.

Abstrakt

V rámci dizertační práce bylo připraveno více než dvacet nových bis(*tpy*)oligothiofenů (*tpy* označuje skupiny 2,2':6',2''-terpyridin-4'-yl) s nesubstituovanými a substituovanými (methyl, hexyl, 6-bromhexyl, 6-(4-methoxyfenoxy)hexyl) mono- až kvaterthiofenovými centrálními bloky. Tyto oligothiofeny byly využity jako stavební bloky (unimery) konstitučně-dynamických polymerů (dynamerů) rozpustných v organických rozpouštědlech (THF, DMSO, $CHCl_3$, CH_2Cl_2 apod). Modifikací 6-bromhexylových bočních skupin trimethylaminem nebo triethylfosfinem byly navíc připraveny unimery a následně i polymery rozpustné v alkoholech a částečně ve vodě.

Spektroskopické studie připravených látek prokázaly, že sterické efekty převažují nad elektron-donorovými efekty substituentů centrálního bloku. Unimery s velkými dihedrálními úhly mezi centrálními thiofenovými cykly vykazují UV/vis absorpční charakteristiky obdobné jako unimery s poloviční délkou centrálního bloku, avšak emisní charakteristiky odpovídající celým blokům, což svědčí o dostatečně rychlé relaxaci jejich excitovaných molekul do koplanárních konformací s chinoidní strukturou a protilehle orientovanými substituenty sousedních cyklů.

Průběh seskupování molekul unimerů s ionty kovů do řetězců supramolekulárních polymerů lze rozdělit do tří stádií: *i*) vznik dimerů U-Mt^{2+}-U, *ii*) seskupování do delších řetězců a *iii*) při nadbytku iontů kovu v systému - jejich vazba na koncové terpyridinové ligandy a rovnovážné zkracování polymerních řetězců. Důkazy byly získány pomocí UV/vis a fluorescenční spektroskopie, SEC a viskozimetrie.

Pozorované změny v optických spektrech prokazují zvýšení rozsahu delokalizace elektronů po uspořádání unimerů do polymerních řetězců. Na druhé straně, hypsochromní posun emisního maxima v tenkých filmech většiny polymerů ve srovnání s příslušnými unimery ukazuje, že objemné *tpy*-Mt^{2+}-*tpy* skupiny potlačují efektivní planarizaci vázaných unimerů v pevných filmech polymerů. Absorpční spektra Fe-polymerů vykazují MLCT pás, který je zodpovědný za jejich typickou modrou barvu. Zatímco Zn-polymery vykazují luminiscenční chování, Fe-polymery jsou neemitující.

Spektroskopická, viskozimetrická a SEC měření ukázala, že konstituční dynamika Zn-polymerů je rychlá, zatímco velmi pomalá dynamika Fe-polymerů umožnila stanovení distribuce molekulových hmotnosti pro Fe-polymery pomocí SEC. Dalšími experimenty v různých rozpouštědlech byl prokázán vliv rozpouštědla na stabilitu vytvořených polymerů.

CONTENT

LIST OF ABBREVIATIONS

MSP	metallo-supramolecular polymer
tpy	2,2':6',2''-terpyridine-4'-yl
terpyridine	2,2':6',2''-terpyridine
U	unimer (general)
MLCT	metal-to-ligand charge transfer
SEC	Size-exclusion chromatography
Th*tpy*	4'-(Thiophene-2-yl)-2,2':6',2''-terpyridine
BrTh*tpy*	4'-(5-Bromothiophene-2-yl)-2,2':6',2''-terpyridine
CIE diagram	full name CIE 1931 XYZ color space is the color space defined by International Commission on Illumination (from French name Commission internationale de l'éclairage) in 1931

1 INTRODUCTION

1.1 Supramolecular approach to linear conjugated polymers

The reversibility of a molecular assembly is the main principle of supramolecular chemistry. From the classical point of view, all reactions are reversible, but for many of them the opposite path from products back to reactants requires huge amount of energy and blocking numerous other easier paths to another compounds. Thus we called these reactions irreversible. The concept of reversible or "weak" interaction is known for ages from biology and biochemistry – typically, the base-pairing in DNA or lock-and-key principle in enzymatic processes are well known and it was good choice to apply these principles in classical organic or material chemistry. The main principles and types of interactions in supramolecular chemistry were defined by Nobel Prize winner J.-M. Lehn as the chemistry beyond the molecule.[1] Constitutional dynamic polymers, so-called dynamers, were then defined in 2005.[2] Dynamers are typically able to exchange or reshuffle their components under specific conditions and thus self-heal or self-repair themselves.

By applying one specific interaction into the supramolecular chemistry – coordination bond, we can constrict the huge group of constitutional dynamic polymers to coordination supramolecular polymers, also referred as metallo-supramolecular polymers (MSPs). Typically, in these polymers/dynamers the monomeric units are held together by coordination bond between some specific organic ligand and metal ions. According to the IUPAC recommendation we can classify the MSPs as the ionenes, since they contain charged main chain atoms. On the other side, polyelectrolytes are typical with pendant ionic groups.[3] It is noteworthy, that the nomenclature in the field of metallo-supramolecular polymers/dynamers is not uniformed and sometimes confusing. Some scientific group called their MSPs inappropriately as metallo-supramolecular polyelectrolytes even if the charged atoms are present only in the main chain of the polymer.[4] The organic molecules utilized as monomeric units in metallo-supramolecular polymers through the Thesis would be called as unimer as proposed by Ciferri.[5]

Other materials concerning this project are conjugated organic oligomers and polymers. Alternation of single and multiple bonds is the basic structural condition for extensive delocalization of π-electrons within an organic molecule that is crucial for obtaining an organic material or polymer with semiconducting properties. Typical conjugated polymers applied as semiconducting materials for organic light-emitting diods, solar cells or field-effect transistors are polythiophenes,[6–11] polyphenylevinylenes,[12–17] polyfluorenes,[18–21] polyacetylenes,[22–24] polyanilines[25–30] and

others[31–35] (**Fig. 1.**). These traditional covalent polymers are nowadays processed either by various coating (film-casting) techniques[36] or by ink-jet printing from solutions or emulsions (dispersions).[37–40] One of the main disadvantages of covalent conjugated polymers is their structural defects formed during both polymerization and subsequent purification and processing. These defects are more or less randomly distributed within semiconducting polymers, mostly act as traps for one type of charge carriers and cannot be rationally removed. The application of supramolecular approaches in a construction of polymeric optoelectronic devices can help to overcome these problems. The supramolecular approach utilizing highly specific coordination bonding of conjugated oligomers is the subject of this Thesis.

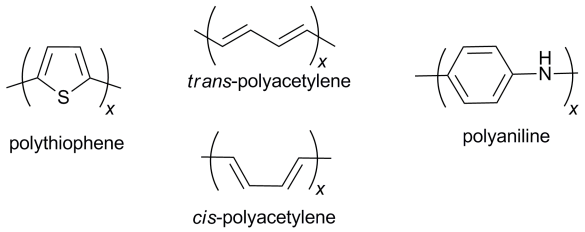

Fig. 1. Examples of traditional conjugated polymers.

By joining above mentioned fields of chemistry we can ideally reach materials, which are (*i*) easy and cheap to prepare; (*ii*) dynamic; (*iii*) easy to process and (*iv*) semiconducting or show other interesting useful properties.

1.2 Ligands and ions used in metallo-supramolecular polymers

Substituted *N*-type ligands such as derivatives of pyridine, 2,2'-bipyridine (*bipy*), phenanthroline (*phen*) or 2,2':6',2''-terpyridine are most often used in the field of MSPs. 2,2':6',2''-Terpyridine can be regarded as an ideal ligand for effective binding of metal ions of the charge number z = 2 or 3 (Mt^{z+}). Terpyridine with its three pyridine nitrogens provides octahedral complexes possessing high stability constant with a large variety of transition metal ions. With 4'-substituted 2,2':6',2''-terpyridine and suitable metal ions one can get plenty of complexes with general scheme $[Mt(tpy)_2]^{2+}$ used preferentially in the research targeted to solar cells. To get linear polymers is necessary to involve ditopic bis(*tpy*) compounds composed of a central block that is capped with two terpyridine end-groups (**Fig. 2.**). Tris(*tpy*) unimers afford more dimensional entities like metallo-organic frameworks, metallo-organic dendrimers *etc*.[41,42]

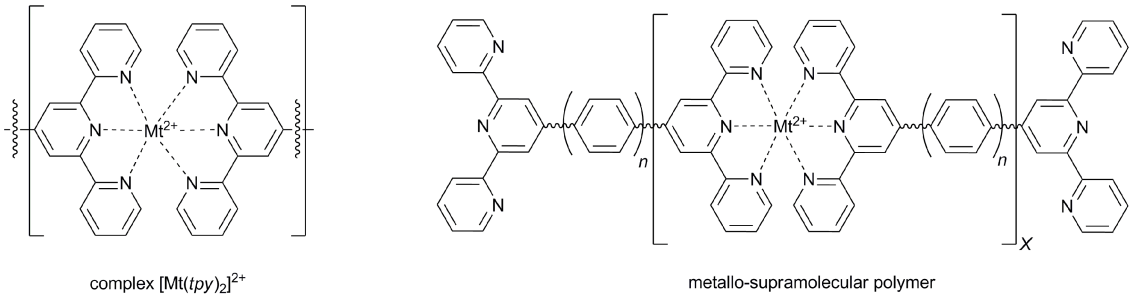

Fig. 2. Schematic representation of $[Mt(tpy)_2]^{2+}$ complex and metallo-supramolecular polymer composed of bisterpyridines.

Terpyridine and its derivatives create complexes with a high number of transition metals including lanthanides. The most often studied are the *tpy*-type complexes with Fe^{2+}, Co^{2+}, Ni^{2+}, Cu^{2+}, Zn^{2+}, Ru^{2+}, Rh^{2+}, Pd^{2+}, Cd^{2+}, Os^{2+}, Ir^{3+} or Pt^{2+}. The complexation equilibrium can be represented by stability constants defined according to the following reactions:

$$Mt^{2+} + tpy \rightarrow [Mt(tpy)]^{2+} \qquad K_1$$

$$[Mt(tpy)]^{2+} + tpy \rightarrow [Mt(tpy)_2]^{2+} \qquad K_2$$

$$Mt^{2+} + 2\ tpy \rightarrow [Mt(tpy)_2]^{2+} \qquad b = K_1 \cdot K_2$$

The stability constants are available for several Mt/*tpy* systems in different solvents, mainly for the systems with unsubstituted parent ligands. However, these values are not easy transferable (generally applicable) to the derived systems, because each stability constant is valid for the given surroundings and conditions (solvent(s), temperature, counterions).

The choice of a proper metal-unimer combination offers the opportunity to control the stability of designed polymers from thermodynamically stable to dynamically equilibrating.[43] Stable linear chains are provided with such metals as Ru^{2+}, Os^{2+}, Ni^{2+} or Ir^{3+}. It is generally meant, that these polymers can be characterized by various techniques also used for conventional polymers such as SEC. On the other hand, other metals like Fe^{2+}, Zn^{2+}, Co^{2+} or lanthanides are considered to build dynamic linear chains not suitable for SEC or even viscometry in some cases and thus the characterization of such polymers became an challenging issue.

The frequently prepared iron/*tpy* complexes $[Fe(tpy)_2]^{2+}$ are low-spin and with octahedral coordination.[44] Their absorption spectra usually show *(i)* the bands at around 280 and 320 nm that belong to the ligand (*tpy*) centered π-π^* transitions, and *(ii)* the band at 550 or more nm, that is responsible for a purple to blue color of these complexes and originates from the metal-to-ligand charge transfer (MLCT) transition.[45] If the central atom of an $[Fe(tpy)_2]^{2+}$ species is oxidized to Fe^{3+} state, the MLCT process does not take place due to the absence of transferable electrons at the iron

ion, and the purple-to-blue color of the complex disappears.[46,47] Reversible oxidation/reduction of iron central ions allows utilization of $[Fe(tpy)_2]^{2+/3+}$ species in electrochromic devices. While *tpy* derivatives give the low-spin Fe^{2+} complexes with MLCT band,[48] *tpy*-derivatives substituted in positions 4, or 6, or 4'', or 6'' (on outer rings) provide the high-spin Fe/*tpy* complexes without the MLCT band.[49]

Iron/*tpy* complexes as well as polymers are completely non-emissive. The lowest excited state of $[Fe(tpy)_2]^{2+}$ species, the d-d triplet state, is close to the ground state.[50] As the d-d triplet state easily depletes upper excited states and potential phosphorescence from the d-d state is spin forbidden, its decay by non-radiative transitions is unambiguously preferred in accord with the energy gap law.[51,52]

The very stable biscomplex $[Fe(tpy)_2]^{2+}$ is preferentially present in the mixture of terpyridine and Fe^{2+} ions,[53–55] while the monocomplex $[Fe(tpy)]^{2+}$ has not been monitored even at very high excess on Fe^{2+} in the mixture.[54,56] Oppositely, the biscomplex $[Zn(tpy)_2]^{2+}$ easily undergo the transformation to monocomplex $[Zn(tpy)]^{2+}$ in the excess of Zn^{2+} ions. Despite rather high stability the $[Fe(tpy)_2]^{2+}$ complexes can be reversibly dismounted by a strong chelating ligands such as by hydroxyethyl(ethylenediaminetriacetic acid) HEEDTA.[57]

Zinc with its fully occupied d^{10} shell is difficult to oxidize or reduce and act as a Lewis acid. Complex formation can be reversed more easily and zinc complexes in solution exist in dynamic equilibrium and thus exchange rapidly.[57] 4′-Aryl substituted terpyridine in complexes with zinc possess absorption band around 320 nm, which originated from intracharge transfer from aryl donor to metalated terpyridine acceptor. This feature is similar for protonated terpyridine, where H^+ promotes intracharge transfer from pendent group to terpyridine.[58] Polymerization of bisterpyridines with Zn^{2+} proceeds under mild conditions resulting in light-emitting polymers with well-defined structure.[59] Highly-luminescent zinc-containing polymers meet potential application as emissive materials in electroluminescent devices.[60]

Lanthanide ions (Ln) with terpyridine can form several types complexes with general scheme $[Ln(tpy)]^{3+}$, $[Ln(tpy)_2]^{3+}$ or $[Ln(tpy)_3]^{3+}$. Formation of particular complex in the Ln/*tpy* mixture is controlled primarily by the counterions of the lanthanide cation and solvent choice. Lanthanide nitrates are known to form mono- and biscomplexes with general scheme $[Ln(tpy)(NO_3)_3]$ and $[Ln(tpy)_2(NO_3)_3]$. The presence of coordinating NO_3^- counterions prevents complexation of additional terpyridine and thus the tris(*tpy*) complex cannot be formed. Similar situation occurs for RCO_2^- counterions, which by itself acts as bridging bidentate ligand. Water has to be used as co-solvent while mixing the lanthanide halides with *tpy* ligands for solubility reasons, but water limits the complexation by generating adducts. Only lanthanide salts with non-coordinating ClO_4^-

counterions in poorly coordinating acetonitrile are known to give complexes of $[Ln(tpy)_2(MeCN)_n]^{3+}$ or $[Ln(tpy)_3]^{3+}$ types. The presence of these complexes in solid state was proved by X-ray analysis,[61] while in solution partial decomplexation of distal pyridine rings is reported.[62]

Lanthanide/*tpy* complexes are often used for their luminescent behavior in nerve-gas detection,[63] optical communication,[64] lasers or components in multilayer organic light-emitting devices.[65–67] Direct light absorption of Ln^{3+} is very weak. Thus the light is absorbed by the organic ligands and transferred to the Ln^{3+}, which then undergo the typical luminescence. The here described process is known as an antenna effect.[68,69] The luminescence originated from lanthanide ions met several advantages such as *i*) high color purity induced by narrow emission band; *ii*) long radiative lifetimes of excited states; *iii*) large Stoke´s shift; *iv*) relatively immovable position.[70–72]

1.3 Metallo-supramolecular polymers and their properties

Bis(*tpy*) with poly(oxyalkylene) central blocks are perhaps the most popular non-conjugated unimers since they are easily soluble in alcohols.[73–76] A high flexibility of their central blocks promotes formation of macrocycles in addition to linear MSPs during assembling with metal cations.[77–79] Oligo(oxyethylene) chains attached to the ortho- position of outer *tpy* ring was also used for improving solubility of the unimer with polyphenylene central block.[80]

Conjugated unimers and MSPs usually suffer from poor solubility, which is a consequence of conformational rigidity and thus also increased probability of stacking their chain segments. Their solubility can be increased by introducing side groups on the unimer central block or outer rings of its *tpy* end-groups.[67,81–86] Of course, optical properties of resulting compounds are changed in both cases. However, the pyridine ring substitution also highly affects binding properties of the whole *tpy* group, mostly in a not desirable way. Hence the central-block substitution is a more promising way. Another way of tuning the solubility of MSPs consists in the choice of proper counterions, which, however, is still to a great extent a question of fortune.

Typical motifs used in central block (also called as spacer) of conjugated bisterpyridines are oligophenylenes,[87,88] oligofluorenes,[89–92] perylene-bisimide,[93–96] anthracene,[96] oligo/polythiophene, ethylene and their combinations. Properties of resulting materials are related with the donor or acceptor origin of the spacer.

Bis(*tpy*)oligophenylenes are most used unimers in MSPs. Nowadays bis(*tpy*)oligophenylenes with up to four directly bonded phenylenes are known.[81,85,97–100] Phenylene in the central block can also alternate with different conjugated

molecules.[101] The smallest one, 1,4-bis(*tpy*)benzene, is perhaps the most popular conjugated unimer for its simple preparation and, nowadays, even commercial availability.[79,82,84,102] Optical properties of its polymers formed by assembling with Fe^{2+}, Co^{2+}, Ni^{2+} and Ru^{2+} ions were investigated by several researchers. The polymers formed with $Fe(OAc)_2$ or $Ni(OAc)_2$ show solubility in water and Fe-polymers exhibit electrochromism.[79,47,103,104] As chains of these MSPs are positively charged, they can be electrophoretically deposited from solutions and layer-by-layer assembled on a support.[41] Schwarz et al.[105] introduced conductometric technique for precise controlling the stoichiometry of assembling. Kurth et al.[106] studied exchanges of Co^{2+} with Fe^{2+} ions in prepared polymers in solution and in the solid state and found out the protocol for exchanging metal ions in a deposited layer.

Although polythiophenes are nowadays used as semiconducting polymers, best to my knowledge bis(*tpy*)oligothiophenes containing only oligothiophene central block are not described in the literature. Only 2,5-bis(*tpy*)thiophene[107] is published as the analogue to 1,4-bis(*tpy*)benzene. On the other hand, thiophene-2,5-diyl alternating with different molecules in the central block of bisterpyridines are reported.[108–110] Ethynediyl has been reported to enhance the electronic communication between thiophene ring and *tpy* ligand. Unimers comprising up to five thiophene-2,5-diyl-*alt*-ethynediyl in the central block have been prepared and assembled with Ru and Os ions to luminescent MSPs[111–113] that were also used as molecular wires.[114,115]

It is worth mentioning here different scientific approach to bis(*tpy*)oligothiophenes. Th*tpy* is quite easy to prepare. Its complexes with different metal ions are considered to be potentially used in solar cells.[77,116–122] When complex $[Mt(Th\textit{tpy})_2]^{2+}$ (Mt stands for Ru or Os) is coated to electrode, it can be electrochemically polymerized.[123,124] By this approach the MSPs consist of unimers with bithiophene central block are obtained directly on the electrode, but these unimers as well as polymers could not be isolated, preciously characterized, and coated to another substrate.

1.4 Cationic polythiophenes

Polythiophenes are prepared by oxidative, catalytic or electrochemical polymerization of thiophene or its derivatives. Cationic polythiophenes can be prepared by the oxidative[125,126] or catalytic polymerization[127,128] of a thiophene with pendant ionic or ionogenic group. However, chains of so prepared polythiophene-polyelectrolytes are regio-irregular (irregular head-tail linking), which is unfavorable for possible optoelectronic applications. Another possibility consists in the catalytic synthesis of a regioregular polythiophene with, e.g., ω-bromoalkyl or ω-bromoalkoxyl side groups

followed by the exchange of terminal Br atoms for ionic groups (modification of the parent polymer).[129]

Cationic polythiophenes prepared so far mostly carry side-chain-capping groups with positively charged nitrogen, originating from the agents such as pyridine, imidazole or trialkylamines.[130–132] Regioregularity of the parent chains remains conserved during these modifications. Unlike non-ionic polythiophenes, cationic polythiophenes are water and alcohol soluble.[133] Potential application of cationic polythiophenes can be found in the field of photovoltaic applications[134–136] or optoelectronic devices.[137,138] Delocalization of main-chain π-electrons is strongly affected by the main-chain conformation, which is controlled by electrostatic and steric interaction of ionic side groups. The conformational changes are directly reflected in changes of solution UV/vis spectra of these compounds, which is frequently used in spectroscopic detection of metal ions[128,130,131] or biomolecules.[139–141]

2 AIMS OF THE THESIS

In accordance with the above described requirements for the novel semiconducting materials and recent findings in the field of supramolecular chemistry, the aims of the Thesis were as follows:

(i) Development of synthesis procedures for preparation of conjugated unimers with an oligothiophene central block capped by terpyridine ligands. The central block has to be either unsubstituted or with symmetrically distributed substituents.

(ii) Modification of unimers with reactive side groups to unimers soluble in alcohols or water, which are well appreciated by green chemistry and also favorable for their processing.

(iii) Assembly of prepared unimers with metal ions to obtain corresponding metallo-supramolecular polymers.

(iv) Characterization of the prepared unimers and polymers with special attention paid to their spectroscopic properties in solution and thin films and correlation of the obtained characteristics with the structure of unimers.

(v) Detailed study of the assembling process in solutions.

(vi) To obtain knowledge on the constitutional dynamics of prepared metallo-supramolecular polymers.

3 RESULTS AND DISCUSSION

3.1 Unimers and their synthesis

Structures and codes of prepared compounds are shown in **Figs. 3.** and **4**. The first letter of a code is related to the number of thiophene rings in the unimer central block: **M** for monothiophene, **B** for bithiophene, **T** for terthiophene, **Q** for quaterthiophene, respectively. Subsequent numbers indicate positions at which hexyl side chains (if present) are attached to the central (oligo)thiophene chain; only β-positions are numbered from the left to the right, see **Fig. 3.**). In two unimers, methyl instead of hexyl side groups is present; they are denoted by the subscript after locants: **B14$_{Me}$**, **T16$_{Me}$**. In all other cases the affix after locants designates the end-capping group (if present) of hexyl side chains: **A** stands for 4-methoxyphenoxy, **Br** for bromo, **N$^+$** for trimethylammonium, **P$^+$** for triethylphosphonium groups, respectively.

Synthesis of unimers **B** and **T** was the subject of the author´s Bachelor Thesis[142] but the synthetic pathway was further modified to obtain higher product yields. Preparation and basic properties of unimers **B14$_{Me}$**, **B14**, **T16$_{Me}$** and **T16** were subject of the author´s Master Thesis.[143] Unimers **Q27Br** and **Q27P$^+$** were synthesized by Ms. Šichová within her Master Thesis.[144] All the other presented unimers were exclusively prepared by the author of this Thesis. For the exact reaction condition see Experimental part, for NMR, IR and HR-MS of the particular compound see related publication specified in Experimental part and attached to the Thesis.

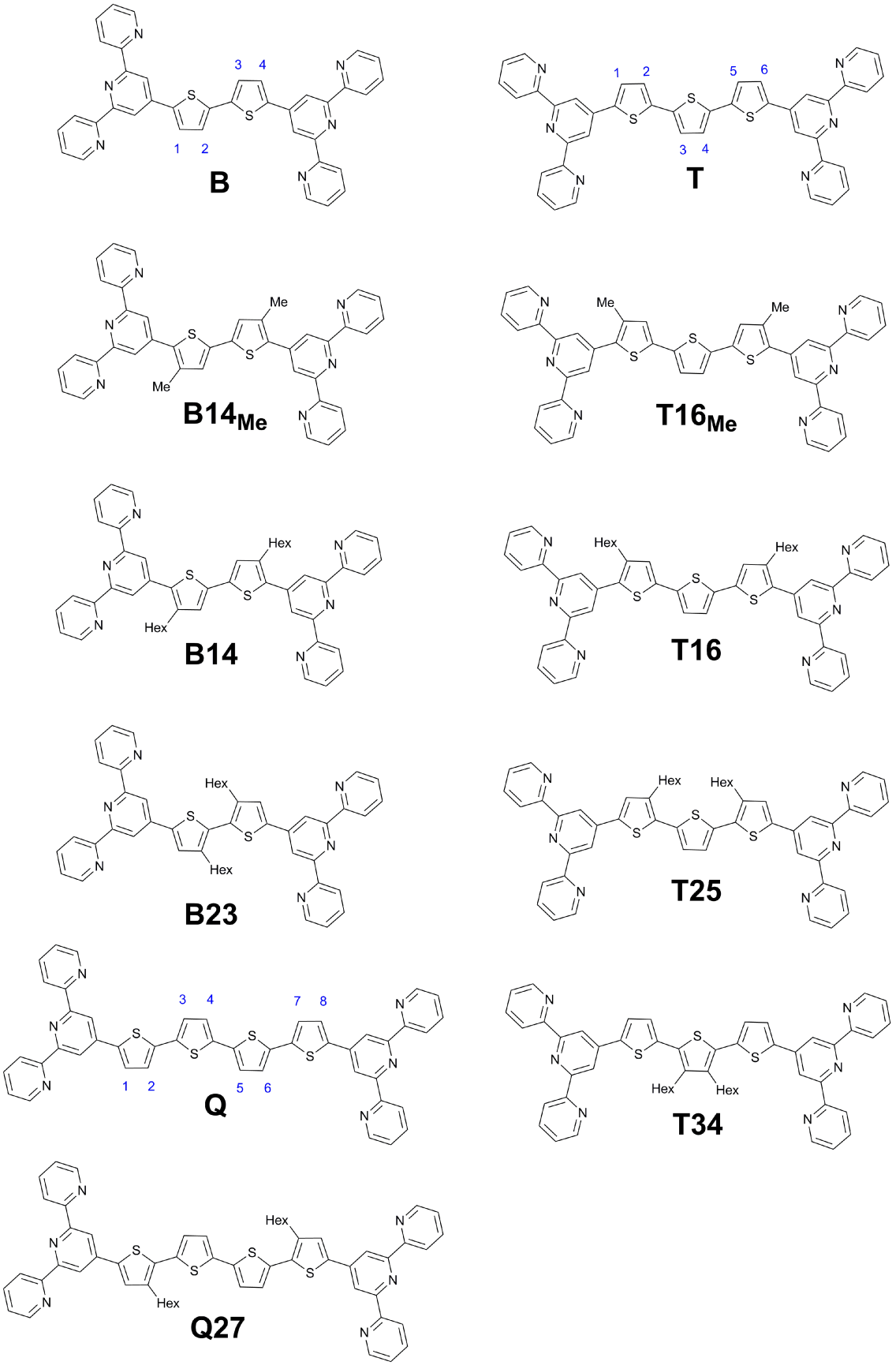

Fig. 3. Structures and codes of prepared non-ionic unimers.

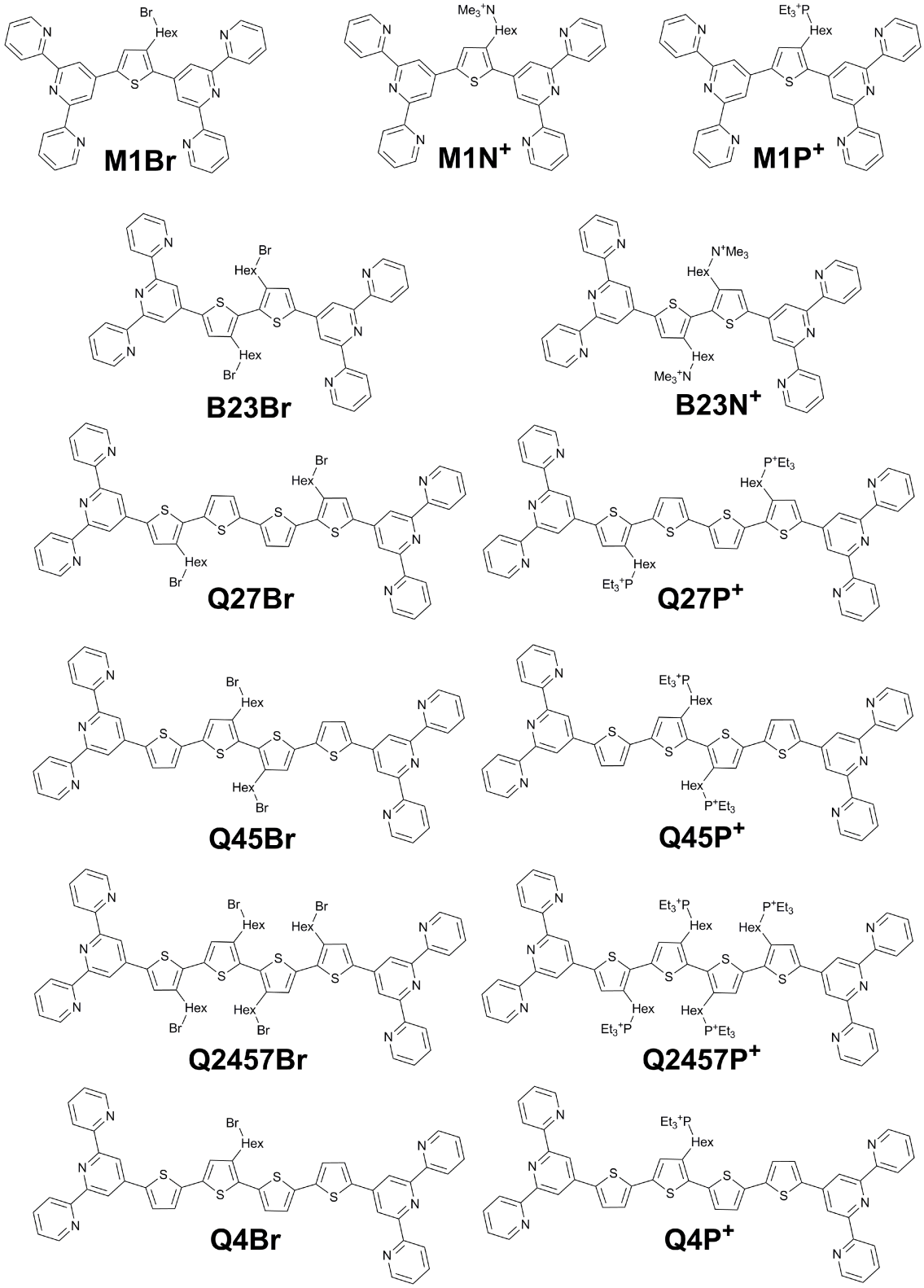

Fig. 4. Structures and codes of prepared brominated and ionic unimers.

Synthetic pathways leading to desired non-ionic and brominated unimers (Br-unimers) can be classified into several groups according to the used strategy: *i)* synthesis of the half of a unimer followed by coupling the halves to give the desired symmetric unimer; *ii)* synthesis of a unimer central block followed by borylation of its ends and coupling

with Br*tpy*; and *iii)* synthesis of a core of the central block followed by its borylation and coupling with BrTh*tpy*. Ionic unimers were “simply” prepared by *iv)* modification of brominated unimers.

Suzuki-Miyaura cross-coupling and direct borylation belong to the most widely used reactions within this Thesis. Stille cross-coupling mostly provided significantly lower yields of the desired products. Moreover Suzuki coupling requires non-toxic organoboron derivatives while Stille coupling toxic organostannanes.[145,146] Direct borylation is extremely efficient for thiophene derivatives giving almost 100% conversions in one reaction step while the classical route through lithiation involves more reaction steps and precious reaction conditions.[147,148] Fortunatelly, all used boron derivatives could be prepared by direct borylation.

Choice of the synthetic strategy for particular unimer depends on the position of substituents on the central oligothiophene block. 3-Substituted thiophenes were the key monomers which were (bi)functionalized by bromination or borylation. In the case of unsubstituted and hexyl substituted thiophenes, there many commercially available derivatives that can be used; for example 2-bromo-3-hexylthiophene, thiophene-2-boronic acid, bithiophene-2-boronic acid, 3-hexylthiophene-2-boronic acid. Other 3-substituted thiophenes such as 3-[6-(4-methoxyphenoxy)hexyl]thiophene and 3-(6-bromohexyl)thiophene) had to be synthesized.

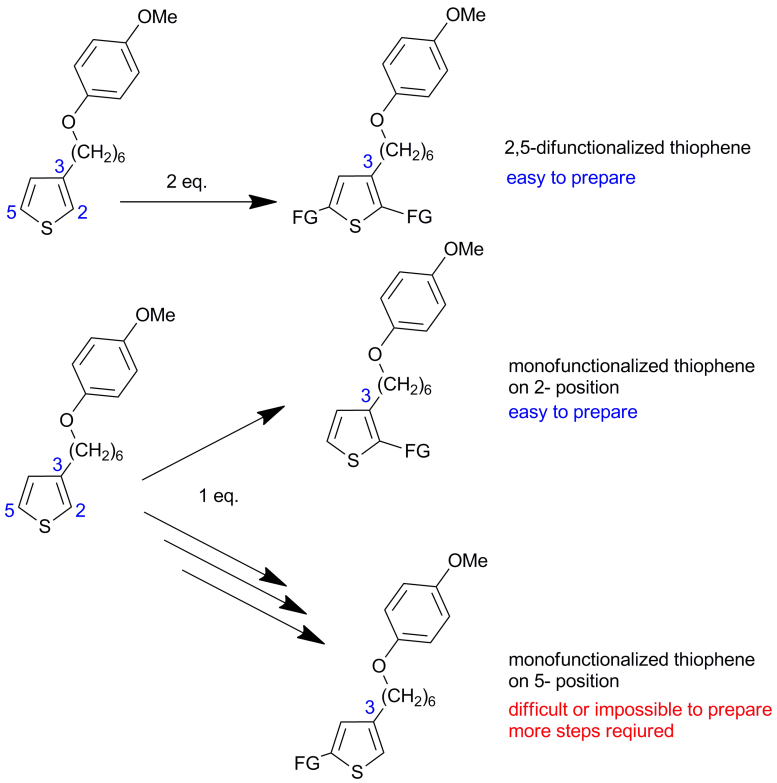

Scheme 1. Schematic representation of possibilities to functionalization of 3-substituted thiophene by functional groups (FG).

From the synthesis point of view (**Scheme 1.**), it is relatively easy to prepare 2,5-difunctional or 2-monofunctional thiophenes since the substituent on position 3 activates position 2 for substitution. Preparation of the opposite 5-derivatives of thiophene is much more difficult and requires more reaction steps and time-demanding separation.

In the first reaction strategy (**Scheme 2.**) Br*tpy* is first reacted with boron derivate of thiophene or bithiophene (substituted by methyl in case of $\mathbf{B14_{Me}}$ or hexyl for **B14**, respectively) to give 4'-(thiophen-2-yl)terpyridine (4'-(2,2'-bithiophen-5-yl)terpyridine respectively) that is subsequently brominated. This mono-*tpy* derivative is then coupled with bis(pinacolato)diboron to get the desired product. This strategy is favorable for preparing non-substituted unimers (**B** or **Q**) whose low solubility simplifies purification of crude products from which rather well soluble side products are simply washed away. This strategy also allows preparing bithiophene unimers with side groups attached at extreme positions of oligothiophene central block (neighborhood of *tpy* end-group, such as in $\mathbf{B14_{Me}}$ and **B14**).

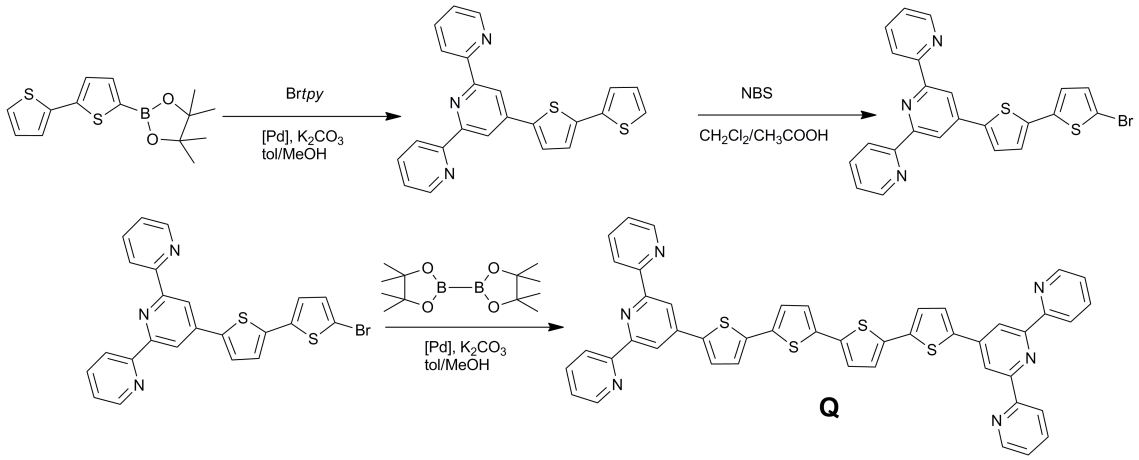

Scheme 2. Route *i)* coupling of two halves leading to unimer **Q**.

The second synthetic pathway (see **Scheme 3.**) starts with the synthesis of central block and continues with its direct borylation and Suzuki-Miyaura cross-coupling of borylated derivative with Br*tpy*. Oligothiophene blocks bearing hexyl substituents on specific positions (central block of **B23** and **T25**) or bromohexyl had to be previously synthesized and preciously purified. Subsequent iridium-catalyzed direct borylation handled with pinacolborane, which is said to be highly moisture-sensitive, but the reaction is easily mastered by the Schlenk technique.

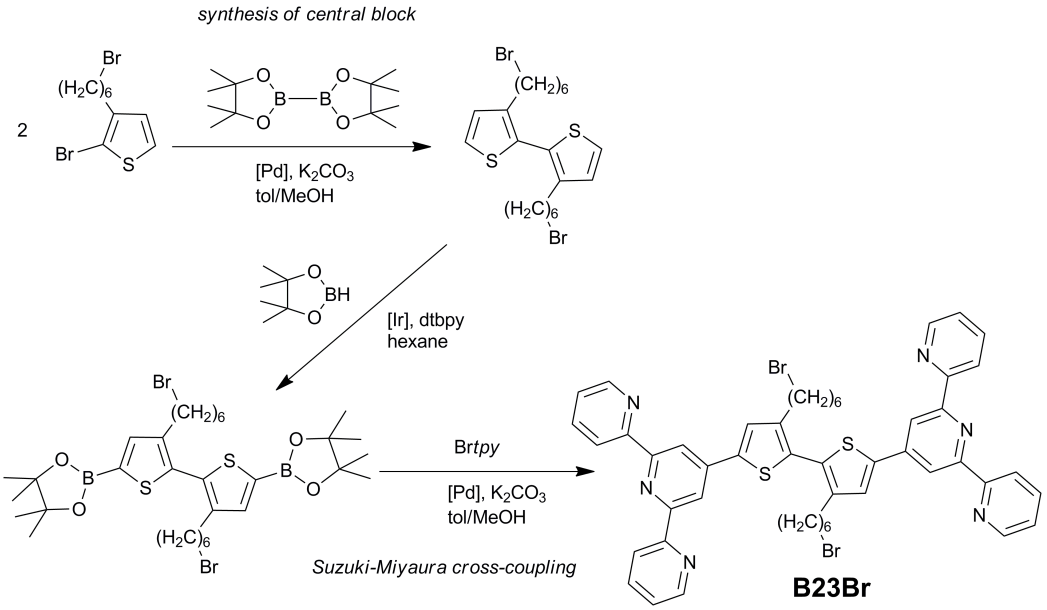

Scheme 3. Reaction pathway *ii)* involving synthesis of central block, direct borylation and final coupling with Br*tpy* leading to unimer **B23Br**.

3-(6-Bromohexyl)thiophene is the key monomer for the synthesis of central blocks of brominated unimers (**M1Br**, **B23Br** and others). It was prepared by dropwise addition of 3-thienyllithium to a fourfold stoichiometric excess of dibromohexane and purified by vacuum distillation. During the last reaction step in which the central block has to be coupled with Br*tpy*, partial elimination of terminal bromine atoms was observed yielding a negligible fraction of unimer with side chains capped with terminal double bonds (hex-5-en-1-yl side groups). It is worth mentioning here that dehydrobromination occurred only in presence of Br*tpy*, while during synthesis of central block under the same reaction conditions the terminal bromine was not affected. Thus 3-[6-(4-methoxyphenoxy)hexyl]thiophene (for exact synthetic route see ref.[149]) was used as the key monomer in following syntheses (**Q45Br**, **Q27Br**, **Q2457Br**). In the last step the isolated and purified unimer bearing methoxyphenoxyhexyl substituents was reacted with BBr_3 in dichloromethane to get the Br-unimers without any terminal double bonds.

The third applied synthetic pathway is a combination of the two preceding strategies: BrTh*tpy* is used instead of Br*tpy* in the last reaction step (**Scheme 4.**). While Br*tpy* is commercially available, BrTh*tpy* had to be prepared by reaction of Br*tpy* with thiophene-2-boronic acid and subsequent bromination of so formed Th*tpy*. This strategy was used in preparing some unimers with terthiophene type central blocks: **T**, **T16** and $\mathbf{T16_{Me}}$. Br*tpy* was first reacted with (3-alkyl)thiophene-2-boronic acid, resulting product was brominated and then coupled with bis(pinacol) ester of thiophene-2,5-diboronic acid. This strategy allows introduction of a substituent to the central-block

position nearest to the *tpy* end-group. Central blocks of other unimers (**T34**, **Q45Br** and **Q4Br**) were synthesized or modified depending on their structure.

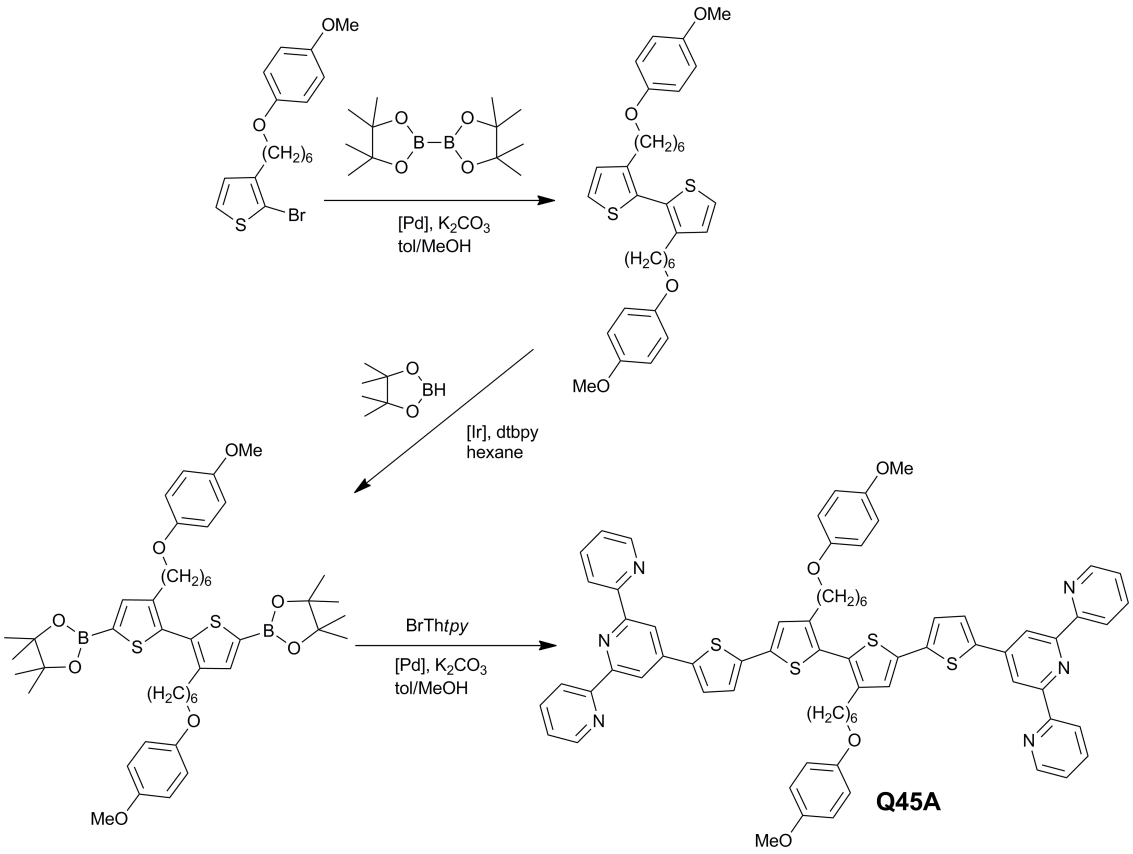

Scheme 4. Synthetic strategy *iii)* comprises synthesis of a part of the unimer central block, its direct borylation and final coupling with BrTh*tpy* resulting in **Q45A**.

The third strategy, at which thiophene directly attached to the terpyridine (BrTh*tpy*) is attached to a core of the central block in the last reaction step, is much more effective than strategy (*ii*), at which the central oligothiophene block build up by the stepwise approach is finally coupled with Br*tpy*. Due to the stepwise synthesis, a final longer oligothiophene central block is always more or less contaminated by chains of shorter oligothiophene(s) and this mixture is usually difficult and time consuming to separate by chromatography techniques.

The fourth strategy consists in the modification of already prepared unimers carrying bromohexyl side chains. New unimers with totally different solubility and some other properties can be thus obtained in a single reaction step. First attempts were done to modify Br-unimers by the reaction with *N*-methylimidazole that is well known quaternization agent for polythiophenes with bromoalkyl side groups[125,150,151] (see **Scheme 5.**) However, this reaction surprisingly did not proceed at all on unimers with *tpy* end-groups, neither in solution nor under the solvent-free conditions at 70°C (for all tested conditions see Experimental part). Dehydrobromination of bromohexyl groups

giving unimers with terminal double bonds was observed instead of the quaternization of the side chain end-groups. Interestingly, quaternization took smoothly place on 3-(6-bromohexyl)thiophene even in the presence of free terpyridine. Hence it seems that this reaction is specifically inhibited by *tpy* end-groups bound to the central block.

Trimethylamine (NMe_3) was used as the second quaternization agent. Its big advantage is low boiling point which allows easy evaporation of the excess of NMe_3 from the reaction mixture. On the other hand, quaternization with NMe_3 is very sensitive to the reaction temperature. At low temperatures below 10°C the reaction does not proceed at all, while at above 50°C the dehydrobromination is preferred. It is only the temperature around 25°C at which the reaction proceeds relatively fast giving a high yield of sufficiently pure ionic unimers. Unimers **M1N$^+$** and **B23N$^+$** were obtained just by this approach.

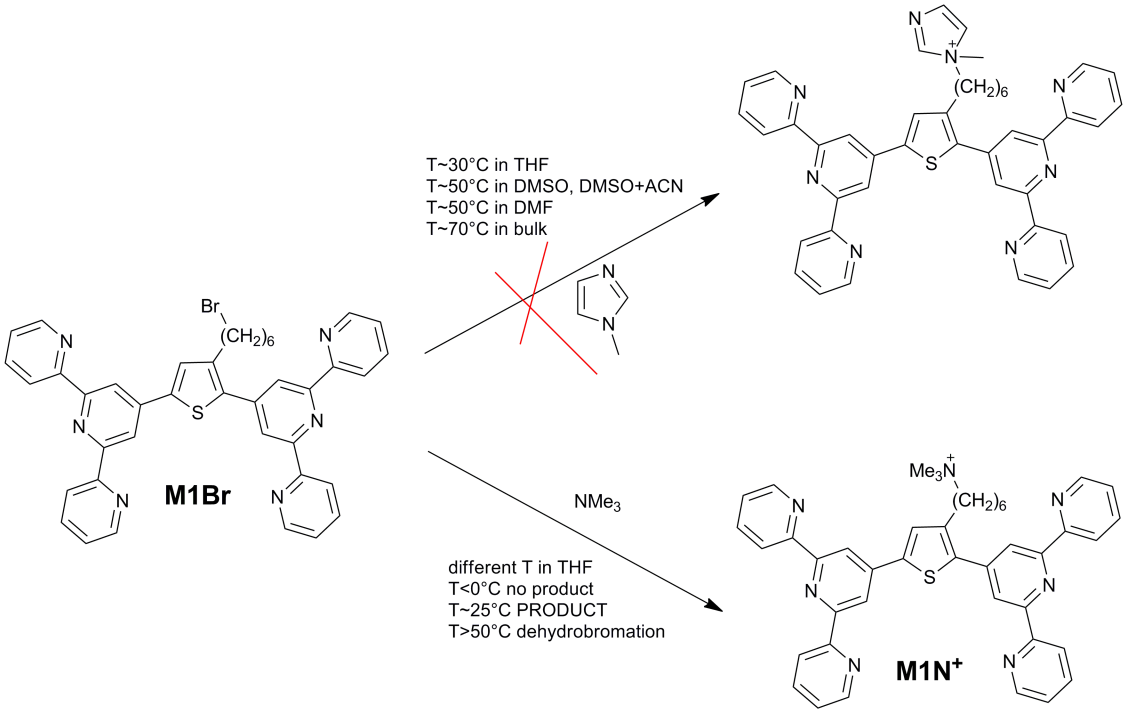

Scheme 5. Modification of Br-unimers by amines.

The second examined quaternization agents were phosphines (**Scheme 6.**). Quaternization of **M1Br** with triphenylphosphine (PPh_3) gave the product in the yield of only 10% while the quaternization with triethylphosphine (PEt_3) gave the yields around 90%. The small yield of the reaction with PPh_3 was probably caused mainly by steric hindrances arising from proximity of the bulky PPh_3 and *tpy* groups. In addition, the unreacted PPh_3 and its oxide $POPh_3$ were difficult to remove. In contrast, PEt_3 is easy to remove by simple evaporation in vacuum and $POEt_3$ can be washed away by

toluene or ether. By applying PEt_3 in toluene at 90°C for four days, ionic unimers **Q27P$^+$**, **Q45P$^+$** and **Q2457P$^+$** were obtained in the yields from 74 % to 95 %.

Unimer **Q4Br** is sparingly soluble in cold toluene. At 90°C its solution seems to be homogenous but after adding the quaternization agent a solid fraction appeared. The precipitate formation in a low-polar solvent typically indicates that the ionization of parent compound took place; it is a typical evidence of successful modification of Br-unimers to the ionic ones. However, in the case of **Q4Br**, the precipitate contained both original and quaternized compounds which was impossible to separate due to the low overall solubility of both compounds. As the phosphonium salts are soluble in DMSO, the quaternization of **Q4Br** was repeated in toluene/DMSO (1/1 by vol.) or chlorobenzene, but the process doesn´t reach any significant success.

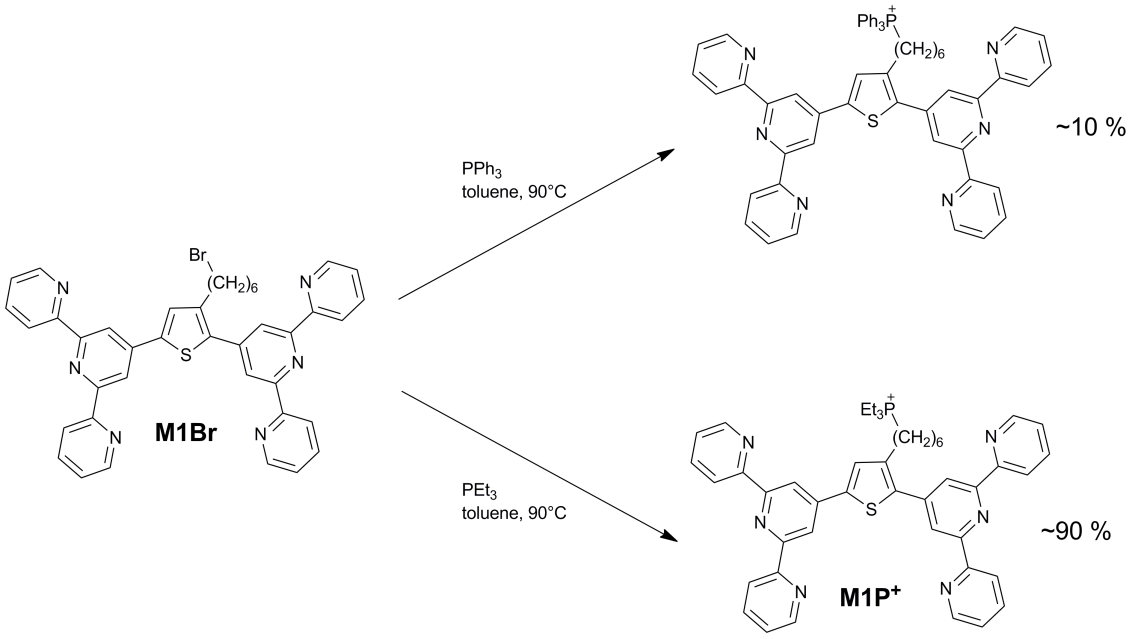

Scheme 6. Modification of Br-unimers by phospines.

The unimers were used for *preparation of MSPs*. According to generally used protocol[152] unimers are dissolved in NMP and solution of equimolar amount of metal salt in NMP is added. After stirring at 100°C overnight, KPF_6 is added and after one hour the polymers are precipitated into methanol. This procedure was applied on MSPs derived from non-ionic **B**- and **T**- type unimers with Zn^{2+} ions. Addition of KPF_6 salt to the reaction mixture resulted in an exchange of counterions giving MSPs poorly soluble in solvents like DMSO or NMP.

Majority of MSPs was prepared by simple mixing solutions of a unimer and metal perchlorate in equimolar stoichiometric ratio (see **Scheme 7.**). Both components were dissolved in chloroform/acetonitrile (1/1 by vol.) mixture, mixed together and evaporate

to obtain a solid MSPs. Assembling of some unimers with metal ions to polymeric species was also performed in THF

MSPs prepared are throughout this Thesis denoted by the prefix $\mathbf{P_{Zn}}$ or $\mathbf{P_{Fe}}$ (for Zn- and Fe-MSPs, respectively) to the name of corresponding unimer (e.g. $\mathbf{P_{Zn}B23}$ is MSP consisting of the unimer **B23** and Zn^{2+} ions, etc.).

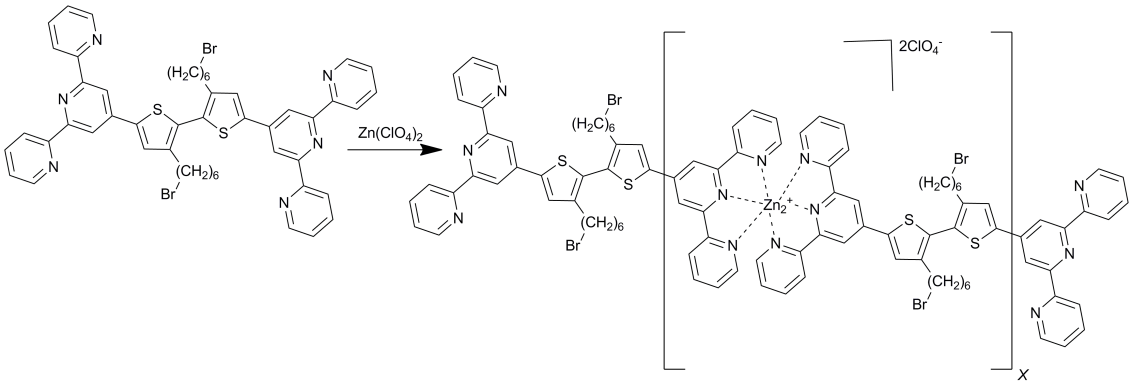

Scheme 7. Schematic representation of polymerization. Note that pyridine rings in *tpy* end-groups undergo the *anti*- to *syn*- conformational change when coordinating to ions.

3.2. Solubility of prepared compounds

As all prepared compounds have fully conjugated central block their solubility is strongly influenced by rigidity of the structure. Unsubstituted unimers **B**, **T** and **Q** suffer from poor solubility in common solvents. They are only partly soluble in DMSO, chloroform or THF giving solutions of low concentrations after several days of dissolving. Introduction of methyl substituent ($\mathbf{B14_{Me}}$, $\mathbf{T16_{Me}}$) onto the central part does not increase solubility at all (therefore these unimers were no further studied in detail). Unimers of the **M**-, **B**- and **T**-types with hexyl and bromohexyl side groups are insoluble in hydrocarbons as well as polar solvents such as water or alcohols, but they are quite good soluble in organic solvents like toluene, chloroform, dichloromethane, THF, NMP or DMSO. Solubility of brominated **Q**-type unimers significantly depends on the number and positions of substituents on the central block. **Q4Br** as the most planar molecule with a single side chain follows the un/solubility of unsubstituted unimers. **Q45Br** and **Q2457Br** are soluble under same conditions as hexyl-bearing unimers, while solubility of **Q27Br** appears in between last mentioned groups.

The introduction of ionic side groups substantially changes solubility of unimers. Generally, all prepared cationic unimers are well soluble in methanol and DMSO, while their solubility in toluene, THF or dichloromethane is lost. Ammonium-bearing unimers are slightly soluble in water, giving solutions of very low concentrations that usually contain a dispersed insoluble part. Phosphonium-bearing unimers $\mathbf{Q27P^+}$ and $\mathbf{Q45P^+}$ are well soluble in methanol and DMSO and partially soluble in water also giving

colloidal solutions. Unimer **Q2457P$^+$** is the only one unimer which is fully soluble in water at concentration $4 \cdot 10^{-5}$ M.

Solubility of Zn-MSPs prepared with PF_6^- counterions is very limited to solvents like DMSO or NMP or 1,1,1,3,3,3-hexafluoro-2-propanol. In other common solvents these Zn-MSPs are totally insoluble. Zn-MSPs with ClO_4^- counterions are soluble in the mixture of chloroform/acetonitrile, in which they were mostly prepared. Solubility of Fe-MSPs is slightly lowered compared to the Zn-MSPs. Ionic unimers are assembled into MSPs in methanol, and the solubility is not significantly affected by the complexation into long chains. As the ammonium-bearing unimers are not fully soluble in water, they were assembled with zinc ions in methanol and evaporated to get a MSP film coated on inner walls of a flask. Water was then added and stirred to promote dissolving. However, complete dissolving has not been achieved even after several days. This shows that though polymer chains contain more ionic groups per unimer unit than a unimer molecule itself, solubility in water is not achieved for any MSP prepared from water-insoluble unimer. Only MSPs prepared from **Q2457P$^+$** were fully soluble in water.

3.3 Absorption spectra of prepared unimers and polymers

Solution UV/vis spectra of unimers.

Absorption as well as photoluminescence characteristics of unimers are summarized in **Tab. 1**. Solution absorption spectra of unimers show two main bands: the band at around 280 nm belonging to the n→π a π→π* transitions within pyridine and thiophene rings[69] and the band centered at a longer wavelength (340 – 400) belonging to the HOMO-LUMO transitions from the HOMO that is orbital spread over the central oligothiophene chain and adjacent pyridine rings (**Fig. 5.**).

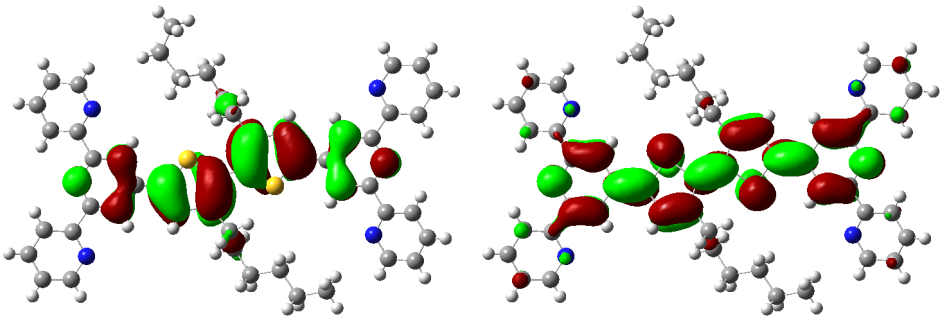

Fig. 5. Electronic density contours for HOMO and LUMO of **B23** obtained by DFT calculations using X-ray crystal structure.

Tab. 1. Absorption and photoluminescence characteristics of prepared unimers. λ_A – apex of absorbance maxima; λ_F – apex of emission maxima; υ – Stokes shift; ϕ – absolute quantum yield of luminescence.

Unimer	UV/vis absorption λ_A (nm)		Luminescence λ_F (nm)		Stokes shift υ (cm^{-1})		Luminescence ϕ (%)	
	Solution	Film	Solution	Film[f]	Solution	Film	Solution	Film
M[a]	344		384, 400					
M1Br[b]	335	344	406	543	5200	10650	3	7
M1N^{+}[c]	334	347	404	460	5200	7150	3	7
M1P^{+}[c]	334	340	405	557	5250	11370	1	1
B[d]	395	390	444, 469	675	2800	10800	33[g]	
B14$_{Me}$[d]	382		445, 466		3700		14[g]	
B14[d]	370	380	448, 470	610	4700	9950	10[g]	
B23[d]	339	400 – 420	450, 470	550	7280	6820 – 5630	3[g]	
B23Br[b]	338	345	452	560	7450	11250	5	4
B23N^{+}[c]	337	345	450	520	7450	9650	5	3
T[d]	420	425	484, 516	765	3150	10400	43[g]	
T16$_{Me}$[d]	411		485, 507		3670		12[g]	
T16[d]	409	420	487, 515	685	3920	9210	20[g]	
T25[d]	403	428	494, 523	612, 720	4570	6970	16[g]	
T34[d]	404	455	492, 522	672	4430	7100	17[g]	
Q[b]	441	435	514, 546	645	4350	7450	30	<1
Q4Br[b]	423	450	525, 554	700	5600	7900	30	<1
Q27[b]	425	460	554	630	5500	5300	26	1
Q27Br[b]	425	455	554	630	5500	6000	31	1
Q27P^{+}[c]	419	455	550	~650	5700	7300	18	<1
Q45Br[b]	397	425	530	610	6300	7000	14	1
Q45P^{+}[c]	393	410	536	550	6800	6200	11	1
Q2457Br[b]	386	500	536	560, 603	7250	3600	14	3
Q2457P^{+}[c]	381	410	536	560	7600	6400	10	1
Q2457P^{+}[e]	400		555		6980			

a) Values for unimer **M** was adopted from ref[107], values in acetonitrile. Solution measurements were done for concentration $2 \cdot 10^{-5}$M in *b)* mixture of chloroform/acetonitrile (1/1 by vol.); *c)* methanol; *d)* THF; *e)* water. *f*) Thin films were coated by drop cast technique onto quartz glass or pyrolytic graphite; *g)* luminescence quantum yields were determined by comparison to quinine sulphate in 0.5M H_2SO_4. Unindexed quantum yields are values determined by integration sphere.

Position of the longer wavelength band mainly depends on the length of the unimers central block[153,154] (**Fig. 6.** *left*) and chain distortion caused by substituents (**Fig. 6.** *right*). Within each structure class: **M**-, **B**-, **T**- and **Q**-type, the unsubstituted unimer always shows the highest lying optical absorption maximum, which well corresponds with the highest co-planarity of rings of the molecular chain that favors delocalization of electrons along the chain.

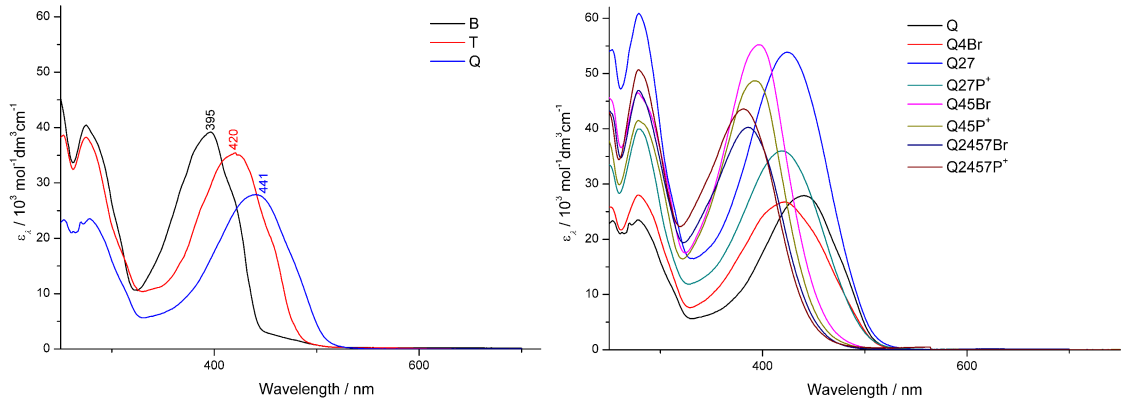

Fig. 6. Absorption spectra of solutions of unsubstituted unimers **B**, **T** and **Q** (*left*); effect of substituent position on absorption spectra of **Q**-type unimers (*right*). Room temperature, concentration of unimer $2 \cdot 10^{-5}$ M.

Introduction of substituents onto oligothiophene central chain disturbs planarity of molecular chains, which induces a blue shift of the absorption maximum with respect to that observed for unsubstituted counterpart. This effect is illustrated on examples of the **Q**-type structures (see **Fig. 6.** *right*). Dihedral angles between adjacent ring planes estimated by the DFT calculations (performed by Dr. Svoboda) are summarized in **Tab. 2**.

The highest local distortion is achieved when substituents are attached at near neighboring positions pertaining to adjacent thiophene rings, which is the case of the unimers of **B23**- and **Q45**- types. Molecules of these unimers behave at the optical absorption almost like two little communicating half-structures. The absorption band of **B23** occurs at the same wavelength as that of Th*tpy***,** being blue shifted about ca 60 nm with respect to the band of **B**. Similar difference is observed for **Q45**-type molecules (blue shift about ca 45 nm with respect to **Q**).

Substitution on each thiophene ring, which is the case of **Q2457**-type unimers, obviously results in the highest total disorder of the whole unimer molecule. Accordingly, these unimers show the lowest-lying absorption maxima of all **Q** unimers in solution. Introduction of substituents to “remote” positions (structures **T25** and **Q27**-type) seems to be a good compromise – substituents do not much interact with each other and thus the coplanarity of rings is not dramatically disturbed. Special case is unimer **T34** with two oppositely oriented substituents on the middle thiophene ring; this unimer behaves similarly like **T25** with isolated substituents.

The hexyl side groups are electron-donating groups increasing the electron density on the oligothiophene backbone, which should result in the red-shift of the absorption band. On the other side, the chain distortion caused by substituents should shift the bands in the blue direction. Comparing the spectra of substituted and

unsubstituted species of the same type one can conclude that the chain-distortion effect prevail the electron-donating effect of side groups.

Tab. 2. Calculated geometry of the molecules; δ_{BC} . . . . . $\delta_{C'B'}$ are dihedral angles between planes of neighboring main-chain rings given in the subscript.

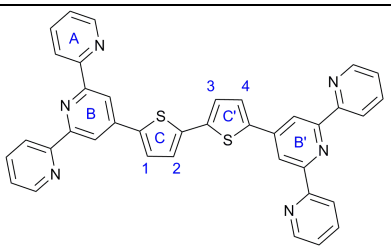

	Ground State			Excited State		
	δ_{BC}	$\delta_{CC'}$	$\delta_{C'B'}$	δ_{BC}	$\delta_{CC'}$	$\delta_{C'B'}$
B	14.5	0.1	14.5	0.0	0.0	0.0
B14	43.9	0.5	42.7	19.9	0.4	22.5
B23	18.9	67.6	18.8	0.0	0.1	0.0

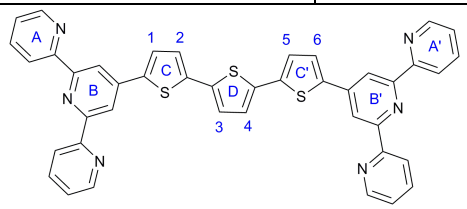

	Ground State				Excited State			
	δ_{BC}	δ_{CD}	$\delta_{DC'}$	$\delta_{C'B'}$	δ_{BC}	δ_{CD}	$\delta_{DC'}$	$\delta_{C'B'}$
T	16.3	14.0	13.8	16.3	0.0	0.0	0.0	0.0
T16	43.4	8.3	7.9	44.7	24.5	2.6	2.7	26.8
T25	17.7	26.0	28.8	17.8	0.0	0.0	0.0	0.0
T34	14.6	37.3	36.7	17.9	0.8	2.7	1.6	0.8

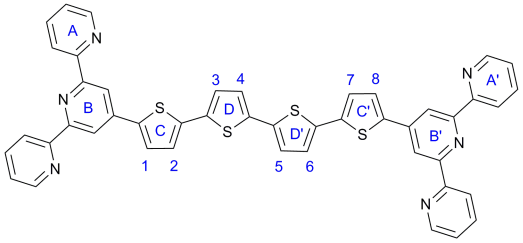

	Ground State			Excited State		
	δ_{BC}	δ_{CD}	$\delta_{DD'}$	δ_{BC}	δ_{CD}	$\delta_{DD'}$
Q	15.8	12.5	0.7	0.0	0.0	0.0
Q27	17.3	28.6	1.0	0.0	0.0	0.0
Q27Br	13.9	22.8	1.0	0.5	3.2	1.3
Q27P$^+$Br$^-$	17.3	32.4	16.3	*	*	*
Q45Br	14.6	18.5	58.9	1.4	3.1	23.7
Q45P$^+$Br$^-$	18.0	15.4	63.5	*	*	*
Q2457Br	19.6	40.8	97.5	*	*	*
Q2457P$^+$Br$^-$	15.8	27.4	124.4	*	*	*

* Values are not available during the first 720 hours

Introduction of ionic groups to the end of hexyl substituents does not significantly affect the unimers absorption in solution. Only very small blue shift up to 6 nm is observed for both **N$^+$**- and **P$^+$**-unimers compared to related **Br**-unimers.

UV/vis spectra of unimers in thin films.

The absorption spectra in thin films of unsubstituted unimers and unimers with side groups interfering with *tpy* end-groups show the HOMO-LUMO band while broadened but centered at a position nearly equal to its position in the solution spectrum ($\Delta\lambda_A$ is ± 5 nm for **B**, **T** and **Q**, and from 7 to 13 nm for **M1**-type, **B14** and **T16**); see **Fig. 7.** and **Tab. 1**. The unimers with side groups sterically non-interfering with each other or with *tpy* end-groups (**T25, T34**, **Q4** and **Q27**-types) show the spectral band position in the thin films red shifted about 25 to 50 nm with respect to its position in the solution spectrum.

The unimers containing substituents at near neighboring positions of adjacent thiophene rings (**B23**-, **Q45**- and **Q2457**- types) show a very wide range of differences between the thin film and solution spectra. The highest red shift of the absorption band when going to the thin films is observed for **B23** ($\Delta\lambda_A$ = 81 nm) and **Q2457Br** ($\Delta\lambda_A$ = 109 nm) Simultaneously, both these relatively heavily substituted unimers exhibit the thin film absorption band at substantially higher wavelengths than their unsubstituted counterparts **B** ($\Delta\lambda_A$ = 40 nm) and **Q** ($\Delta\lambda_A$ = 65 nm). On the other hand, the thin film vs. solution shift observed for **Q45Br** ($\Delta\lambda_A$ = 28 nm) is similar to the shifts observed for unimers with sterically non-interfering side chains and the thin film absorption band of **Q45Br** is blue shifted about 10 nm compared to the band of **Q**.

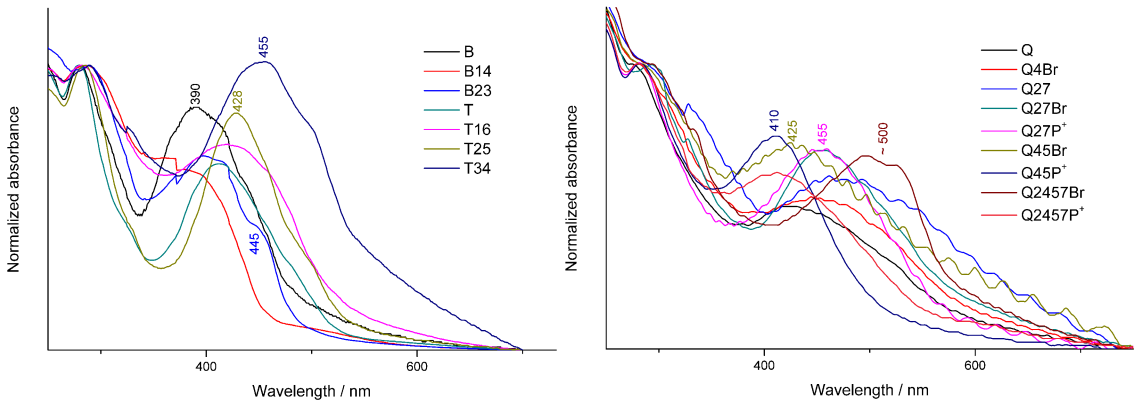

Fig. 7. UV/vis spectra of unimers in thin films.

In the thin films of polyarylenes, the π-stacking of constitutional units is generally supposed to cause planarization of chains due to which the red shift of the absorption band compared to its position in the solution spectrum appears. The thin film absorption band of **B23** is very broad (400 – 420 nm) and shows a pronounced shoulder at ca 450 nm, which indicates the presence of domains containing molecules of increased planarity in a film of **B23**. It is worth noting here that **B23** is the only

unimer that was successfully crystallized giving macroscopic yellow needles (melting point 227 °C) suitable for X-ray analysis. The crystal structure of **B23** (**Fig. 8.**) showed coplanarity of pyridine rings in *tpy* end-groups, only slightly twisted thiophene-*tpy* bonds (20 °) and, mainly: (*i*) *anti-* conformation of sulfur atoms as well as hexyl groups of the central block; (*ii*) layered packing of **B23** molecules, which tentatively suggests the π-stacking and (*iii*) proximity of ends of hexyl groups to pyridine rings of neighboring molecules, which indicates attractive interaction between these moieties. Regarding the very blue shifted position of the absorption band of **B** compared to the band of **B23**, the generally supposed π-stacking does not seems to be the main reason of the observed co-planarization of **B23** molecules in the thin film. The main reason should be seen in the effect of hexyl side groups that act as anchors attenuating the amplitude of thermal twisting of thiophene rings and thus increase the extent of delocalization of π-electrons along unimer chains. The fact that **Q2457Br** shows so exceptionally high red shift when going from solution to the thin film (110 nm) whereas the shift for **Q45Br** is rather low (28 nm) points to the importance of side groups for planarization of unimer molecules of the studied type.

The ionic unimers generally show the absorption band blue shifted compared to their bromohexyl precursors. This observation can be attributed to the effect of counterions whose disturb packing of the ionic unimer molecules into significantly regularly organized nanostructures.

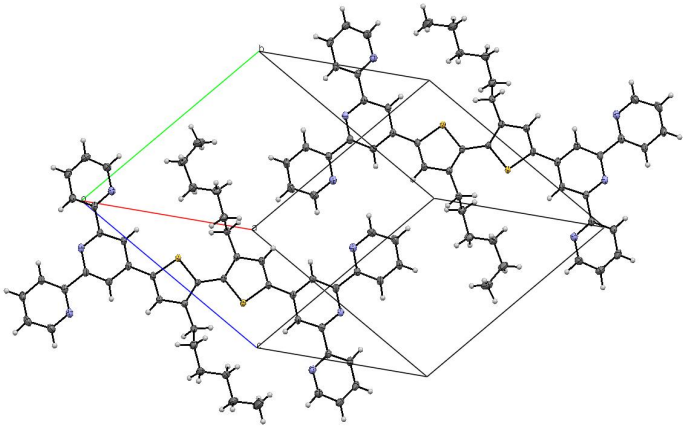

Fig. 8. X-ray crystal structure and molecular packing of **B23** in the crystal lattice. Ellipsoids are plotted at 50% probability level. Crystal data at 150 K: $C_{50}H_{48}N_6S_2$, yellow crystalline needles, triclinic space group $P\bar{1}$, a = 12.0931(3) Å, b = 13.3397(3) Å, c = 14.2693(4) Å, V = 2015.42 Å3, α = 73.2800(10)°, β = 71.1120(10)°, γ = 70.9350(10)°, Z = 2, Z' = 0, R-Factor = 3.97%.

UV/vis spectra of Zn-MSPs.

Absorption characteristics of prepared Zn-MSPs are summarized in **Tab. 3**. Compared to the UV/vis spectra of corresponding unimers, the spectra of Zn-MSPs (**Fig. 9.**) show sharpening of the band belonging to transitions within *tpy* groups and thiophene rings, resulting in a small shift of the band maximum to 287 ± 2 nm. The second, relatively weak band occurs at about 330 nm. Such band is also present in the spectrum of protonized terpyridine[155] and can be attributed to the *syn*-conformation of pyridine rings. Pyridine rings of the *tpy* end-group are in *anti*-conformation in a free unimer molecule (see scheme of assembling in **Scheme 7.**).

Tab. 3. Absorption and photoluminescence characteristics of prepared Zn-MSPs. λ_A – apex of absorbance maxima; λ_F – apex of emission maxima; υ – Stokes shift; ϕ – absolute quantum yield of luminescence.

Zn-MSP	UV/vis absorption λ_A (nm)		Luminescence λ_F (nm), ϕ (%)		Stokes shift υ (cm^{-1})	
	Solution	Film	Solution	Film[e]	Solution	Film
P_{Zn}M1Br[a]	380	407	440	460 (3)	3600	2850
P_{Zn}M1N$^+$[b]	370	395	444	473 (1)	4500	4300
P_{Zn}M1P$^+$[b]	368	395	446	466 (11)	4750	3920
P_{Zn}B[c]	443, 460sh	435, 465sh	562	600 (11)	4780 (3950sh)	6270 (4840sh)
P_{Zn}B14[c]	440	455	560	570	4870	4430
P_{Zn}B23[c]	390	390	535	545	6950	7230
P_{Zn}B23Br[a]	385	395	550	525 (4)	7800	6200
P_{Zn}B23N$^+$[b]	375	390	550	538 (3)	8500	6900
P_{Zn}T[c]	479	470	635	686	5130	6750
P_{Zn}T16[c]	466	465	650	595	6350	4700
P_{Zn}T25[c]	474	500	635	660	5350	4850
P_{Zn}T34[c]	480	495	620	640	4700	4580
P_{Zn}Q[a]	486	500	656	~690 (1)	5350	5050
P_{Zn}Q4Br[a]	467	492	672	702 (<1)	6550	6100
P_{Zn}Q27[a]	468	490	673	~640 (2)	6500	5250
P_{Zn}Q27Br[a]	470	510	675	~710 (1)	6450	5450
P_{Zn}Q27P$^+$[b]	483	500	550	~705 (<1)	2500	5700
P_{Zn}Q45Br[a]	447	455	673	585 (3)	7500	4850
P_{Zn}Q45P$^+$[b]	426	430	536	660 (1)	4800	8050
P_{Zn}Q2457Br[a]	432	430	668	590 (3)	8200	5800
P_{Zn}Q2457P$^+$[b]	439	440	552	625 (1)	4650	6450
P_{Zn}Q2457P$^+$[d]	462		720		7750	

MSPs were assembled and the absorption spectra were measured at $2 \cdot 10^{-5}$M in *a)* mixture of chloroform/acetonitrile (1/1 by vol.); *b)* methanol; *c)* THF; *d*) water. *e)* Thin films were coated by drop cast technique onto quartz glass from the particular solutions.

The position of the absorption band of the lowest energy transition of a Zn-MSP depends on both the chain length and the chain distortion, as can be seen from the survey given below:

P_{Zn}M-type	*solution:*	370 – 380 nm;
	thin film:	395 – 410 nm;
P_{Zn}B-type	*solution:*	440 – 460 nm (undistorted unimers chains);

		375 – 390 nm (distorted **P_{Zn}B23**-types);
	thin film:	450 – 460 nm (undistorted unimers chains);
		395 nm (distorted unimers chains);
P_{Zn}T-type	*solution:*	465 – 480 nm;
	thin film:	465 – 500 nm;
P_{Zn}Q-type	*solution:*	467 – 486 nm (undistorted unimers chains);
		425 – 445 nm (distorted unimers chains);
	thin film:	490 – 500 nm (undistorted unimers chains);
		430 – 455 nm (distorted unimers chains);

First this overview shows that the difference in the band position between the solution and the thin film spectrum is relatively low, which indicates the absence of organized stacking of polymer molecules in cast films. Secondly it is seen that the band wavelength of the Zn-MSPs significantly increases only when going from the **P_{Zn}M**-type to **P_{Zn}T**-type MSPs. The absorption characteristics of the **P_{Zn}T**-type and **P_{Zn}Q**-type MSPs are namely nearly the same. This indicates that the extent of the delocalization of electrons within Zn-MSP chains approaches its limiting value in the **P_{Zn}Q**-type MSPs. The corresponding **Q**-type unimers comprise 14 conjugated double bonds (taking into account only central rings of *tpy* end-groups contributing to HOMO).

The above overview further shows that, for both solution and spectra in thin films, the λ_A values of MSPs derived from a unimer with distorted central block occur in the same wavelength range as λ_A values of MSPs derived from a unimer with undistorted central block comprising just a half of thiophene rings:

λ_A for **P_{Zn}B**-type (distorted) $\cong$ λ_A for **P_{Zn}M**-type (undistorted)

λ_A for **P_{Zn}Q**-type (distorted) $\cong$ λ_A for **P_{Zn}B**-type (undistorted)

This observation corresponds with that found for free unimers and thus confirms that the unimers with distorted central blocks behave in the light absorption like unimers with undistorted central blocks of half length.

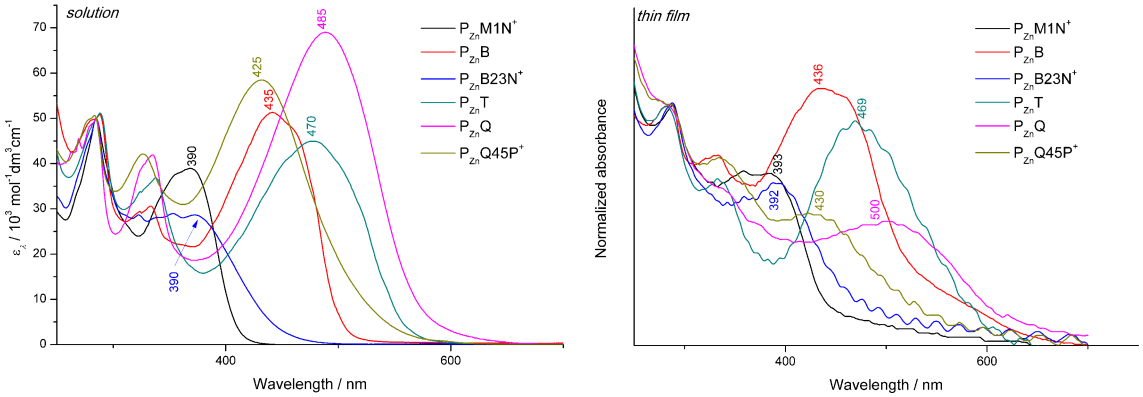

Fig. 9. Solution (*left*) and thin film (*right*) UV/vis spectra of selected Zn-MSPs.

For both, solution and thin film UV/vis spectra, the HOMO-LUMO absorption band of a given Zn-MSPs is red shifted in average about + 50 nm compared to the corresponding band of the parent unimer. Great exceptions of this "rule" exhibit spectra of thin film of unimers with distorted central block chains: the couples **P_{Zn}B23** – **B23** and **P_{Zn}Q2457Br** – **Q2457Br**, for which a blue shift of ca –30 nm and –70 nm, respectively, accompanies the unimer transformation into Zn-MSPs. Note that these unimers show exceptionally high lying absorption bands (420 nm for **B23** and 500 nm for **Q2457Br**), which indicates a highly over-average degree of planarization of their free molecules in the thin films. This is most probably driven by an association of hexyl side chains to alifatic domains, which might promote π-π stacking stabilizing coplanar conformations of the molecules in a film. Hence the blue shift due to complexation can be explained by impossibility of forming an assembly of polymer chains similar to the assembly of free unimer molecules, most probably owing to the perpendicular arrangement of *tpy* end-groups coordinated to Zn^{2+} ions, which might give to the bound unimer units quite high conformational freedom.

UV/vis spectra of Fe-MSPs.

Absorption characteristics of prepared Fe-MSPs are summarized in **Tab. 4**. The absorption spectra of Fe-MSPs in solution cover four areas (see **Fig. 10.**). In the area of lower wavelengths the maximum around 280 – 290 nm dominates. As it was discussed earlier this band is contributed by several n-π and π-π* transitions. Fe-MSPs are good example of the fact that this band is contributed by different transitions, as they often show a doublet band. The band about 320 – 330 nm connected with the *anti-* and *syn-* conformational changes in *tpy* is more pronounced compared to the Zn-MSPs.

Tab. 4. Absorption characteristics of prepared Fe-MSPs. λ_A – apex of absorbance maxima; λ_{MLCT} – apex of the MLCT band.

Fe-MSP	UV/vis absorption λ_A (nm)			
	Solution	(MLCT)	Film[d]	(MLCT)
P_{Fe}M1Br[a]	373	590	394	606
P_{Fe}M1N$^+$[b]	370	587	388	601
P_{Fe}M1P$^+$[b]	370	598	372	608
P_{Fe}B23[a]	370	587		
P_{Fe}B23Br[a]	370	594	386	598
P_{Fe}B23N$^+$[b]	366	591	380	599
P_{Fe}Q[a]	(395), 471	603	475	621
P_{Fe}Q4Br[a]	(395), 443	603	454	624
P_{Fe}Q27[a]	437	601	460	622
P_{Fe}Q27Br[a]	(387), 452	601	465	621
P_{Fe}Q27P$^+$[b]	(386), 436	593	465	611
P_{Fe}Q45Br[a]	405	598	410	613
P_{Fe}Q45P$^+$[b]	399	593	410	609
P_{Fe}Q2457Br[a]	(384), 423sh	594	395	609
P_{Fe}Q2457P$^+$[b]	384	591	395	604
P_{Fe}Q2457P$^+$[c]	400	607		

MSPs were assembled and the absorption spectra were measured at $2 \cdot 10^{-5}$M in *a)* mixture of chloroform/acetonitrile (1/1 by vol.); *b)* methanol; *c*) water. *d*) Thin films were coated by drop cast technique onto quartz glass from the particular solutions.

Compared to the absorption spectra of Zn-MSPs, the spectra of Fe-MSPs contain additional band with maximum centered at around 600 nm. This band is typical of $[Fe(tpy)_2]^{2+}$ complexes and responsible for the typical blue color of these complexes. This band originates from the metal-to-ligand charge transfer (MLCT); an MLCT band is also present in $[Ru(tpy)_2]^{2+}$ complexes where it occurs at around 500 nm. The MLCT band maximum in solution ranges from 587 to 603 nm depending on the structure of parent unimer. This observation prompted that the MLCT transition is not localized exclusively within the *tpy* end-groups but includes also other parts of the molecule, i.e., its central block. This was proven by the resonance and off-resonance Raman spectra of Fe-MSPs obtained with different excitation wavelength.[149,156] Another indication of the participation of the transitions involving the central block in the MLCT band provides the fact that the position of the band attributable to the central blocks in an Fe-MPS is as a rule blue-shifted compared to the band position for Zn-MSP derived from the same unimer. This can be ascribed just to the shift of these transitions to the MLCT band. The only exception from this rule are spectra of **P_{Fe}M**-type MSPs in which this band seems to be significantly contributed by the band at around 325 nm belonging to *tpy* end-groups in *syn*-conformation.

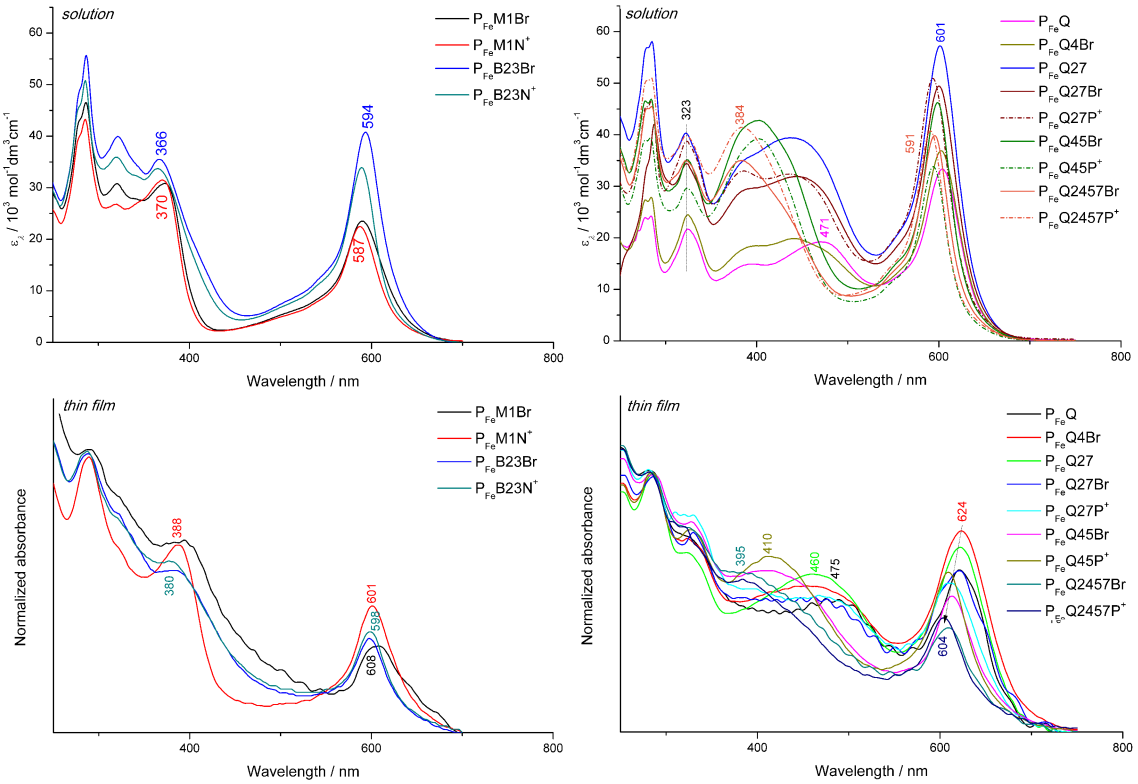

Fig. 10. Solution (*up*) and thin film (*down*) UV/vis spectra of Fe-MSPs. Room temperature, concentration of MSPs $2 \cdot 10^{-5}$ M.

Thin film absorption spectra of Fe-MSPs do not exhibit any dramatic changes or dependence on the molecule structure. Moreover, the decreased intensity of the band of transitions involving central blocks of unimer units (due to indicated transfer of some transitions to the region of the MLCT band) makes determining this band position difficult. Nevertheless, the latter band seems to be slightly red-shifted (about 5 to 35 nm) compared to its position in the solution spectra without an exception, which indicates that the Fe-MSP chains can be in the thin films slightly more planarized than in solutions. MLCT band is also in all cases red-shifted when going from a solution to the thin films; the shift ranges from 5 to 25 nm without any clear dependence. The shift of MLCT band can be ascribed to better dipolar coupling of MLCT bands in thin films, which was described by Kurth et al.[106] when $[Fe(tpy)_2]^{2+}$ complexes in Fe-MSPs accumulates and by Janini et al.[157] based on the prolongation of MSP chain during a unimer complexation with Ru^{2+} ions.

3.4 Photoluminescence characteristics of prepared unimers and polymers

Photoluminescence spectra of unimers.

The measured photoluminescence characteristics of prepared unimers are collected in **Tab. 1**. Their spectra in solution usually show a broad emission band with the position steadily increasing from the **M**- to **Q**-type unimers. The emission bands occur at 405 nm for **M**-type unimers, between 441 and 470 nm for **B**-type, 484 – 523 for **T**-type species and 514 – 554 nm for **Q**-type unimers. The unsubstituted unimer has always the highest emission maximum compared to its substituted analogues, same as in the UV/vis spectra. The areas occupied by particular unimers are clearly visible from the CIE diagram (**Fig. 11.** *right*) as clusters in specific color areas. Solution spectra of unimers **M1Br**, **B**, **T** and **Q** are depicted in **Fig. 11** *left*. Maxima of some spectra are split by the vibronic structure.[158,159] This phenomenon is mostly pronounced for planar structures or spectra measured in THF.

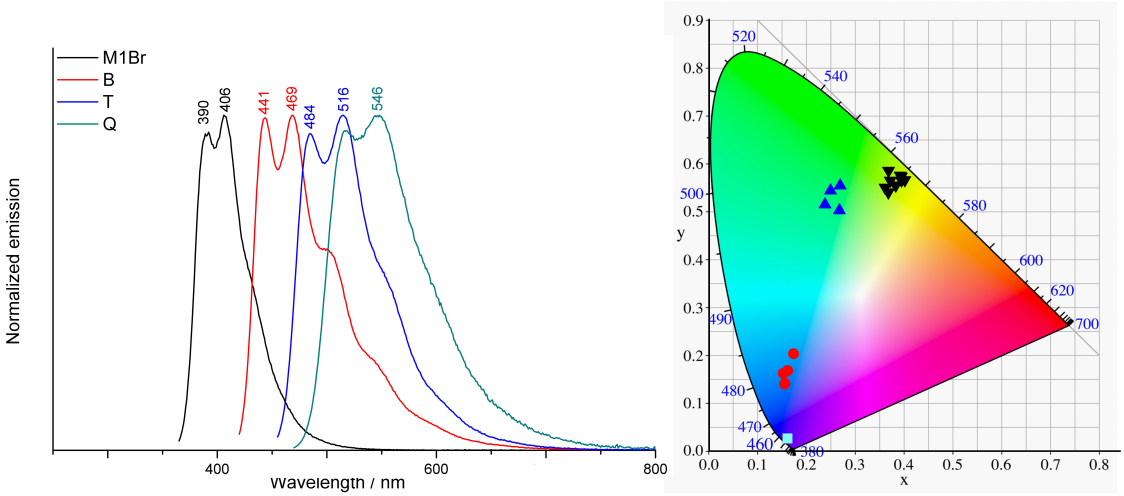

Fig. 11. Normalized emission spectra of unsubstituted unimers **M1Br**, **B**, **T** and **Q** (*left*), room temperature, concentration $2 \cdot 10^{-5}$ M; CIE diagram with groups of points showing areas occupied by emission of prepared unimers :■ for **M**-type unimers, ● for **B**-type unimers, ▲ for **T**-type unimers, ▼ for **Q**-type unimers (*right*).

The spectra of thin films of unimers (**Fig. 12.**) are always red-shifted compared to the spectra taken from solution. The shift ranges from 15 to 250 nm. This relatively high difference should be attributed the differences in ability of given unimer molecules to undergo planarization in the excited state from which the luminescence is emitted. In the excited state the rings in unimer backbone acquire the quinoidal structure with the LUMO orbital mostly spread over the bonds connecting thiophene units together with

the central pyridine ring.[160] Typical characteristics of luminescence of particular compound is the Stokes shift, which is defined as the energy difference between the absorption and emission maxima of the corresponding electronic transitions. As can be seen from the **Tab. 1.**, introduction of substituent to oligothiophene central part of unimer caused significant blue-shift in solution emission maxima of these compounds, however the Stokes shift follows opposite trend.

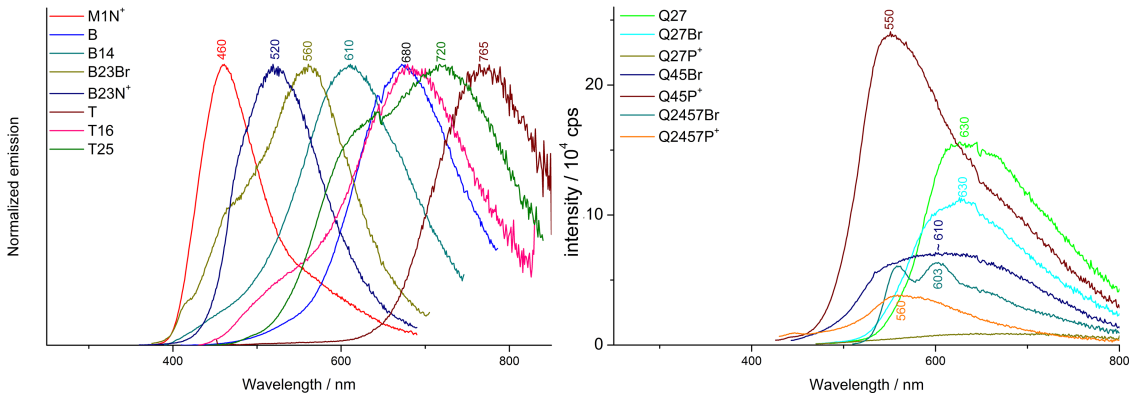

Fig. 12. Emission spectra of thin films of unimers.

Fluorescence quantum yields in solutions are rather low for **M**-type and **B23**-type structures (3, resp. 5%) and medium for **B14**-type unimers, substituted **T**-type and **Q**-type unimers with distorted central block chains. Relatively higher quantum yields (26 – 43%) are obtained for unimers with close to coplanar-ring structures: **B**, **T**, **Q**, **Q4Br**, **Q27** and **Q27Br**. These values are comparable with other unimers of this type found by different research groups.[60,83,89,115] Quantum yields in thin films are only about a few percent, which means that the excitation energy is preferably dissipated by non-radiative transitions.

Photoluminescence spectra of MSPs.

Luminescence characteristics of Zn-MSPs are summarized in **Tab. 3**. Solution spectra ($2 \cdot 10^{-5}$ M) of Zn-MSPs exhibit a broad unimodal emission band (**Fig. 13.** *left*) with maximum at around 440 nm (**M**-type MSPs); 548 ± 14 nm (**B**-type MSPs); 635 ± 15 nm (**T**-type MSPs); and 658 ± 18 nm (**Q**-type MSPs). Except for the **M**-type, all other Zn-MSPs occupy the yellow to red area of the CIE diagram (see **Fig. 13.** *right*) and their emission maxima are red shifted about 100 nm or more compared to the emission maximum of the corresponding free unimer. This observation is in accord with literature knowledge that the coordination to Zn^{2+} ions stabilizes the LUMO level, which induces the intramolecular charge transfer in non-charge transfer compounds that cause the red-shift and significant quenching of the fluorescence.[161,162]

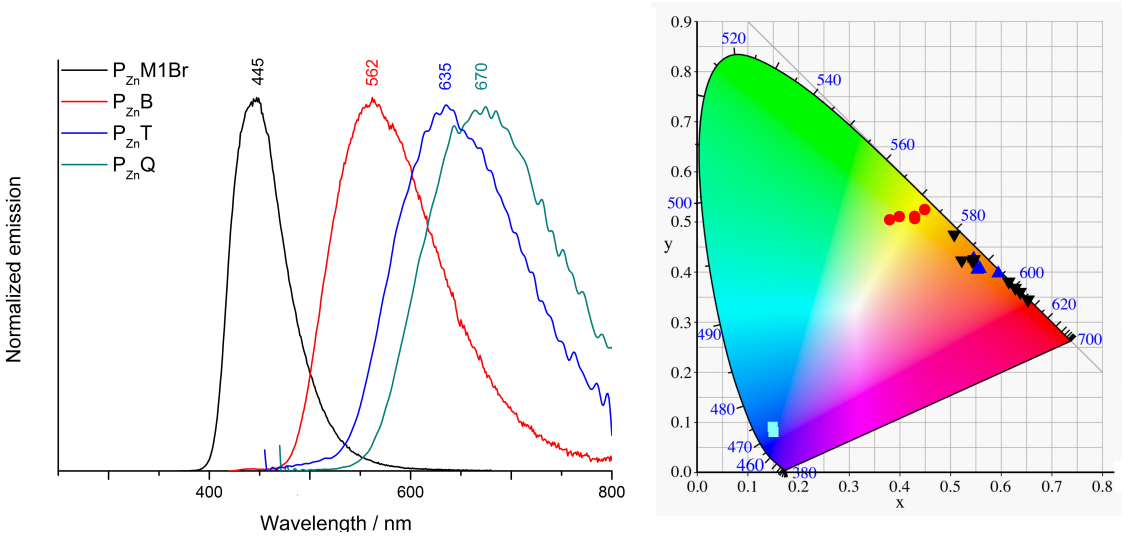

Fig. 13. Solution spectra of Zn-MSPs prepared from **M1Br**, **B**, **T** and **Q** (*left*), room temperature, concentration $2 \cdot 10^{-5}$ M; CIE diagram pointing out areas occupied by emission of Zn-MSP solutions: ■ for **M**-type MSPs, ● for **B**-type MSPs, ▲ for **T**-type MSPs, ▼ for **Q**-type MSPs (*right*).

The thin film emission of Zn-MSPs (**Fig. 14.**) is quite weak showing the quantum yields comparable to those observed for thin films of unimers. Moreover, in some cases (**P_{Zn}B23Br**, **P_{Zn}B23N$^+$**, **P_{Zn}T16**, **P_{Zn}Q27**, **P_{Zn}Q45Br** and **P_{Zn}Q2457Br**), the emission band of Zn-MSP in thin films is even blue-shifted with respect to its position in solution, which points to distorted geometry of excited states of these compounds in films. A blue shift of the luminescence is also mostly observed when going from a unimer in thin films to the corresponding Zn-MSP in thin films. This indicates that, in a film, the unimer molecules adopt more planar geometry than their units built in Zn-MSPs. This might be caused by interactions of the central blocks of unimer units with bulky $[Zn(tpy)_2]^{2+}$ linkages, which should hinder planarization of the blocks.

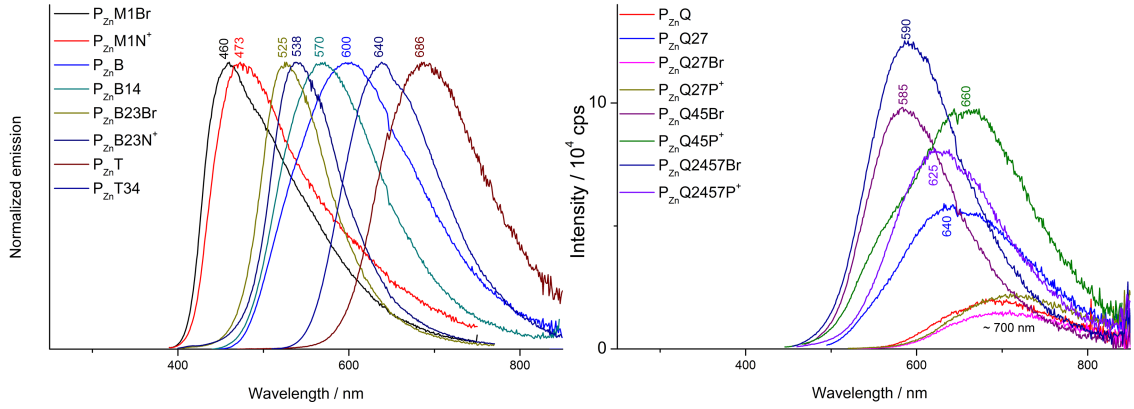

Fig. 14. Emission spectra of Zn-MSPs in thin films.

Fe-MSPs do not show luminescence at all, which is attributed to the fact that their lowest excited state is a d-d triplet state that is very close to the ground state.[50] As the potential d-d phosphorescence is spin forbidden, the d-d triplet state easy depletes the upper excited states and decays by unambiguously preferred non-radiative transitions in accord with the energy gap law.[52,163]

3.5 Assembling of unimers to metallo-supramolecular polymers

Examination of assembling process was performed using the optical absorption and emission spectroscopy, size exclusion chromatography and viscometry. For the spectroscopic measurements set of samples with initial concentration of unimer $2 \cdot 10^{-5}$ M and increasing amount of metal ions were prepared and allowed to equilibrate for 24 hours before measurements. For the SEC and viscometry measurements, the initial concentration of unimer was increased to $5 \cdot 10^{-4}$ M. The metal ions-to-unimer ratio *r* varied from 0.0 to 3.0. Zn^{2+} and Fe^{2+} perchlorates were used in these experiments.

3.5.1 Absorption spectra

The assembling process was monitored in several solvents. Non-ionic **B** and **T** unimers were assembled in THF. Methanol was used as solvent for assembling of ionic unimers. The other unimers (**M1Br, B23Br**, and non-ionic **Q**-type structures) were assembled in the mixture of chloroform/acetonitrile (1/1 by vol.). Unimer **B23** was assembled in both THF and the chloroform/acetonitrile mixture. Unimer **Q2457P$^+$**, as the only unimer fully soluble in water, was assembled in both methanol and water.

Assembling with Zn^{2+} ions can be formally divided into three stages (**Fig. 15.**). The first stage of assembling occurred for *r* values up to 0.5 – 0.6. During this stage original band of free unimer gradually attenuates and new absorption band starts to develop as a shoulder on the unimer band at higher wavelengths. The set of spectra relating to this phase always exhibits one or more isosbestic points, which indicates a transition between two distinct species. One of them is the free unimer while the second one should be according to the stoichiometry dimer U-M^{2+}-U (where U stands for a unimer species).

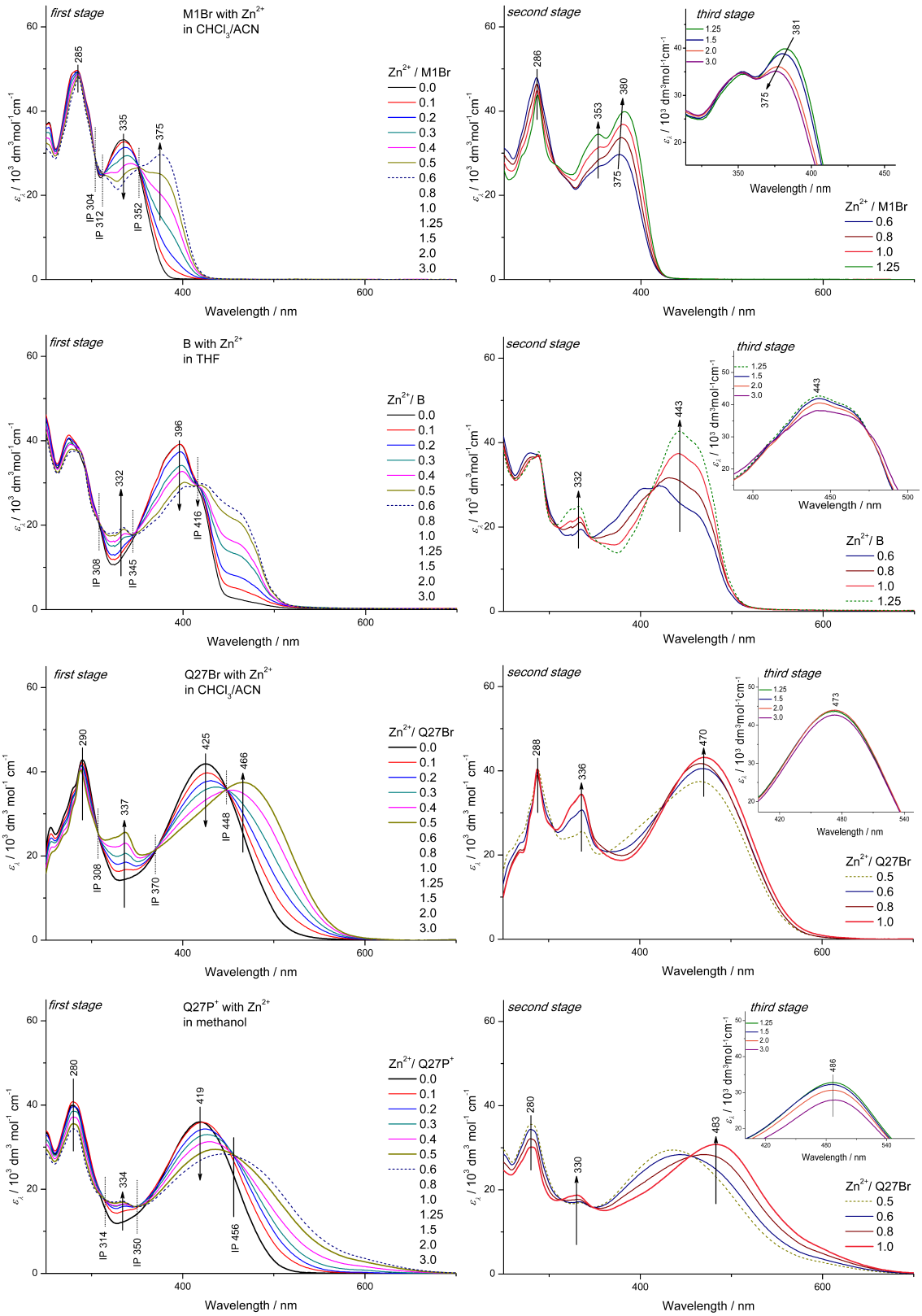

Fig. 15. UV/vis spectra of assembling of selected unimers with Zn^{2+} ions. Room temperature, initial unimer concentration $2 \cdot 10^{-5}$ M.

The *second stage* occurs for *r* values in the region from 0.5 to ca 1. It is characterized by the disappearance of the unimer main band and full development of the new bands belonging to MSP chains. The stepwise monitored absorption spectra usually do not pass through isosbestic points in this stage of assembly, which corresponds to the stepwise growth of MSP chains with the random choice of reacting species. Changes in absorption spectra are observed in several areas.

(i) Decrease in absorption at 280 nm resulting in sharpening of the band in this region and shift of its maximum to almost 290 nm; this feature is more pronounced for the non-ionic compared to the ionic unimers.

(ii) Development of the band at 320 – 330 nm attributed to *tpy* units in *syn* conformation. Also this feature is more pronounced the non-ionic compared to the ionic MSPs, however, it is not seen for **M**-type and **B23**-type MSPs owing to overlap with the band of enchained unimer units.

(iii) Development of the new band belonging to the corresponding MSP (see above, spectra of MSPs). A continuous red shift of this band maximum with increasing value of the ratio *r* is the evidence for the prolongation of the conjugated MSP chains.

Third stage of assembly is characterized either by conservation of the absorption spectrum of already assembled MSP or by its slight changes mainly in the area of higher wavelengths. The overstoichiometric amount of metal ions present in this stage is proposed to result in the end-capping of MSP chains with the surplus ions and/or equilibrium shortening of the chains. Absorption spectroscopy cannot provide an exact view of the processes running in this stage, but only help to detect a constitutional dynamics of the system.

Assembling with Fe^{2+} ions was carried out with the unimers of the **M1**-, **B23**- and **Q**-types. An example of changes in the UV/vis spectra accompanying assembling with Fe^{2+} ions is shown in **Fig.16.**; complete sets of the absorption spectra can be seen in refs[149,156,](attached to the Thesis). The spectra monitored in the *first stage* of assembling show several isosbestic points resulting from attenuation of the free unimer band and formation of the bands of MSP including the MLCT band. Sharpening and a small red shift of the maximum in the region 280 – 290 nm are also seen.

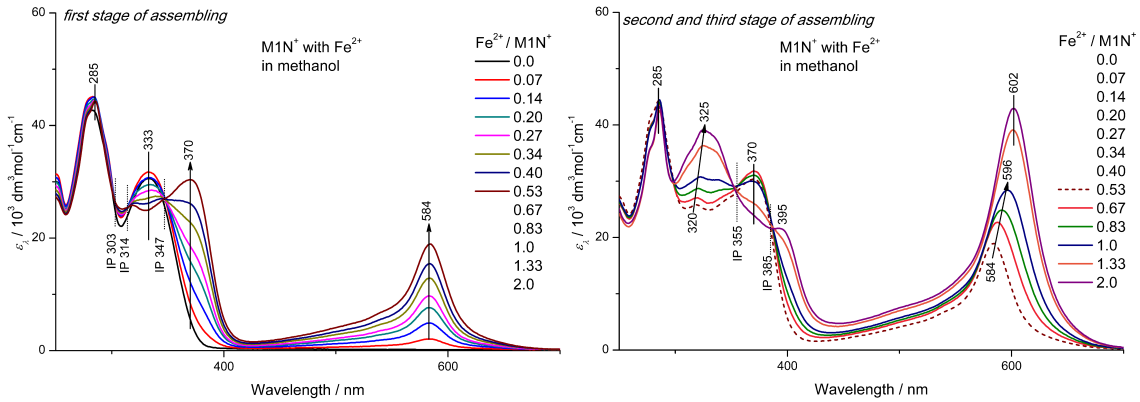

Fig. 16. UV/vis spectra of assembling of **M1N$^+$** with Fe^{2+} ions into MSPs. Room temperature, initial unimer concentration $2 \cdot 10^{-5}$ M.

During the *second stage* usually weaker new band is forming belonging to the HOMO-LUMO transitions in conjugated backbone. MLCT band in **M**-type and **B23**-type assembling sets shifts to higher wavelengths, which should originate from dipolar coupling of individual MLCT complexes.[106] For **Q**-type structures the position of MLCT band is fixed in all stages of assembling. This can be ascribed to the decreased dipolar coupling of the MLCT complexes due to increased length of the oligothiophene central block between the MLCT complexes of *tpy* end-groups. During the *third stage* of assembling with Fe^{2+} the UV/vis spectra mostly showed only small changes that can be ascribed to the end-capping of MSP chains with surplus Fe^{2+} ions.

3.5.2 Luminescence spectra

Luminescence spectra of systems at various stages of assembling were recorded with excitations at isosbestic points of the UV/vis spectral sets.[149,111,115] The spectra for Fe^{2+}/any unimer systems exhibited exclusively a monotonous luminescence decay with the increasing composition ratio *r*. Luminescence completely quenched for *r* up to 0.6 seldomly at higher *r* (see examples in **Fig. 17.**). Therefore, next discussion concerns the systems with Zn^{2+} ions whose all showed luminescence at all examined ratios *r*.

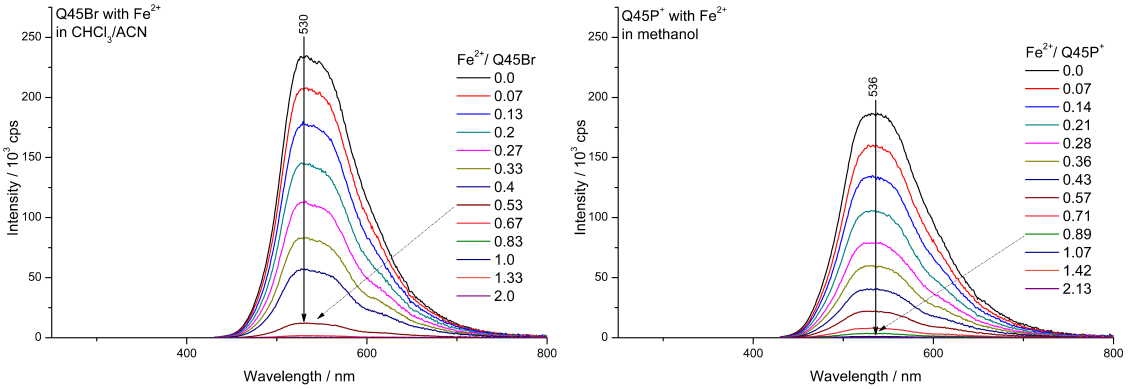

Fig. 17. Monotonous luminescence decay accompanied the assembling of with Fe^{2+} ions into MSPs. Room temperature, initial unimer concentration $2 \cdot 10^{-5}$ M.

As can be seen from examples shown in **Fig. 18.**, luminescence spectra show three stages of the unimer assembling with Zn^{2+} ions, same as the UV/vis spectra. The spectral set for the system Zn^{2+}/**M1N^{+}** in methanol shows attenuation of the unimer band for ratios *r* up to 0.6 and simultaneous development of a new band pertaining to the complexed species formed. This spectral set shows an isosbestic point at 420 nm, which represents the additional evidence (to that derived from absorption spectra) for the formation of dimers U-M^{2+}-U. Quite similar development of spectral features exhibits the system Zn^{2+}/**M1Br** in the mixed chloroform/acetonitrile (1/1 by vol.) solvent. For both these systems the emission band of dimers is more intense than the band of corresponding unimer, which is typical of the $[Zn(tpy)_2]^{2+}$ species derived from monotopic terpyridine-4'-yl derivatives.[54]

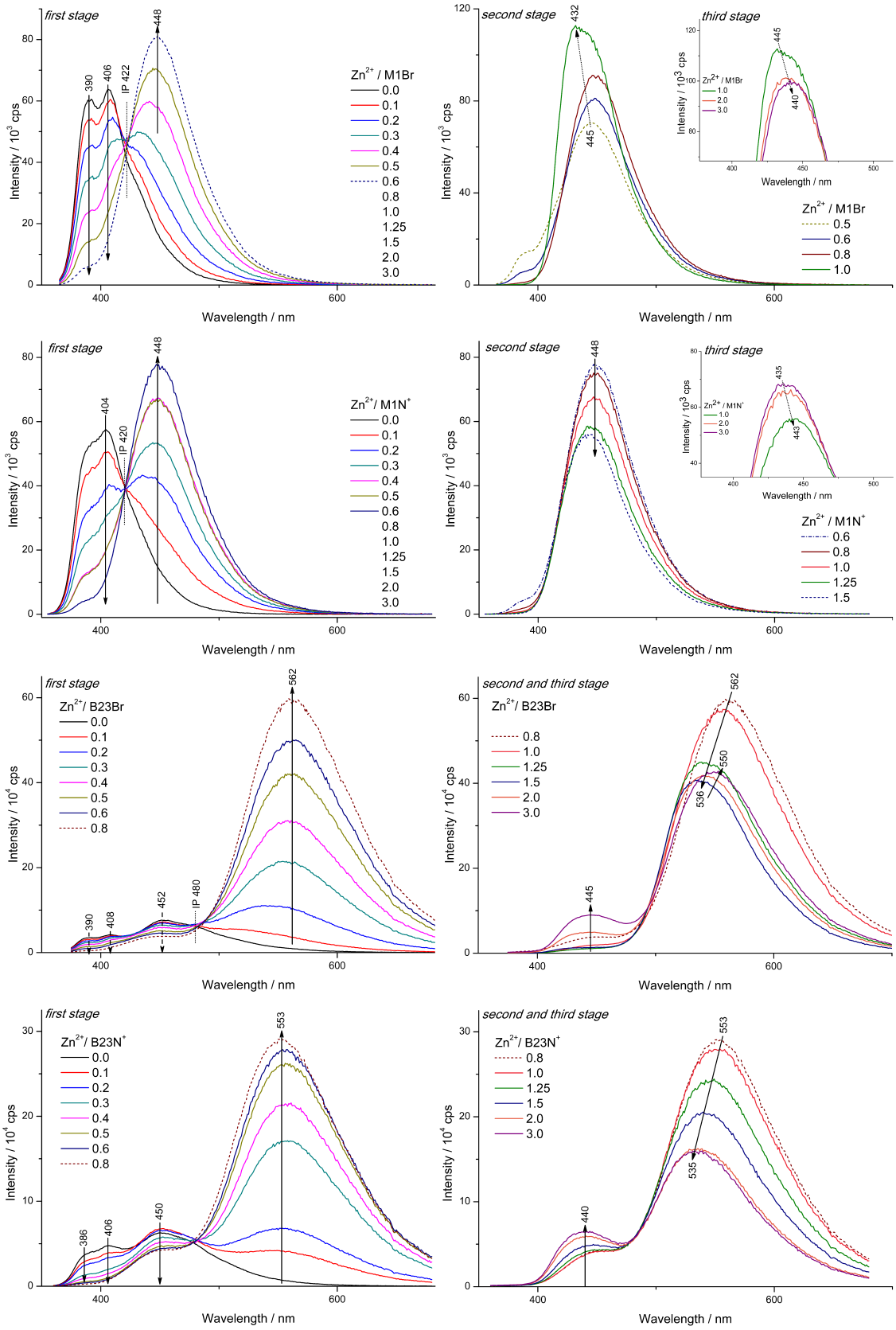

Fig. 18. Luminescence spectra of assembling of selected unimers with Zn^{2+}. Room temperature, initial unimer concentration $2 \cdot 10^{-5}$ M.

Fig. 18. also shows the spectral sets for the systems with ionic and non-ionic unimers with distorted bithiophene central blocks: Zn^{2+}/**B23N**$^{+}$ and Zn^{2+}/**B23Br**. As can be seen, these spectral sets show features very similar to those observed for systems Zn^{2+}/**M1N**$^{+}$ and Zn^{2+}/**M1Br** and the emission intensity of complexed species much higher than that of the unimers. The spectral set for the Zn^{2+}/**B23** system in THF solvent[160] (not shown) also exhibits the same features. Hence these observations strongly support the conclusion drawn from the UV/vis spectral sets that the molecules as well as the enchained unit of the unimers with distorted bithiophene central blocks spectroscopically nearly behave like two independent monotopic Th*tpy* species. Note that the discussed spectral sets with nearly identical main features were obtained using three different solvents (methanol, THF and chloroform/acetonitrile mixture). Thus it seems sure that these common spectral features originates from the the unimer structure, not from a solvent effect.

For all other studied systems (**B**-type except **B23**-type, **T**-type, **Q**-type), the observed luminescence emission intensity of assembled unimers was substantially weaker than the intensity of the parent unimer, regardless the extent of the central block distortion. Unlike the UV/vis spectra, the effect of the central block distortion on the luminescence of MSPs is quite small as can be seen from examples in **Fig. 19**.

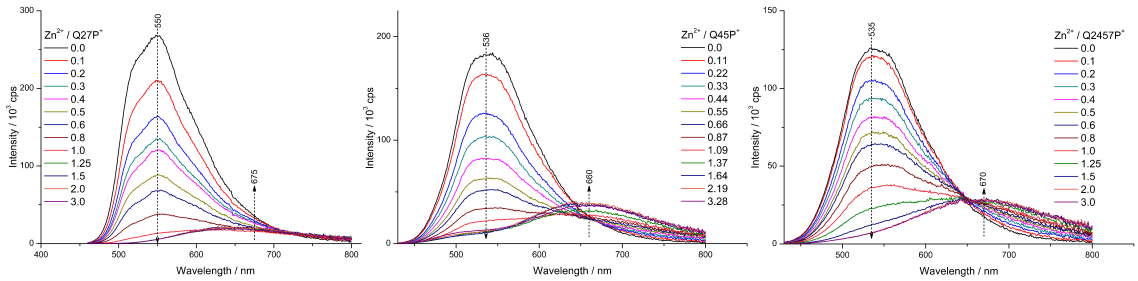

Fig. 19. Sets of the luminescence spectra for assembling of the **Q**-type unimers; the central block distortion increases from left to right. Room temperature, initial unimer concentration $2 \cdot 10^{-5}$ M in methanol.

*Assembling of unimer **Q2457P**$^{+}$ in water*

The water-soluble unimer **Q2457P**$^{+}$ has been assembled with metal ions also in water. Since its molecular dissolving in water takes a long time (see **Fig. 20.**) a month-old solution of **Q2457P**$^{+}$ was used in these experiments. The optical spectral changes accompanying the assembly in water substantially differ from those observed for the assembly in methanol (see **Fig. 21.**).

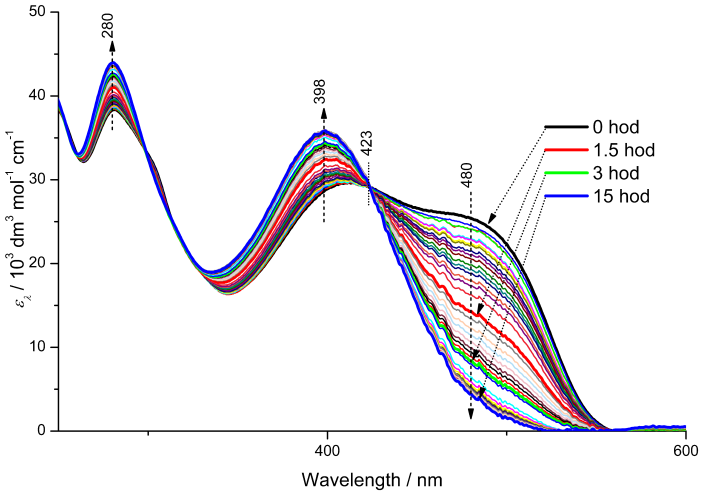

Fig. 20. Dissolving of **Q2457P$^+$** in water monitored for 15 hours.

(i) The absorption maxima of **Q2457P$^+$** (λ_A = 400 nm) and its Zn-MSP (r = 2, λ_A = 462 nm) as well as the luminescence maximum of the unimer (λ_F = 555 nm) are red shifted about ca 20 nm compared to their positions in methanol solutions, which indicates that the free as well as enchained unimer species acquire in water more planar conformations than in methanol. This can be attributed to the substantial increase in the solvent permittivity, which, in accord with the Coulomb law, reduces repulsive ionic interactions among neighbouring P^+Et_3 groups as well as their attractive interactions with counterions.

(ii) The UV/vis spectra for assembling of **Q2457P$^+$** with Zn^{2+} ions show a single set of isosbestic points and fluent course of changes up to r = 2. Luminescence spectra indicate the presence of free unimer in solution up to r equal to at least 1.5. These features consistently indicate a lowered stability and increased constitutional dynamics of **P_{Zn}Q2457P$^+$** in aqueous solutions.

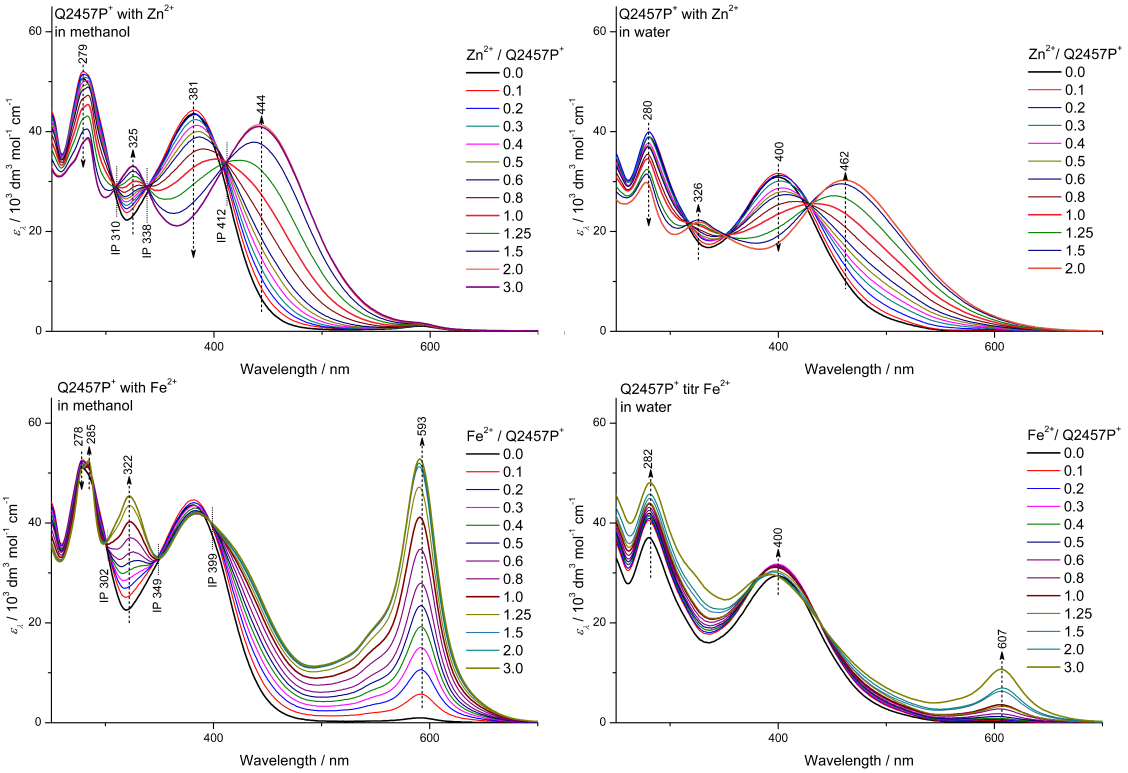

Fig. 21. Changes in UV/vis spectra accompanying assembling of **Q2457P$^+$** with Zn^{2+} (*up*) or Fe^{2+} (*down*) ions in methanol (*left*) or water (*right*) at room temperature. Initial unimer concentration $2 \cdot 10^{-5}$M.

(iii) The emission band observed for **P_{Zn}Q2457P$^+$** (λ_F = 720 nm) is enormously red shifted (about 180 nm) compared to the band of **Q2457P$^+$** in methanol solution (**Fig. 22.**). Stokes shift for **P_{Zn}Q2457P$^+$** in water (7 750 cm^{-1}) is much higher than the shift in methanol (4 650 cm^{-1}, **Tab. 3.**), which proves much higher extent of conformational relaxation of excited states in aqueous compared to methanol solutions.

(iv) Surprisingly, but in accord with the preceding observations, the UV/vis spectra for the Fe^{2+}/**Q2457P$^+$** system show small changes and weak MLCT band while the luminescence spectra show emission up to r = 3. Note that no new emission band occurs, only reluctant luminescence quenching with increasing r is observed. These features indicate that the chains of highly ionic **P_{Fe}Q2457P$^+$** are in aqueous solution less stable than the chains of related Zn-MSPs. This observation represents quite surprising flip in the stability of Fe- and Zn-MSPs derived from bisterpyridines compared to perhaps all so far reported data.[53–55,164,165]

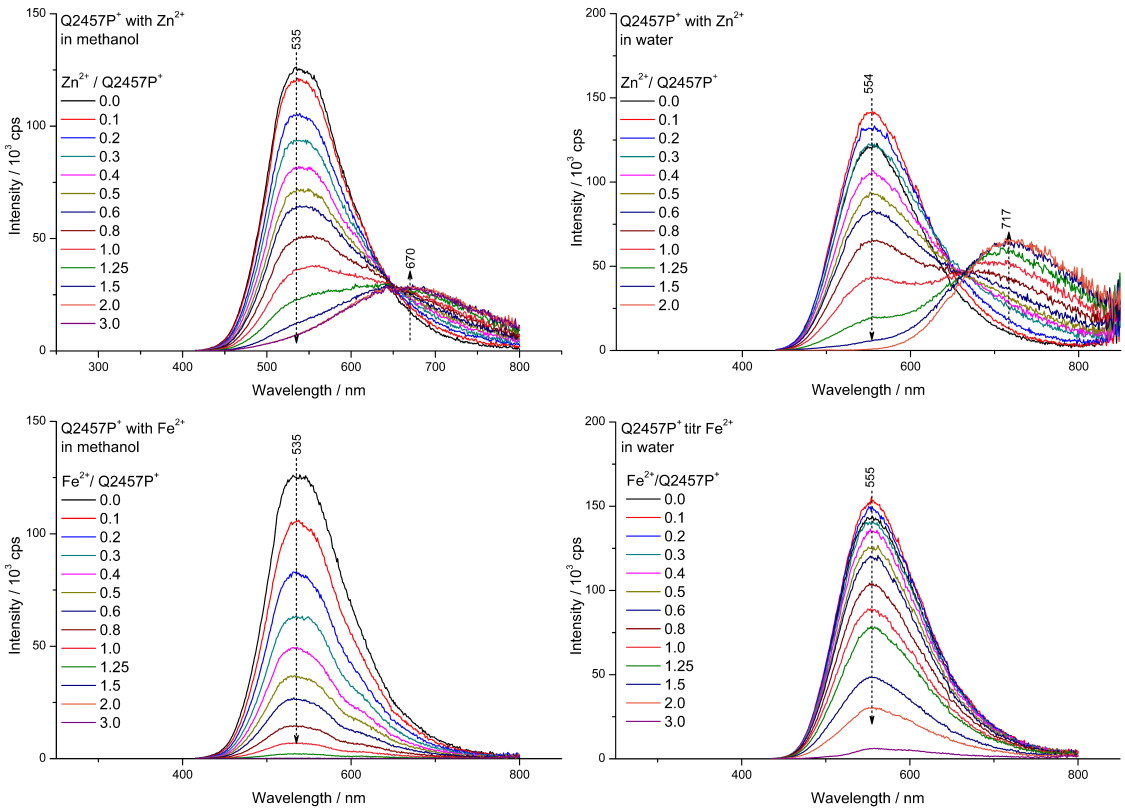

Fig. 22. Emission spectra accompanying the assembling of **Q2457P⁺** with Zn^{2+} (*up*) and Fe^{2+} (*down*) in methanol (*left*) of water (*right*) at room temperature. Initial unimer concentration $2 \cdot 10^{-5}$M.

3.5.3 Size exclusion chromatography and viscometry

There is only limited number of methods suitable for determination of the degree of polymerization of the constitutional dynamic MSPs. Size exclusion chromatography is considered to be the method suitable only for MSPs with stable coordination bonds (with Ru or Os ions) with very slow kinetics. In our case we were able to perform SEC measurements for systems with Fe^{2+}, which is quite unique using the conditions specified in Experimental part. These results helped us to bring awareness about chain-lengths of resulting MSPs in such dynamic systems. SEC measurements were successfully performed for systems of **M1Br,**[156] **B23**, **Q27Br** and **Q45Br**[149] with Fe^{2+} ions. Systems with Zn^{2+} ions were also tested on SEC, but fast dynamics in that system caused complete dissociation of polymer chains and detection only signal belonging to the free unimer. Unfortunately, similar study on MSPs derived from ionic unimers was not possible owing to the strong adsorption of their chains inside SEC column. Systems of different composition of non-ionic unimer and Fe^{2+} ions were allowed to equilibrate for one day and then injected to SEC equipped with DAD detector resulting in composition-dependent chromatograms similar to those of conventional polymers (see **Fig. 23.**).

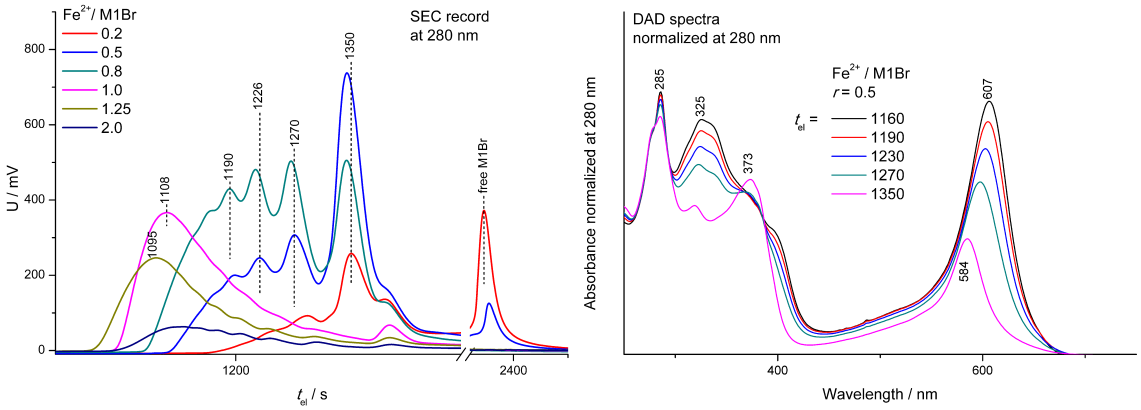

Fig. 23. Well resolved SEC chromatograms for different *r* (*left*) and DAD spectra belonging to the Fe-MSPs with different lengths (*right*).

Well resolved chromatograms were obtained for systems with composition ratio $r \leq 1$, while those with $r > 1$ provide worse resolve records with decreasing area under curve. This indicates retention of longer chain obviously end-capped with Fe^{2+} on column, which had to be washed away using different chelating compounds. SEC record provides well resolved peaks which can be ascribed to the species with different length (dimers at 1350 s, trimers at 1270 s, etc.). This assignment provides semi-logarithmic dependence of number of repeating units on elution time, which was then used to calculation of average degrees of polymerization. The number-average and weight-average degrees of polymerization were estimated to be up to 10 for 0.5mM solutions. It is seen from **Fig. 24.** that the stoichiometric excess of Fe^{2+} ions results in the formation of shorter chains. This is supported by the results of viscometric measurements that also indicate shortening of the MSP chains in the presence of excess Fe^{2+} ions.

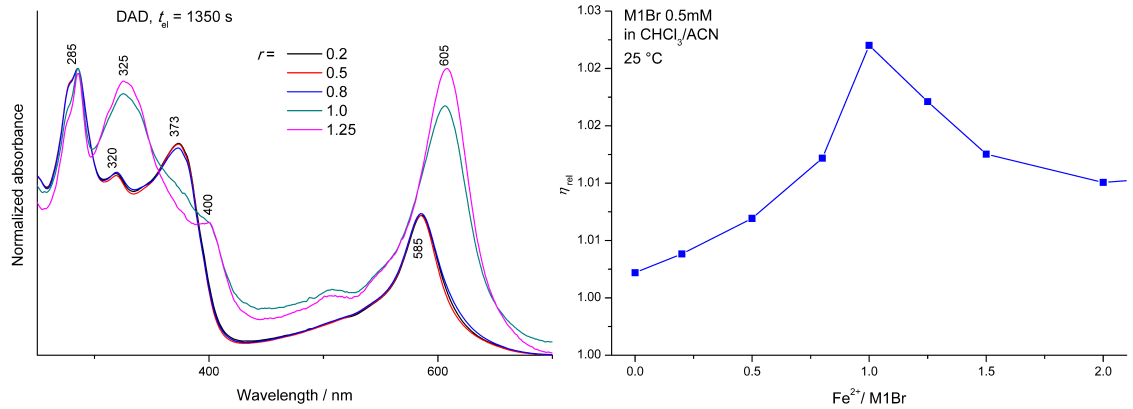

Fig. 24. Comparison of the spectra of the last fraction (dimers; t_{el} = 1350 s) of Fe^{2+}/**M1Br** systems with the different composition ratio (*left*) and the relative viscosity of solutions of the system Fe^{2+}/**M1Br** as a function of composition (*right*).

Number-average (X_n) and weight-average (X_w) degrees of polymerization of Fe/**M1Br** and Fe/**Q45Br** systems with different *r* are depicted in **Tab. 5**. These two systems consist of unimers with the shortest and the longest central part. It is clearly visible, that for a given initial concentration and the same experimental setup the values are about the same. Thus it can be concluded, that the length of the unimer central block does not dramatically influence the degree of polymerization.

Tab. 5. Number-average (X_n) and weight-average (X_w) degrees of polymerization and dispersity index (D) of Fe/**M1Br** and Fe/**Q45Br** systems in solution of initial concentration $5 \cdot 10^{-4}$ M calculated from SEC records.

	Fe / **M1Br**			Fe / **Q45Br**		
r	X_n	X_w	D	X_n	X_w	D
0.2	2.26	2.46	1.09	3.07	4.23	1.36
0.5	2.62	3.10	1.18	3.24	4.77	1.47
0.8	3.31	4.04	1.22	4.43	6.02	1.36
1.0	5.43	6.62	1.22	6.13	7.23	1.18
1.25	5.94	7.48	1.26	6.26	6.84	1.09

The reported halftime of the $[Fe(terpyridine)_2]^{2+}$ complex is ca 8400 min but the halftime of the $[Zn(terpyridine)_2]^{2+}$ is below 0.1 min.[165] Fast reversibility of assembling process was found for Zn-MSPs in DMSO. Prepared MSPs with PF_6^- counterions was dissolved in DMSO and stepwise diluted. The UV/vis spectrum was measured immediately after dilution. As can be seen, the λ_A value continuously decreases with increasing dilution of the Zn-MSPs solution (see **Fig. 25.**). Such changes indicate fast equilibrium depolymerization of conjugated supramolecular chains and prove the fast constitutional dynamics of this system.

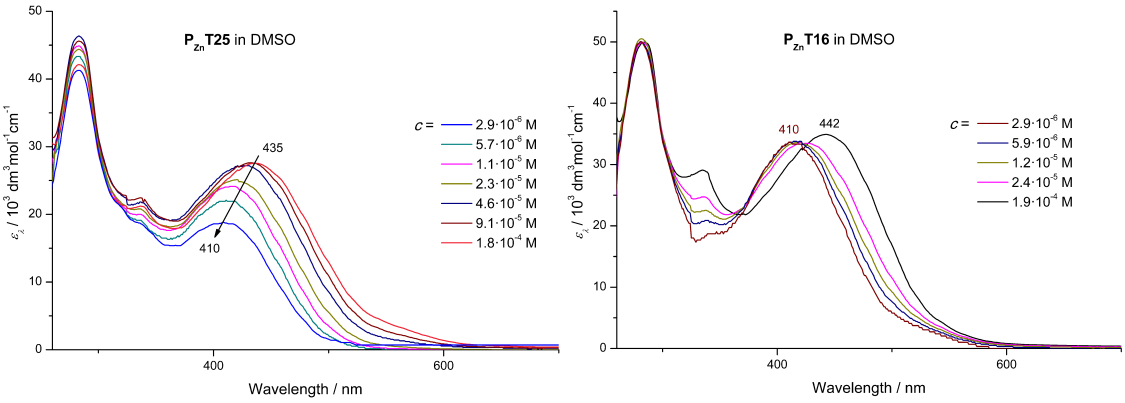

Fig. 25. Dependence of Uv/vis spectra on MSPs concentration in DMSO. **PZnT25** (*left*) and **P_{Zn}T16** (*right*).

Despite the aforementioned fast dynamics of Zn-MSPs, the time-resolved *transient absorption spectroscopy* provided a value of the degree of polymerization for Zn-MSPs in DMSO solution of the concentration of $1 \cdot 10^{-4}$,[166] which is hardly accessible by others methods. Comparison of the time development of the transient absorption spectra of free unimers and corresponding Zn-MSPs afforded the fraction of free unimers in DMSO solutions of $\mathbf{P_{Zn}T}$ and $\mathbf{P_{Zn}T16}$, from which the following values of X_n and X_w were calculated: $X_n \approx 11$ and $X_w \approx 21$ for $\mathbf{P_{Zn}T}$ and $X_n \approx 5$ and $X_w \approx 9$ for $\mathbf{P_{Zn}T16}$ (for 10^{-4} M solutions in DMSO).[166] These values are comparable with those obtained for Fe-MSPs from SEC records.

3.5.4 Assembling course of B23 and Th*tpy with lanthanides*

Lanthanide ions are known to bind up to three *tpy* ligands. When binding α,ω-bis(*tpy*), formation of a 3D coordination network can be expected. To examine this idea, several experiments on assembling unimer **B23** with lanthanide salts were performed using the same experimental procedure as described above. A set of mixed solutions of different Ln^{3+}/**B23** mole ratio were prepared (europium nitrate, lanthanum nitrate and lanthanum perchlorate were used as inorganic components), allowed to equilibrate and their UV/vis and luminescence spectra were measured. The obtained sets of the absorption and emission spectra are shown in **Fig. 26**.

Absorption spectra during the assembling experiments of **B23** with different lanthanide salts followed almost the same trends. The band of free unimer at 339 nm continuously attenuates while new band with maximum at 356 nm and shoulder at 370 nm develops. These changes are also accompanied by sharpening and small red shift of the band around 280 nm. The changes are smooth without any significant break.

Luminescence spectra for the Eu^{3+}/**B23** system show a continuous decrease of the intensity of the unimer band and formation of new sharp bands at 594, 617 and 650 nm that are typical of the $^5D_0 \rightarrow {}^7D_J$ electronic transitions within the Eu^{3+} ions.[167] Hence it follows that the binding with Eu^{3+} ions results in quenching the luminescence originating from unimer units. Unlike the system with Eu^{3+} ions, both systems with La^{3+} ions show formation of a new band with flat maximum at about 540 nm, which can be attributed to the transitions from LUMO that is spread over conjugated polymer backbone.

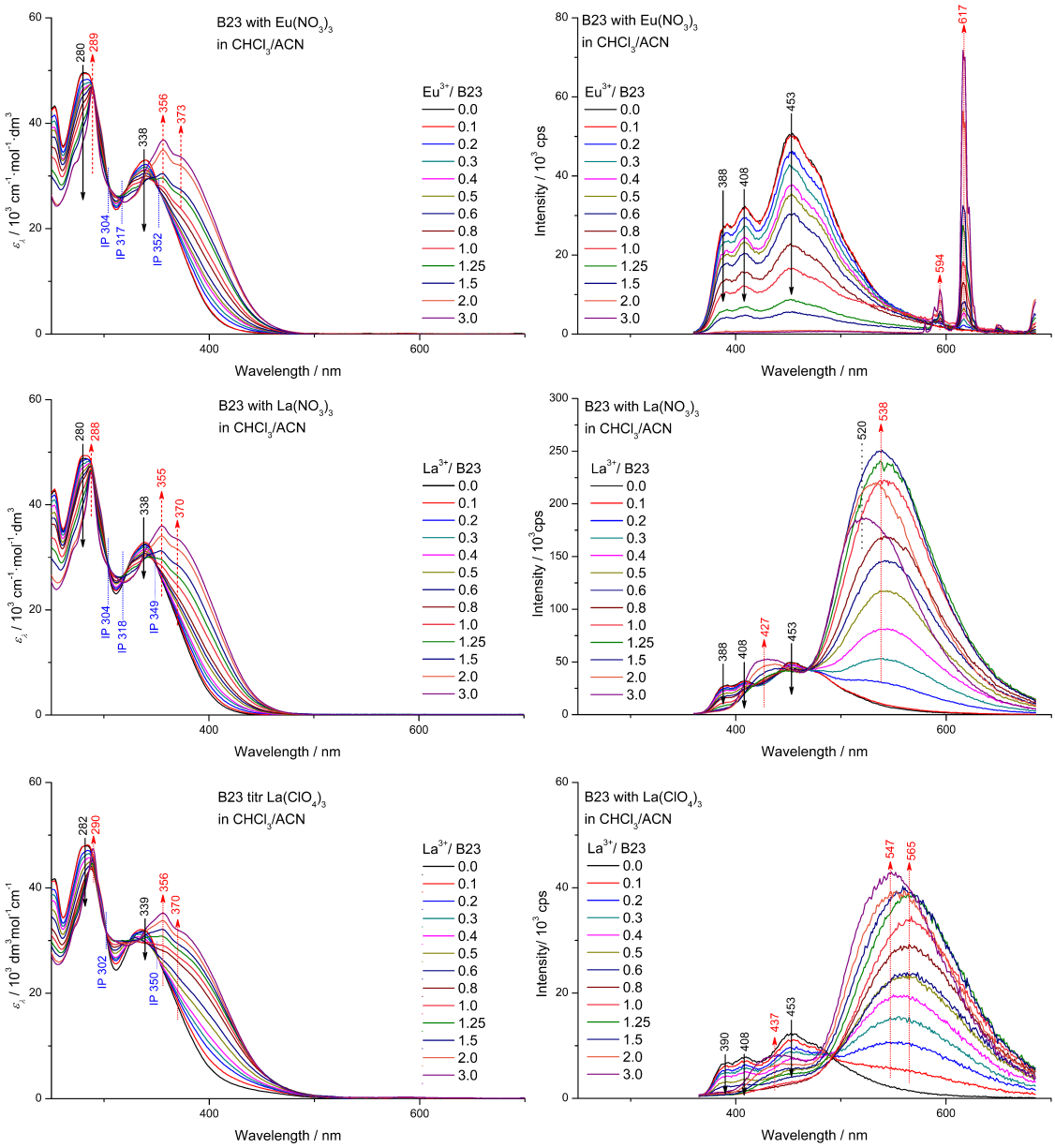

Fig. 26. Spectral sets for assembling unimer **B23** with different lanthanide salts in $CHCl_3$/ACN (1/1 by vol.), initial concentration $2 \cdot 10^{-5}$ M, room temperature.

Lanthanum nitrate is known to bind only two terpyridine units, which means that it can form only linear chains. On the other hand, lanthanum perchlorates is reported to bind three *tpy* ligands[61] and thus it might be supposed to provide an MSP network when binding ditopic unimer molecules. Nevertheless, the spectral changes observed for both lanthanum nitrate and lanthanum perchlorate are almost the same, which insinuates formation of linear chains also with $LaClO_4$.

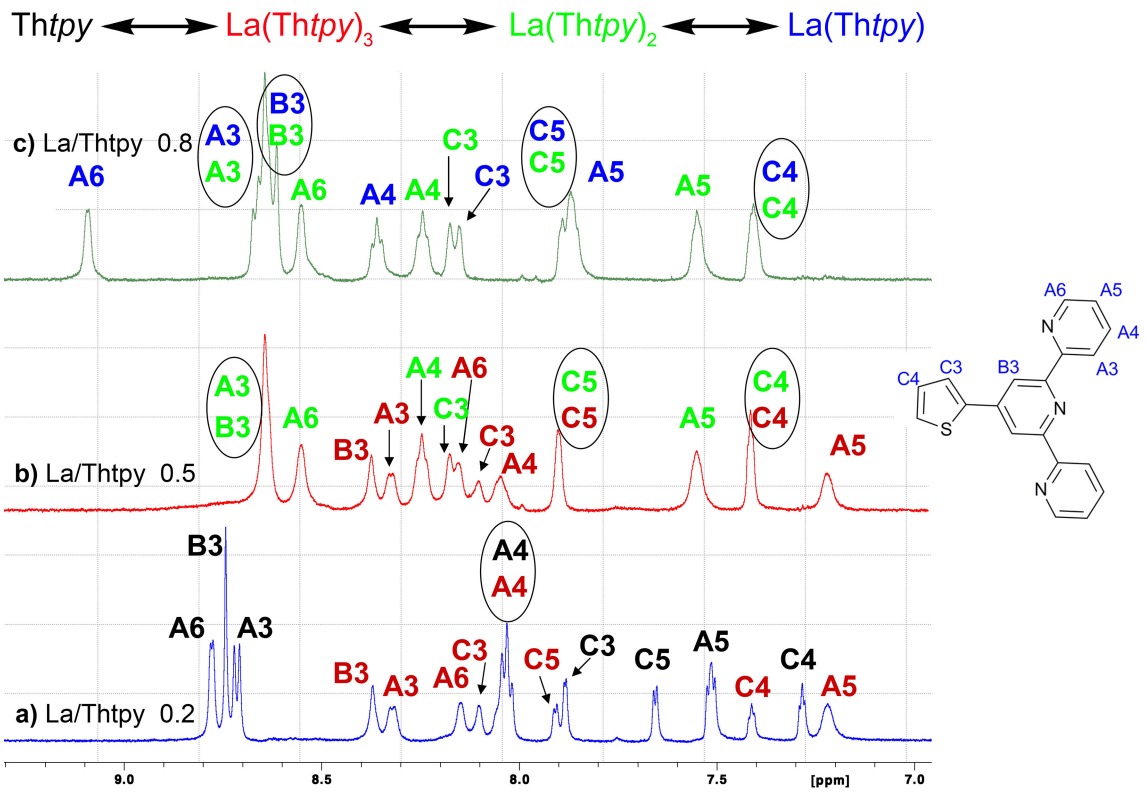

Fig. 27. ^{1}H NMR spectra and the signal assignment (by colors) for La^{3+}/Th*tpy* systems of different ratios *r*; spectra measured in pure acetonitrile.

To examine stoichiometry of this assembling, independent NMR experiments with the monotopic model ligand Th*tpy* were performed. The ligand was mixed with $LaClO_4$ in different ratios *r* in pure acetonitrile and the $CHCl_3$/ACN (1/1 by vol.) mixed solvent and NMR spectra of both solutions were measured and evaluated as to the solute stoichiometry. The ^{1}H NMR spectra measured in ACN are displayed in **Fig. 27.** together with assignment of the signals belonging to the mono- (in blue), bis- (in green) and tris- (in red) Th*tpy* complexes. The signal assignment was done with help of EXSY NMR spectra. These spectra thus conclusively show that the tris(*tpy*) species: $[La(Thtpy)_3]^{3+}$ really form, however, only in pure acetonitrile, because the "red" signals of tris(*tpy*) species are absent in ^{1}H NMR spectra taken from the $CHCl_3$/ACN mixed solvent. Hence it follows that the presence of chloroform inhibits formation of 3D MSP network.

4 EXPERIMENTAL PART

4.1 Materials

- Ligands:

The ligand 4'-bromo-2,2':6',2''-terpyridine was purchased from TCI Europe N.V within the Thesis framework. The ligands based on 4'-(thiophene-2-yl)-2,2':6',2''-terpyridine were synthesized via modified Kröhnke reaction of thiophene-2-carbaldehyde with 2-acetylpyridine and treating with ammonium acetate.[168] Next portion of ligands based on 4'-(thiophene-2-yl)-2,2':6',2''-terpyridine was prepared by Suzuki coupling of purchased 4'-bromo-2,2':6',2''-terpyridine and particular thiophene derivatives.

- Thiophenes and compounds for central block synthesis

Thiophene-2-boronic acid pinacol ester, 3-methylthiophene-2-boronic acid, 3-hexylthiophene-2-boronic acid pinacol ester, 2,2'-bithiophene, 2-bromothiophene, 3,3'''-dihexyl-2,2':5',2'':5'',2'''-quaterthiophene, thiophene-2,5-diboronic acid bis(pinacol) ester, 3,4-dibromothiophene, 3-bromothiophene, hexylmagnesiumbromide solution (2.0M in diethylether), *n*-butyllithium solution (2.5M in hexane), 1,6-dibromohexane, 4-methoxyphenol, 4,4,5,5-tetramethyl-1,3,2-dioxaborolane (HBpin) and 4,4,4',4',5,5,5',5'-octamethyl-2,2'-bi-1,3,2-dioxaborolane (B_2pin_2) were all purchased from Sigma Aldrich and used as received.

- Catalysts

[1,3-Bis(2,6-Diisopropylphenyl)imidazol-2-ylidene](3-chloropyridyl)palladium(II) dichloride known as PEPPSI-IPr, (1,5-cyclooctadiene)(methoxy)iridium(I) dimer and 4,4'-di-tert-butyl-2,2'-dipyridyl (dtbpy) as co-catalyst were exclusively used in preparation of unimers and their precursors. All purchased from Sigma Aldrich.

- Common chemicals and metal salts

Potassium carbonate, sodium carbonate and magnesium sulfate were purchased from Lach-ner and used as received; Boron tribromide, *N*-methylimidazole, trimethylamine (31-35 wt. % in ethanol, 4.2 M), triethylphosphine (1.0 M in THF) and *N*-bromosuccinimide were purchased from Sigma Aldrich. Zinc(II) perchlorate hexahydrate, iron(II) perchlorate hydrate, europium(III) nitrate pentahydrate, lanthanum(III) nitrate hexahydrate and ammonium hexafluorophosphate were purchased from Sigma Aldrich. Lanthanum(III) perchlorate hexahydrate was purchased from ABCR GmbH.

- Solvents

Toluene was distilled prior to use from sodium/benzophenone system, tetrahydrofurane was distilled from suspension with lithium aluminium hydride. Hexane was dried over

molecular sieves 3Å. Methanol, dimethyl sulfoxide, 1-methyl-2-pyrrolidinone, dimethylformamide, dichloromethane, chloroform, diethyl ether, hydrochloric acid and sulfuric acid 98% were purchased from Lach-Ner and used as obtained.

4.2 Methods

- Nuclear magnetic resonance spectroscopy (NMR)

^{1}H, ^{13}C and ^{11}B NMR spectra were measured on a Varian ^{UNITY}INOVA 400 and Varian SYSTEM 300 spectrometer. Samples were dissolved in d_8-THF, d-$CDCl_3$, d_2-CD_2Cl_2, d_4-MeOD or d_6-DMSO. Chemical shifts δ are reported in parts per million relatively to residual solvents peak (for ^{1}H 1.73 or 3.58 (d_8-THF), 7.24 (d-$CDCl_3$), 5.32 (d_2-CD_2Cl_2), 3.32 (d_4-MeOD), 2.50 (d_6-DMSO) and ^{13}C 67.57 (d_8-THF), 77.23 (d-$CDCl_3$), 54.0 (d_2-CD_2Cl_2), 39.5 (d_4-MeOD) and 49.2 (d_6-DMSO)). Coupling constants J (in Hz) were obtained by first-order analysis.

- Infrared and Raman spectroscopy (IR)

Infrared spectra were recorded on Thermo Nicolet 7600 FTIR spectrometer equipped with a Spectra Tech InspectIR Plus microscopic accessory. Samples were diluted with KBr and diffuse reflectance (DRIFT) method was used. Raman spectra of solid samples were recorded on a DXR Raman microscope (Thermo Scientific) using excitations across the whole visible region (λ_{ex} = 445, 532, 633 and 780 nm) and usual laser power at the sample 0.1 to 0.4 mW. Raman spectra were measured by Dr. Šloufová.

- Gas chromatography (GC)

Conversion of reactants in syntheses of central blocks and purity of particular non-ionic compounds up to ca Mr~800 were checked by GC-2010 Gas Chromatograph, Shimadzu. Samples were diluted with suitable solvent and 1μL of sample was injected.

- Size exclusion chromatography (SEC)

Conversion of reactants during final Suzuki coupling were checked by size exclusion chromatography on Agilent Technologies 1100 Series apparatus fitted with UV/vis Diode Array Detector (DAD) operating in the wavelength region 200-700 nm. A series of two PLgel columns (Mixed-E, Polymer Laboratories, UK) and THF (flow rate 0.7 mL/min) were used. Application of DAD detector allowed monitoring of UV/vis spectra of substances eluted from columns.

SEC records for samples with different Fe^{2+}/unimer ratio were obtained on a Spectra Physics Analytical HPLC pump P1000 with two PLgel columns Polymer Labs (Bristol, UK) Mixed-D, Mixed-E. System was equipped with THERMO UV6000 DAD detector. 0.05M Tetrabutylammonium hexafluorophosphate in chloroform/acetonitrile

(1/1, v/v, CHROMASOLV, Riedel-deHaen) was used as an eluent (0.7 mL/min). Initial concentration of injected samples was $5 \cdot 10^{-4}$M, injected volume 20μL.

- Absorption spectroscopy

Absorption spectra were measured on Shimadzu UV-2401PC instrument or SPECORD S600 instrument. Samples were diluted in particular solvent to concentration of $2 \cdot 10^{-5}$ M and measured in quartz cuvettes with optical length 1 cm. Thin films were coated by drop cast technique onto surface of quartz cuvette.

- Photoluminescence spectroscopy

Photoluminescence spectra were measured on a Fluorolog 3-22 Jobin Yvon Spex instrument, using four-window quartz cuvette (1 cm) for solutions and using quartz glass for films. The emission spectra were recorded with excitation wavelength, λ_{ex}, matching the absorption maximum of measured compound. Quantum yields, λ_F, of photoluminescence were measured using integration sphere Quanta-φ F-3029 or determined by means of a comparison of the integrated spectrum of the compound with that of quinine sulfate diluted solution in 0.5M H_2SO_4 used as standard with λ_F = 0.54. Fluorescence decays were recorded on FluoroHub single photon counting controller on a Fluorolog 3-22 Jobin Yvon Spex instrument using excitation at λ_{ex} = 378 nm for solutions and λ_{ex} = 472 nm for thin films.

- High-resolution mass spectroscopy (HR-MS)

HR-MS were measured by Dr. Cvačka on Institute of Organic Chemistry and Biochemistry AS CR, v.v.i in Prague.

- Viscosity measurements

Viscometric measurements were processed at Microviscometer Lovis 2000 M/Me (Anton Paar) at 25°C using solutions of the concentration of $5 \cdot 10^{-4}$M in given solvents.

4.3 Syntheses

The following paragraphs describe only general procedures applied within this project. For specific reaction conditions and characterization of particular compound the reader is kindly asked to look into the attached publications. Syntheses and basic spectroscopic characteristics of unimers **B**, **B14Me**, **T** and **T16 Me** and their precursors are published in ref[168]. Ref[160] contains preparation of unimers **B14**, **B23**, **T16**, **T25** and **T34**, their precursors and related Zn-MSPs, spectroscopic properties of all already prepared compounds (all non-ionic **B**- and **T-**type structures) and also related Zn-MSPs and course of assembling to Zn-MSPs. Complete preparation of **M1Br**, **B23Br** and related methylammonium salts are described in ref[156]. Their spectroscopic characteristics and assembling stages with Zn^{2+} and Fe^{2+} ions are presented together

with Zn- and Fe- MSPs soluble in alcohols. Set of unimers of **Q**-type, related MSPs with zinc and iron and all available characteristics are published in ref[149].

- General procedure to bromination of ligands and thiophenes

Bromination was usually performed on 4'-(3-alkylthiophene-2-yl)terpyridine. Ligand (1 eq.) was dissolved in mixture of dichloromethane/acetic acid (1/1 by vol.) and NBS (1.2 eq) was added in one portion in the dark. The solution was stirred overnight and then neutralized with saturated solution of potassium carbonate. The two-phase solution was extracted with dichloromethane. The organic layer was collected, washed with water, dried with $MgSO_4$, filtered off and evaporated to get the product. By application this procedure the product usually does not require additional purification.

Selective bromination of 3-substituted thiophene to the adjacent 2- position (selectively 2-bromo-3-substituted thiophene required) required more careful approach. Thiophene (1 eq.) was dissolved in DMF, packed in aluminium foil to protect from the light and cooled down to ca 3°C in an ice bath. The solution of NBS (1 eq.) in DMF was prepared and added in ca. one hour intervals in ca. 5 portions. Twenty minutes after each addition the conversion was monitored by GC analysis. After addition of all NBS, the reaction mixture was withdrawn from the cooling bath and stirred for next two hours. After that water was added and the solution was extracted with dichloromethane, the organic layer was dried with $MgSO_4$, filtered off and evaporated to get the product. If the product was contamined by the 2,5-dibromothiophene, it had to be purified by column chromatography. Careful cooling down and slow addition of NBS solution usually provided exclusively the desired product.

- General procedure to direct borylation of (oligo)thiophenes

The procedure was adopted from Chotana et al.[148] Direct borylation allowed only preparation of α,ω-bifuncionalized thiophenes in our case. Particular (oligo)thiophene (1 eq.), [Ir] catalyst (5 mol% of Ir) and dtbpy (5 mol.%) were placed in the Schlenk tube and three vacuum-argon cycles are carefully applied. Hexane (or hexane/thf 1/1 by vol. mixture for hardly soluble compounds, e.g. longer oligothiophenes) is added through septum using whole-glass syringe under argon. HBpin (3 – 4 eq.) was added through septum and the reaction mixture was heated to ca. 50°C overnight. Conversion of smaller compounds to related α,ω-bisboronates was monitored by GC. After cooling to room temperature the reaction mixture was diluted with water in an open vessel and allowed to react for one hour to deactivate the unreacted HBpin. The aqueous solution was extracted with chloroform, the organic layer was dried with $MgSO_4$, filtered off and evaporated to get the product. This reaction procedure usually provides full conversion

of reactants. Moreover the resulting products are not suitable for purification by column chromatography as the functional groups decomposed in interaction with stationary phase. It is noteworthy that prepared compounds are not recommended to longer storage and are safely ready to use within ca one month after preparation and subsequent storage in the fridge.

- General procedure to Suzuki-Miyaura cross-coupling reaction

In Suzuki-Miyaura cross-coupling reaction one equivalent of bromo-group reacts with one equivalent of boronic-group. This has to be kept in mind while designing the reaction ratios, as in some cases slight excess of one of the reactants provide better reaction yields (See **Tab. 6.**). Usually boronic derivate, bromo derivate, PEPPSI-IPr (2 – 5 mol%) and potassium carbonate (3 eq. per one reaction center) were placed in the Schlenk tube and three vacuum-argon cycles were carefully applied. Toluene and methanol (1/1 by vol.) were added through septum and the reaction mixture was heated to 90°C overnight. After cooling to room temperature the reaction mixture was either filtered of (in case of hardly soluble products **B**, **T**, **Q** or **Q4Br**) and washed with toluene or water was added and the mixture was extracted with chloroform. The organic phase was dried with $MgSO_4$, filtered off and evaporated to get the crude product. Usually the product had to be purified by column chromatography.

- General procedure for introduction of bromine to the terminal carbon of the attached hexyl

A unimer was dissolved in dichloromethane (to concentration ca. 0.02 M), the solution was then cooled in an ice bath and the BBr_3 was added (excess). After 4 hours of stirring the cooling bath was removed and the solution was poured into water. The mixture was carefully neutralized with saturated solution of K_2CO_3. Then the product was extracted with dichloromethane, dried with $MgSO_4$, filtered off and evaporated to get the desired product.

- General procedure of quaternization reaction

Quaternization with trimethylamine. The particular Br-unimer was dissolved in THF (to concentration $4 \cdot 10^{-3}$M) and trimethylamine was added (10 eq.) as ethanolic solution (4.2M). The reaction proceeded at 25°C for four days, when the product precipitated from the solution. After four days the product was isolated by centrifugation and washed with THF. Finally, the product was dried in vacuum.

Tab. 6. Ratio of bromo- and boronic- derivatives in Suzuki-Miyaura cross-coupling reaction used for optimal yields within the Thesis:

Bromo derivate	Boronic derivate	Bromo derivate to boron derivate ratio	Example of products
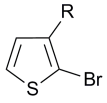	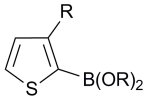	1 : 1.3	**B23-**type central block, **Q4Br** central block
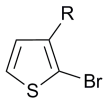	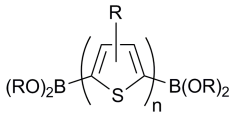	2.5 : 1	**Q27-**type central block, **Q2457-**type central block
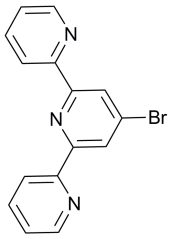	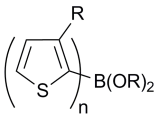	1 : 1.2	oligo-(3-alkyl)thiophene-2-ylterpyridine
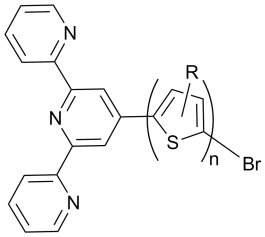	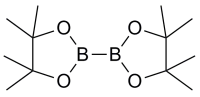	2 : 1.5	Unimers **B**, **B14Me**, **B14**, **Q**
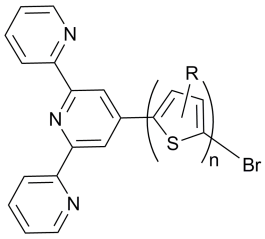	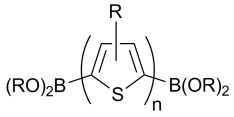	2.2 : 1	Unimers **T**, **T16Me**, **T16**, **B23-**type, **T25**, **T34**, **Q27-**type, **M1Br**, **Q45-**type, **Q2457-**type

R substituents onto thiophene ring could be hydrogen, meth-1-yl, hex-1-yl, 6-bromohex-1-yl or 6-(4-methoxyphenoxy)hex-1-yl group, *n* usually ranges between 0 and 2.

Unsuccessful quaternization procedures with other amines. Usually 10 eq. of quaternizing agent was used in combination with unimer **M1Br** or **B23Br**. Reaction temperature, solvent and applied quaternizing agent are presented in **Tab. 7**.

Tab. 7. Reaction conditions applied in unsuccessful quaternization reaction.

Amine – quaternizing agent	Solvent	Temperature / °C
N-methylimidazole	THF	30
N-methylimidazole	DMSO	50
N-methylimidazole	DMSO + acetonitrile	50
N-methylimidazole	DMF	50
N-methylimidazole	bulk	70
Trimethylamine	THF	< 0
Trimethylamine	THF	> 50
Triethylamine	THF	75
Triethylamine	bulk	75

Quaternization with triethylphosphine. A unimer was dissolved in toluene (to concentration ca. 6.5mM) and the flask was flushed with argon. Triethylphosphine (PEt_3) was added as 1M solution in THF (ca. 20 eq.) and the reaction was heated to 110°C for four days during these the quaternized product precipitated from the solution. After cooling to room temperature the product was filtered and washed with toluene and diethylether. The desired product was dried in vacuum.

- General procedure to polymerization/assembling to metallo-supramolecular polymers

Polymers with PF_6^- counterions. Procedure was adopted from ref.[152] Unimer (1 eq.) was dissolved in *N*-methylpyrrolidone and solution of Zn^{2+} salt (1 eq.) in NMP was added. The solution was stirred at 100 °C overnight. An excess of NH_4PF_6 (30 eq.) was added to the hot solution and stirring was continued for an hour. The solution was poured into methanol and resulting MPS was collected by sedimentation and washed with methanol. The product was dried under vacuum.

Polymers with ClO_4^- counterions. MSPs with perchlorate counterions were prepared simply by mixing the solution of unimer (1 eq.) in mixture of chloroform/acetonitrile (1/1 by vol., $2 \cdot 10^{-5}$M) for non-ionic unimers or methanol for unimers with ionic substituent with solution of appropriate metal salt (1 eq.) in the same

solvent (100×more concentrated, $2 \cdot 10^{-3}$M). After vigorous stirring the solvents were evaporated to get the solid MSPs.

4.4. Samples preparation

- Assembling experiments

For assembling experiments set of usually 13 samples (**Tab. 8.**) with constant unimer content and increasing amount of metal ions were prepared. Solutions were allowed to equilibrate for 24 hours and measured by spectroscopic methods. The initial concentration of unimer for spectroscopic measurements was $2 \cdot 10^{-5}$ M and was mixed with appropriate volume of 100× more concentrated volume of metal salt ($2 \cdot 10^{-3}$ M). Addition of 100× more concentrated solution of metal salt only slightly dilute the initial unimer solution thus this dilution is taken into account in ε in absorption spectra, but is neglected in the luminescence measurements. Perchlorate metal salts were exclusively used for preparation of these samples. **B**- and **T-**type non-ionic unimers were assembled in THF, brominated unimers were assembled in chloroform/acetonitrile (1/1 by vol.) while methanol was used as solvent for ionic unimers.

Tab. 8. Protocol for preparation of set of solutions for spectroscopic measurements.

Sample Nr.	V_U / mL	V_{Mt2+} / μL	c_U / 10^{-5} M	***r***
0	2	0	2.0	**0.0**
1	2	2	1.998	**0.1**
2	2	4	1.996	**0.2**
3	2	6	1.994	**0.3**
4	2	8	1.992	**0.4**
5	2	10	1.990	**0.5**
6	2	12	1.988	**0.6**
7	2	16	1.984	**0.8**
8	2	20	1.980	**1.0**
9	2	25	1.975	**1.25**
10	2	30	1.970	**1.5**
11	2	40	1.961	**2.0**
12	2	60	1.942	**3.0**

Initial concentration for unimer was $2 \cdot 10^{-5}$ M, metal salts were added from solution with concentration $2 \cdot 10^{-3}$ M, *r* is defined as metal-to-unimer mole ratio (n_U/n_{Mt2+}).

- Preparation of samples for SEC and viscosity measurements

For the SEC and viscosity measurements 25×more concentrated solutions compared to the spectroscopic measurements were required (**Tab. 9.**). The unimer solution of the concentration of 0.5 mM and was mixed with an appropriate volume of the metal salt solution (0.05 M). Each sample was allowed to equilibrate for 24 hours prior measurements.

Tab. 9. Protocol for preparation of set of solutions for SEC and viscosity measurements.

Sample Nr.	V_U / mL	V_{Mt2+} / μL	***r***
1	2	0	**0.0**
2	2	4	**0.2**
3	2	10	**0.5**
4	2	16	**0.8**
5	2	20	**1.0**
6	2	25	**1.25**
7	2	30	**1.5**
8	2	40	**2.0**

Initial concentration for unimer was 0.5 mM, metal salts were added from solution with concentration 0.05 M, *r* is defined as metal-to-unimer mole ratio (n_U/n_{Mt2+}).

- Samples in thin films

Thin films for spectroscopic measurements were prepared by repeated casting a layer from ca $2 \cdot 10^{-5}$ M solution of a unimer or MSP onto highly oriented pyrolytic graphite, or a quartz cuvette wall, or simple quartz glass, and subsequent solvent evaporation.

5 CONCLUSIONS

New synthesis routes have been developed for the preparation of the unimers with oligothiophene central blocks substituted at different positions and *tpy* end-groups. Using the procedures developed, more than twenty new unimers with linear central blocks containing one to four thiophene-2,5-diyl units were prepared, purified and adequately characterized. α,ω-Bis(*tpy*)oligothiophenes of the following types were prepared:

1. with unsubstituted (up to quaterthiophene) central blocks (**B**, **T** and **Q**);
2. with asymmetric: 3-(6-Rhexyl)thiophene-2,5-diyl central block (**M1**-type) and non-ionic (**Br**) or ionic (**N$^+$** or **P$^+$**) side-chain end-capping groups R;
3. with symmetrically substituted bi-, tri- and quaterthiophene central blocks (**B-**, **T-** and **Q-**type) with non-ionic side groups;
4. with symmetrically substituted central blocks and ionic side groups: **B23N$^+$** and **Q**-type with **P$^+$** side groups.

The prepared ionic unimers are all soluble in alcohols, some of them are sparingly soluble in water and one (**Q2457P$^+$**) even well soluble in water.

The unimers prepared were assembled with Zn^{2+} as well as Fe^{2+} ions to give corresponding MSPs and electronic spectra of both unimers and MSPs were studied with the aim to establish the correlation between their structure and spectroscopic properties, which reflects influences of the central block length and the electronic and steric effects of the side groups on the delocalization of electron along their chains. The results obtained indicate that the extent of the delocalization of electrons approaches its limiting value for unimers with quaterthiophene central block and that the steric effects of side groups are much more important than their electronic effects. Unimers with high steric hindrances (distortion) in the middle of the central oligothiophene block were found to behave nearly like the unimers with half central block.

A more detailed study of the course of the MSP assembly from unimers and ions identified three stages of the overall process in solutions: (*i*) assembly of the U-Mt^{2+}-U dimers, (*ii*) growth of MSP chains to certain length limited by the thermodynamic equilibrium between the chains and their constituents which, however, also depends on the rate of establishing the equilibrium, and (*iii*) end-capping the MSPs chain with surplus Mt^{2+} ions and, at still higher excess of the ions, also equilibrium depolymerization of the MSP chains.

Evidences were obtained by the spectroscopic, viscometric and SEC techniques that the constitutional dynamics of non-ionic MSPs is fast for Zn- while very slow for Fe-MSPs. The dynamics of Fe-MSPs is so slow that they could be analyzed by the

SEC method and their molecular-mass characteristics in solution, otherwise hardly accessible for dynamic MSPs, could be determined. In contrast, a surprising flip in the stability of Zn- and Fe-MSPs was found for **Q2457P**$^{+}$ based MSPs dissolved in water, the Zn-MSPs being more stable that the Fe-MSPs. Remarkable influence of the solvent was found also for assembling of the *tpy* derivatives with La^{3+} ions that form tris(*tpy*) complexes in pure acetonitrile but only bis(*tpy*) complexes in the chloroform/acetonitrile mixed solvent.

6 REFERENCES

1 J.-M. Lehn, *Proc. Natl. Acad. Sci. USA.*, 2002, **99**, 4763–4768.
2 J.-M. Lehn, *Prog. Polym. Sci.*, 2005, **30**, 814–831.
3 M. Hess, R. G. Jones, J. Kahovec, T. Kitayama, P. Kratochvíl, P. Kubisa, W. Mormann, R. F. T. Stepto, D. Tabak, J. Vohlídal and E. S. Wilks, *Pure Appl. Chem.*, 2006, **78**, 2067–2074.
4 F. Caruso, C. Schüler and D. G. Kurth, *Chem. Mater.*, 1999, **11**, 3394–3399.
5 A. Ciferri, *Macromol. Rapid Commun.*, 2002, **23**, 511–529.
6 K. Kaneto, S. Ura, K. Yoshino and Y. Inuishi, *Jpn. J. Appl. Phys.*, 1984, **23**, L189–L191.
7 T.-A. Chen, X. Wu and R. D. Rieke, *J. Am. Chem. Soc.*, 1995, **117**, 233 – 244.
8 R. D. McCullough, *Adv. Mater.*, 1998, **10**, 93–116.
9 B. S. Ong, Y. Wu, P. Liu and S. Gardner, *J. Am. Chem. Soc.*, 2004, **126**, 3378–3379.
10 Y. Liang, D. Feng, Y. Wu, S.-T. Tsai, G. Li, C. Ray and L. Yu, *J. Am. Chem. Soc.*, 2009, **131**, 7792–7799.
11 B. C. Schroeder, C. B. Nielsen, P. Westacott, J. Smith, S. Rossbauer, T. D. Anthopoulos, N. Stingelin and I. McCulloch, *MRS Commun.*, 2015, **5**, 435–440.
12 N. C. Greenham, S. C. Moratti, D. D. C. Bradley, R. H. Friend and A. B. Holmes, *Nature*, 1993, **365**, 628–630.
13 V. L. Colvin, M. C. Schlamp and A. P. Alivisatos, *Nature*, 1994, **370**, 354–357.
14 I. D. Parker, *J. Appl. Phys.*, 1994, **75**, 1656.
15 G. Yu, J. Gao, J. C. Hummelen, F. Wudl and A. J. Heeger, *Science*, 1995, **270**, 1789–1791.
16 S. A. McDonald, G. Konstantatos, S. Zhang, P. W. Cyr, E. J. D. Klem, L. Levina and E. H. Sargent, *Nat. Mater.*, 2005, **4**, 138–142.
17 P. C. Rodrigues, B. D. Fontes, B. B. M. Torres, W. S. Sousa, G. C. Faria, D. T. Balogh, R. M. Faria and L. Akcelrud, *J. Appl. Polym. Sci.*, 2015, **132**, 42579–42587.
18 Q. Pei, *J. Am. Chem. Soc.*, 1996, **118**, 7416–7417.
19 M. T. Bernius, M. Inbasekaran, J. O'Brien and W. Wu, *Adv. Mater.*, 2000, **12**, 1737–1750.
20 L. Li, Z. Wang, Q. Chen, X. Zhou, T. Yang, Q. Zhao and W. Huang, *J. Solid State Chem.*, 2015, **231**, 47–52.
21 Z. Li, J. Ding, J. Lefebvre and P. R. L. Malenfant, *Org. Electron.*, 2015, **26**, 15–19.
22 P. J. Nigrey, *J. Electrochem. Soc.*, 1981, **128**, 1651–1654.
23 H. Naarmann and N. Theophilou, *Synth. Met.*, 1987, **22**, 1–8.
24 K. Gurunathan, A. V. Murugan, R. Marimuthu, U. P. Mulik and D. P. Amalnerkar, *Mater. Chem. Phys.*, 1999, **61**, 173–191.
25 A. G. MacDiarmid, L. S. Yang, W. S. Huang and B. D. Humphrey, *Synth. Met.*, 1987, **18**, 393–398.
26 A. G. MacDiarmid, J. C. Chiang, A. F. Richter and A. J. Epstein, *Synth. Met.*, 1987, **18**, 285–290.
27 R. J. Tseng, J. Huang, J. Ouyang, R. B. Kaner and Y. Yang, *Nano Lett.*, 2005, **5**, 1077–1080.
28 L.-Z. Fan, Y.-S. Hu, J. Maier, P. Adelhelm, B. Smarsly and M. Antonietti, *Adv. Funct. Mater.*, 2007, **17**, 3083–3087.
29 J. Xu, K. Wang, S.-Z. Zu, B.-H. Han and Z. Wei, *ACS Nano*, 2010, **4**, 5019–5026.
30 A. Chiolerio, S. Bocchini, F. Scaravaggi, S. Porro, D. Perrone, D. Beretta, M. Caironi and C. F. Pirri, *Semicond. Sci. Technol.*, 2015, **30**, 104001–104011.
31 D. T. McQuade, A. E. Pullen and T. M. Swager, *Chem. Rev.*, 2000, **100**, 2537–2574.
32 E. Bundgaard and F. C. Krebs, *Sol. Energy Mater. Sol. Cells*, 2007, **91**, 954–985.

33 J. Hou, H.-Y. Chen, S. Zhang, G. Li and Y. Yang, *J. Am. Chem. Soc.*, 2008, **130**, 16144–16145.
34 J. Chen and Y. Cao, *Acc. Chem. Res.*, 2009, **42**, 1709–1718.
35 Z. He, C. Zhong, X. Huang, W.-Y. Wong, H. Wu, L. Chen, S. Su and Y. Cao, *Adv. Mater.*, 2011, **23**, 4636–4643.
36 A. Teichler, J. Perelaer and U. S. Schubert, *J. Mater. Chem. C*, 2013, **1**, 1910–1925.
37 B.-J. de Gans, P. C. Duineveld and U. S. Schubert, *Adv. Mater.*, 2004, **16**, 203–213.
38 E. Tekin, B.-J. de Gans and U. S. Schubert, *J. Mater. Chem.*, 2004, **14**, 2627–2632.
39 Y. Yoshioka and G. E. Jabbour, *Synth. Met.*, 2006, **156**, 779–783.
40 E. Tekin, P. J. Smith and U. S. Schubert, *Soft Matter*, 2008, **4**, 703–713.
41 T. K. Sievers, A. Vergin, H. Möhwald and D. G. Kurth, *Langmuir*, 2007, **23**, 12179–12184.
42 T.-Z. Xie, S.-Y. Liao, K. Guo, X. Lu, X. Dong, M. Huang, C. N. Moorefield, S. Z. D. Cheng, X. Liu, C. Wesdemiotis and G. R. Newkome, *J. Am. Chem. Soc.*, 2014, **136**, 8165–8168.
43 M. Chiper, R. Hoogenboom and U. S. Schubert, *Macromol. Rapid Commun.*, 2009, **30**, 565–578.
44 W. M. Reiff, W. A. A. Baker and N. E. E. Erickson, *J. Am. Chem. Soc.*, 1968, **435**, 4794–4800.
45 P. S. Braterman, J.-I. Song and R. D. Peacock, *Inorg. Chem.*, 1992, **31**, 555–559.
46 M. D. Hossain, J. Zhang, R. K. Pandey, T. Sato and M. Higuchi, *Eur. J. Inorg. Chem.*, 2014, **2014**, 3763–3770.
47 M. Schott, H. Lorrmann, W. Szczerba, M. Beck and D. G. Kurth, *Sol. Energy Mater. Sol. Cells*, 2014, **126**, 68–73.
48 E. C. Constable and A. M. W. C. Thompson, *J. Chem. Soc. Dalton Trans.*, 1992, **2**, 3467–3475.
49 E. C. Constable, G. Baum, E. Bill, R. Dyson, R. van Eldik, D. Fenske, S. Kaderli, D. Morris, A. Neubrand, M. Neuburger, D. R. Smith, K. Wieghardt, M. Zehnder and A. D. Zuberbühler, *Chem. Eur. J.*, 1999, **5**, 498–508.
50 J. N. Demas and B. A. DeGraft, *Topics in Fluorescence Spectroscopy: Volume 4: Probe Design and Chemical Sensing*, 1994.
51 R. Siebert, A. Winter, M. Schmitt, J. Popp, U. S. Schubert and B. Dietzek, *Macromol. Rapid Commun.*, 2012, **33**, 481–497.
52 R. Englman and J. Jortner, *Mol. Phys.*, 1970, **18**, 145–164.
53 R. Dobrawa and F. Würthner, *J. Polym. Sci. Part A: Polym. Chem.*, 2005, **43**, 4981–4995.
54 T. Vitvarová, J. Zedník, M. Bláha, J. Vohlídal and J. Svoboda, *Eur. J. Inorg. Chem.*, 2012, **2012**, 3866–3874.
55 R. H. Holyer, C. D. Hubbard, S. F. A. Kettle and R. G. Wilkins, *Inorg. Chem.*, 1966, **5**, 622–625.
56 R. A. Dobrawa, Bayerischer Julius-Maximilians-Universität Würzburg, *Dissertation Thesis*, 2004.
57 H. Hofmeier and U. S. Schubert, *Macromol. Chem. Phys.*, 2003, **204**, 1391–1397.
58 W. Goodall and J. A. G. Williams, *Chem. Commun.* , 2001, 2514–2515.
59 R. Dobrawa, M. Lysetska, P. Ballester, M. Grüne and F. Würthner, *Macromolecules*, 2005, **38**, 1315–1325.
60 Y. Y. Chen and H. C. Lin, *J. Polym. Sci. Part A: Polym. Chem.*, 2007, **45**, 3243–3255.
61 A. Escande, L. Guénée, K.-L. Buchwalder and C. Piguet, *Inorg. Chem.*, 2009, **48**, 1132–1147.
62 R. D. Chapman, R. T. Loda, J. P. Riehl and R. W. Schwartz, *Inorg. Chem.*, 1984, **23**, 1652–1657.
63 R. Shunmugam and G. N. Tew, *Chem. Eur. J.*, 2008, **14**, 5409–5412.

64 T. Lazarides, N. M. Tart, D. Sykes, S. Faulkner, A. Barbieri and M. D. Ward, *Dalton Trans.*, 2009, 3971–3979.
65 L. D. Carlos, R. a S. Ferreira, V. De Zea Bermudez and S. J. L. Ribeiro, *Adv. Mater.*, 2009, **21**, 509–534.
66 A. de Bettencourt-Dias, *Dalton Trans.*, 2007, 2229–2241.
67 E. S. Andreiadis, R. Demadrille, D. Imbert, J. Pécaut and M. Mazzanti, *Chem. Eur. J.*, 2009, **15**, 9458–9476.
68 N. Sabbatini, M. Guardigli, I. Manet, R. Ungaro, A. Casnati, R. Ziessel, G. Ulrich, Z. Asfari and J.-M. Lehn, *Pure Appl. Chem.*, 1995, **67**, 135–140.
69 Y.-W. Yip, H. Wen, W.-T. Wong, P. A. Tanner and K.-L. Wong, *Inorg. Chem.*, 2012, **51**, 7013–7015.
70 X. L. Li, K. J. Zhang, J. J. Li, X. X. Cheng and Z. N. Chen, *Eur. J. Inorg. Chem.*, 2010, 3449–3457.
71 J.-C. G. Bünzli and C. Piguet, *Chem. Soc. Rev.*, 2005, **34**, 1048–1077.
72 J.-C. G. Bünzli, *Acc. Chem. Res.*, 2006, **39**, 53–61.
73 S. Schmatloch, A. M. J. Van Den Berg, A. S. Alexeev, H. Hofmeier and U. S. Schubert, *Macromolecules*, 2003, **36**, 9943–9949.
74 M. Al-Hussein, W. H. de Jeu, B. G. G. Lohmeijer and U. S. Schubert, *Macromolecules*, 2005, **38**, 2832–2836.
75 M. Chiper, R. Hoogenboom and U. S. Schubert, *Eur. Polym. J.*, 2010, **46**, 260–269.
76 M. Chiper, M. A. R. Meier, J. M. Kranenburg and U. S. Schubert, *Macromol. Chem. Phys.*, 2007, **208**, 679–689.
77 E. Figgemeier, V. Aranyos, E. C. Constable, R. W. Handel, C. E. Housecroft, C. Risinger, A. Hagfeldt and E. Mukhtar, *Inorg. Chem. Commun.*, 2004, **7**, 117–121.
78 H. S. Chow, E. C. Constable, C. E. Housecroft and M. Neuburger, *Dalton Trans.*, 2003, 4568–4569.
79 G. Schwarz, Y. Bodenthin, T. Geue, J. Koetz and D. G. Kurth, *Macromolecules*, 2010, **43**, 494–500.
80 R. R. Pal, M. Higuchi and D. G. Kurth, *Org. Lett.*, 2009, **11**, 3562–3565.
81 T. Sato, R. K. Pandey and M. Higuchi, *Dalton Trans.*, 2013, **42**, 16036–16042.
82 J.-H. Li and M. Higuchi, *J. Inorg. Organomet. Polym.*, 2010, **20**, 10–18.
83 F. S. Han, M. Higuchi and D. G. Kurth, *Tetrahedron*, 2008, **64**, 9108–9116.
84 F. S. Han, M. Higuchi and D. G. Kurth, *J. Am. Chem. Soc.*, 2008, **130**, 2073–2081.
85 F. S. Han, M. Higuchi and D. G. Kurth, *Adv. Mater.*, 2007, **19**, 3928–3931.
86 J. Husson and M. Knorr, *J. Heterocycl. Chem.*, 2012, **49**, 453–478.
87 P. D. Vellis, J. A. Mikroyannidis, C. Lo and C. Hsu, *J. Polym. Sci. Part A: Polym. Chem.*, 2008, **46**, 7702–7712.
88 G. Schwarz, I. Haßlauer and D. G. Kurth, *Adv. Colloid Interface Sci.*, 2014, **207**, 107–120.
89 Y. Y. Chen and H. C. Lin, *Polymer* , 2007, **48**, 5268–5278.
90 X. Chen, L. Ma, Y. Cheng, Z. Xie and L. Wang, *Polym. Int.*, 2007, **56**, 648–654.
91 K. W. Cheng, C. S. C. Mak, W. K. Chan, A. M. Ching NG and A. B. Djurišič, *J. Polym. Sci. Part A: Polym. Chem.*, 2008, **46**, 1305–1317.
92 A. Wild, F. Schlütter, G. M. Pavlov, C. Friebe, G. Festag, A. Winter, M. D. Hager, V. Cimrova and U. S. Schubert, *Macromol. Rapid Commun.*, 2010, **31**, 868–874.
93 R. Dobrawa and F. Würthner, *Chem. Commun.*, 2002, 1878–1879.
94 Y. Y. Chen, Y.-T. Tao and H.-C. Lin, *Macromolecules*, 2006, **39**, 8559–8566.
95 V. Stepanenko, M. Stocker, P. Müller, M. Büchner and F. Würthner, *J. Mater. Chem.*, 2009, **19**, 6816–6826.
96 A. Wild, C. Friebe, A. Winter, M. D. Hager, U.-W. Grummt and U. S. Schubert, *Eur. J. Org. Chem.*, 2010, **2010**, 1859–1868.

97 T. Lin, G. Kuang, X. S. Shang, P. N. Liu and N. Lin, *Chem. Commun.*, 2014, **50**, 15327–15329.
98 W. Wang, S. Wang, X. Li, J.-P. Collin, J. Liu, P. N. Liu and N. Lin, *J. Am. Chem. Soc.*, 2010, **132**, 8774–8778.
99 R. R. Pal, M. Higuchi, Y. Negishi, T. Tsukuda and D. G. Kurth, *Polym. J.*, 2010, **42**, 336–341.
100 S. Kelch and M. Rehahn, *Macromolecules*, 1999, **32**, 5818–5828.
101 A. Wild, A. Winter, F. Schlütter and U. S. Schubert, *Chem. Soc. Rev.*, 2011, **40**, 1459–1511.
102 Y. Bodenthin, G. Schwarz, Z. Tomkowicz, T. Geue, W. Haase, U. Pietsch and D. G. Kurth, *J. Am. Chem. Soc.*, 2009, **131**, 2934–2941.
103 M. Higuchi and D. G. Kurth, *Chem. Rec.*, 2007, **7**, 203–209.
104 D. G. Kurth, W. Szczerba, M. Schott, H. Riesemeier, A. F. Thünemann and D. G. Kurth, *Phys. Chem. Chem. Phys.*, 2014, **16**, 19694–19701.
105 G. Schwarz, T. K. Sievers, Y. Bodenthin, I. Hasslauer, T. Geue, J. Koetz and D. G. Kurth, *J. Mater. Chem.*, 2010, **20**, 4142–4148.
106 D. G. Kurth, M. Schütte and J. Wen, *Colloids Surfaces A Physicochem. Eng. Asp.*, 2002, **200**, 633–643.
107 S. Encinas, L. Flamigni, F. Barigelletti, E. C. Constable, C. E. Housecroft, E. R. Schofield, E. Figgemeier, D. Fenske, M. Neuburger, J. G. Vos and M. Zehnder, *Chem. Eur. J.*, 2002, **8**, 137–150.
108 E. C. Constable, E. Figgemeier, C. E. Housecroft, E. A. Medlycott, M. Neuburger, S. Schaffner and S. Reymann, *Polyhedron*, 2008, **27**, 3601–3606.
109 S. Etienne and M. Beley, *Inorg. Chem. Commun.*, 2006, **9**, 68–71.
110 P. Manca, M. I. Pilo, G. Casu, S. Gladiali, G. Sanna, R. Scanu, N. Spano, A. Zucca, C. Zanardi, D. Bagnis and L. Valentini, *J. Polym. Sci. Part A: Polym. Chem.*, 2011, **49**, 3513–3523.
111 A. Barbieri, B. Ventura, F. Barigelletti, A. De Nicola, M. Quesada and R. Ziessel, *Inorg. Chem.*, 2004, **43**, 7359–7368.
112 A. De Nicola, C. Ringenbach and R. Ziessel, *Tetrahedron Lett.*, 2003, **44**, 183–187.
113 A. Harriman, A. Mayeux, A. De Nicola and R. Ziessel, *Phys. Chem. Chem. Phys.*, 2002, **4**, 2229–2235.
114 E. C. Constable, C. E. Housecroft, E. R. Schofield, S. Encinas, N. Armaroli, F. Barigelletti, L. Flamigni, E. Figgemeier and J. G. Vos, *Chem. Commun.*, 1999, **532**, 869–870.
115 C. Ringenbach, A. De Nicola and R. Ziessel, *J. Org. Chem.*, 2003, **68**, 4708–4719.
116 M. Beley, D. Delabouglise, G. Houppy, J. Husson and J.-P. Petit, *Inorg. Chim. Acta*, 2005, **358**, 3075–3083.
117 E. C. Constable, R. Handel, C. E. Housecroft, M. Neuburger, E. R. Schofield and M. Zehnder, *Polyhedron*, 2004, **23**, 135–143.
118 C. Houarner-Rassin, E. Blart, P. Buvat and F. Odobel, *J. Photochem. Photobiol., A* , 2007, **186**, 135–142.
119 R. López, D. Villagra, G. Ferraudi, S. A. Moya and J. Guerrero, *Inorg. Chim. Acta*, 2004, **357**, 3525–3531.
120 Z. Naseri, A. Nemati, A. Banavand, A. Bakhoda and S. Foroutannejad, *Polyhedron*, 2012, **33**, 396–403.
121 S. Caramori, J. Husson, M. Beley, C. A. Bignozzi, R. Argazzi and P. C. Gros, *Chem. Eur. J.*, 2010, **16**, 2611–2618.
122 E. C. Constable, C. E. Housecroft, E. Medlycott, M. Neuburger, F. Reinders, S. Reymann and S. Schaffner, *Inorg. Chem. Commun.*, 2008, **11**, 518–520.
123 J. Hjelm, E. C. Constable, E. Figgemeier, A. Hagfeldt, R. Handel, C. E. Housecroft, E. Mukhtar and E. Schofield, *Chem. Commun.*, 2002, 284–285.

124 J. Hjelm, R. W. Handel, A. Hagfeldt, E. C. Constable, C. E. Housecroft and R. J. Forster, *Inorg. Chem.*, 2005, **44**, 1073–1081.
125 A. Viinikanoja, S. Areva, N. Kocharova, T. Aäritalo, M. Vuorinen, A. Savunen, J. Kankare and J. Lukkari, *Langmuir*, 2006, **22**, 6078–6086.
126 C. T. Burns, S. Lee, S. Seifert and M. A. Firestone, *Polym. Adv. Technol.*, 2008, **19**, 1369–1382.
127 L. Zhai and R. D. Mccullough, *Adv. Mater.*, 2002, **14**, 901–905.
128 M. Knaapila, T. Costa, V. M. Garamus, M. Kraft, M. Drechsler, U. Scherf and H. D. Burrows, *Macromolecules*, 2014, **47**, 4017–4027.
129 S. Clément, A. Tizit, S. Desbief, A. Mehdi, J. De Winter, P. Gerbaux, R. Lazzaroni and B. Boury, *J. Mater. Chem.*, 2011, **21**, 2733–2739.
130 H.-A. Ho and M. Leclerc, *J. Am. Chem. Soc.*, 2003, **125**, 4412–4413.
131 F. Le Floch, H.-A. Ho, P. Harding-Lepage, M. Bédard, R. Neagu-Plesu and M. Leclerc, *Adv. Mater.*, 2005, **17**, 1251–1254.
132 D. Bondarev, J. Zedník, I. Šloufová, A. Sharf, M. Procházka, J. Pfleger and J. Vohlídal, *J. Polym. Sci. Part A : Polymer Chem.*, 2010, **48**, 3073 – 3081.
133 S. Das, D. P. Chatterjee, R. Ghosh and A. K. Nandi, *RSC Adv.*, 2015, **5**, 20160–20177.
134 Y. Kim, S. Cook, S. M. Tuladhar, S. A. Choulis, J. Nelson, J. R. Durrant, D. D. C. Bradley, M. Giles, I. McCulloch, C.-S. Ha and M. Ree, *Nat. Mater.*, 2006, **5**, 197–203.
135 D. A. Rider, B. J. Worfolk, K. D. Harris, A. Lalany, K. Shahbazi, M. D. Fleischauer, M. J. Brett and J. M. Buriak, *Adv. Funct. Mater.*, 2010, **20**, 2404–2415.
136 Y.-M. Chang, R. Zhu, E. Richard, C.-C. Chen, G. Li and Y. Yang, *Adv. Funct. Mater.*, 2012, **22**, 3284–3289.
137 G. Zotti, S. Zecchin, A. Berlin, G. Schiavon and G. Giro, *Chem. Mater.*, 2001, **13**, 43–52.
138 B. Senthilkumar, P. Thenamirtham and R. Kalai Selvan, *Appl. Surf. Sci.*, 2011, **257**, 9063–9067.
139 H.-A. Ho and M. Leclerc, *J. Am. Chem. Soc.*, 2004, **126**, 1384–1387.
140 H.-A. Ho, M. Boissinot, M. G. Bergeron, G. Corbeil, K. Doré, D. Boudreau and M. Leclerc, *Angew. Chemie Int. Ed.*, 2002, **41**, 1548–1551.
141 X. Duan, L. Liu, F. Feng and S. Wang, *Acc. Chem. Res.*, 2010, **43**, 260–70.
142 P. Štenclová, Charles University in Prague, *Bachelor Thesis*, 2009.
143 P. Štenclová, Charles University in Prague, *Diploma Thesis*, 2011.
144 K. Šichová, Charles University in Prague, *Diploma Thesis*, 2014.
145 A. F. Littke and G. C. Fu, *Angew. Chem. Int. Ed.* , 2002, **41**, 4176–4211.
146 K. C. Nicolaou, P. G. Bulger and D. Sarlah, *Angew. Chemie Int. Ed.*, 2005, **44**, 4442–4489.
147 T. Ishiyama, Y. Nobuta, J. F. Hartwig and N. Miyaura, *Chem. Commun.*, 2003, 2924–2925.
148 G. A. Chotana, V. A. Kallepalli, R. E. Maleczka and M. R. Smith, *Tetrahedron*, 2008, **64**, 6103–6114.
149 P. Štenclová, K. Šichová, I. Šloufová, J. Zedník, J. Svoboda and J. Vohlídal, *Dalton Trans.*, 2015, DOI: 10.1039/C5DT04133C.
150 J. Pretula, K. Kaluzynski, B. Wisniewski, R. Szymanski, T. Loontjens and S. Penczek, *J. Polym. Sci. Part A: Polym. Chem.*, 2008, **46**, 830–843.
151 K. Zilberberg, A. Behrendt, M. Kraft, U. Scherf and T. Riedl, *Org. Electron.*, 2013, **14**, 951–957.
152 A. Winter, C. Friebe, M. Chiper, M. D. Hager and U. S. Schubert, *J. Polym. Sci. Part A: Polym. Chem.*, 2009, **3**, 4083–4098.
153 S. Gondo, Y. Goto and M. Era, *Mol. Cryst. Liq. Cryst.*, 2007, **470**, 353–358.
154 C. L. Huisman, A. Huijser, H. Donker, J. Schoonman and A. Goossens, *Macromolecules*, 2004, **37**, 5557–5564.
155 W. Goodall and J. A. G. Williams, *Chem. Commun.*, 2001, 2514–2515.

156 P. Štenclová-Bláhová, J. Svoboda, I. Šloufová and J. Vohlídal, *Phys. Chem. Chem. Phys.*, 2015, **17**, 13743–13756.
157 T. E. Janini, J. L. Fattore and D. L. Mohler, *J. Organomet. Chem.*, 1999, **578**, 260–263.
158 R. Siebert, D. Akimov, M. Schmitt, A. Winter, U. S. Schubert, B. Dietzek and J. Popp, *ChemPhysChem*, 2009, **10**, 910–919.
159 Z. Ji, S. Li, Y. Li and W. Sun, *Inorg. Chem.*, 2010, **49**, 1337–1346.
160 P. Bláhová, J. Zedník, I. Šloufová, J. Vohlídal and J. Svoboda, *Soft Mater.*, 2014, **12**, 214–229.
161 D. R. Bai, C. Romero-Nieto and T. Baumgartner, *Dalton Trans.*, 2010, **39**, 1250–1260.
162 C. Goze, G. Ulrich, L. Charbonnière, M. Cesario, T. Prangé and R. Ziessel, *Chem. Eur. J.*, 2003, **9**, 3748–3755.
163 R. Siebert, A. Winter, B. Dietzek, U. S. Schubert and J. Popp, *Macromol. Rapid Commun.*, 2010, **31**, 883–888.
164 U. S. Schubert, H. Hofmeier and G. R. Newkome, *Modern Terpyridine Chemistry*, Wiley-VCH Verlag GmbH, Weinheim, 2006.
165 R. Hogg and R. G. Wilkins, *J. Chem. Soc.*, 1962, 341–350.
166 D. Rais, M. Menšík, P. Štenclová-Bláhová, J. Svoboda, J. Vohlídal and J. Pfleger, *J. Phys. Chem. A*, 2015, **119**, 6203–6214.
167 R. Ziessel, S. Diring, P. Kadjane, L. Charbonnière, P. Retailleau and C. Philouze, *Chem. Asian J.*, 2007, **2**, 975–982.
168 J. Svoboda, P. Stenclova, F. Uhlík, J. Zedník and J. Vohlídal, *Tetrahedron*, 2011, **67**, 75–79.

7 LIST OF PUBLICATIONS

1) Štenclová P., Šichová K., Šloufová I., Zedník J., Svoboda J. Vohlídal J.: Alcohol- and water-soluble bis(*tpy*)quaterthiophenes with phosphonium side groups: new conjugated units for metallo-supramolecular polymers; *Dalton Trans*. 2015, DOI: 10.1039/C5DT04133C.
2) Rais D., Menšík M., Štenclová-Bláhová P., Svoboda J., Vohlídal J., Pfleger J.: Time-Resolved Transient Optical Absorption Study of Bis(terpyridyl)oligothiophenes and Their Metallo-Supramolecular Polymers with Zn(II) Ion-Couplers; *J. Phys. Chem. A* 2015, **119**, 6203 – 6214.
3) Štenclová-Bláhová P., Svoboda J., Šloufová I., Vohlídal J.: Alcohol-Soluble Bis(*tpy*)thiophenes: New Building Units for Constitutional Dynamic Conjugated Polyelectrolytes; *Phys. Chem. Chem. Phys.* 2015, **17**, 13743 – 13756.
4) Bláhová P., Zedník J.; Šloufová I., Vohlídal J., Svoboda J.: Synthesis and Photophysical Properties of New α,ω-Bis(Tpy)Oligothiophenes and Their Metallo-Supramolecular Polymers With Zn^{2+} Ion Couplers; *Soft Mater.* 2014, **12**, 214 – 229.
5) Svoboda J., Štenclová P., Uhlík F., Zedník J., Vohlídal J.: Synthesis and Photophysical Properties of α,ω-Bis(terpyridine)oligothiophenes; *Tetrahedron* 2011, **67***,* 75 – 79.

8 ATTACHEMENTS

A) Svoboda J., Štenclová P., Uhlík F., Zedník J., Vohlídal J.: Synthesis and Photophysical Properties of α,ω-Bis(terpyridine)oligothiophenes; *Tetrahedron* 2011, **67***,* 75 – 79.

B) Bláhová P., Zedník J.; Šloufová I., Vohlídal J., Svoboda J.: Synthesis and Photophysical Properties of New α,ω-Bis(Tpy)Oligothiophenes and Their Metallo-Supramolecular Polymers With Zn^{2+} Ion Couplers; *Soft Mater.* 2014, **12**, 214 – 229.

C) Štenclová-Bláhová P., Svoboda J., Šloufová I., Vohlídal J.: Alcohol-Soluble Bis(*tpy*)thiophenes: New Building Units for Constitutional Dynamic Conjugated Polyelectrolytes; *Phys. Chem. Chem. Phys.* 2015, **17**, 13743 – 13756.

D) Štenclová P., Šichová K., Šloufová I., Zedník J., Svoboda J. Vohlídal J.: Alcohol- and water-soluble bis(*tpy*)quaterthiophenes with phosphonium side groups: new conjugated units for metallo-supramolecular polymers; *Dalton Trans*. 2015, DOI: 10.1039/C5DT04133C.

ATTACHEMENT A

Svoboda J., Štenclová P., Uhlík F., Zedník J.,
Vohlídal J.:Synthesis and Photophysical Properties
of α,ω-Bis(terpyridine)oligothiophenes;
Tetrahedron 2011, **67***,* 75 – 79.

Tetrahedron 67 (2011) 75–79

Contents lists available at ScienceDirect

Tetrahedron

journal homepage: www.elsevier.com/locate/tet

Synthesis and photophysical properties of α,ω-bis(terpyridine)oligothiophenes

Jan Svoboda *, Pavla Štenclová, Filip Uhlík, Jiří Zedník, Jiří Vohlídal

Department of Physical and Macromolecular Chemistry, Charles University in Prague, Faculty of Science, Hlavova 2030, CZ-128 40, Prague 2, Czech Republic

ARTICLE INFO

Article history:
Received 11 August 2010
Received in revised form 20 October 2010
Accepted 8 November 2010
Available online 13 November 2010

ABSTRACT

Four novel fully π-conjugated α,ω-bis(terpyridine)oligothiophenes characterized by NMR, IR, and HR-mass spectroscopy are presented and their electronic absorption/emission and redox properties are described based on both experiments and theoretical calculations. These compounds can be potentially utilized as building blocks for preparation of conjugated metallo-supramolecular polymers or dynamers and related functional materials.

1. Introduction

Ditopic compounds with terpyridine (*terpy*) end-groups are of scientific interest as suitable materials for preparation of metallo-supramolecular polymers[1,2] and dynamers (constitutional-dynamic polymers).[3] The specific configuration of nitrogen atoms allows easy tridentate facial or meridian coordination of a *terpy* group as a ligand to various metal atoms (ions), such as to atoms/ions of Ru, Os, Ir, Fe, Zn, and Co, giving rise to linear chains.[4–6] This feature, which is absent in many other modules,[7] allows metallo-supramolecular assemblies with well-defined stereochemistry, which is important for the reproducible preparation of functional materials.

The optical properties of *terpy* compounds are important for their applications as probes (sensors), active materials for light-emitting devices and dye-sensitized solar cells. The chemical structure of a *terpy* compound directly affects functionality of a metallo-supramolecular assembly comprising this compound, in particular the prevalence of the light-emitting or charge transporting properties. Therefore, the tailored synthesis of *terpy* compounds is a fundamental step in the preparation of high-performance metal-coordination functional materials. The main interest has been focused to mono-*terpy* compounds that are applied in dye-sensitized solar cells.[8–12] Among α,ω-bis(*terpy*)compounds, those in molecules of which conjugated oligomeric chains link two *terpy* end-units are of interest for optoelectronic applications because they can be used for preparation of conjugated dynamers, constitutional-dynamic counterparts of conjugated polymers.[3,13–27]

The choice of the linker between two *terpy* end-units has a strong influence on ligand properties. Low band-gap polythiophenes and oligothiophenes are one of the most important classes of conjugated compounds with a wide range of applications, such as conducting film, electrochromics, and field-effect transistors.[28–30] On the other hand, based to the best of our knowledge, bis-terpyridines containing only oligothiophene linker have not been reported to date.

In the present paper we describe the preparation and photophysical properties of four novel conjugated α,ω-bis(*terpy*)oligothiophenes that differ in the central-chain length and substitution of thiophene rings. The results of theoretical calculations on these molecules, which provide a useful tool for interpretation of photophysical measurements are also presented.

2. Results and discussion

2.1. Synthesis of α,ω-bis(*terpy*)oligothiophenes

Mono-terpyridines reported in this paper were prepared using the procedures based on the two-step Kröhnke methodology.[31] First thiophene-2-carbaldehyde (or its 3-methyl- derivative) reacted with 2-acetylpyridine to give the dicarbonyl precursor (Scheme 1). In the second step, the central pyridine ring was closed by treating the precursor with an excess of ammonium acetate. Preparation of 4′-(thiophen-2-yl)-2,2′;6′,2″-terpyridine has been described in the literature.[32] The derivative of this compound with a methyl-substituted thiophene ring, it was prepared with the aim to increase solubility of target bis(*terpy*) compounds. Brominations of both 4′-(thiophen-2-yl)terpyridines were carried out in the standard way using NBS[33] provided us monotopic precursors of α,ω-bis(*terpy*) compounds **1a** and **1b** (Scheme 1).

The desired α,ω-bis(*terpy*)oligothiophenes were prepared by Suzuki coupling of **1a** and **1b**, respectively, with: (i) bis(pinacolato) diborane—to obtain compounds **2a** and **2b** with dithiophene linkers between terminal *terpy* groups, and (ii) 2,5-thiophenediboronic acid—to obtain compounds **3a** and **3b** with terthiophene linkers (Scheme 2). Their low solubility in toluene enables easy isolation of **2a**, **2b**, and **3a** by simple filtration. On the other hand, **3b** had to be

* Corresponding author. Tel.: +420 221951311; fax: +420 224919752; e-mail address: js@vivien.natur.cuni.cz (J. Svoboda).

0040-4020/$ – see front matter © 2010 Elsevier Ltd. All rights reserved.
doi:10.1016/j.tet.2010.11.039

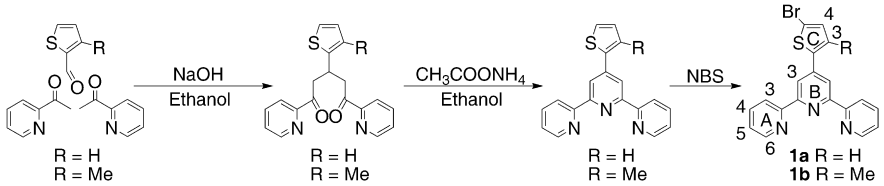

Scheme 1. Preparation of 4′-(thiophen-2-yl)terpyridines.

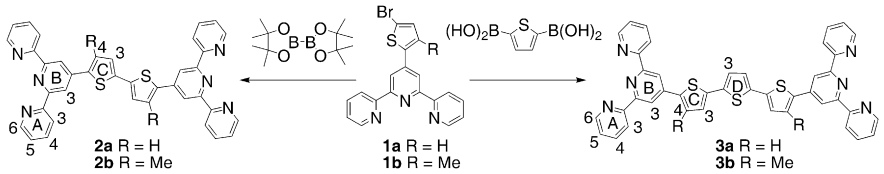

Scheme 2. Preparation of α,ω-bis(terpyridine)oligothiophenes.

purified using column chromatography as it was significantly soluble in toluene. All ligands were prepared in quite good yields (45–85%) except for **3b** (mainly owing to a loss of the product during the liquid-phase purification). Couplings of **1a** and **1b** were carried out using the Stille method gave lower yields of all bis(*terpy*) compounds.

The successful transformation of **1a** and **1b** to corresponding bis(*terpy*) compounds was confirmed by NMR and HRMS analyses (see Experimental section). Occurrence of bands pertaining to π–π* transitions in conjugated oligothiophene linkers in the optical spectra of **2a** to **3b** (Fig. 1) provides additional evidence since a similar band is absent in spectra of **1a** and **1b**.

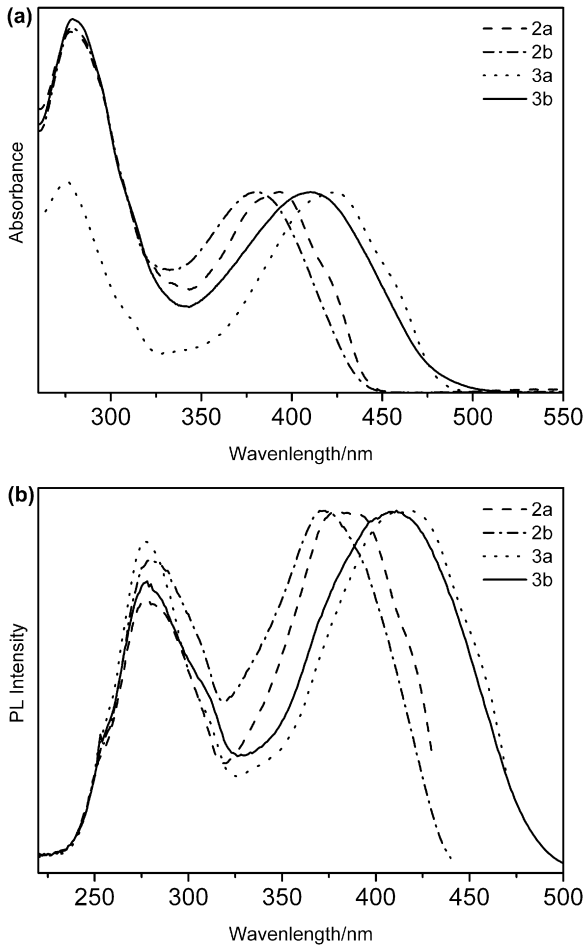

Fig. 1. UV/vis (a) and excitation photoluminescence (b) spectra of prepared bis(terpyridine)s; THF, room temperature.

A comparison of the IR spectra of all α,ω-bis(*terpy*)oligothiophenes with the spectrum of 2,2′;6′,2″-terpyridine shows that the bands of vibrational modes in the *terpy* end-groups unambiguously predominate in the spectra of bis(*terpy*) compounds (see Experimental section). Bands pertaining to vibrations in the oligothiophene chains are mostly reduced to shoulders. Similar features show IR spectra of polythiophene carrying 6-(1-methylimidazolium-3-yl)hexyl side groups,[34] in which bands of imidazolium groups predominate. The much higher transition dipole moments of nitrogen heterocycles compared to that of sulfur heterocycles is the reason for it. Ordinary FT Raman spectra (λ_{ex}=1064 nm) of bis(*terpy*) compounds are not accessible due to high-intensity fluorescence of the samples.

2.2. Spectroscopic and redox characterizations

The absorption UV/vis spectra and the excitation photoluminescence spectra of prepared bis(*terpy*) compounds **2a** to **3b** are compared in Fig. 1 and the absorption spectra obtained from DFT calculations in Fig. 2. Each spectrum exhibits a band at

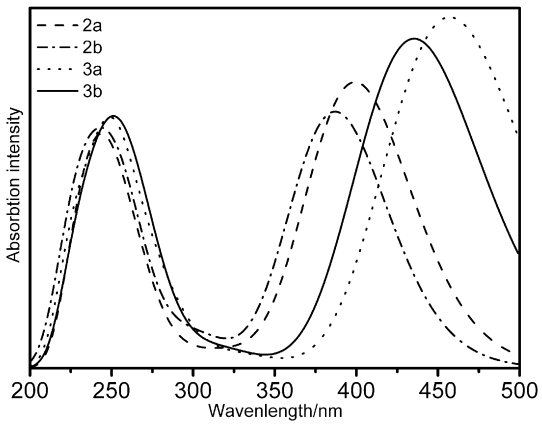

Fig. 2. Absorption spectra obtained using DFT calculation.

280 nm due to π–π* and *n*–π* transitions within pyridine and thiophene rings and a strong broad band with weak shoulders and a flat maximum occurring in the region from 370 nm to 425 nm (see Table 1). The latter band shifts to longer wavelengths when going from the dithiophene (compounds **2**) to the terthiophene (compounds **3**) linker. This proves that this band is associated with π–π* (HOMO–LUMO) transitions in the molecule's backbone. DFT calculations have shown that both HOMO and LUMO are of π-nature typical of conjugated systems and

Table 1
Spectroscopic and redox data for prepared α,ω-bis(*terpy*) compounds at room temperature

Compound	λ_{abs}[a] [nm]	λ_{ex}[b] [nm]	λ_F[c] [nm]	φ_F[d] [%]	τ_F[e] [ns]	E_{ox}[f] [V]	E_{red}[f] [V]
2a	393	379	441	33	0.57	1.55	−1.57
2b	382	370	445	14	0.77	1.48	−1.65
3a	425	420	481	43	0.53	1.51	−1.57
3b	411	411	507	12	0.54	1.53	−1.66

[a] λ_{abs}, the absorption maximum from the UV/vis spectra in THF solution.
[b] λ_{ex}, the maximum in photoluminescence excitation spectra in THF solution.
[c] λ_F, the photoluminescence emission maximum in THF solution.
[d] φ_F, photoluminescence quantum yield in THF solution relative to quinine sulfate in 0.5 M H_2SO_4. Excitation wavelength was 380 nm for all samples.
[e] τ_F, the lifetime of excited states in THF solution. Excitation wavelength was 370 nm for all samples.
[f] Potentials E_{oxy} and E_{red} determined by cyclic voltammetry of thin film on disc graphite electrode. Potentials referred versus Ag/AgCl reference electrode.

localized mainly over the thiophene central chain and adjacent pyridine rings (see Fig. 3). As for the HOMO, the C=C bonds are π-bonding and have an alternating phase with respect to their adjacent C=C bonds, whereas for the LUMO, the C=C bonds are π-antibonding and the inter-ring C^{β}–$C^{\beta'}$ bonds are bonding. This means that the excited oligomeric chain acquires the quinoid-like electronic configuration.

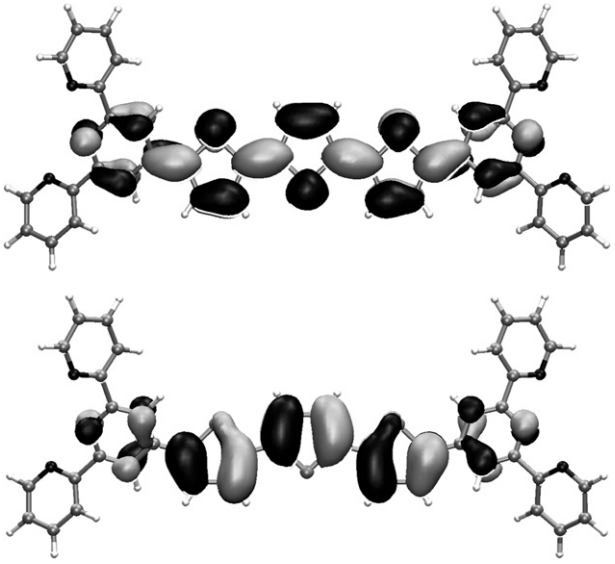

Fig. 3. Electronic density contours for LUMO (up) and HOMO (down) of **3a** obtained using DFT calculations.

The spectra presented in Fig. 1 show that the position of the band of π–π* transitions in the molecule backbone shifts to lower wavelengths when going from compounds **a** (without CH_3 groups on thiophene rings) to compounds **b** (with CH_3 groups on thiophene rings). This proves the decreased extent of delocalization of π-electrons upon substitution of thiophene rings with CH_3 groups, which can be ascribed to increased chain distortion caused by substitution of thiophene rings. The effect of CH_3 substituents is also seen on the shape of the π–π* band. More distinct shoulders and flatter maxima are seen on the bands of **2a** and **3a** (without CH_3) compared to those of **2b** and **3b** (with CH_3). This indicates a higher conformational disorder of oligomeric chains with methyl-substituted rings stemming from the decreased symmetry of the rings, which makes rotation of the rings caused by interactions with solvent molecules faster.

The effect of the linker length on the photoluminescence of α,ω-bis(*terpy*)oligothiophenes is seen visually: dithiophene compounds **2** show blue-light emission while the terthiophene ones (**3**) emit green light. Unlike the absorption spectra, the photoluminescence emission spectra of α,ω-bis(*terpy*)oligothiophenes (Fig. 4) show certain vibrational structure, that is better seen in the spectra of unsubstituted compounds **a** than in those of the substituted ones (**b**). In addition, the photoluminescence emission maxima, λ_F, of samples **b** occur at longer wavelengths than the maxima of corresponding samples **a**. Decreased vibrational structure of and longer wavelength of emission bands of compounds **b** reflects can be explained by faster rotational dynamics of **b**-type molecules. This explanation is supported by the results of measurements of the photoluminescence emission quantum yields, φ_F, which were found to be 33% and 43% for **2a** and **3a** (without CH_3), respectively, and 12–14% for **2b** and **3b** (with CH_3). This drop in φ_F when going from **a** to **b** molecules can be also ascribed to a lowered torsion robustness of the S_1 excited state of type **b** chains (with CH_3 groups), which enhances (facilitates) a non-radiative decay of excited states. The mean lifetimes of excited states found for α,ω-bis(*terpy*) compounds prepared are rather short but comparable (0.53–0.77 ns; Table 1).

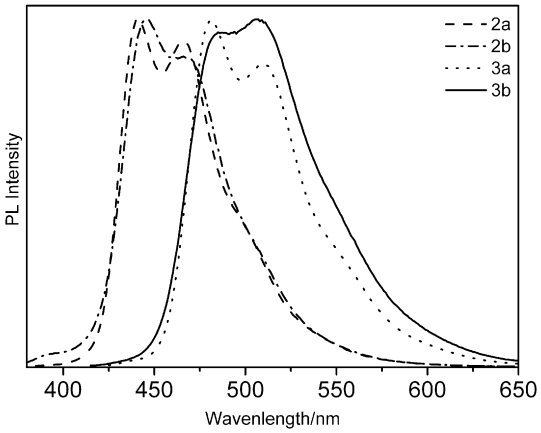

Fig. 4. Emission photoluminescence spectra of prepared α,ω-bis(terpyridine) oligothiophenes.

The cyclic voltammetry spectra of the ligands (Fig. 5) exhibit band-gap energy values from 3.07 to 3.19 eV (Table 1), which relatively is in a good agreement with data obtained from optical measurements.

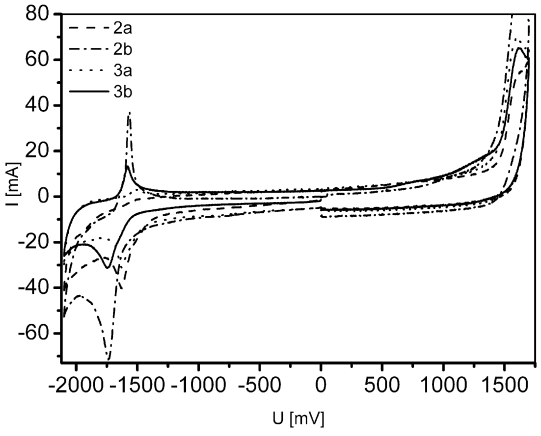

Fig. 5. Cyclic voltammogram of a thin film of prepared bis(terpyridine)s on a 1 mm diameter graphite disc electrode at 50 mV s^{-1} in CH_3CN containing 0.1 M [*n*-Bu_4N][PF_6] as supporting electrolyte.

3. Experimental section

3.1. Measurements

^{1}H and ^{13}C NMR spectra were measured on a Varian ^{UNITY}INOVA 400 or Varian SYSTEM 300 spectrometer in d_8-THF or $CDCl_3$. Chemical shifts δ are reported in parts per million relative to the solvent peak (for ^{1}H 7.25 ppm ($CDCl_3$) or 3.58 ppm (d_8-THF); for ^{13}C 77.0 ppm ($CDCl_3$) or 67.57 ppm (d_8-THF)). Coupling constants, J (in Hz), were obtained by first-order analysis. Infrared spectra were recorded on a Nicolet Magna 760 IR instrument equipped with an Inspector IR module using KBr-diluted samples and diffuse reflectance technique (DRIFT) (128 or more scans at resolution 4 cm^{-1}). UV/vis spectra were measured using a Shimadzu UV-2401PC and solutions of prepared compounds in THF. Photoluminescence spectra were measured on a Fluorolog 4 Jobin Yvon Spex instrument (Jobin Yvon Instruments S. A., Inc., USA) using four-window quartz cuvette (1 cm) and THF solutions of the samples. The photoluminescence emission spectra were recorded using excitation wavelength, λ_{ex} equal to the position of absorption maximum of particular compound. Quantum yields, φ_F, of photoluminescence were determined by means of a comparison of the integrated spectrum of the compound in question with that of quinine sulfate diluted solution in 0.5 M H_2SO_4 used as the standard with φ_F=0.54; λ_{ex}=380 nm was used for all measured samples. Time-resolved fluorescence decays were monitored on an Edinburgh Instruments ED 299 T fluorometer equipped with a laser diode with excitation wavelength 370 nm by means of the time-correlated single-photon-counting technique. Cyclic voltammograms (CV) were measured on a potentiostat UMμE Eco-Trend using films of compounds deposited on a carbon disc electrode (diameter 1 mm) by the drop-casting technique (Bu_4N)(PF_6) solution (0.1 M) in acetonitrile as the supporting electrolyte, Ag/AgCl reference electrode and the scanning rate of 380 mV s^{-1}.

3.2. Materials

Thiophene-2-carbaldehyde, 3-methylthiophene-2-carbaldehyde, 2-acetylpyridine, ammonium acetate, *N*-bromosuccinimide (NBS), bis-(pinacolato)-diboran, thiophene-2,5-diboronic acid and PEPPSI-Ipr catalyst (all Aldrich) as well as K_2CO_3 (Lachner) were used as received. 4′-(Thiophen-2-yl)-2,2′;6′,2″-terpyridine was prepared using the two-step synthesis described in literature[32] and then brominated with NBS to obtain 4′-(5-bromothiophen-2-yl)-2,2′;6′,2″-terpyridine **1a**.[33]

3.3. Calculations

Theoretical calculations were done using the density functional theory (DFT), namely the Becke's three parameter functional with the non-local Lee-Yang-Parr correlation functional (B3LYP) with the standard 6-31G(d) basis set as implemented in Ref. 35 After optimization of the geometry and ensuring that the found stationary point is a local minimum we calculated excited states up to corresponding photon wavelength of 250 nm. After convolution with a Gaussian kernel with width of 0.25eV we obtained theoretical electronic spectra of studied molecules.

3.4. Synthesis of monoterpyridine compounds

3.4.1. 4′-[3-Methylthiophen-2-yl]-2,2′;6′,2″-terpyridine. A solution of 3-methyl-2-thiophenecarbaldehyde (5.56 mL; 6.80 g; 60 mmol) in ethanol (1000 mL) was mixed with a solution of NaOH (16.0 g; 400 mmol) in deionized water (100 mL) in a three-neck round-bottomed flask and a solution of 2-acetylpyridine (13.36 mL; 14.44 g; 120 mmol) in ethanol (800 mL) was added dropwise under stirring during 30 min. The resultant reaction mixture was stirred for 20 h at room temperature, then ethanol and was removed on a rotary evaporator and the crude intermediate was extracted into CH_2Cl_2 (1000 mL). The obtained organic phase was successively washed with deionized water (3×800 mL) and brine (100 mL), dried over magnesium sulfate and CH_2Cl_2 was evaporated to obtain oil intermediate to which ethanol (400 mL) and stoichiometric excess of ammonium acetate (120 g;) was added. The resulting mixture was kept under reflux for 18 h, then cooled down to room temperature, ethanol was evaporated, the residue was taken up in toluene (1000 mL) and the organic phase was washed with distilled water (3×400 mL), dried over magnesium sulfate, and concentrated. The obtained crude product was dissolved in aqueous HCl (0.5 M; 300 mL) and washed with CH_2Cl_2 (3×280 mL). Then the aqueous layer was neutralized using aqueous NaOH, which gave a brown oil product that was extracted into CH_2Cl_2 and isolated by evaporating the solvent. Purified using column chromatography (silica gel, 10% methanol/$CHCl_3$). Isolated yield: 1.67 g; 8.5%. R_f (10% methanol/$CHCl_3$) 0.34. δ_H (400 MHz, $CDCl_3$) 8.71 (ddd, ^3J=4.8 Hz, ^4J=1.6 Hz, ^5J=0.8 Hz, 2H, A^6), 8.62–8.66(m, 2H, A^3), 8.58 (s, 2H, B^3), 7.86 (ddd, $^3J\approx$7.8 Hz, ^4J=1.7 Hz, 2H, A^4), 7.33 (ddd, ^3J=7.5 and 4.7 Hz, ^4J=1.2 Hz, 2H, A^5), 7.32 (d, ^3J=5.1 Hz, 1H, C^5), 6.98 (d, ^3J=5.1 Hz, 1H, C^4), 2.51 (s, 3H, CH_3). δ_C (100.6 MHz, $CDCl_3$) 156.1 (A^2), 155.8 (B^2), 149.2 (A^6), 144.5 (B^4), 136.8 (A^4), 136.3 (C^3), 135.7 (C^2), 131.6 (C^4), 125.0 (C^5), 123.8 (A^5), 121.3 (A^3), 120.3 (B^3), 15.5 ($-CH_3$). HRMS found *m*/*z*: 330.1056 $[M+H]^+$; $C_{20}H_{16}N_3S$ requires: 330.1059. IR (DRIFT), cm^{-1}: 3054 and 3009 (merged ν_{CH} pyridine and thiophene rings); 2949, 2920, and 2866 (ν_{CH} methyl); 1600, 1583, 1568, 1469, 1447, and 1398 (ν_{CC} pyridine rings); 1548 (ν_{CC} thiophene rings, weak); 1266 (s), 1215 (s), 1130 (s), 994 (s), 890 (s), 793 (vs), 743 (s), 660 (s), 621 (s).

3.4.2. 4′-(5-Bromo-3-methylthiophen-2-yl)-2,2′;6′,2″-terpyridine ***1b***. 4′-(3-Methylthiophen-2-yl)-2,2′;6′,2″-terpyridine (0.835 g; 0.7 mmol), acetic acid (10 mL), NBS (0.146 g; 0.8 mmol), and CH_2Cl_2 (10 mL) were placed into a round-bottomed flask and the resulting mixture was stirred at room temperature overnight. Then the reaction mixture was cautiously neutralized with a saturated solution of $NaHCO_3$, the aqueous phase was extracted with CH_2Cl_2 (3×50 mL) and both organic phases were combined, washed with brine (50 mL), dried over magnesium sulfate and concentrated by evaporating CH_2Cl_2. Isolated yield: 0.53 g; 52%. δ_H (400 MHz, $CDCl_3$) 8.68 (ddd, ^3J=4.8 Hz, ^4J=1.7 Hz, ^5J=0.8 Hz, 2H, A^6), 8.61 (ddd, ^3J=7.9 Hz, $^4J\approx{}^5J\approx$1.0 Hz, 2H, A^3), 8.50 (s, 2H, B^3), 7.84 (ddd, ^3J=7.7 Hz, ^4J=1.8 Hz, 2H, A^4), 7.31 (ddd, ^3J=7.5, 4.8 Hz, ^4J=1.1 Hz, 2H, A^5), 6.92 (s, 1H, C^4), 2.42 (s, 3H, CH_3). δ_C (100.6 MHz, $CDCl_3$) 155.8 (A^2+B^2), 149.2 (A^6), 143.3 (B^4), 137.0 (C^2), 136.9 (A^4), 136.3 (C^3), 134.2 (C^4), 123.9 (A^5), 121.3 (A^3), 120.0 (B^3), 112.2 (C^5), 15.4 (-CH_3). HRMS found *m*/*z*: 408.0161 $[M+H]^+$; $C_{20}H_{15}N_3BrS$ requires: 408.0165. IR (DRIFT), cm^{-1}: 3053 and 3007 (merged ν_{CH} pyridine and thiophene rings); 2952, 2924 and 2866 (ν_{CH} methyl); 1599, 1584, 1567, 1467, 1450, and 1397 (ν_{CC} pyridine rings); 1553, 1535 (ν_{CC} thiophene rings, weak); 1265 (s), 991 (s), 879 (s), 790 (vs), 746 (s), 734 (s), 675 (s), 660 (s), 622 (s).

3.5. Synthesis of α,ω-bis(*terpy*) compounds

3.5.1. General procedure for the synthesis by Suzuki–Miyaura coupling. Monoterpyridine compound (0.656 mmol), diboronic compound (0.328 mmol); bis-(pinacolato)-diboran (synthesis of type **2** compounds) or 2,5-thiophenediboronic acid (synthesis of type **3** compounds) and K_2CO_3 (120 mg, 0.868 mmol) were dissolved in a degassed toluene/methanol mixture (5 mL, 1:1), argon was bubbled through the solution for 10 min, then PEPPSI-IPr catalyst (6 mg) was added and the reaction mixture kept under stirring for 18 h at 100°C. The mixture was diluted with toluene (20 mL), water was added (20 mL) and the formed two-phase system was filtered.

The obtained greenish or brownish sediment was dissolved in a large amount of hot THF, filtered and solvent was evaporated to obtain the desired product.

3.5.2. 5,5′-Bis(terpy)-2,2′-dithiophene ***2a***. Greenish powder prepared from **1a**; isolated yield: 143 mg; 69%. δ_H (400 MHz, d_8-THF) 8.85 (s, 4H, B^3), 8.74–8.67 (m, 8H, A^6+A^3), 7.94–7.88 (m, 4H, A^4), 7.88 (d, J=3.9, 2H, C^3), 7.53 (d, J=3.9, 2H, C^4), 7.39 (ddd, J=1.2, 4.7, 7.4, 4H, A^5). HRMS found m/z: 629.1568 $[M+H]^+$; $C_{38}H_{25}N_6S_2$ requires: 629.1577. IR (DRIFT), cm^{-1}: 3085 and 3050 (ν_{CH} thiophene rings); 3064 and 3015 (ν_{CH} pyridine rings); 1601, 1584, 1567, 1480, 1467, 1448, and 1398 (ν_{CC} pyridine rings); 1547, 1516 (ν_{CC} thiophene rings, weak); 1268 (s), 1010 (s), 879 (s), 783 (vs), 743 (s), 737 (s), 728 (s), 681 (s), 658 (s), 624 (s).

3.5.3. 5,5′-Bis(terpy)-(4,4′-dimethyl-2,2′-dithiophene) ***2b***. Greenish powder prepared from **1b**; isolated yield: 72 mg; 45%. δ_H (400 MHz, d_8-THF) 8.77 (s, 4H, B^3), 8.75–8.66 (m, 8H, A^6+A^3), 7.95–7.87 (m, 4H, A^4), 7.42–7.36 (m, 4H, A^5), 7.33 (s, 2H, C^3), 2.58 (s, 6H, CH_3). HRMS found m/z: 657.1880 $[M+H]^+$; $C_{40}H_{29}N_6S_2$ requires: 657.1890. IR (DRIFT), cm^{-1}: 3087 and 3049 (ν_{CH} thiophene rings); 3062 and 3012 (ν_{CH} pyridine rings); 2955, 2923, and 2853 (ν_{CH} methyl); 1601, 1585, 1567, 1478, 1467, 1446, and 1397 (ν_{CC} pyridine rings); 1549 (ν_{CC} thiophene rings, weak); 1376 (ν_{CC} methyl-thiophene); 1267 (s), 880 (s), 789 (vs), 731 (s), 686 (s), 666 (s), 658 (s), 643 (s), 623 (s), 493 (s).

3.5.4. 5,5″-Bis(terpy)-2,2′;5′,2″-terthiophene ***3a***. Brown powder prepared from **1a**; isolated yield: 196 mg; 85%. δ_H (400 MHz, d_8-THF) 8.83 (s, 4H, B^3), 8.73–8.69 (m, 8H, A^6+A^3), 7.95–7.88 (m, 4H, A^4), 7.87 (d, J=3.9, 2H, C^3), 7.43 (d, J=3.9, 2H, C^4), 7.41 (s, 2H, D^3), 7.39 (ddd, J=1.0, 4.4, 6.1, 4H, A^5). δ_C (100.6 MHz, d_8-THF) 157.5, 156.9, 152.8, 150.2, 138.3, 137.7, 129.0, 128.1, 126.5, 126.1, 125.0, 121.8, 117.2, 111.8. HRMS found m/z: 711.1451 $[M+H]^+$; $C_{42}H_{27}N_6S_3$ requires: 711.1454. IR (DRIFT), cm^{-1}: 3061 and 3010 (merged ν_{CH} pyridine and thiophene rings); 1600, 1584, 1568, 1467, 1456, and 1400 (ν_{CC} pyridine rings); ν_{CC} of thiophene rings are not resolved; 1267 (w), 1010 (s), 879 (m), 782 (vs), 740 (m), 728 (m), 685 (m), 659 (s), 623 (s).

3.5.5. 5,5″-Bis(terpy)-(4,4″-dimethyl-2,2′;5′,2″-terthiophene) ***3b***. Brown powder prepared from **1b**; isolated yield: 25 mg; 14%. δ_H (400 MHz, d_8-THF) 8.74 (s, 4H, B^3), 8.73–8.68 (m, 8H, A^6+A^3), 7.94–7.87 (m, 4H, A^4), 7.38 (ddd, J=1.4, 5.0, 5.9 4H, A^5), 7.31 (s, 2H), 7.26 (s, 2H), 2.56 (s, 6H, CH_3). δ_C (100.6 MHz, d_8-THF) 157.2, 156.9, 150.3, 144.6, 138.3, 137.7, 137.3, 135.6, 129.7, 126.2, 125.0, 121.8, 120.7, 120.2, 16.2. HRMS found m/z: 739.1755 $[M+H]^+$; $C_{44}H_{31}N_6S_2$ requires: 739.1767. IR (DRIFT), cm^{-1}: 3065 and 3010 (merged ν_{CH} pyridine and thiophene rings); 2955, 2920, and 2853 (ν_{CH} methyl); 1600, 1583, 1568, 1467, 1447, and 1398 (ν_{CC} pyridine rings); ν_{CC} of thiophene rings are not resolved; 1264 (s), 879 (s), 789 (vs), 740 (s), 730 (s), 677 (s), 660 (s), 622 (s).

4. Conclusions

In summary, novel π-conjugated bis-terpyridines with oligothiophene linker were synthesized using a Suzuki-type cross-coupling strategy. The photophysical properties of the obtained compounds are presented. On the basis of our results, we can draw several principal conclusions: (i) the wavelength of the longer-wavelength maximum of the ligand absorption increases with oligothiophene linker prolongation and (ii) decreases with introduction of methyl group onto thiophene ring, (iii) the emission maximum in photoluminescence spectra increases with conjugated chain prolongation. The lifetimes of excited states are relatively short (0.55–0.77 ns) and the photoluminescence emission quantum yields are 33–43% for bis-terpyridines with non-substituted thiophene rings and 12–14% for compounds with methyl-substituted thiophene rings. Thus, these novel compounds are promising candidates for the construction of metallo-supramolecular polymers. Further work concerning the photophysical properties of the polymer material is currently underway in our laboratory.

Acknowledgements

Financial support from the Ministry of Education of the Czech Republic no.: MSM0021620857 and Grant Agency of Czech Republic no.: 104/09/1435 is gratefully acknowledged.

Supplementary data

Supplementary data associated with this article can be found in the online version at doi:10.1016/j.tet.2010.11.039.

References and notes

1. Harriman, A.; Ziessel, R. *Chem. Commun.* **1996**, 1707.
2. Dobrawa, R.; Wurthner, F. *J. Polym. Sci., Part A: Polym. Chem.* **2005**, *43*, 4981.
3. Lehn, J. M. *Prog. Polym. Sci.* **2005**, *30*, 814.
4. Constable, E. C.; Thompson, A. M. W. C. *J. Chem. Soc., Dalton Trans.* **1992**, 3467.
5. Barigelletti, F.; Flamigni, L. *Chem. Soc. Rev.* **2000**, *29*, 1.
6. Chiper, M.; Hoogenboom, R.; Schubert, U. S. *Macromol. Rapid Commun.* **2009**, *30*, 565.
7. Mortimer, R. J.; Dyer, A. L.; Reynolds, J. R. *Displays* **2006**, *27*, 2.
8. Goze, C.; Ulrich, G.; Charbonniere, L.; Cesario, M.; Prange, T.; Ziessel, R. *Chem. Eur. J.* **2003**, *9*, 3748.
9. Hjelm, J.; Handel, R. W.; Hagfeldt, A.; Constable, E. C.; Housecroft, C. E.; Forster, R. J. *Inorg. Chem.* **2005**, *44*, 1073.
10. Houarner, C.; Blart, E.; Buvat, P.; Odobel, F. *Photochem. Photobiol. Sci.* **2005**, *4*, 200.
11. Houamer-Rassin, C.; Blart, E.; Buvat, P.; Odobel, F. *J. Photochem. Photobiol., A* **2007**, *186*, 135.
12. Krebs, F. C.; Biancardo, M. *Sol. Energy Mater. Sol. Cells* **2006**, *90*, 142.
13. El-ghayoury, A.; Schenning, A. P. H. J.; Meijer, E. W. *J. Polym. Sci., Part A: Polym. Chem.* **2002**, *40*, 4020.
14. Harriman, A.; Mayeux, A.; De Nicola, A.; Ziessel, R. *Phys. Chem. Chem. Phys.* **2002**, *4*, 2229.
15. Benniston, A. C.; Harriman, A.; Lawrie, D. J.; Mayeux, A.; Rafferty, K.; Russell, O. D. *Dalton Trans.* **2003**, 4762.
16. Yu, S. C.; Kwok, C. C.; Chan, W. K.; Che, C. M. *Adv. Mater.* **2003**, *15*, 1643.
17. Andres, P. R.; Schubert, U. S. *Adv. Mater.* **2004**, *16*, 1043.
18. Barbieri, A.; Ventura, B.; Barigelletti, F.; De Nicola, A.; Quesada, M.; Ziessel, R. *Inorg. Chem.* **2004**, *43*, 7359.
19. Lopez, R.; Villagra, D.; Ferraudi, G.; Moya, S. A.; Guerrero, J. *Inorg. Chim. Acta* **2004**, *357*, 3525.
20. Dobrawa, R.; Lysetska, M.; Ballester, P.; Grune, M.; Wurthner, F. *Macromolecules* **2005**, *38*, 1315.
21. Iyer, P. K.; Beck, J. B.; Weder, C.; Rowan, S. J. *Chem. Commun.* **2005**, 319.
22. Han, F. S.; Higuchi, M.; Kurth, D. G. *Tetrahedron* **2008**, *64*, 9108.
23. Vellis, P. D.; Mikroyannidis, J. A.; Lo, C. N.; Hsu, C. S. *J. Polym. Sci., Part A: Polym. Chem.* **2008**, *46*, 7702.
24. Schwarz, G.; Bodenthin, Y.; Geue, T.; Koetz, J.; Kurth, D. G. *Macromolecules* **2010**, *43*, 494.
25. Chen, Y. Y.; Lin, H. C. *J. Polym. Sci., Part A: Polym. Chem.* **2007**, *45*, 3243.
26. Chen, Y. Y.; Lin, H. C. *Polymer* **2007**, *48*, 5268.
27. Winter, A.; Friebe, C.; Chiper, M.; Hager, M. D.; Schubert, U. S. *J. Polym. Sci., Part A: Polym. Chem.* **2009**, *47*, 4083.
28. Roncali, J. *Chem. Rev.* **1992**, *92*, 711.
29. McCullough, R. D. *Adv. Mater.* **1998**, *10*, 93.
30. Jeffries-El, M.; McCullough, R. D. In *Conjugated Polymers*, 3rd ed.; Skotheim, T. A., Reynolds, J. R., Eds.; CRC, Taylor and Francis Group: London, 2007; Vol. 1; pp 9.1–9.49.
31. Kröhnke, F. *Synthesis* **1976**, *1*.
32. Encinas, S.; Flamigni, L.; Barigelletti, F.; Constable, E. C.; Housecroft, C. E.; Schofield, E. R.; Figgemeier, E.; Fenske, D.; Neuburger, M.; Vos, J. G.; Zehnder, M. *Chem. Eur. J.* **2002**, *8*, 137.
33. Beley, M.; Delabouglise, D.; Houppy, G.; Husson, J.; Petit, J. P. *Inorg. Chim. Acta* **2005**, *358*, 3075.
34. Bondarev, D.; Zednik, J.; Sloufova, I.; Sharf, A.; Prochazka, M.; Pfleger, J.; Vohlidal, J. *J. Polym. Sci., Part A: Polym. Chem.* **2010**, *48*, 3073.
35. Frisch, M. J., et al. *Gaussian 03, Revision C.01*; Gaussian: Wallingford CT, 2004.

ATTACHEMENT B

Bláhová P., Zedník J.; Šloufová I., Vohlídal J., Svoboda J.: Synthesis and Photophysical Properties of New α,ω-Bis(Tpy)Oligothiophenes and Their Metallo-Supramolecular Polymers With Zn^{2+} Ion Couplers; *Soft Mater.* 2014, **12**, 214 – 229.

Soft Materials (2014) **12**, 214–229

ISSN: 1539-445X print / 1539-4468 online
DOI: 10.1080/1539445X.2013.858358

Taylor & Francis
Taylor & Francis Group

Synthesis and Photophysical Properties of New α,ω-Bis(*Tpy*)Oligothiophenes and Their Metallo-Supramolecular Polymers With Zn^{2+} Ion Couplers

PAVLA BLÁHOVÁ, JIŘÍ ZEDNÍK, IVANA ŠLOUFOVÁ, JIŘÍ VOHLÍDAL, and JAN SVOBODA*

Department of Physical and Macromolecular Chemistry, Charles University in Prague, Faculty of Science, Prague, Czech Republic

Received July 15, 2013; Accepted October 20, 2013

Five new α,ω-bis(*tpy*)bithiophenes and terthiophenes, each comprising two hexyl groups attached to oligothiophene block at different positions, were prepared using the Suzuki coupling strategy, characterized (NMR, IR, Raman, HRMS, UV/vis, fluorescence, cyclic voltammetry) and transformed to corresponding conjugated metallo-supramolecular polymers with Zn^{2+} ion-couplers. Reference oligomers with unsubstituted central blocks and their polymers are also reported. Photophysical properties of oligomers and polymers are described, analyzed with a help of DFT calculations, and correlated with the chemical constitution of oligomeric building blocks. Steric effects were shown to exceed the electronic effects of hexyl groups, and twisting the thiophene-thiophene bonds were shown to influence electronic spectra of oligomers and polymer more deeply than twisting the thiophene-*tpy* bonds. Outlying photoluminescence characteristics observed for some oligomers and polymers were shown to be consistent with the other data based on their analysis by the Stokes shift approach. Polymers prepared exhibited good constitutional dynamics in DMSO but only limited dynamics in THF solutions. IR and Raman spectra allowing identification of solid oligomers and polymers are also presented.

Keywords: Conjugated polymer, Dynamer, Hexylthiophene, Metallo-supramolecular polymer, Terpyridine

Introduction

A macromolecule of a metallo-supramolecular polymer (MSP) is composed of defined oligomeric molecules with chelate end-groups, which are linked together via coordination of the chelate groups to metal ions (so called ion couplers) (1). Depending on the strength of interactions between chelate end-groups and ion couplers, molecules of MSP can be as stable as current covalent macromolecules or they can exhibit the constitutional dynamics either at increased temperature or in solution or both—such polymers are referred to as dynamers (2). The constitutional dynamics gives to MSPs (i) significant processing advantages, (ii) responsiveness to external/internal stimuli (adaptability), (iii) possibility of additional tuning the properties by post-synthesis exchanges of oligomer molecules and/or ion-couplers, and (iv) in some cases a capability of self-healing. The constitutional dynamics of an MSP is qualitatively controlled by the involved thermodynamic equilibria and kinetically controlled by the rates of reversible reactions underlying the coordination equilibria (i.e., by the rate of chemical relaxation of the system).

Ditopic conjugated oligomers with 2,2′:6′,2″-terpyridine-4′-yl (*tpy*) end-groups are of interest as building blocks for the construction of electromagnetic-field-responsive MSPs (3–6) with applications based on the light/electricity inter-conversion and non-linear optical phenomena (light-emitting devices, photovoltaic cells, etc.) (7–21). Specific configuration of nitrogen atoms prefers tridentate facial or meridian coordination of *tpy* group to metal ions such as ions of Ru, Os, Ir, Fe, Zn, and Co, which gives rise to linear chains (22–24). This aspect allows a reproducible formation of defined MSPs. Stability and dynamics of these MSPs are mainly controlled by the position and kinetics of establishing of coordination equilibrium state whereas functional properties of MSPs are mainly controlled by the structure of central blocks of ditopic oligomers.

The previously described bis(*tpy*) oligomers mainly comprised high-band-gap central blocks of the oligoarylene or oligoaryleneethynylene types that mostly show a good quantum efficiency of the luminescence. On the other hand, bis(*tpy*) compounds with low-band-gap oligothiophene central blocks are almost unknown materials, though polythiophenes and oligothiophenes belong among the most important polymer materials with applications in organic optoelectronics including photovoltaics.

*Address correspondence to: Jan Svoboda, Department of Physical and Macromolecular Chemistry, Charles University in Prague, Faculty of Science, Hlavova 2030, CZ-128 40, Prague 2, Czech Republic. Email: jan.svoboda@natur.cuni.cz
Color versions of one or more of the figures in the article can be found online at www.tandfonline.com/lsfm.

We have recently reported on dimeric and trimeric α,ω-bis(*tpy*)oligothiophenes with unsubstituted central blocks and central blocks with two methyl groups each located right next to the one of *tpy* end-groups (25) and on the complexation of terpyridine, ethynyl*tpy* and (2-thienyl)*tpy* with Zn^{2+} and Fe^{2+} ions (26). In the present paper, we report the preparation of five new α,ω-bis(*tpy*) bithiophenes and terthiophenes, each carrying just two hexyl groups located at various positions of oligothiophene central blocks. Further, we report the transformation of these new oligomers and corresponding unsubstituted oligomers into metallo-supramolecular polymers, and mainly photophysical properties of all prepared oligomers and polymers. Complete sets of the IR and Raman spectra that allow easy identification of all these materials in the solid state are also included.

Experimental Section

Materials

The 2,2′;6′,2″-terpyridine (H*tpy*), 2-(3-hexylthiophen-2-yl)-4,4,5,5-tetramethyl-1,3,2-dioxaborolane (HexThBor), 2-bromo-3-hexylthiophene, *N*-bromosuccinimide (NBS), 4,4,4′,4′,5,5,5′,5′-octamethyl-2,2′-bi-1,3,2-dioxaborolane (Bor_2), thiophene-2,5-diboronic acid, [1,3-bis(2,6-diisopropylphenyl)imidazol-2-ylidene](3-chloropyridyl)palladium(II) dichloride (PEPPSI-IPr), 4,4′-di-*tert*-butyl-2,2′-dipyridyl (dtbpy), 4,4,5,5-tetramethyl-1,3,2-dioxaborolane (HBor), bis(1,5-cyclooctadiene)di-μ-methoxydiiridium(I) ($[Ir(OMe)(COD)]_2$), 3,4-dibromothiophene, 1,3-bis(diphenylphosphino)propane nickel(II) chloride (Ni(dppp)Cl_2), zinc acetate (all Aldrich), and 4′-bromo-2,2′;6′,2″-terpyridine (Br*tpy*) (TCI) were used as received. The 4′-(5-Bromothiophen-2-yl)-2,2′:6′,2″-terpyridine (BrTh*tpy*) was prepared by Suzuki coupling of Br*tpy* with 2-thienylboronic acid and then brominated with NBS (27).

Toluene (Lachner) was distilled under argon from sodium/benzophenone prior to use; methanol (Aldrich) and hexane (Lachner) were bubbled with argon prior to use; and dichloromethane (Lachner), N-methylpyrrolidone (NMP) and acetic acid (Lachner) were used as obtained.

Synthesis of α,ω-Bis(tpy)oligothiophenes

4′-(3-Hexylthiophen-2-yl)-2,2′:6′,2″-terpyridine, ***HexThtpy***

HexThBor (610 mg, 1.97 mmol, 30% excess) was added to a solution of Br*tpy* (496 mg, 1.52 mmol) and K_2CO_3 (636 mg, 4.6 mmol) in degassed toluene/methanol (30 + 30 mL) under argon atmosphere, then PEPPSI-IPr catalyst (10mg) was added and the resulting reaction mixture was refluxed for 3 hours. After 3 hours, when Br*tpy* was consumed (monitoring by GC), the reaction mixture was cooled to room temperature, diluted with toluene (50 mL), washed with water (3 × 150 mL), the organic layer was dried with $MgSO_4$ and evaporated to give a pink oil, which was distilled on a Kugelrohr apparatus (110°C) to remove 3-hexylthiophene and get the desired product (572 mg, 94%). ^{1}H NMR (300 MHz, $CDCl_3$) δ 8.72 (d, $J = 4.6$, 2H, A^6), 8.66 (d, $J =$ 8.2, 2H, A^3), 8.58 (s, 2H, B^3), 7.88 (m, A^4), 7.37–7.33 (m, 3H, A^5+C^5), 7.04 (d, $J = 5.2$, 1H, C^4), 2.83 (t, $J = 7.6$, 2H, Hex^1), 1.74–1.67 (m, 2H, Hex^2), 1.40–1.26 (m, 6H, Hex^3-Hex^5), 0.84 (t, $J = 6.4$, 3H, Hex^6). ^{13}C NMR (101 MHz, $CDCl_3$) δ 156.10(A^2), 155.69(B^2), 149.18 (A^6), 144.58 (B^4), 140.99 (C^2), 136.75 (A^4), 135.31 (C^3), 130.04 (C^4), 125.21 (C^5), 123.77 (A^5), 121.22 (A^3), 120.78 (B^3), 31.62 (Hex^1), 30.94 (Hex^2), 29.15–29.11 (Hex^3-Hex^5), 22.58 (Hex^6). IR (DRIFT), cm^{-1}: 3061 and 3012 (merged ν_{CH} pyridine and thiophene rings); 2954, 2927, and 2856 (ν_{CH} in CH_3 and CH_2 groups); 1600, 1584, 1567, 1466, 1430, and 1395 (ν_{CC} pyridine ring); 1548 (ν_{CC} thiophene ring, w); 1265 (m), 1210 (s), 1123 (s), 987 (m), 890 (s), 793 (s), 740 (s), 655 (m), 622 (m). HRMS found m/z: 400.1839 $[M_+H]^+$, $C_{25}H_{26}N_3S$ requires: 400.1842.

4′-(5-Bromo-3-hexylthiophen-2-yl)-2,2′:6′,2″-terpyridine, ***BrHexThtpy***

HexTh*tpy* was dissolved in CH_2Cl_2 (20 mL) and acetic acid (20 mL) and NBS (416 mg, 2.3mmol) were added. The reaction mixture was stirred overnight in dark at room temperature, and then neutralized with a saturated aqueous solution of $NaHCO_3$ until a gas was evolving. The obtained two-phase liquid mixture was extracted with dichloromethane, the obtained organic layer was washed with water, dried with $MgSO_4$, and evaporated to give the product (389 mg, 57%). ^{1}H NMR (400 MHz, $CDCl_3$) δ 8.72 (d, $J = 4.7$, 2H, A^6), 8.65 (d, $J = 8.1$, 2H, A^3), 8.52 (s, 2H, B^3), 7.88 (t, $J = 7.7$, 2H, A^4), 7.37–7.34 (m, 3H, A^5), 7.00 (s, 1H, C^4), 2.76 (t, $J = 7.7$, 2H, Hex^1), 1.70–1.63 (m, 2H, Hex^2), 1.39–1.27 (m, 6H, Hex^3 – Hex^5), 0.84 (t, $J =$ 6.8, 3H, Hex^6). ^{13}C NMR (101 MHz, $CDCl_3$) δ 155.87 (A^2), 155.85 (B^2), 149.21 (A^6), 143.33 (B^4), 141.62 (C^2), 136.91 (C^3), 136.80 (A^4), 132.70 (C^4), 123.89 (A^5), 121.20 (A^3), 120.48 (B^3), 112.25 (C^5), 31.57 (Hex^1), 30.77 (Hex^2), 29.00 (Hex^3–Hex^5), 22.55 (Hex^6). IR (DRIFT), cm^{-1}: 3071, 3060, 3049, and 3012 (merged ν_{CH} pyridine and thiophene rings); 2953, 2930, and 2868 (ν_{CH} methyl), 2854 (ν_{CH} methylen), 1696 (m), 1600, 1584, 1567, 1464, 1456, and 1394 (ν_{CC} pyridine rings), 1555 and 1541 (ν_{CC} thiophene rings); 1269 (m), 1266 (m), 997 (s), 793 (vs), 746 (s), 670 (s), 660 (m), 622 (s). HRMS found m/z: 478.0945 $[M_+H]^+$, $C_{25}H_{26}N_3BrS$ requires: 478.0947.

5,5′-Bis(2,2′:6′,2″-terpyridine-4′-yl)-4,4′-dihexyl-2,2′-bithiophene, ***B14***

BrHexTh*tpy* (100 mg, 0.21 mmol), Bor_2 (29 mg, 0.11 mmol) and K_2CO_3 (38 mg, 0.27 mmol) were dissolved in a mixture of distilled toluene (8 mL) and methanol (8 mL) under argon atmosphere and PEPPSI-IPr catalyst (5 mg) was added. The reaction mixture was allowed to react at 100°C for 2 hours, then cooled to room temperature, diluted with chloroform (10 mL), washed with water (3 × 30 mL), dried with $MgSO_4$ and evaporated to give a crude product that was purified on a preparative HPLC device (UV/vis and IR detection) using chloroform/methanol (3:2) with ammonium hydroxide (2%) as a solvent system. Isolated yield 13 mg (14%). ^{1}H NMR (300 MHz, $CDCl_3$) δ 8.73 (d, $J = 4.5$, 4H, A^6), 8.66 (d, $J = 7.9$, 4H, A^3), 8.63 (s, 4H, B^3), 7.88 (t, $J = 7.1$, 4H, A^4), 7.38 – 7.33 (m, 4H, A^5), 7.18 (s, 2H, C^3), 2.88 – 2.81 (m, 4H, Hex^1), 1.79–1.71 (m, 4H, Hex^2), 1.36–1.26 (m, 12H, Hex^3 – Hex^5), 0.89–0.81 (m, 6H, Hex^6). IR (DRIFT), cm^{-1}: 3063 and 3013 (ν_{CH} pyridine); 2953, 2927, and 2867 (ν_{CH} methyl); 2856 (ν_{CH} methylene); 1598, 1582, 1566, 1466, 1454, and 1396 (ν_{CC} pyridine); 1546 (ν_{CC} thiophene, w); 1264 (s); 884 (s); 792 (vs); 742 (s); 683 (s); 657 (s); 657 (s); 622 (s); 498 (s). HRMS found m/z: 797.3452 $[M_+H]^+$, $C_{50}H_{49}N_6S_2$ requires: 797.3455.

5,5″−Bis(2,2′:6′,2″−terpyridine−4′−yl)−4,4″−dihexyl-2,2′:5′,2″−terthiophene, ***T16***

BrHexTh*tpy* (75 mg, 0.16 mmol), thiophene-2,5-diboronic acid (13 mg, 0.08mmol) and K_2CO_3 (38 mg, 0.27 mmol) were dissolved in the mixture of distilled toluene (2.5 mL) and methanol (2.5 mL) under argon atmosphere and PEPPSI-IPr catalyst (2 mg) was added. The reaction mixture was allowed to react at 100°C for 2 hours, then cooled to room temperature, diluted with chloroform (5 mL) and washed with water (3 × 10 mL). The organic layer was dried with $MgSO_4$, solvents were evaporated of filtrate and the crude product was purified by preparative HPLC fitted with UV/vis and IR detectors using chloroform/methanol (3:2) with 2% of ammonium hydroxide as a mobile phase. Yield 44 mg (63%). ^{1}H NMR (300 MHz, $CDCl_3$) δ 8.73 (d, J = 4.7, 4H, A^6), 8.66 (d, J = 7.9, 4H, A^3), 8.62 (s, 4H, B^3), 7.88 (t, J = 7.9, 4H, A^4), 7.28–7.34 (m, 4H, A^5), 7.14 (s, 2H, D^4), 7.15 (s, 2H, C^3), 2.88–2.81 (m, 4H, Hex^1), 1.79–1.71 (m, 4H, Hex^2), 1.35–1.2 (m, 12H, Hex^3–Hex^5), 0.9–0.8 (m, 6H, Hex^6). ^{13}C NMR (101 MHz, $CDCl_3$) δ 156.04, 155.83, 149.20, 144.30, 142.17, 136.79, 136.24, 129.02, 126.76, 124.60, 123.83, 121.22, 120.31, 114.28, 31.63, 30,82, 29.66, 29.33, 29.14, 22.61. IR (DRIFT), cm^{-1}: 3061 and 3012 (merged ν_{CH} pyridine and thiophene), 2961, 2929, and 2867 (ν_{CH} methyl), 2854 (ν_{CH} methylene), 1659 (m), 1600, 1583, 1567, 1465, 1447, and 1396 (ν_{CC} pyridine), 1262 (s); 885 (s), 795 (vs), 740 (s), 731 (s), 677 (s); 659 (s); 622 (s). HRMS found m/z: 879.3326 $[M_+H]^+$, $C_{54}H_{51}N_6S_3$ requires: 879.3332.

3,3′-Dihexyl-2,2′-bithiophene, ***Hex$_2$Th$_2$***

HexThBor (1 mL, 3.17 mmol), 2−bromo−3−hexylthiophene (0.62 mL, 3 mmol) and K_2CO_3 (460 mg, 3.33 mmol) were dissolved in degassed distilled toluene (10 mL) and methanol (10 mL) and PEPPSI−IPr catalyst (100 mg) was added. The reaction mixture was heated at 95°C for 4 hours, and then cooled to room temperature, diluted with chloroform and washed with water. The organic layer was dried with $MgSO_4$ and evaporated to give the crude product that was distilled on a Kugelrohr apparatus (100°C, 1 hour) to remove residues of hexylthiophene. The distillation residue was dissolved in hexane and filtered through a small column of silica to obtain the desired product as a yellowish oil (685 mg, 68%). ^{1}H NMR (400 MHz, CD_2Cl_2) δ 7.30 (d, J = 5.1, 2 H, A^4), 6.98 (d, J = 5.1, 2 H, A^5), 2.49 (t, J = 7.8, 4 H, Hex^1), 1.57–1.49 (m, 4 H, Hex^2), 1.28–1.23 (m, 12H, Hex^3–Hex^5), 0.85 (t, J = 6.8, 6 H, Hex^6). ^{13}C NMR (101 MHz, CD_2Cl_2) δ 143.1 (A^3), 129.1 (A^2), 129.1 (A^5), 125.8 (A^4), 32.2 (Hex^3), 31.3 (Hex^2), 29.7 (Hex^4), 29.3 (Hex^1), 23.2 (Hex^5), 14.4 (Hex^6). IR (DRIFT), cm^{-1}: 3102 (w), 3061 (w), 2955 (s), 2927 (s), 2856 (s), 1748 (w), 1522 (m), 1465 (s), 1459 (s), 1409 (m), 1377(m), 1304 (w), 1231 (m), 1172 (w), 1088 (m), 1049 (w), 1011 (w), 920 (m), 875 (m), 832 (s), 720 (s), 694 (m), 652 (m), 597 (w), 514 (w). HRMS found m/z: 335.1862 $[M_+H]^+$, $C_{20}H_{31}S_2$ requires: 335.1861

5,5′-Bis(4,4,5,5-tetramethyl−1,3,2-dioxaborolane-2-yl)-3,3′-dihexyl-2,2′-bithiophene, ***Hex$_2$Th$_2$Bor$_2$***

General procedure for synthesis of boronates was adopted from Chotana (28). **Hex$_2$Th$_2$** (784 mg, 2.34 mmol) was dissolved in dry hexane (10 mL) under argon atmosphere, dtbpy (30 mg, 0.11 mmol) and $[Ir(OMe)(COD)]_2$ (22 mg, 0.033 mmol) were added, the mixture was bubbled with argon for 10 minutes and then HBor (1.4 mL, 9.6 mmol) was added. The reaction mixture was stirred for 24 hours at 40°C, diluted with CH_2Cl_2 (15 mL), washed with water (3 × 30 mL). The organic layer was dried with $MgSO_4$, filtered through a short silica column, and the filtrate was evaporated to get the desired product (1.307 g, 81%). ^{1}H NMR (400 MHz, CD_2Cl_2) δ 7.47 (s, 2 H, A^4), 2.50 (t, J = 7.6, 4 H, Hex^1), 1.55–1.52 (m, 4 H, Hex^2), 1.34 (s, 24H, B–*CH$_3$*), 1.26–1.20 (m, 12 H, Hex^3–Hex^5), 0.86–0.83 (m, 6 H, Hex^6). ^{13}C NMR (101 MHz, CD_2Cl_2) δ 144.35, 139.29, 136.53, 84.70, 32.18, 31.22, 29.64, 29.21, 25.14, 23.13, 14.41. ^{11}B NMR (128 MHz, CD_2Cl_2) δ 22.44 (s, 2B). IR (DRIFT), cm^{-1}: 3058 (w), 2976 (m), 2956 (m), 2929 (s), 2856 (s), 1655 (w), 1594 (m), 1533 (s), 1467 (s), 1459 (m), 1444 (m), 1380 (s), 1331 (s), 1300 (m), 1269 (m), 1213 (m), 1166 (m), 1143 (s), 1111 (m), 1098 (m), 1031 (m), 997 (m), 957 (m), 925 (w), 853 (s), 830 (m), 773 (m), 725 (m), 688 (m), 666 (s), 607 (w), 578 (m), 519 (w), 436 (w). HRMS found m/z: 609.3387 $[M_+Na]^+$, $C_{32}H_{52}O_4B_2NaS_2$ requires: 609.3385

5,5-Bis(2,2′:6′,2″-terpyridine-4′-yl)-3,3′-dihexyl-2,2′-bithiophene, ***B23***

Br*tpy* (656 mg, 2.1 mmol), **Hex$_2$Th$_2$Bor$_2$** (616 mg, 1.05 mmol) and K_2CO_3 (462 mg, 3.34 mmol) were dissolved in a mixture of toluene/methanol (10 + 10 mL) under argon atmosphere and the PEPPSI-IPr catalyst (82 mg) was added. The prepared mixture was refluxed for 3 hours, then cooled to room temperature, diluted with toluene (20 mL), washed with water (3 × 50 mL), the isolated organic layer was dried with $MgSO_4$, solvents were evaporated of filtrate to obtain a crude product that was purified by chromatography on aluminum oxide, hexan:toluene (3:2). Yield 150 mg (18%). ^{1}H NMR (400 MHz, d_8-THF) δ 8.83 (s, 4H, B^3), 8.72–8.70 (m, 8H, A^6 + A^3), 7.91 (td, 4H, J = 7.9 Hz, J = 1.8 Hz, A^4), 7.85 (s, 2H, C^4), 7.40–7.37 (m, 4H, A^5), 2.74 (t, J = 7.9, 4H, Hex^1), 1.77–1.73 (m, 8H, Hex^2–Hex^3), 1.41–1.29 (m, 8H, Hex^4–Hex^5), 0.88 (t, J = 7.0, 6H, Hex^6). ^{13}C NMR (101 MHz, *d8*-THF) δ 156.88, 150.22, 145.46, 143.98, 142.82, 137.67, 131.21, 128.82, 124.99, 121.82, 117.39, 107.58, 55.92, 32.78, 31.76, 30.27, 23.66, 14.61. IR (DRIFT), cm^{-1}: 3060 (w), 3011 (w), 2959 (m), 2928 (m), 2856 (m), 1598 (m), 1581 (s), 1566 (s), 1551 (m), 1530 (w), 1467 (m), 1444 (m), 1404 (m), 1383 (w), 1360 (w), 1264 (w), 1211 (w), 1093 (w), 1072 (w), 1036 (w), 1019 (w), 989 (w), 880 (w), 836 (w), 790 (s), 774 (s), 744 (m), 733 (m), 676 (w), 658 (m), 632 (w), 622 (w), 506 (w), HRMS found m/z: 797.3449 $[M_+H]^+$, $C_{50}H_{49}N_6S_2$ requires: 797.3455.

3,3″-Dihexyl-2,2′:5′,2″-terthiophene, ***Hex$_2$Th$_3$***

Thiophene-2,5-diboronic acid (344 mg, 2 mmol), 2-bromo-3-hexylthiophene (988 mg, 4 mmol), and K_2CO_3 (635 mg, 5.29 mmol) were dissolved in a degassed toluene/methanol (25 mL, 1:1) and bubbled with Ar (g) for 10 min; PEPPSI-IPr (15 mg) catalyst was added. The obtained mixture was stirred at 100°C for 2 hour, then diluted with toluene (100 mL) and filtered; the filtrate was washed with water, dried ($MgSO_4$), solvents were evaporated and distilled on a Kugelrohr apparatus (250°C) to provide a product that was a yellow oil (yield 669 mg, 80%). ^{1}H

NMR (300 MHz, CD_2Cl_2) δ 7.20 (d, $J = 5.2$, 2H), 7.04 (s, 2H), 6.97 (d, $J = 5.2$, 2H), 2.79 (t, $J = 7.9$ 4H, Hex^1), 1.71–1.61 (m, 4H, Hex^2), 1.41–1.27 (m, 12H, Hex^3–Hex^5), 0.91–0.86 (m, 6H, Hex^6). ^{13}C NMR (101 MHz, CD_2Cl_2) δ 140.49, 136.61, 130.79, 130.74, 126.63, 124.35, 31.31, 29.81, 27.51, 25.82, 23.24, 14.46. IR (DRIFT), cm^{-1}: 3103 (w), 3066 (w), 2954 (s), 2926 (s), 2856 (s), 1465 (s), 1377 (m), 1244 (w), 1195 (w), 1087 (w), 1050(w), 876 (w), 834 (s), 797 (s), 723 (m), 692 (m), 656 (m). HRMS found m/z: 417.1735 $[M_+H]^+$, $C_{24}H_{33}S_3$ requires: 417.1739.

5,5″-Bis(4,4,5,5-tetramethyl-1,3,2-dioxaborolane-2-yl)-3,3″-dihexyl-2,2′:5′,2″-terthiophene, ***Hex$_2$Th$_3$Bor$_2$***

Hex$_2$Th$_3$ (225 mg; 0.54 mmol), catalyst $[Ir(OMe)(COD)]_2$ (10 mg, 0.015 mmol) and co-catalyst dtbpy (15 mg, 0,08 mmol) were dissolved in hexane (10 mL, stored over molecular sieve, bubbled with argon before use). HBor (0.3 mL; 260 mg; 2.07 mmol) was added under an argon atmosphere. The reaction mixture was stirred for 3 hours at room temperature until the terthiophene disappeared, as was monitored by GC. Then, the reaction mixture was diluted with water and stirred for 1 hour. The product was extracted with hexane, which was finally dried with $MgSO_4$ and evaporated to provide a yellowish oil (280 mg, 78%). ^1H NMR (300 MHz, CD_2Cl_2) δ 7.43 (s, 2H, A), 7.15 (s, 2H, B), 2.8 (t, $J = 7.9$, 4 H, Hex^1), 1.72–1.62 (m, 4H, Hex^2), 1.43–1.25 (m, 36H, Hex^3–Hex^5, B–*CH_3*), 0.89 (t, $J = 6.9$, 6H, Hex^6). ^{13}C NMR (101 MHz, CD_2Cl_2) δ 141.64, 140.75, 137.77, 127.0, 118.51, 84.75, 32.26, 31.23, 30.94, 29.84, 25.15, 23.20, 14.43. ^{11}B NMR (128 MHz, CD_2Cl_2) δ 24.45 (s, 2B). IR (DRIFT), cm^{-1}: 3404 (w), 3067 (w), 2977 (s), 2956 (s), 2929 (s), 2857 (s), 1735 (w), 1655 (w), 1594 (w), 1552 (m), 1522 (s), 1448 (s), 1372 (s), 1332 (s), 1298 (s), 1269 (s), 1214 (m), 1194 (s), 1144 (s), 1111 (m), 1090 (w), 1028 (m), 983 (m), 960 (w), 853 (s), 799 (m), 774 (w), 725 (w), 665 (s), 578 (w), 551 (w), 520 (w), 437 (w). HRMS found m/z: 669.3440 $[M_+H]^+$, $C_{36}H_{55}O_4B_2S_3$ requires: 669.3443.

5,5″-Bis(2,2′:6′,2″-terpyridine-4′-yl)-3,3″-dihexyl-2,2′:5′,2″-terthiophene, ***T25***

Hex$_2$Th$_3$Bor$_2$ (280 mg, 0.42 mmol), Br*tpy* (266 mg, 0.85 mmol) and K_2CO_3 (170 mg, 1.23 mmol) were dissolved in degassed toluene/methanol (15 + 15 mL) under an Argon atmosphere. The PEPPSI-IPr catalyst (10 mg) was added and the reaction mixture was stirred at 100°C for 3 hours. The reaction mixture was diluted with toluene, washed with water. The organic part was dried over $MgSO_4$, filtered and evaporated to get the crude product. Purification on aluminum oxide with hexane + THF (3:2) as a mobile phase gave the pure product as an orange solid (69 mg, 18%). ^1H NMR (400 MHz, *d8*-THF) δ 8.82 (s, 2H, B^3), 8.73 – 8.69 (m, 8H, A^6 + A^3), 7.91 (td, $J = 7.6$, $J = 2.3$, 4H, A^4), 7.81 (s, 2H, C^4), 7.41–7.37 (m, 4H, A^5), 7.36 (s, D^3), 2.96 (t, $J = 7.8$, 4H, Hex^1), 1.56–1.49 (m, 8H, Hex^2–Hex^3), 1.41–1.38 (m, 8H, Hex^4–Hex^5), 0.95–0.87 (m, 6H, Hex^6). ^{13}C NMR (101 MHz, *d8*-THF) δ 157.38, 156.88, 150.21, 143.75, 137.69, 137.17, 133.30, 130.25, 125.00, 120.86, 117.17, 32.88, 31.67, 30.83, 30.49, 23.74, 14.66. IR (DRIFT), cm^{-1} 3060 (w), 3011 (w), 2956 (m), 2925 (s), 2855 (m), 1599 (m), 1583 (s), 1567 (m), 1545 (m), 1467 (m), 1451 (m), 1434 (w), 1403 (m), 1386 (w), 1265 (m), 1197 (w), 1125 (w), 1094 (w), 1072 (w), 1019 (w), 991 (m), 881(m), 835 (m), 789 (s), 743 (m), 731 (m), 659 (m), 622 (m). HRMS found m/z: 879.3323 $[M_+H]^+$, $C_{54}H_{51}N_6S_3$ requires: 879.3332.

3,4-Dihexylthiophene, ***Hex$_2$Th***

The desired product was synthesized according to the known procedure (29). 3,4-Dibromothiophene (686 mL, 6.2 mmol) and $Ni(dppp)Cl_2$ (177 mg, 0.33 mmol) were dissolved in distilled THF (35 mL). The 2.0 M solution of hexylmagnesiumbromide in diethyl ether (8 mL, 0.016 mmol) was added drop-wise under an argon atmosphere at 0°C. After the addition was completed the reaction was heated at 80°C overnight. The reaction was quenched with 1M HCl (50 mL) and extracted with dichloromethane (3 × 40 mL). The organic phase was dried with $MgSO_4$, filtered and evaporated to provide brownish oil. The product was purified on column chromatography (Silica/hexane) to obtain the desired product as colorless oil (509 mg, 33%). ^1H NMR (300 MHz, $CDCl_3$) δ 6.92 (s, 2H, A^2), 2.54 (t, $J = 7.8$, 4H, Hex^1), 1.71 – 1.61 (m, 4H, Hex^2), 1.47–1.30 (m, 12H, Hex^3–Hex^5), 0.94 (t, $J = 6.1$, 6H, Hex^6). ^{13}C NMR (101 MHz, $CDCl_3$) δ 142.08, 119.86, 31.75, 29.64, 29.29, 28.82, 22.64, 14.08. IR (DRIFT), cm^{-1} 2956 (s), 2963 (s), 2858 (s), 1466 (m), 1459 (m), 1378 (m), 1304 (w), 1174 (w), 1114 (w), 1080 (w), 868 (m), 836 (m), 783 (s), 725 (m), 679 (w). HRMS found m/z: 253.1984 $[M_+H]^+$, $C_{16}H_{29}S$ requires: 253.1985.

2,5-Bis(4,4,5,5-tetramethyl-1,3,2-dioxaborolane-2-yl)-3,4-dihexylthiophene, ***Hex$_2$ThBor$_2$***

Hex$_2$Th (509 mg; 2.016 mmol), catalyst $[Ir(OMe)(COD)]_2$ (20 mg, 0.03 mmol), and co-catalyst dtbpy (16 mg, 0,08 mmol) were dissolved in hexane (10 mL, stored over molecular sieve, bubbled with argon prior to use). HBor (1.25 mL; 8.6 mmol) was added under an argon atmosphere. The reaction mixture was stirred for 7 days at 45–50°C. The product was extracted with hexane (40 mL) and washed with water (3 × 40 mL), the organic layer was dried with $MgSO_4$ and evaporated to get the desired product as brownish oil (838 mg, 82%). ^1H NMR (400 MHz, $CDCl_3$) δ 2.80 (t, $J = 7.8$, 4H, Hex^1); 1.50–1.44 (m, 4H, Hex^2), 1.40–1.27 (m, 36H, Hex^3–Hex^5, B–*CH_3*), 0.90 (t, $J = 6.6$, 6H, Hex^6). ^{13}C NMR (101 MHz, $CDCl_3$) δ 154.06, 83.41, 32.28, 31.67, 29.46, 28.49, 24.75, 22.62, 14.12. IR (DRIFT), cm^{-1} 2977 (m), 2957 (m), 2929 (s), 2857 (w), 1529 (m), 1467 (m), 1371 (s), 1345 (s), 1309 (m), 1271 (m), 1214 (m), 1140 (s), 1097 (m), 1049 (m), 959 (m), 856 (s), 832 (w), 724 (w), 696 (m), 684 (m), 669 (m), 578 (w). HRMS found m/z: 527.3510 $[M_+Na]^+$, $C_{28}H_{50}O_4B_2NaS$ requires: 527.3508.

5,5″-Bis(2,2′:6′,2″-terpyridine-4′-yl)-3′,4′-dihexyl-2,2′:5′,2″-terthiophene, ***T34***

BrTh*tpy* (364 mg, 0.92 mmol), **Hex$_2$ThBor$_2$** (245 mg, 0.49 mmol) and K_2CO_3 (350 mg, 2.5 mmol) were dissolved in toluene and methanol (15 + 15 mL). The PEPPSI-IPr catalyst (10 mg) was added under an Argon atmosphere and the reaction mixture was heated to reflux for 4 hours. The solution was diluted with dichloromethane (30 mL) and washed with water (3 × 50 mL). The organic layer was dried with $MgSO_4$ and evaporated to get crude product. The product was purified on column chromatography (aluminum oxide/hexan+THF 3:2) to get the

product as orange solid (130 mg, 31%). ^{1}H NMR (600 MHz, *d8*-THF) δ 8.82–8.84 (m, 4H, A^6), 8.71–8.73 (m, 4H, A^3), 8.70 (s, 2H, B^3), 7.91 (td, $J = 7.63$, $J = 1.76$, 4H, A^4), 7.89 (d, $J = 3.52$, 2H, C^3), 7.38 – 7.41 (m, 4H, A^5), 7.36 (d, $J = 3.52$, 2H, C^4), 2.92–2.90 (m, 4H, Hex^1), 1.56–1.54 (m, 4H, Hex^2), 1,41–1,40 (m, 12H, Hex^3–Hex^5), 0.96–0.93 (m, 6H, Hex^6). ^{13}C NMR (151 MHz, *d8*-THF) δ 157.42, 156.87, 150.24, 143.85, 142.53, 142.03, 138.88, 137.71, 131.38, 128.26, 127.64, 125.04, 121.86, 117.31, 32.65, 31.69, 30.82, 30.62, 29.20, 14.63. IR (DRIFT), cm^{-1} 3060 (w), 3011 (w), 2926 (s), 2870 (m), 2854 (m), 1598 (m), 1583 (s), 1567 (s), 1466 (m), 1456 (m), 1400 (m), 1377 (w), 1364 (w), 1268 (w), 1219 (w), 1094 (m), 1088 (m), 1041 (w), 1008 (m), 879 (m), 788 (s), 741 (m), 729 (m), 659 (m). HRMS found *m/z*: 879.3330 $[M_+H]^+$, $C_{54}H_{51}N_6S_3$ requires: 879.3332.

Synthesis of Metallosupramolecular Polymers with PF_6^- Counterions

The α,ω-Bis(*tpy*) oligomers were transformed to corresponding metallosupramolecular polymers by adopting the procedure described by Winter (21). Briefly, a solution of zinc acetate (0.05 mmol) in N-methylpyrrolidone (NMP) (1 mL) was added to a solution of particular bis(*tpy*)dihexyloligothiophene (0.05 mmol) in NMP (5 mL) and the resulting mixture was stirred at 100°C under argon atmosphere for 12 hours. An excess of NH_4PF_6 (100 mg) was added to the hot solution and stirring was continued for 1 hour. Then the solution was poured into methanol (50 mL), and the resulting polymer was filtered off and washed with methanol (10 mL). Finally, the product was dried under vacuum at 40°C for 24 hours. The isolated polymer yield ranged from 52% to 79%.

Characterization

The ^{1}H and ^{13}C NMR spectra were recorded on a Bruker Avance 600 MHz, Varian ^{UNITY}INOVA 400 or Varian SYSTEM 300 instruments in d_8-THF, CD_2Cl_2, $CDCl_3$, or d_6-DMSO and referenced to the solvent signal: 7.25 ppm ($CDCl_3$), 5.32 ppm (CD_2Cl_2), 3.58 ppm (d_8-THF), or 2.50 ppm (d_6-DMSO) for ^{1}H and 77.0 ppm ($CDCl_3$), 53.84 ppm (CD_2Cl_2), or 67.57 ppm (d_8-THF) for ^{13}C spectra. Coupling constants, J (in Hz), were obtained by first-order analysis. Infrared spectra were recorded on a Thermo Nicolet 7600 FTIR spectrometer equipped with a Spectra Tech InspectIR Plus microspectroscopic accessory. The spectra were processed using Omnic (version 6) software. KBr-diluted samples and diffuse reflectance technique (DRIFT) (128 or more scans at resolution 4 cm^{-1}) were used. Raman spectra were recorded on a DXR Raman microscope (Thermo Scientific) using excitation at 780 nm (usual laser power at the sample 0.1 to 0.4 mW) and undiluted samples. UV/VIS spectra were recorded on a Shimadzu UV-2401PC using THF or DMSO solutions of prepared compounds. Photoluminescence spectra were measured on a Fluorolog 3-22 Jobin Yvon Spex instrument (Jobin Yvon Instruments S. A., Inc., USA) in THF solutions using four-window quartz cuvette (1 cm) or film deposited on highly oriented pyrolytic graphite (NT-MDT Co., Russia). The emission spectra were recorded with excitation wavelength, λ_{ex}, equal to the position of the absorption maximum of particular compound.Quantum yields, ϕ_F, of photoluminescence were determined by means of a comparison of the integrated spectrum of the compound in question with that of the standard: quinine sulfate diluted solution in 0.5 M H_2SO_4 ($\phi_F = 0.54$; $\lambda_{ex} = 380$ nm). Fluorescence decay was monitored with a FluoroHub single photon counting controller on a Fluorolog 3-22 Jobin Yvon Spex instrument using excitation at $\lambda_{ex} = 378$ nm for solutions and $\lambda_{ex} = 472$ nm for films. Cyclic voltammograms (CV) were recorded on a potentiostat UMμE Eco-Trend using the scanning rate of 137 mVs^{-1}, Saturated calomel reference electrode and acetonitrile solution of Bu_4NPF_6 (0.1 M) as the supporting electrolyte. Films were deposited by the drop-casting technique (from THF solution) on a carbon disc working electrode (diameter 1 mm).

UV/vis Study of Complexation

In a typical complexation experiment, a mixed solution containing Zn^{2+} ions ($2\cdot10^{-3}$ mol·dm^{-3}) and a measured oligomer ($2\cdot10^{-5}$ mol·dm^{-3}) in THF was step-wise added to a THF solution (2 mL) of the oligomer ($2\cdot10^{-5}$ mol·dm^{-3}) and the UV/vis absorption and the photoluminescence emission spectra were taken after each addition.

Calculation

The geometry of ground and excited states was optimized using the density functional theory (DFT), transition energies of absorption/emission were calculated by TD-DFT using optimized ground/excited state geometry. In all the computations, we used the Becke's three parameter functional with the non-local Lee-Yang-Parr correlation functional (B3LYP) with the standard 6-31G(d) basis set as implemented in Gaussian (30).

Results and Discussion

Two series of new well-defined oligomers with dihexyloligothiophene central block and *tpy* end-groups: α,ω-bis(*tpy*)dihexyloligothiophenes were prepared in order to examine the effect of hexyl side groups bonded to the central block at various positions on the properties of the oligomers and corresponding metallosupramolecular polymers. Abbreviations of names of bis(*tpy*) oligomers and their metallosupramolecular polymers used throughout this paper are as follows:

- **B** α,ω-bis(*tpy*)dimer with unsubstituted bithiophene central block
- **B14B** with hexyl groups attached at positions **1** and **4** of the central block (for numbering the central block see Fig. 1.)
- **B23** **B** with hexyl groups attached at positions **2** and **3** of the central block
- **T** α,ω-bis(*tpy*)trimer with unsubstituted terthiophene central block
- **T16** **T** with hexyl groups attached at positions **1** and **6** of the central block
- **T25** **T** with hexyl groups attached at positions **2** and **5** of the central block
- **T34** **T** with hexyl groups attached at positions **3** and **4** of the central block

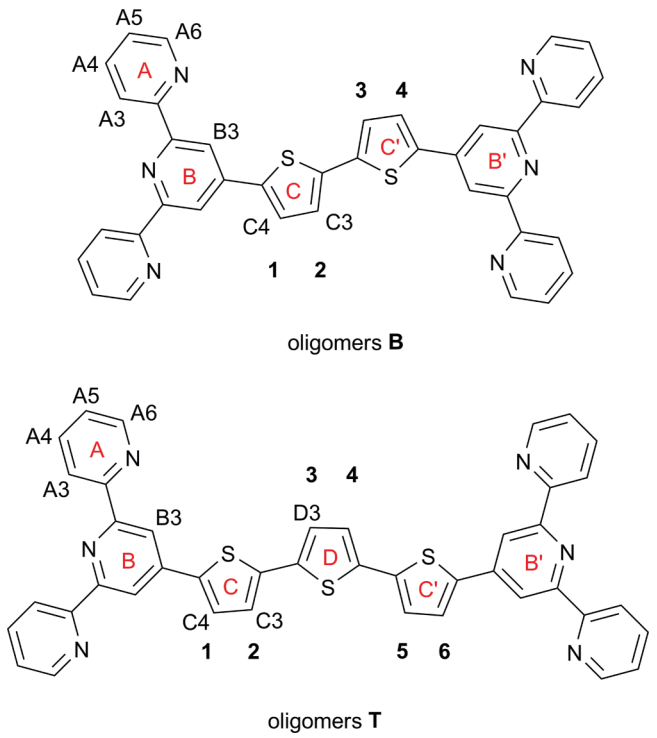

Fig. 1. Numbering of the central block positions of bis(*tpy*) oligomers (in bold) and ring carbons for the NMR spectra assignment (A3 to D3). 83 x 94 mm (600 x 600 DPI).

PB, PB14, PB23, PT, PT16, PT25, and **PT34** – metallosupramolecular polymer composed of chains containing the corresponding oligomer molecules connected with Zn^{2+} ion couplers.

Preparation and Basic Characterizations of Oligomers and Polymers

Unlike the unsubstituted and twice methyl-substituted bis(*tpy*)oligothiophenes that we prepared (25) by the procedure based on Kröhnke methodology (31), the herein described oligomers of the **B** and **T** series were prepared from commercially available Br*tpy* using synthesis paths involving two subsequent Suzuki-Miyaura couplings (see Scheme 1).

The preparation of compounds **B14** and **T16** started with coupling of Br*tpy* and borolane of 3-hexylthiophene to obtain **HexTh*tpy*** which was brominated to give **BrHexTh*tpy*** that was utterly reacted with bisborolane to give **B14**, or thiophene-2,5-diboronic acid to give **T16**.

Preparations of **B23** and **T25** started with syntheses of the corresponding central blocks, continued with a direct α,ω-bis-borylation of these blocks by the Ir-catalyzed reaction with 4,4,5,5-tetramethyl-1,3,2-dioxaborolane (32), and was completed by Suzuki-Miyaura coupling of the obtained bis(borolane)s with Br*tpy*. This reaction pathway was much more effective than the alternative approach: bromination of the central block followed by coupling of the brominated block with *tpy*-4′-borolane. The latter coupling namely gave the desired **B** or **T** type compound in a yield below 10 %. On the other hand, the central dihexyloligothiophene blocks as well as their bis(borolane)s were obtained in good yields and could be directly used in coupling with Br*tpy* without any purification by column chromatography, at which, moreover, a decomposition of bis(borolane)s on silica was observed.

A synthesis of **T34** started with preparation of bis(borolane) of 3,4-dihexylthiophene, which was then allowed to react with BrTh*tpy* prepared using the earlier applied procedure (27). The isolated yield in the last coupling step was gradually increased from 14% to 63% by improving this process.

The **B** and **T** type oligomers were assembled to linear metallosupramolecular polymers in their reactions with the stoichiometric equivalents of zinc acetate in *N*-methylpyrrolidinone. An excess of KPF_6 was added at the end of assembling process to exchange CH_3COO^- with PF_6^- counterions. Addtionally, the complexation of oligomers with Zn^{2+} ions was studied in dilute THF solutions under monitoring by the UV/vis and luminescence spectroscopy (see further).

Assignment of the ^{1}H NMR signals of bis(*tpy*) oligomers is summarized in Table 1. The ^{1}H NMR spectra of isolated polymers dissolved in d_6-DMSO (see example in Supplementary Information, Fig. S1) were free of signals of the corresponding oligomers; however, the number of observed signals was always higher than the number expected for a pure polymer. This made a reliable assignment of ^{1}H NMR signals difficult; a conclusive assignment was obtained only for **PB23** (see Table 1). The other signals most probably originated from end-groups and near-neighboring units, which indicates rather low degree of polymerization of MSP chains in DMSO solutions. For example, the degree of polymerization of **PB23** in DMSO solution (conc. equal to 15 mg/mL) used for the measurement of the ^{1}H NMR spectrum was estimated to be ca 25 assuming that the low-intensity signals at 8.9 and 9.0 ppm belongs to *tpy* end groups coordinated to zinc ions. Nevertheless, molar mass in solution is not an important characterstics of a dynamer as it changes with the concentration of the solution.

The IR spectra of bis(*tpy*)oligothiophenes are similar to each other and they resemble the spectrum of terpyridine rather than the spectrum of bithiophene or terthiophene (Supplementary Information, Figs. S2 and S3). Nevertheless, certain differences in the spectra are apparent. The most of the uniformity deviating are spectra of oligomers **B14** and **T16** with hexyl groups oriented toward *tpy* end-groups. Both these spectra exhibit (i) intense band at ca. 1265 cm^{-1}, (ii) strong, very broad band ranging from 1150 to 970 cm^{-1}, in which ca. 10 bands resolved in the spectra of other oligomers are merged, and (iii) significant broadening of a strong band of deformation modes at about 790 cm^{-1}. Spectra of other oligomers show only minor differences that, however, allow a reliable fingerprint identification of a given oligomer.

The assembly of bis(*tpy*)oligothiophenes into corresponding MSPs is displayed in IR spectra by a substantial change in the bands of stretching modes of *tpy* groups (they undergo the anti-to-syn conformational transition of nitrogen atoms during coordination to Zn^{2+} ions) and an overall decrease in the spectral resolution. Strong bands that occurred at *ca.* 842 cm^{-1} as well as medium-intensity bands at 558 cm^{-1} belong to PF_6^- counterions (33).

Raman spectra of solid oligomers as well as their MSPs were measured on a dispersion Raman microscope in the

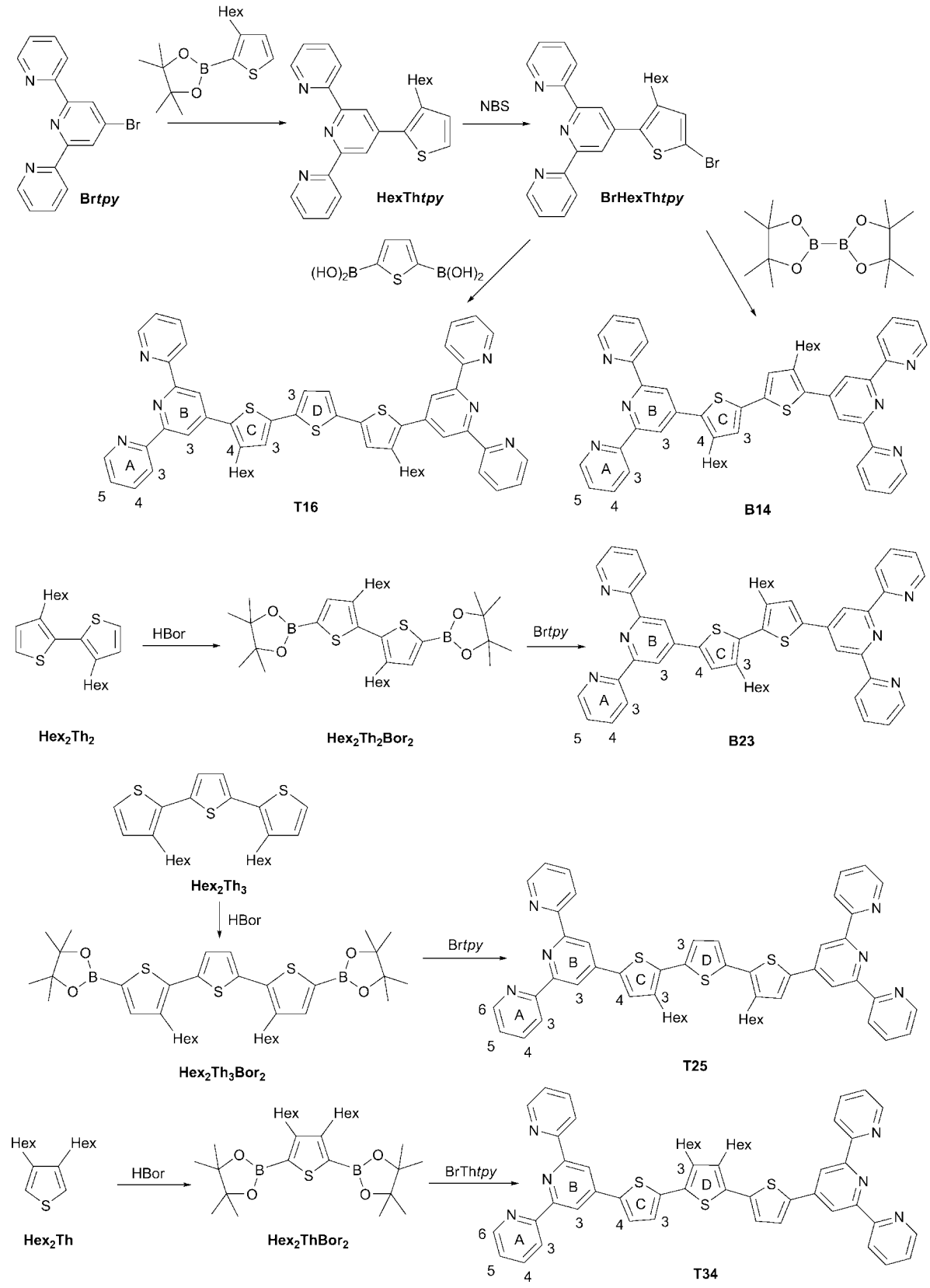

Scheme 1. Preparation of α,ω-bis(tpy)oligothiophenes. 218 x 304 mm (600 x 600 DPI).

Table 1. H NMR shifts of the prepared oligomers (in d_8-THF) and polymer **PB23** (in d_6-DMSO)

	A3	A4	A5	A6	B3	C3	C4	D3
B	8.74 – 8.67	7.94 – 7.88	7.39	8.74 – 8.67	8.85	7.88	7.53	/
B14	8.66	7.88	7.38 – 7.33	8.73	8.63	7.18	/	/
B23	8.72 – 8.70	7.91	7.40 – 7.37	8.72 – 8.70	8.83	/	7.85	/
T	8.73 – 8.69	7.95 – 7.88	7.39	8.73 – 8.69	8.83	7.87	7.43	7.41
T16	8.66	7.88	7.38 – 7.34	8.73	8.62	7.15	/	7.17
T25	8.73 – 8.69	7.90	7.41 – 7.37	8.73 – 8.69	8.82	/	7.81	7.36
T34	8.73 – 8.71	7.91	7.41 – 7.38	8.84 – 8.82	8.70	7.89	7.36	/
PB23	9.08	8.27	7.49	7.97	9.20	/	8.67-8.59	/

off-resonance mode using a low energy power at the sample (0.1 to 1 mW). FT Raman spectra were not measurable due to too high luminescence of the samples. Unlike the IR spectra, in the Raman spectra of bis(*tpy*)oligothiophenes dominate the bands of central oligothiophene blocks, in particular the bands of symmetric stretching modes of C=C bonds of thiophene rings ($\nu_{C=C}$). These bands occur in the region from 1440 to 1490 cm^{-1} and their position and fine structure are quite sensitive to the main structure parameters of central oligothiophene blocks: the length of central oligothiophene block and the presence and position of substituents (see Supplementary Information, Figs. S4 and S5). This allows a simple and reliable spectroscopic identification of both a particular oligomer and its MSP. The medium-intensity bands of antisymmetric stretching modes (1555 cm^{-1} for bithiophene and 1529 cm^{-1} for terthiophene) are very weak or almost absent in the Raman spectra of bis(*tpy*)oligothiophenes. The *tpy* end-groups contribute to the Raman spectra of bis(*tpy*)oligothiophenes mainly by weak bands of pyridine stretching modes occurring at *ca.* 1565 – 1610 cm^{-1} and the band of pyridine ring-breathing mode at 995 cm^{-1}.

Unbound oligomers mostly show a single broad $\nu_{C=C}$ band centered at a wavelength from 1467 to 1477 cm^{-1}. Exceptions are oligomers **B23** and **T25** exhibiting the $\nu_{C=C}$ band at lowered frequency: 1458 and 1460 cm^{-1}, respectively, and, in addition, a clearly resolved band at 1434 and 1440 cm^{-1}, respectively. A comparison of structures of these oligomers indicates that these spectral features are typical of (4-hexylthiophene-2,5-yl)terpyridine end-grouping. The other observed weaker Raman bands should be contributed by vibrational modes of both *tpy* and thiophene units. A reliable assignment of these bands requires a more detailed spectroscopic study that is beyond the scope of this paper.

Transformation of oligomers into MSPs appeared in the Raman spectra mainly by splitting the $\nu_{C=C}$ band into two bands or a band with shoulder. One of the new bands, that of higher intensity, occurs at a lower frequency while the second band (shoulder) at a higher frequency compared to the $\nu_{C=C}$ band of the parent oligomer. Same as above, spectra of polymers **PB23** and **PT25** differ from spectra of others MSPs and, in addition, from each other. **PB23** exhibits two strong bands of comparable intensity, both shifted to a higher frequency (1460 and 1487 cm^{-1}) compared to the bands of **B23**. Polymer **PT25** shows a broad $\nu_{C=C}$ band in the region from *ca.* 1490 to 1420 cm^{-1} with distinct maximum at 1440 cm^{-1} and at least five shoulders. The difference between spectra of **PB23** and **PT25** indicates much higher extent of delocalization of electrons and thus higher coplanarity of rings in **PT25** chains compared to **PB23** chains. Actually, such outcome can be expected regarding the lowered steric hindrances in central blocks of **PT25** chains; however, it is surprising and interesting that this difference in the steric effects is not manifested in the Raman spectra of the oligomers.

UV/vis Spectroscopy Properties of Oligomers and Polymers

UV/vis spectra of oligomers taken from THF solutions each exhibited two absorption bands: (i) the structure-independent band centered at about 280 nm, and (ii) the structure-dependent band located at a wavelength, λ_{abs}, from 340 to 390 nm for the **B** type and from 400 to 430 nm for the **T** type oligomers (Table 2). The band ad (i) was typical of the spectra of terpyridine and 4′-substituted terpyridines (26). DFT calculations showed that this band is contributed with the π - π^* and n - π^* transitions in *tpy* end-groups (HOMO-1 orbital, Fig. 2). The structure dependent band was dominantly contributed with the transitions in the central oligothiophene block. The **T** type oligomers with longer central blocks obviously showed a higher λ_{abs} compared to the **B** type oligomers.

The DFT calculations further proved the π-nature of both HOMO and LUMO as well as localization of these orbitals mainly on the central oligothiophene block and, partly, on the adjacent (i.e., middle) pyridine rings of *tpy* end-groups (Fig. 2). In HOMO, the main-chain intra-ring C=C bonds are π-bonding and have an alternating phase with respect to adjacent C=C bonds. In LUMO, the intra-ring C=C bonds are π-antibonding and the inter-ring C^{β}-$C^{\beta'}$ bonds are π-bonding, which means that the central-block rings acquire the quinoid-like electronic configuration in the excited oligomer molecule.

Regarding the DFT-calculated geometry of oligomer molecules (Table 3) it is evident that an increase in the thiophene-thiophene torsion angle in the central block decreases the λ_{abs} value more profoundly than an increase in the thiophene-*tpy* torsion angle. A comparison of λ_{abs} values of oligomers of the same family (**B** or **T**) proves that steric hindrances prevail over electronic effects of hexyl side groups. The highest steric hindrances are present in molecules of **B23**, in the spectrum of which the HOMO-LUMO band is reduced to a small satellite peak at 339 nm on the *tpy* band. In addition, the molar absorption coefficient of the *tpy* band (~280 nm) is twice the coefficient observed for 4′-(2-thienyl)terpyridine (26). Obviously, the high

Table 2. Spectroscopic characteristics of prepared oligomers and polymers

	λ_{abs}, nm			λ_F, nm								
	THF	*DFT*	film	THF	*DFT*	film	ϕ^{THF} %	$I^{film}.10^{-6}$ count/s	$\nu_S{}^{THF}$ cm^{-1}	$\nu_S{}^{film}$ cm^{-1}	$\tau_F{}^{THF}$ ns	$\tau_F{}^{film}$ ns
B	395	*420*	390 415_{sh}	444 469	*482*	674	33	0.49	2800 3060_{DFT}	10800 9260_{sh}	0.53	0.63 (31%) 2.04 (55%) 6.65 (13%)
PB	443 460_{sh}	/	436 465_{sh}	562	/	600	/	0.59	4780 3950_{sh}	6270 4840_{sh}		0.06 (75%) 0.38 (21%) 1.90 (4%)
B14	370	*400*	~380	448 470	*482*	611	10	0.29	4700 4250_{DFT}	9950	0.03 (19%) 0.24 (73%) 0.90 (8%)	0.07 (68%) 0.49 (24%) 2.02 (9%)
PB14	440	/	455	560	/	570	/	0.34	4870	4430		0.05 (63%) 0.57 (29%) 3.38 (7%)
B23	339	*363*	400 to 420 450_{sh}	450 470	*486*	550	3	0.19	7280 6970_{DFT}	6820 to 5630 4040_{sh}	0.003 (100%)	0.61 (49%) 1.59 (45%) 7.61 (6%)
PB23	390	/	391	535	/	545	/	4.70	6950	7230		0.31 (40%) 1.14 (53%) 5.40 (7%)
T	420	*464*	426	484 516	*544*	765	43	0.07	3150 3170_{DFT}	10400	0.57 (100%)	0.17 (52%) 0.62 (42%) 2.73 (5%)
PT	479	/	469	635	/	686	/	0.12	5130	6750		0.19 (35%) 0.88 (50%) 2.57 (15%)
T16	409	455	420	487 515	539	685	20	0.12	3920 3430_{DFT}	9210	0.005 (98%) 0.5 (2%)	0.01 (98%) 0.63 (1%) 11.4 (1%)
PT16	466	/	465	~ 650	/	595	/	0.06	6350	4700		0.14 (63%) 0.63 (31%) 4.17 (6%)

(*Continued*)

Table 2. (Continued)

	λ_{abs}, nm			λ_F, nm								
	THF	*DFT*	film	THF	*DFT*	film	ϕ^{THF} %	$I^{film}.10^{-6}$ count/s	$\nu_S{}^{THF}$ cm^{-1}	$\nu_S{}^{film}$ cm^{-1}	$\tau_F{}^{THF}$ ns	$\tau_F{}^{film}$ ns
T25	403	*446*	428	494 523	*555*	612	16	0.58	4570 4400 $_{DFT}$	6970	0.01 (36%) 0.41 (56%) 0.61 (8%)	0.17 (20%) 0.85 (55%) 2.51 (25%)
PT25	474	/	500	635	/	660	/	0.78	5350	4850		0.13 (42%) 0.79 (41%) 3.11 (17%)
T3	404	*437*	455	492 522	*548*	672	17	0.69	4430 4640 $_{DFT}$	7100	0.02 (10%) 0.46 (61%) 0.54 (28%)	0.19 (48%) 0.97 (39%) 3.90 (14%)
PT34	480	/	495	620	/	640	/	1.56	4700	4580		0.22 (40%) 1.13 (46%) 3.97 (14%)

λ_{abs} and λ_F, the absorption and photoluminescence emission maximum in THF solution; DFT, calculated and in solid film; ϕ_F, photoluminescence quantum yield in THF solution relative to quinine sulfate in 0.5 M H_2SO_4. The excitation wavelength was 380 nm for all samples. I^{film}, count per second in the emission maximum (solid film); $\nu_S{}^{THF}$ and $\nu_S{}^{film}$, stokes shift in THF solution and in solid film; $\tau_F{}^{THF}$ and $\tau_F{}^{film}$, the lifetime of excited states in THF solution and in solid film. Footnote $_{sh}$, spectral shoulder position; $_{DFT}$, DFT calculated values.

Table 3. Calculated geometry of the B and T type molecules; δ_{BC} . . . . $\delta_{C'B'}$ are dihedral angles between planes of neighboring main-chain rings given in the subscript (for ring labels see Fig. 1)

	Ground State				Excited State			
	δ_{BC}	$\delta_{CC'}$		$\delta_{C'B'}$	δ_{BC}	$\delta_{CC'}$		$\delta_{C'B'}$
B	14.50	0.13		14.50	0.00	0.00		0.00
B14	43.86	0.54		42.65	19.93	0.44		22.49
B23	18.83	67.55		18.83	0.04	0.05		0.02
	δ_{BC}	δ_{CD}	$\delta_{DC'}$	$\delta_{C'B'}$	δ_{BC}	δ_{CD}	$\delta_{DC'}$	$\delta_{C'B'}$
T	16.33	13.97	13.80	16.34	0.00	0.01	0.01	0.00
T16	43.36	8.33	7.90	44.66	24.50	2.60	2.66	26.78
T25	17.70	26.03	28.73	17.71	0.01	0.00	0.01	0.01
T34	14.60	37.30	36.69	17.88	0.80	2.70	1.58	0.75

torsion angle between thiophene rings (ca 68°) formally makes a free (dissolved) **B23** molecule a system composed of two, rather weakly electronically interconnected 4′-(2-thienyl)*tpy* subunits.

A UV/vis spectrum measured on a solid poly- or oligothiophene (packed molecules) usually shows a value of λ_{abs} higher than a spectrum taken from a solution (single molecules) due to increased coplanarity of main-chain rings in the solid state (34–36). However, our oligomers exhibited a wide variety of shifts of λ_{abs} when going from THF solution to the solid state. The simplest oligomer: **B** showed a blue shift: $\Delta\lambda_{abs} = -5$ nm (shoulders are not considered) while the other oligomers a red shift increasing in the order: **T** (+ 6 nm) ≤ **B14** and **T16** (+ 10 nm) < **T25** (+ 25 nm) ≪ **T34** (+ 51 nm) < **B23** (+ 61 nm). Thus, the oligomers with low-hindered rotation around thiophene-thiophene bonds exhibited a small $\Delta\lambda_{abs}$ (from -5 to + 10 nm) whereas those with the thiophene-thiophene rotation hindered by hexyl groups show a higher shift: $\Delta\lambda_{abs}$ up to *ca.* 60 nm. Small values of $\Delta\lambda_{abs}$ prove that the conformational freedom of central blocks of molecules **B, T, B14,** and **T16** has only little changed upon packing dissolved molecules into a film. On the other hand, the higher values of $\Delta\lambda_{abs}$ observed for **T25, T34,** and **B23** indicate a considerable increase in the coplanarity of backbone rings upon packing these molecules into a film. This reduction of conformational freedom in the solid state should be ascribed to the effect of attached hexyl side-groups rather than to the π-π aromatic stacking interactions.

The last outcome is supported by the substantially different conformations of free and packed-in-crystal **B23** molecules. It is worth noting here that **B23** is the only oligomer that was crystallized from a THF solution and gave macroscopic yellow needles (melting point 227°C) suitable for X-ray analysis. The calculated lowest-energy conformation of a free **B23** molecule shows the planarity of *tpy* end-groups, low torsion angle of thiophene-*tpy* bonds (19°), closely spaced hexyl side-groups and a high thiophene-thiophene torsion angle (68°). The crystal structure of **B23** (Fig. 3) also showed coplanarity of pyridine rings in *tpy* end-groups and only slightly twisted thiophene-*tpy* bonds (20°), but (i) anti conformation of sulfur atoms as well as hexyl groups of the central block, (ii) layered packing of **B23** molecules, which suggests the presence of stacking interactions, and (iii) proximity of ends of hexyl groups to pyridine rings of neighboring molecules, which indicates attractive interactions between these moieties. Thus, partially anchored hexyl groups should attenuate the amplitude of thermal twisting of thiophene rings and increase the extent of delocalization of π-electrons. This fact obviously should result in a significant red shift of λ_{abs} when going from a solution to the solid state. The DFT calculations for a free **B23** molecule in the planar conformation observed in the crystal provided λ_{abs} red shifted *ca.* 50 nm compared to λ_{abs} of a free twisted **B23** molecule, which corresponded well with the difference $\Delta\lambda_{abs} = 61$ nm observed experimentally.

Edges of UV/vis bands of oligomers were examined through voltammetric measurements of redox properties of oligomers (Supplementary Information, Fig. S6). Several redox cycles were recorded for each oligomer. The redox wave amplitude decreased with the increasing cycle-order number. All oligomers exhibited a reversible reduction wave: the **B** type at approximately -1.72 V; the **T** type at -1.63 to -1.69 V. Oxidation wave was clearly observed only for the **T** type oligomers at 0.92 to 0.96 V. The obtained band-gap energy values range from 2.58 to 2.62 eV, which correspond to wavelengths from 474 to 481 nm that are in accord with the cut-off wavelengths of the HOMO-LUMO bands of the **T** type oligomers.

Complexation of oligomers with Zn^{2+} ions was spectroscopically studied in THF using a series of 13 mixed solutions of the oligomer ($2\cdot10^{-5}$ M) and Zn^{2+} ions (mole ratio Zn/oligomer varied from 0 to 3, ClO_4^- counterions) for each oligomer. The UV/vis and luminescence spectra of each solution were measured (Figs. 4 and 5). Changes in the UV/vis spectra caused by the gradual increase in the Zn/olig ratio were characterized by the attenuation of absorption bands of free oligomer molecules and occurrence of new bands pertaining to formed polymer chains. The changes in the region up to 350 nm: (i) attenuation of the band of transitions in tpy groups together with the band shift to ca. 288 nm, and (ii) occurrence of a new band at 330 to 340 nm and an isosbestic point at about 310 nm, resemble the changes observed earlier for the complexation of unsubstituted terpyridine and mono-*tpy* compounds with Zn^{2+} or Fe^{2+} ions (26). Hence, these changes are characteristic of the coordination of *tpy* groups to the metal ions. Atypical spectral changes observed during the complexation of **B23** are obviously because the HOMO-LUMO band of **B23** occurs at 339 nm and thus its

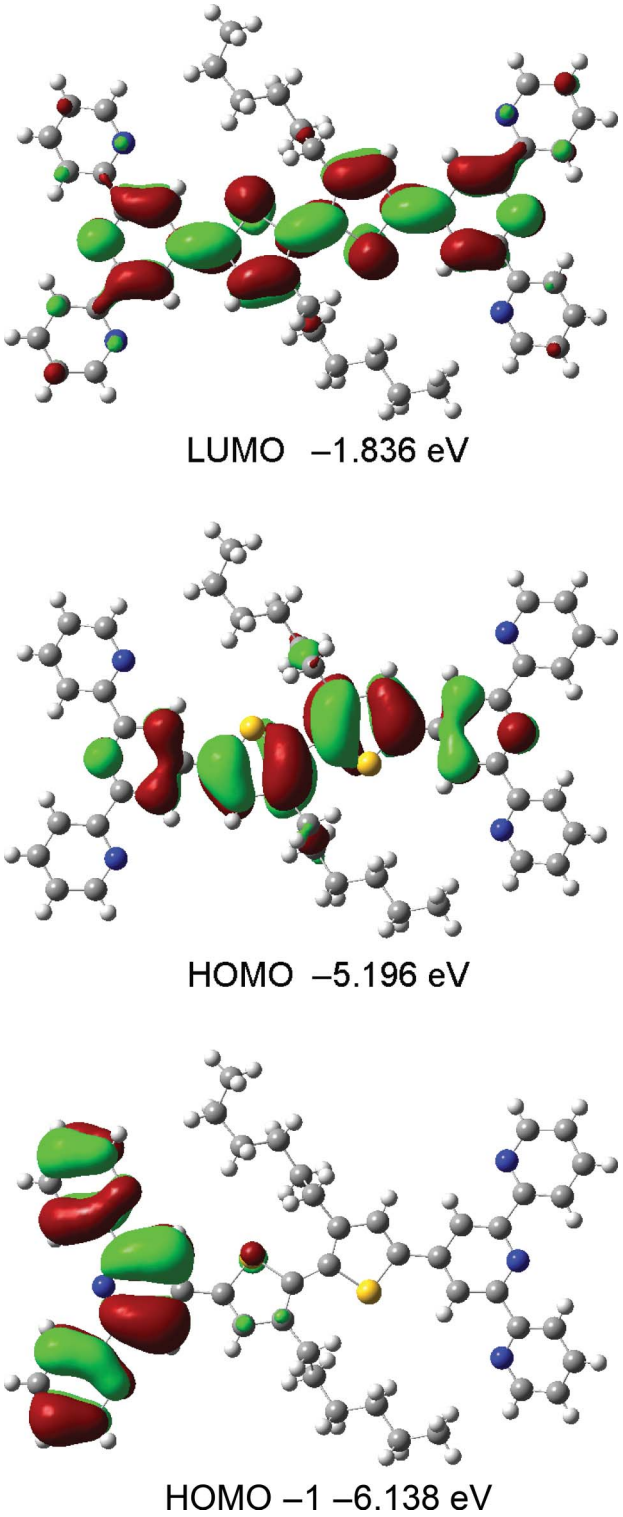

Fig. 2. Electronic density contours for LUMO, HOMO, and HOMO-1 of B23 obtained by DFT calculations using X-ray crystal structure. 62 x 150 mm (300 x 300 DPI).

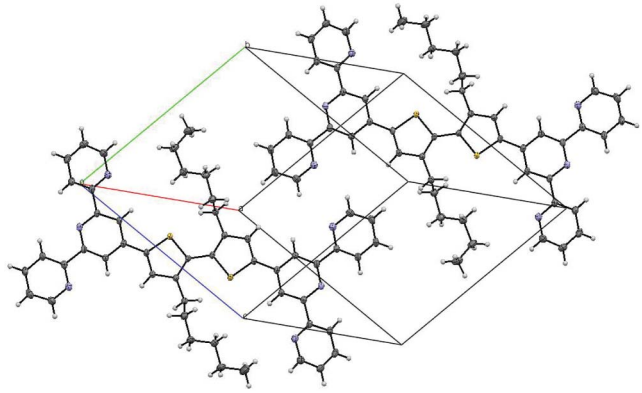

Fig. 3. X-ray crystal structure and molecular packing of B23 in the crystal lattice. Ellipsoids are plotted at 50% probability level. Crystal data at 150 K: $C_{50}H_{48}N_6S_2$, yellow crystalline needles, triclinic space group P 1, a = 12.0931(3) Å, b = 13.3397(3) Å, c = 14.2693(4) Å, V = 2015.42 Å3, α = 73.2800(10)°, β = 71.1120(10)°, γ = 70.9350(10)°, Z = 2, Z' = 0, R-Factor = 3.97%. For the CIF file see Supporting Information. 50 x 31 mm (300 x 300 DPI).

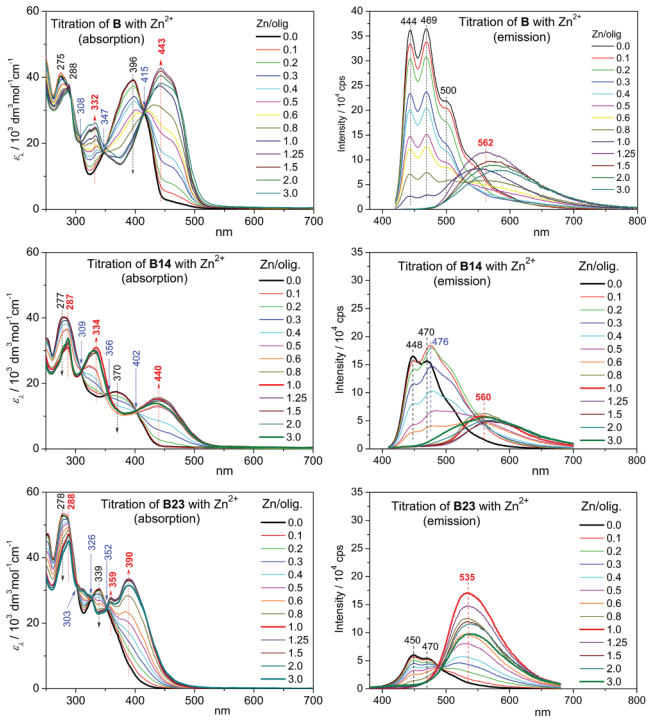

Fig. 4. Changes in UV/vis (left) and photoluminescence (right) spectra accompanied titrations of B oligomers with Zn 2+ ions. Initial oligomer concentration 2·10–5 mol·dm -3; THF, room temperature. 178 x 198 mm (300 x 300 DPI).

attenuation compensates a growth of the band of coordinated *tpy* groups.

Spectral changes observed in the region above 350 nm are characteristic of the central blocks. Those are: (i) attenuation of the HOMO-LUMO band of free oligomer molecules, (ii) development of a new, approximately ca. 70 nm red shifted band that pertains to the HOMO-LUMO transitions in polymeric chains, and (iii) occurrence of two additional isosbestic points, the first one at about 355 nm and another one in the region from 400 to 435 nm depending on the central block constitution. The

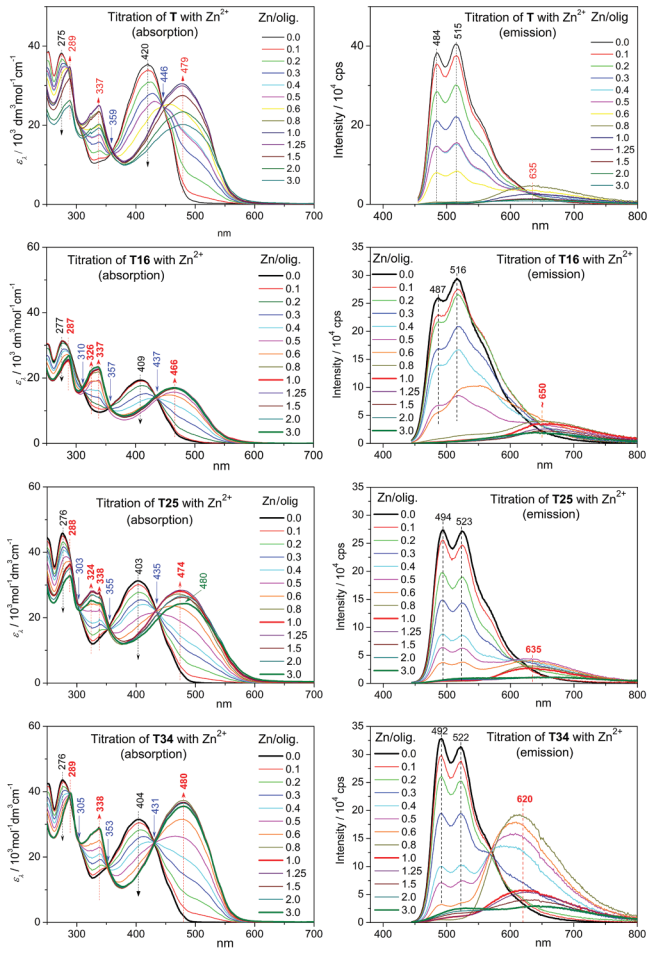

Fig. 5. Changes in UV/vis (left) and photoluminescence (right) spectra accompanied titrations of T oligomers with Zn 2+ ions. Initial oligomer concentration 2·10–5 mol·dm -3; THF, room temperature. 237 x 352 mm (300 x 300 DPI).

presence of isosbestic points proves that there are equilibriums involving a limited number of spectroscopically distinct species in studied systems, which is in accord with the transformation of oligomer molecules to supramolecular chains. An atypical behavior observed for **B23**, i.e., remarkably blue-shifted positions of the HOMO-LUMO band and both additional isosbestic points, should be ascribed to the high torsion angle between thiophene rings, which makes the delocalization of electrons within bithiophene central block difficult.

The formed metallosupramolecular polymers exhibited a low constitutional dynamics in THF solutions indicated by a slight shift of the absorption maximum at over-stoichiometric Zn/oligomer ratios. If an already prepared metallo-supramolecular polymer is dissolved in DMSO, it exhibits lower λ_{abs} compared to its solution in THF. It can be, at the first look, ascribed to a solvatochromic effect. However, if we would like to determine the molar absorption coefficient of the polymer in DMSO, we immediately find that it is not so, because λ_{max} value continuously decreases with increasing dilution of the polymer solution (see examples in Fig. 6). Such changes indicate equilibrium depolymerization of conjugated supramolecular chains and thus prove the reversibility of assembling process in DMSO—a ground of the constitutional dynamics. In addition, this observation indicates significant solvent dependence of complexation constants.

Photoluminescence Properties of Oligomers and Polymers

Photoluminescence spectra of oligomers dissolved in THF show bimodal emission bands (Figs. 4 and 5): the **B** type oligomers in the blue region (maxima/shoulders at λ_F = 441–449 nm and 466–469 nm) whereas the **T** type oligomers in the green region (λ_F = 481–493 nm and 511–524 nm) (Table 2). The quantum yields of photoluminescence, ϕ^{THF}, were found to be higher (i) for the **T** type compared to the **B** type oligomers, and (ii) for oligomers with unsubstituted compared to those with substituted central blocks (Table 2). This proves that the attached hexyl groups facilitated a non-radiative decay of excited states. The time-resolved luminescence spectra showed the fastest fluorescence decay for **B23** (τ_{THF} = 3 ps, 100%) and **T16** (τ_{THF} = 5 ps, 98%). Surprisingly, these oligomers differ in both the central block length and the orientation of hexyl groups with respect to the neighboring *tpy* end-groups.

Unlike the photoluminescence spectra of dissolved oligomers (Fig. 5), the spectra of oligomer films (Fig. 7) showed unimodal bands and rather wide interval of λ_F values within each series: 550 to 674 nm for the **B** type and 612 to 765 nm for the **T** type oligomers. The solid-state emission bands are red shifted about $\Delta\lambda_F$ from *ca.* 90 nm (**B23** and **T25**) to 250 nm (for **T**) compared to the corresponding emission bands observed in solution spectra. The time-resolved spectra showed the three-component fluorescence decay for all solid oligomers. The fastest decay exhibited **T16** (τ_{film} = 10 ps, 98%), which also showed next to the fastest decay in solution. In contrast, **B23** that showed the fastest fluorescence decay in solution, surprisingly showed one the slowest decays in the solid state (τ_{film} = 610 ps, 49%; and 1 590 ps, 45%). This is undoubtedly caused by significantly increased planarity of **B23** molecules packed in a film.

Complexation of oligomers with Zn^{2+} ions to MSPs in THF solutions resulted in a red shift (approximately 100–150 nm)

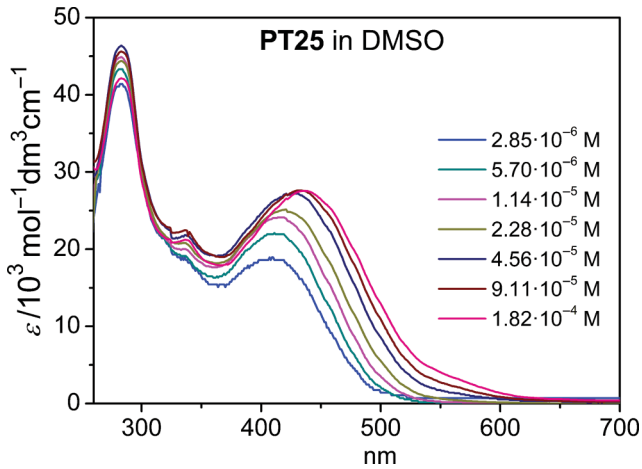

Fig. 6. Dependence of UV/vis spectra on concentration of PT25 in DMSO. 57 x 41 mm (600 x 600 DPI).

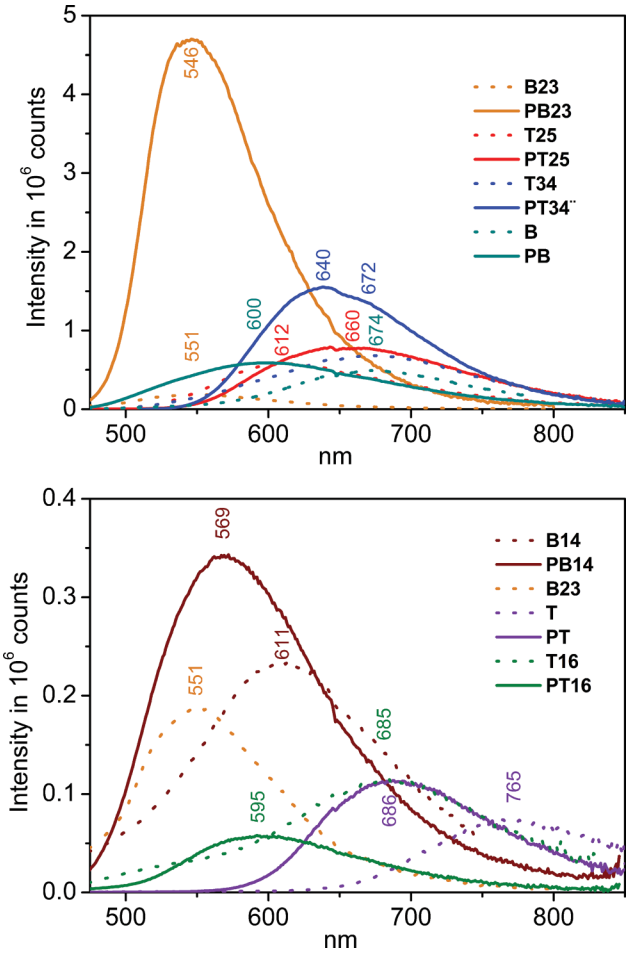

Fig. 7. Photoluminescence spectra of the oligomer and polymer (with Zn(PF 6)2) films. 118 x 174 mm (600 x 600 DPI).

and attenuation of the emission band intensity (Figs. 4 and 5). This indicates increased efficiency of the non-radiative decay of excited states in MSPs compared to free oligomers, which obviously is due to the increased extent of the delocalization of electrons along polymer chains. It is worth mentioning here that a complexation of mono-*tpy* compounds with Zn^{2+} ions is accompanied by just the opposite change, an increase in the photoluminescence intensity of the system (26). However, similar change we purely observed only at the complexation of **B23**. This indicates that, in solution, even enchained **B23** units behave as being composed of two, electronically rather weakly communicating thienyl-*tpy* subunits, as we already concluded from the UV/vis spectra of free oligomer.

The solid-state photoluminescence spectra of polymers (Fig. 7) showed unimodal emission bands with maxima red shifted about $\Delta\lambda_F$ ranging from *ca.* 10 nm (**PB14, PB23**) to 50 nm (**PT**) compared to the bands in spectra taken from solutions. A large exception was observed for **PT16** that reproducibly showed a high blue shift: $\Delta\lambda_F = -67$ nm.

Another exception was seen comparing the emission bands of solid oligomers and polymers (Fig. 7, Table 2). A blue shift about $\Delta\lambda_F$ ranging from – 6 nm (observed for transformation **B23** → **PB23**) to – 90 nm (**T16** → **PT16**) was typically observed when going from an oligomer to the corresponding polymer. However, the system **T25** → **PT25** has reproducibly exhibited the red shift: $\Delta\lambda_F = +38$ nm. On the other hand, exclusively red shift, without any exception was observed when comparing the spectra taken from solutions: $\Delta\lambda_F$ have ranged from + 85 nm (**B23** → **PB23**) to + 160 nm (**T16** → **PT16**). It is very interesting, if not surprising, that the system **T16** → **PT16** shows the highest red shift (+160 nm) for the solution spectra but the highest blue shift (– 90 nm) for the solid-state spectra.

The observed apparent discrepancies among emission spectra should be analyzed in the context with absorption spectra, taking into account that the position of emission band was strongly affected by the rotational-vibrational relaxation of each excited molecule prior to the photon emission. The extent of this relaxation was quantified by Stokes shift, $\Delta\nu_S$ (typical unit cm^{-1}), that corresponds to the energy difference between maxima of the absorption and emission bands pertaining to transitions between the same electronic levels. The relaxation of here studied molecules consists in their transitions from the "benzenoid" to "quinoid" conformations/configurations; the former one being characteristic of the ground state while the latter one of the excited state.

Values of Stokes shift calculated from spectral data as well as those obtained from DFT calculations are summarized in Table 2. As can be seen, the experimental values of $\Delta\nu_S$ found for dissolved oligomers are in good agreement with those obtained from DFT calculations. Dissolved polymers show $\Delta\nu_S = 5\,000 \pm 300$ cm^{-1}, except for **PB23** (6 950 cm^{-1}) and **PT16** ($\sim$ 6 000 cm^{-1}). The Stokes shift obtained for **PT16** is slightly biased by the weakness and flatness of the luminescence band. However, the value found for **PB23** is reliable, and it shows that the relaxation of an excited **PB23** molecule into quinoidal conformation requires the highest change in the thiophene-thiophene torsion angle of all studied polymers.

Solid oligomers show a good correlation between the Stokes shift and molecular structure:

$\Delta\nu_S \cong 10\,600 \pm 200$ cm^{-1} for **B** and **T** – no hexyl groups; low-twisted thiophene-thiophene as well as thiophene-*tpy* bond(s);

$\Delta\nu_S \cong 9600 \pm 400$ cm^{-1} for **B14** and **T16** – low-twisted thiophene-thiophene bond(s); high-twisted thiophene-*tpy* bond(s);

$\Delta\nu_S \cong 7000 \pm 200$ cm^{-1} for (**B23**), **T25,** and **T34** – high-twisted thiophene-thiophene bond(s); low-twisted thiophene-*tpy* bond(s).

As to the solid **B23**, its absorption band is not smooth but shows two pronounced shoulders located at *ca.* 420 and 450 nm, which indicates the presence of domains containing molecules of increased planarity in a film of **B23** (see the aforementioned crystal structure of **B23**). The Stokes shift corresponding to the shoulder at 450 nm is only 4 040 cm^{-1}, which indicates lowered extent of relaxation of excited molecule to acquire the quinoidal form.

The solid-state spectra of polymers provided the following Stokes shifts: $\Delta\nu_S \cong 6\,500 \pm 250$ cm^{-1} for **PB** and **PT**, and $\Delta\nu_S \cong 4\,600 \pm 250$ cm^{-1} for the other polymers. Again, an exception is **PB23** ($\Delta\nu_S = 7\,260$ cm^{-1}). Actually, both **B23** and **PB23**

exhibit similar Stokes shifts of *ca.* 7 000 ± 250 cm^{-1} for both the solution and the solid state spectra (if shoulders are neglected).

In summary, the aforementioned analysis of Stokes shifts provided quite consistent views of the extent of relaxation of excited molecules of studied oligomers and polymers depending on their structure and, in addition, the evidence that some apparently outlying values of λ_F of these materials are coherent with the other λ_F values.

Conclusions

The developed synthesis strategy enables preparation of bithiophenes and terthiophenes with *tpy* end-groups and alkyl substituents attached at various positions to oligothiophene block. Newly prepared α,ω-bis(*tpy*)oligothiophenes differ from each other mainly in the conformational distortion of molecular chains, which obviously influences the photophysical properties of both oligomers and polymers. Spectroscopic data together with outputs of DFT calculations have conclusively shown that increasing the twisting of the thiophene-thiophene bond(s) decreases the value of λ_{abs} much more dramatically than increasing the twisting of the thiophene-*tpy* bonds. These data also conclusively show that the steric effects considerably exceed the electronic effects of hexyl side groups. This is best seen on oligomer **B23**, whose free molecules are highly twisted due to head-to-head linking of thiophene rings, which strongly reduces the extent of delocalization of electrons along their chains. A free molecule of **B23** therefore behaves like a species consisting of two electronically poorly interconnected half-molecules. However, when packed in a crystal, the **B23** molecule acquires almost planar conformation due to a stabilizing effect of hexyl side groups interacting with *tpy* end-groups of near-neighboring molecules. Nevertheless, the UV/vis spectrum of a film of **B23** contains only distinctive shoulders on the red arm of its main absorption band, which anticipates the presence of only small domains but not extended continuous phase of coplanar molecules in the film of **B23**. A better controlled assembly process might hopefully provide more regular **B23** films.

Assembly of bis(*tpy*)oligomers to metallosupramolecular polymers provides materials that mostly exhibit the red-shifted both absorption (up to 80 nm) and emission (up to 135nm) in solution as well as absorption in the solid state (up to 80 nm) but the blue-shifted emission in the solid state (up to - 90 nm) compared to the adsorption or emission of the corresponding oligomer. The observed red shifts are fully consistent with the increased extent of the delocalization of electrons upon linking the conjugated oligomer molecules into polymer chains, whereas the blue shifts observed for solid systems apparently are not. Because the emission appears from LUMO that is mainly spread over the central oligothiophene block, the blue shifts observed during the oligomer-to-polymer transitions indicate that twisting of these blocks in a polymer film is higher than twisting in a film of pure oligomer. This means that the central blocks are better packed in oligomer films compared to polymer films. This outcome is in line with bulkiness of linking units that each consists of two mutually perpendicular *tpy* groups coordinated to one Zn^{2+} ion. These bulky units provide to central blocks more conformational freedom compared to that they have in a film of pure oligomer. Analysis of apparently exceptional values of the positions of emission maxima in terms of the Stokes shift theory revealed that these λ_F values are not exceptional but in conformity with the other ones.

Another important result is that the prepared conjugated metallo-supramolecular polymers exhibit the solvent-dependent constitutional dynamics. Therefore, it is hardly to identify and/or characterize them using only the spectra taken from solutions, including NMR spectra. Therefore, potential identification of these oligomers and polymers based on vibrational spectra is of practical importance. The IR spectra are particularly useful for the identification of free as well as coordinated *tpy* end-groups while the Raman spectra for identification and/or characterization of the state of oligothiophene central blocks.

Acknowledgement

We would like to thank Dr. I. Císařová (Charles University in Prague) for X-ray structure analysis.

Funding

Financial support of the Czech Science Foundation (P108/12/1143), the Ministry of Education of the Czech Republic (MSM0021620857), and the Grant Agency of Charles University (project 64213) is greatly acknowledged. The access to computing and storage facilities owned by parties and projects contributing to the National Grid Infrastructure MetaCentrum, provided under the program "Projects of Large Infrastructure for Research, Development, and Innovations" (LM2010005) is appreciated.

Supplemental Material

Supplemental data for this article can be accessed on the publisher's website.

References

1. Steed, J.W., and Atwood, J. L. (2009) *Supramolecular Chemistry*, 2nd edition ed.; John Wiley & Sons, Ltd.
2. Lehn, J. M. (2005) *Prog. Polym. Sci*., 30:814–831.
3. Thompson, A. M. W. C. (1997). *Coord. Chem. Rev*. 160:1–52.
4. Kurth, D. G., and Higuchi, M. (2006) *Soft Matter*., 2:915–927.
5. Constable, E. C. (2007) *Chem. Soc. Rev*., 36:246–253.
6. Wild, A., Winter, A., Schlutter, F., and Schubert, U. S. *Chem. Soc. Rev*., 40:1459–1511.
7. El-ghayoury, A., Schenning, A. P. H. J., and Meijer, E. W. (2002) *J. Polym. Sci., Part A: Polym. Chem*. 40:4020–4023.
8. Harriman, A., Mayeux, A., De Nicola, A., and Ziessel, R. (2002) *Phys. Chem. Chem. Phys*., 4:2229–2235.
9. Benniston, A. C., Harriman, A., Lawrie, D. J., Mayeux, A., Rafferty, K., and Russell, O. D. (2003) *Dalton Trans*., 4762–4769.
10. Yu, S. C., Kwok, C. C., Chan, W. K., and Che, C. M. (2003) *Adv. Mater*., 15:1643.
11. Andres, P.R., and Schubert, U. S. (2004) *Adv. Mater*., 16:1043–1068.
12. Barbieri, A., Ventura, B., Barigelletti, F., De Nicola, A., Quesada, M., and Ziessel, R. (2004) *Inorg. Chem*. 43:7359–7368.
13. Lopez, R, Villagra, D., Ferraudi, G., Moya, S. A., and Guerrero, J. (2004) *Inorg. Chim. Acta* 357:3525–3531.
14. Dobrawa, R., Lysetska, M., Ballester, P., Grune, M., and Wurthner, F. (2005) *Macromolecules*, 38:1315–1325.

15. Iyer, P. K., Beck, J. B., Weder, C., and Rowan, S. J. (2005) *Chem. Commun*. 319–321.
16. Han, F. S., Higuchi, M., and Kurth, D. G. (2008) *Tetrahedron*, 64:9108–9116.
17. Vellis, P. D., Mikroyannidis, J. A., Lo, C. N. Hsu, C. S. (2008) *J. Polym. Sci.*, *Part A* 46:7702–7712.
18. Schwarz, G., Bodenthin, Y., Geue, T., Koetz, J., and Kurth, D. G. (2010) *Macromolecules*, 43:494–500.
19. Chen, Y. Y., and Lin, H. C. (2007) *J. Polym. Sci.*, *Part A* 45:3243–3255.
20. Chen, Y. Y., and Lin, H. C. (2007) *Polymer*, 48:5268–5278.
21. Winter, A., Friebe, C., Chiper, M., Hager, M. D., and Schubert, U. S. (2009) *J. Polym. Sci.*, *Part A* 47:4083–4098.
22. Constable, E. C., and Thompson, A. M. W. C. (1992) *J. Chem. Soc., Dalton Trans*. 3467–3475.
23. Barigelletti, F. and Flamigni, L. (2000) *Chem. Soc. Rev*. 29:1–12.
24. Chiper, M., Hoogenboom, R., and Schubert, U. S. (2009) *Macromol. Rapid Commun*. 30:565–578.
25. Svoboda, J., Stenclova, P., Uhlik, F., Zednik, J., and Vohlidal, J. (2011) *Tetrahedron*, 67:75–79.
26. Vitvarova, T., Zednik, J. Blaha, M., Vohlidal, J., and Svoboda, J. (2012) *Eur. J. Inorg. Chem*., 3866–3874.
27. Beley, M., Delabouglise, D., Houppy, G., Husson, J., and Petit, J. P. (2005) *Inorg. Chim. Acta*, 358:3075–3083.
28. Chotana, G. A., Kallepalli, V. A., Maleczka, R. E., and Smith, M. R. (2008) *Tetrahedron*, 64: 6103–6114.
29. Banishoeib, F., Henckens, A., Fourier, S., Vanhooyland, G., Breselge, M., Manca, J., Cleij, T. J., Lutsen, L., Vanderzande, D., Nguyen, L. H., Neugebauer, H., and Sariciftci, N. S. (2008) *Thin Solid Films*, 516:3978–3988.
30. Frisch, M. J., Trucks, G. W., Schlegel, H. B., Scuseria, G. E., Robb, M. A., Cheeseman, J. R., Scalmani, G., Barone, V., Mennucci, B., Petersson, G. A., Nakatsuji, H., Caricato, M., Li, X., Hratchian, H. P., Izmaylov, A. F., Bloino, J., Zheng, G., Sonnenberg, J. L., Hada, M. Ehara, M., Toyota, K., Fukuda, R., Hasegawa, J., Ishida, M., Nakajima, T., Honda, Y., Kitao, O., Nakai, H., Vreven, T., Montgomery, T. A., Peralta, J. E., Ogliaro, F., Bearpark, M., Heyd, J. J., Brothers, E., Kudin, K. N., Staroverov, V. N., Kobayashi, R., Normand, J., Raghavachari, K., Rendell, A., Burant, A. C., Iyengar, S. S., Tomasi, J., Cossi, M., Rega, N., Millam, J. M., Klene, M., Knox, J. E., Cross, J. B., Bakken, V., Adamo, C., Jaramillo, J., Gomperts, R., Stratmann, R. E., Yazyev, O., Austin, A. J., Cammi, R., Pomelli, C., Ochterski, J. W. Martin, R. L., Morokuma, K., Zakrzewski, V. G., Voth, G. A., Salvador, P., Dannenberg, J. J., Dapprich, S., Daniels, A. D., Farkas, O., Foresman, J. B., Ortiz, J. V., Cioslowski, J., and Fox, D. J. (2009) *Gaussian 09*, Revision A.02, Gaussian, Inc.: Wallingford, CT.
31. Kröhnke, F. (1976) *Synthesis-Stuttgart*, 1–24.
32. Ishiyama, T., Nobuta, Y., Hartwig, J. F., and Miyaura, N. (2003) *Chem. Commun*., 2924–2925.
33. *Spectral Database for Organic Compounds, SDBS*, Web Address: http://sdbs.riodb.aist.go.jp/sdbs/cgi-bin/cre_index.cgi
34. Yamamoto, T., Komarudin, D., Arai, M., Lee, M. L., Suganuma, H., Asakawa, N., Inoue, Y., Kubota, K., Sasaki, S., Fukuda, T., and Matsuda, H. (1998) *J. Am. Chem. Soc*., 120:2047–2058.
35. Chen, T. A., Wu, X. M., and R. D. Rieke. (1995) *J. Am. Chem. Soc*., 117:233–244.
36. Bondarev, D., Zednik, J., Sloufova, I., Sharf, A., Prochazka, I., Pfleger, J., and Vohlidal, J. (2010) *J. Polym. Sci., Part A* 48: 3073–3081.

Supporting Information

Synthesis and photophysical properties of new α,ω-bis(*tpy*)oligothiophenes and their metallo-supramolecular polymers with Zn^{2+} ion couplers

Pavla Bláhová, Jiří Zedník, Ivana Šloufová, Jiří Vohlídal and Jan Svoboda*

Department of Physical and Macromolecular Chemistry, Charles University in Prague, Faculty of Science, Hlavova 2030, CZ-128 40, Prague 2, Czech Republic
* jan.svoboda@natur.cuni.cz
Phone: +420221951311
Fax: +420224919752

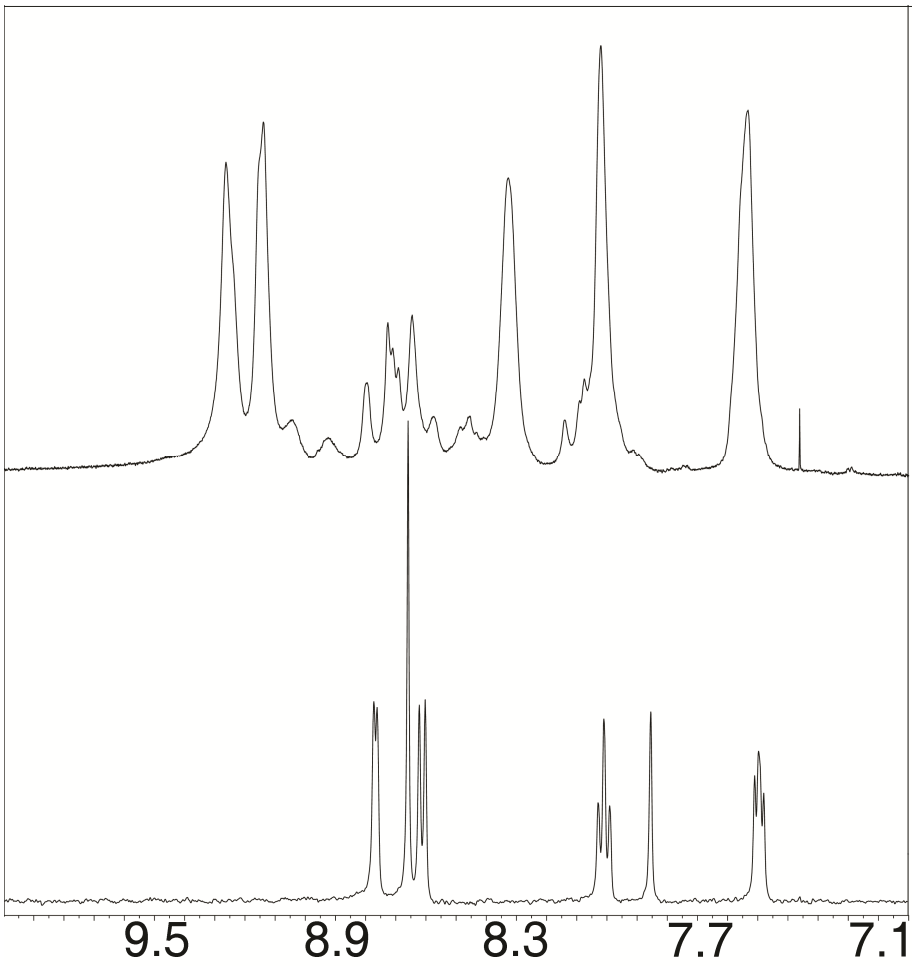

Fig. S1 ^{1}H NMR spectra of oligomer **B23** (down) and polymer PB23 (up). d_6-DMSO, 400MHz.

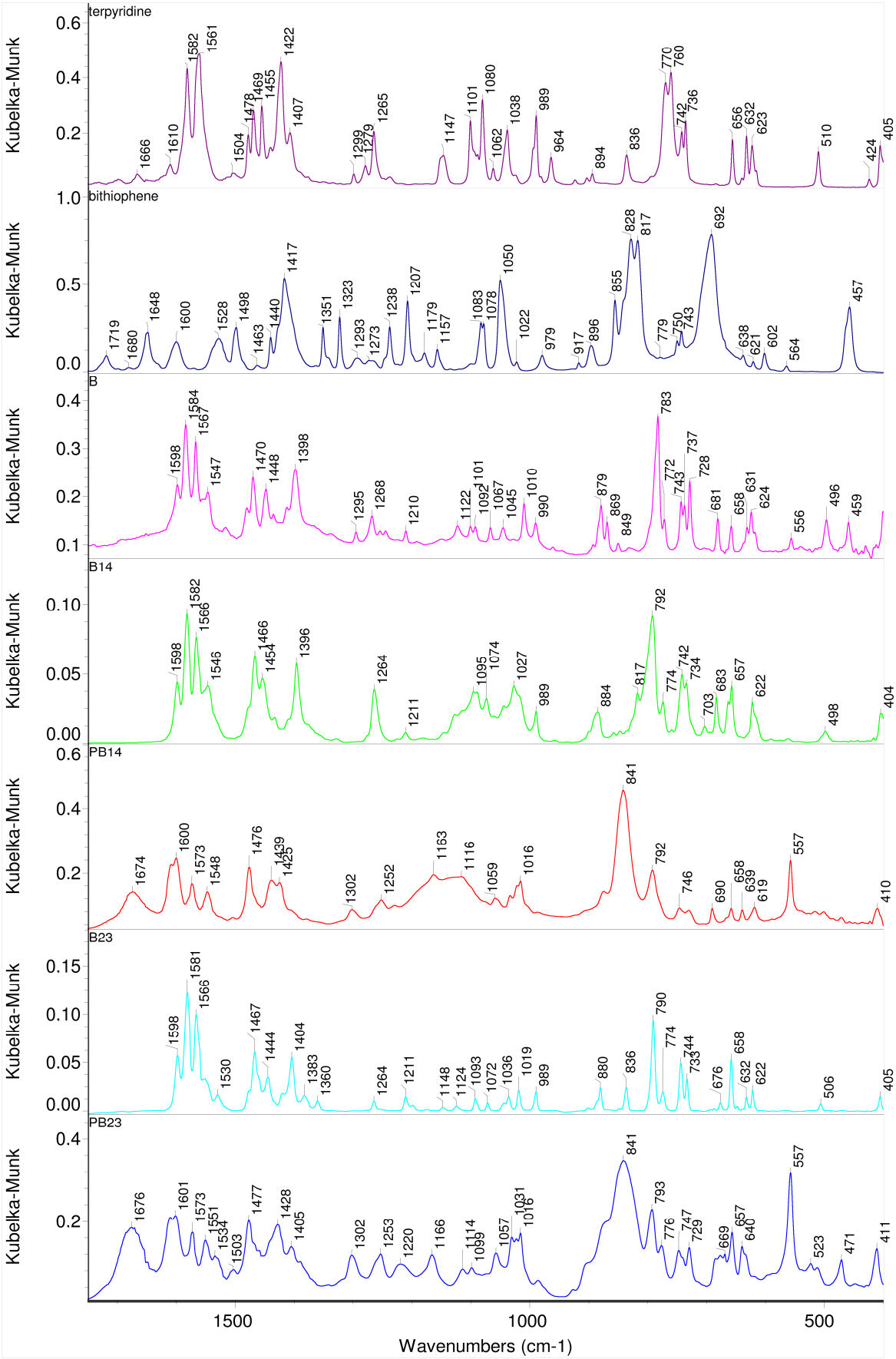

Fig. S2 IR spectra of H*tpy*, bithiophene and **B**-type oligomers and polymers.

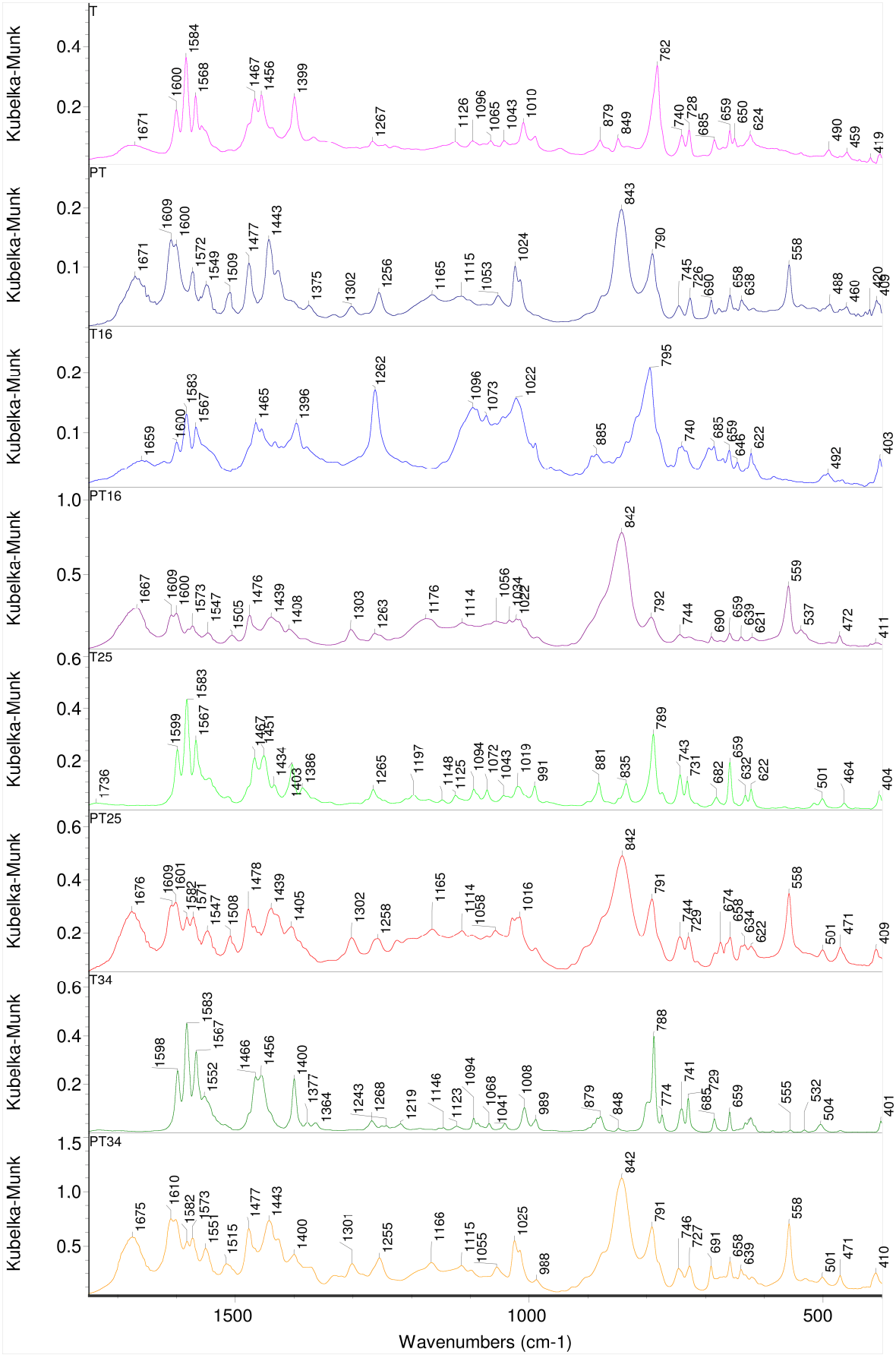

Fig. S3 IR spectra of **T**-type oligomers and polymers.

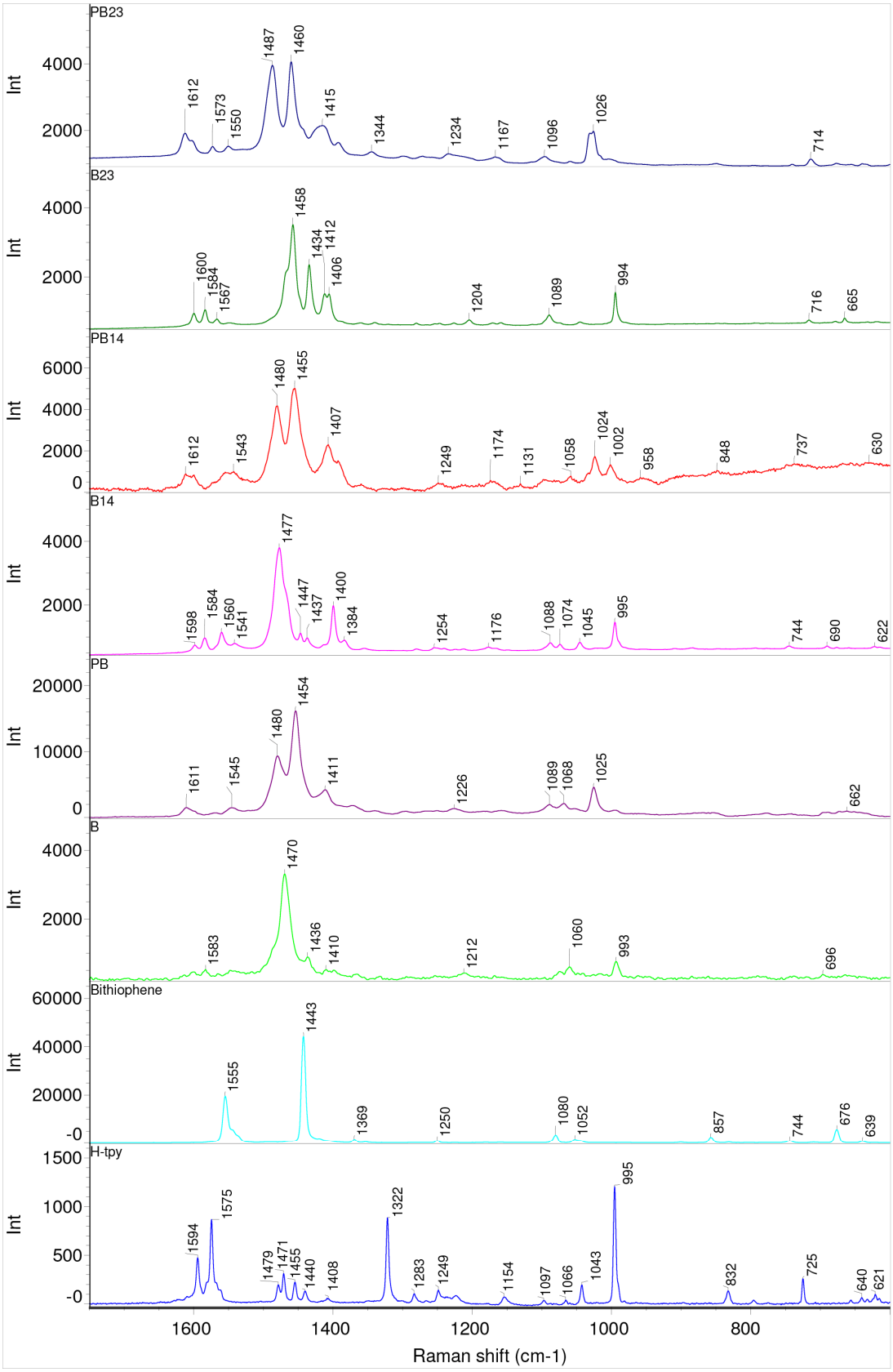

Fig. S4 Raman scattering spectra of H*tpy*, bithiophene and **B**-type oligomers and polymers.

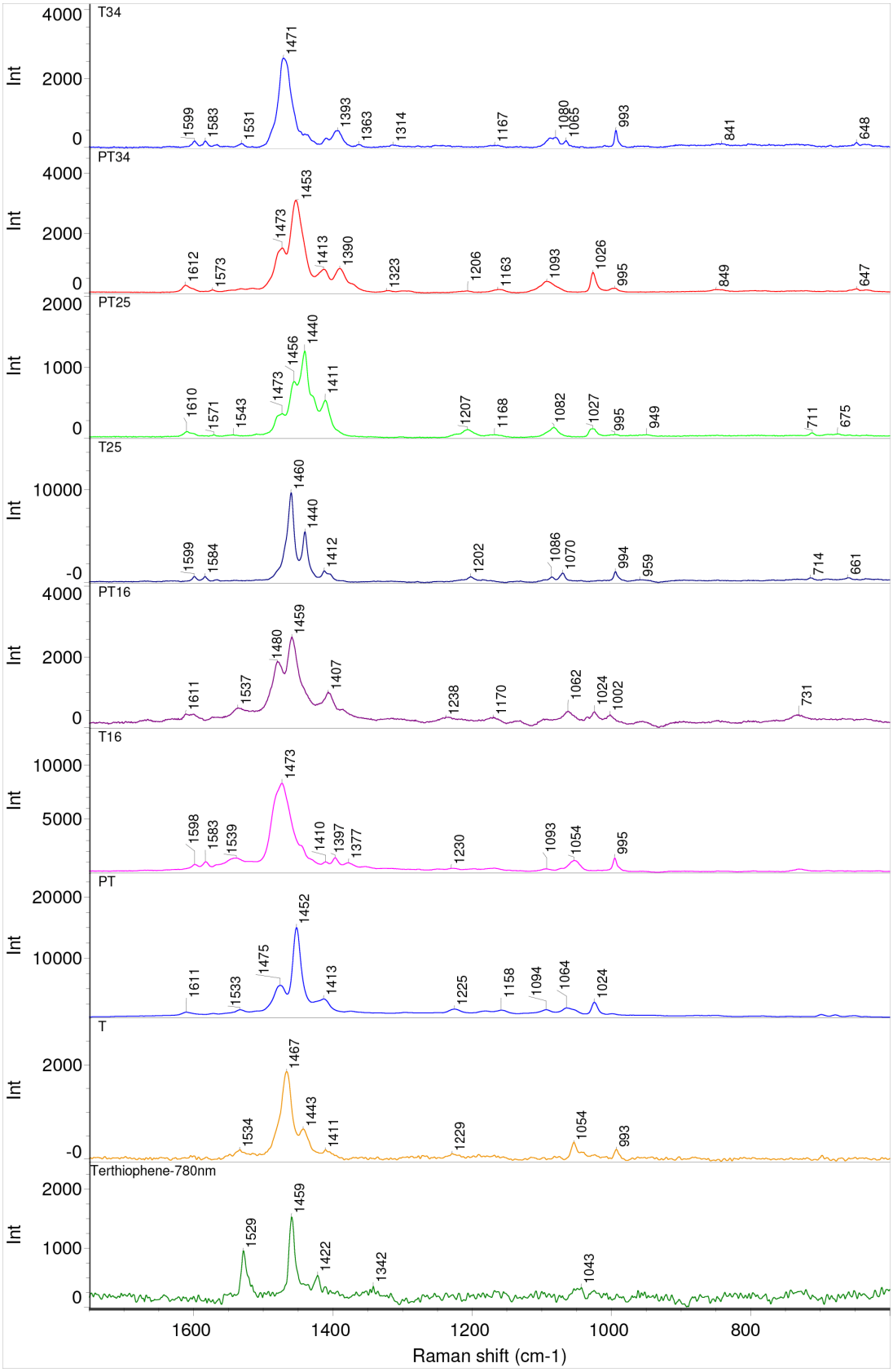

Fig. S5 Raman scattering spectra of terthiophene and **T**-type oligomers and polymers.

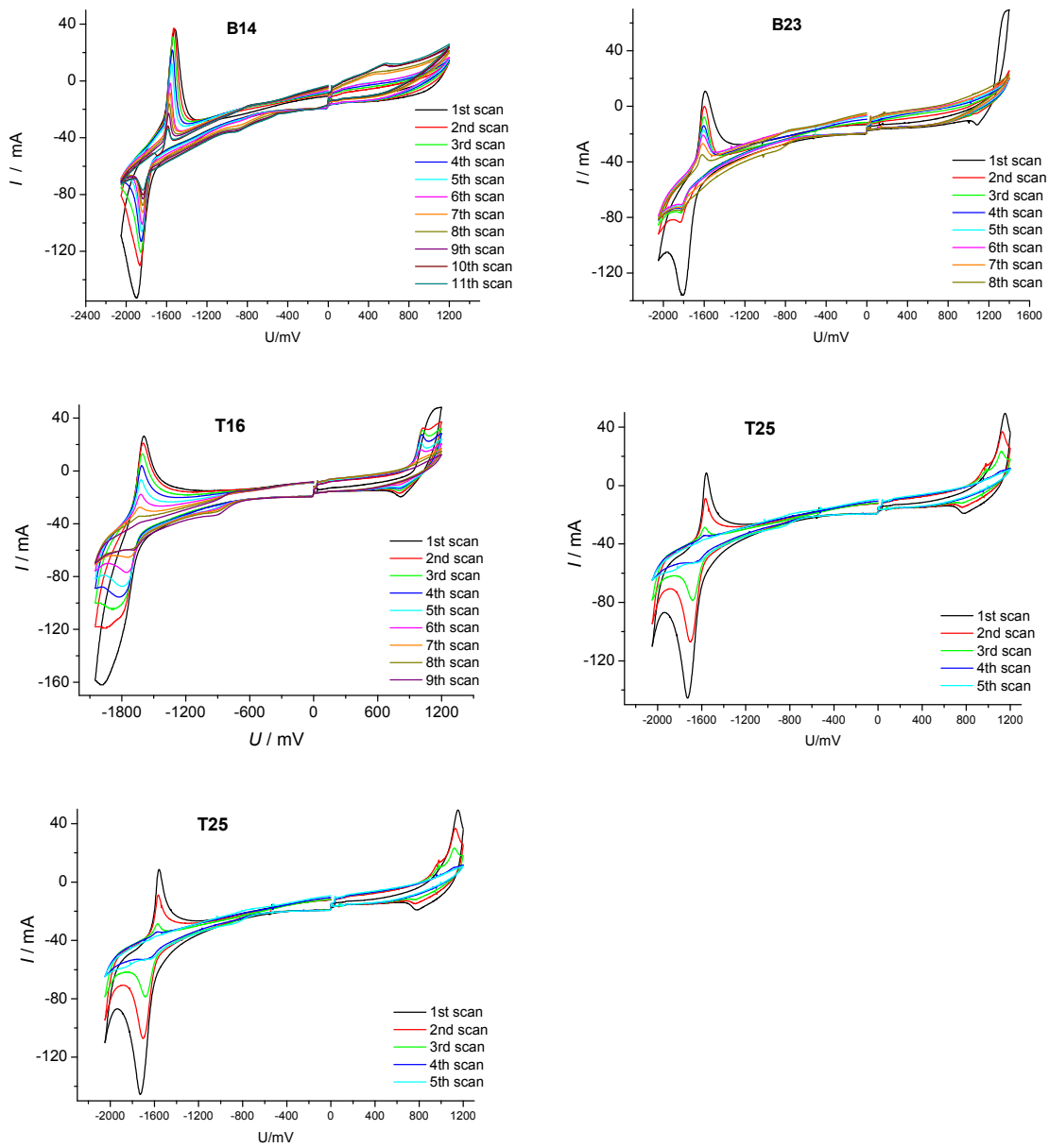

Fig. S6 Cyclic voltammogram of a thin film of prepared bis(*tpy*)oligothiophenes on a 1 mm diameter graphite disc electrode at 137 mV s^{-1} in CH_3CN containing 0.1 M [n-Bu_4N][PF_6] as supporting electrolyte.

ATTACHEMENT C

Štenclová-Bláhová P., Svoboda J., Šloufová I., Vohlídal J.: Alcohol-Soluble Bis(*tpy*)thiophenes: New Building Units for Constitutional Dynamic Conjugated Polyelectrolytes;
Phys. Chem. Chem. Phys. 2015, **17**, 13743 – 13756.

PCCP

PAPER

Cite this: *Phys. Chem. Chem. Phys.*, 2015, **17**, 13743

Alcohol-soluble bis(*tpy*)thiophenes: new building units for constitutional dynamic conjugated polyelectrolytes†

Pavla Štenclová-Bláhová, Jan Svoboda,* Ivana Šloufová and Jiří Vohlídal*

Received 16th February 2015,
Accepted 20th April 2015

DOI: 10.1039/c5cp01000d

www.rsc.org/pccp

New building units (unimers) for metallo-supramolecular polymers 2,5-bis(2,2′:6′,2″-terpyridine-4′-yl)-thiophene, **M**, and 5,5′-bis(2,2′:6′,2″-terpyridine-4′-yl)(2,2′-bithiophene), **B**, with ionic groups attached to thiophene rings are prepared by the modification of corresponding bromo-precursors and assembled with Zn^{2+} and Fe^{2+} ions into alcohol-soluble conjugated constitutional-dynamic polyelectrolytes (polyelectrolyte dynamers). Ionization of side groups only slightly affects the absorption spectra of unimers as well as dynamers but dramatically changes their solubility. Cyclic conformations of unimer molecules resulting from intramolecular interactions between *tpy* end-groups and cationic or polar ($-CH_2Br$) side groups are proposed to explain the spectral conformity of the **M**- and **B**-type unimers and their dynamers and also inhibition of the ionization reaction with *tpy* end-groups. The absorption spectra and excitation profiles of Raman spectra show that mainly the red arm of the metal-to-ligand charge transfer band of Fe-dynamers is significantly contributed with transitions involving thiophene rings. The constitutional dynamics of Zn-dynamers is fast while that of Fe-dynamers is so slow that it allows effective separation of the dynamer to fractions in SEC columns. Electronic spectra and viscosity measurements proved that excess of Fe^{2+} ions results in shortening of the dynamer chains and their end-capping by these ions.

Introduction

Metallo-supramolecular polymers (MSP) are an important subclass of dynamers.[1,2] A molecule of a linear MSP is composed of low-molar-mass or oligomeric units with two chelating end-groups (metal-ion receptors) that enable metal-ion induced reversible self-assembly of the units into chains. Metal ions that facilitate this self-assembly are usually referred to as ion couplers. Depending on the strength of interactions between the end-groups and ion couplers and solubility, molecules of MSPs exhibit constitutional dynamics either at increased temperature, or in solution, or both. The constitutional dynamics gives to MSPs (i) processing advantages, (ii) responsiveness to external stimuli (adaptability), (iii) possibility of tuning the properties or healing structure defects by post-synthesis exchanges of oligomer molecules and/or ion-couplers. The dynamics of MSPs is controlled by the rates of opposite reactions underlying coordination equilibriums, *i.e.*, by the rate of chemical relaxation.

Charles University in Prague, Faculty of Science, Department of Physical and Macromolecular Chemistry, Hlavova 2030, CZ-128 40, Prague 2, Czech Republic. E-mail: jan.svoboda@natur.cuni.cz, jiri.vohlidal@natur.cuni.cz; Fax: +420 224919752; Tel: +420 221951310

† Electronic supplementary information (ESI) available. See DOI: 10.1039/c5cp01000d

As the field of dynamers is relatively new, the related terminology has not yet been established, which brings about ambiguity of the term oligomer. Under the dynamics promoting conditions, dynamer molecules are typically composed of only less number of assembled units, most often oligomeric molecules. Such a dynamer is a "superior oligomer" of hierarchically lower oligomer(s). Ambiguity of the term oligomer is thus obvious. Therefore, we use throughout this paper the term unimer for an oligomer utilized as a "monomer" in the preparation of a dynamer, as proposed by Ciferri *et al.*[3]

The MSPs composed of conjugated unimers are of interest as potential materials for devices with applications based on the light/electricity inter-conversion and non-linear optical phenomena (light-emitting devices, photovoltaic cells, *etc.*).[4–22] High attention has been paid to MSPs derived from conjugated oligomers with tridentate 2,2′:6′,2″-terpyridine-4′-yl (*tpy*) end units that prefer facial and meridian coordination to metal ions such as Ru^{2+}, Fe^{2+}, Zn^{2+} and Co^{2+}, thus giving well defined linear chains.[20,23–25] However, conjugated MSPs as well as their unimers suffer from poor solubility in solvents suitable for their solution processing. MSPs constituted of bis(*tpy*)oligoarylenes are poorly soluble or insoluble in overwhelming majority of solvents. They are not very easily soluble in solvents such as dimethylsulfoxide (DMSO), acetonitrile (AN), and dimethylformamide (DMF), which are not very favorable for preparing good MSP layers.

Poor solubility of conjugated linear MSPs originates from rather high stiffness of their chains that strongly supports the inter-chain interactions and suppresses the intra-chain ones. The stiffness of conjugated MSP chains is a logical consequence of their chemical constitution. It mainly stems from two effects: (i) increased rigidity of conjugated chains of inbuilt unimers, and (ii) ionene structure causing extension of MSP chains due to the electrostatic repulsion between main-chain cations.

An increase in the solubility of conjugated MSPs in medium-polar solvents achieved by introducing pendant alkyl groups to unimeric units[24] is insufficient. Future technologies require materials soluble in "green solvents" such as alcohols and aqueous solutions and in solvents providing good polymer films. Such solubility of conjugated MSPs can be potentially achieved by introducing pendant ionic groups into unimers. In the present paper, we report on the preparation and basic properties of the ionic unimers of the bis(*tpy*)thiophene type and their transformation into conjugated MSPs by means of coordination to Zn^{2+} and Fe^{2+} ion couplers. These compounds might be classified as conjugated polyelectrolyte dynamers though, according to the molecular structure they are hybrids of polyelectrolytes and ionenes since their chains contain pendent ionic groups as well as charged main chain atoms.[26,27]

Results and discussion

The unimers prepared and studied as well as their abbreviations are shown in Chart 1. Metallo-supramolecular dynamers prepared from these unimers are denoted with the prefix $\mathbf{P_{Zn}}$ (dynamers with Zn^{2+} ion couplers) or $\mathbf{P_{Fe}}$ (Fe^{2+} ion couplers) before the unimer label: for example **PZnM-Br** denotes the dynamer formed from **M-Br** and Zn^{2+} ions; $\mathbf{P_{Fe}B\text{-}N^+}$ the dynamer formed from $\mathbf{B\text{-}N^+}$ and Fe^{2+} ions, *etc.*

Synthesis of unimers and dynamers

Bromohexyl unimers **M-Br** and **B-Br** carrying 6-bromohexyl groups were prepared using the Suzuki–Miyaura coupling strategy (Scheme 1) and conditions applied earlier.[28] The key monomer: 3-(6-bromohexyl)thiophene, **BrHexTh**, was prepared by the dropwise addition of 3-thienyllithium to a four-fold stoichiometric excess of 1,6-dibromohexane in hexane and purified by vacuum fractionation. A part of **BrHexTh** was transformed into corresponding 2,5-bis-(borolane)[29,30] which was then reacted with Br*tpy* to give unimer **M-Br**. Another portion of **BrHexTh** was brominated with NBS to give 2-bromoderivative, which in the reaction with diborolane gave 3,3′-bis(6-bromohexyl)-2,2′-bithiophene. The latter was then transformed to bis(boronate) which, in the reaction with Br*tpy*, gave unimer **B-Br**.

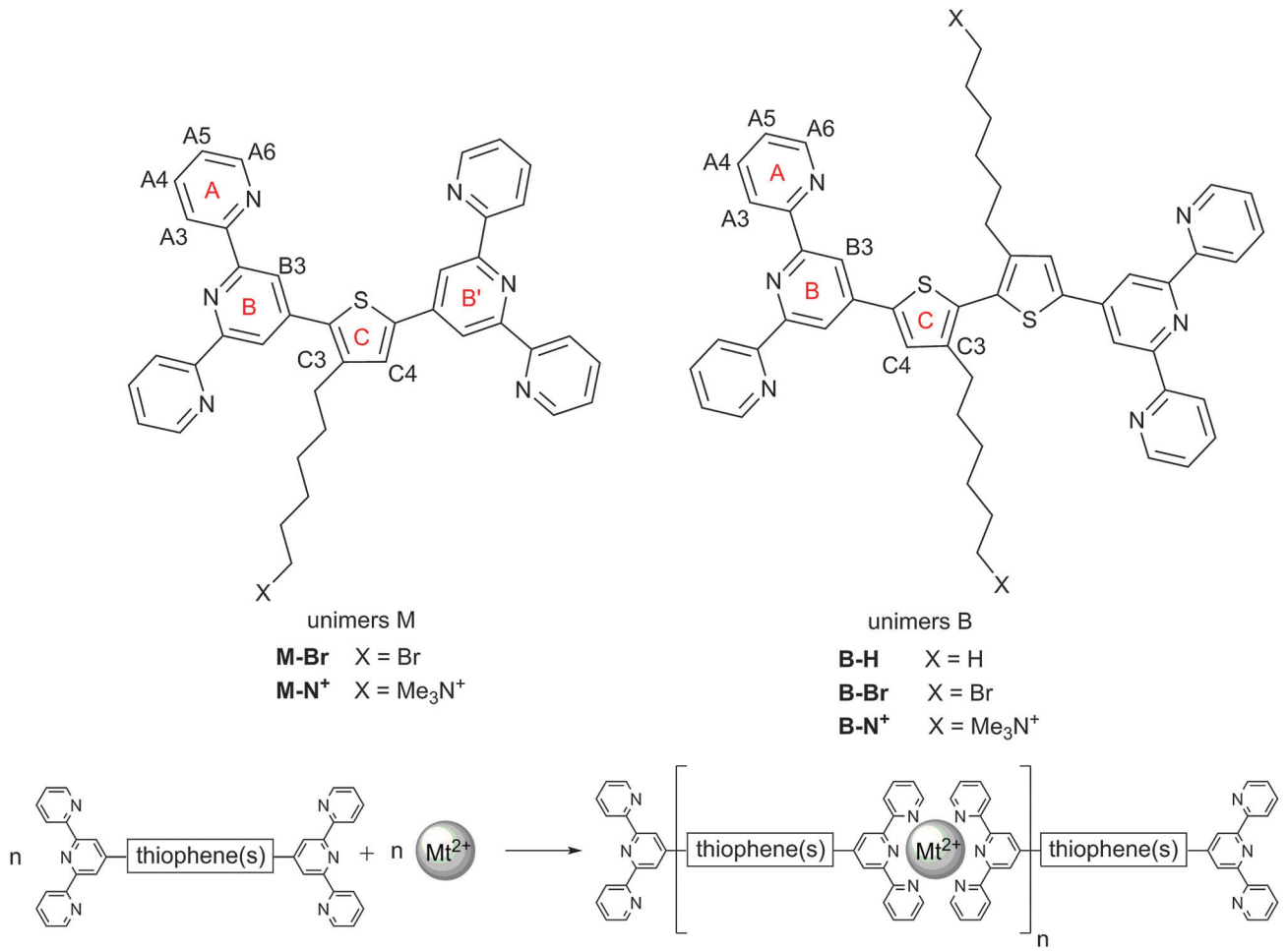

Chart 1 Structures and codes of prepared unimers and the schematic structure of the metallo-supramolecular dynamer.

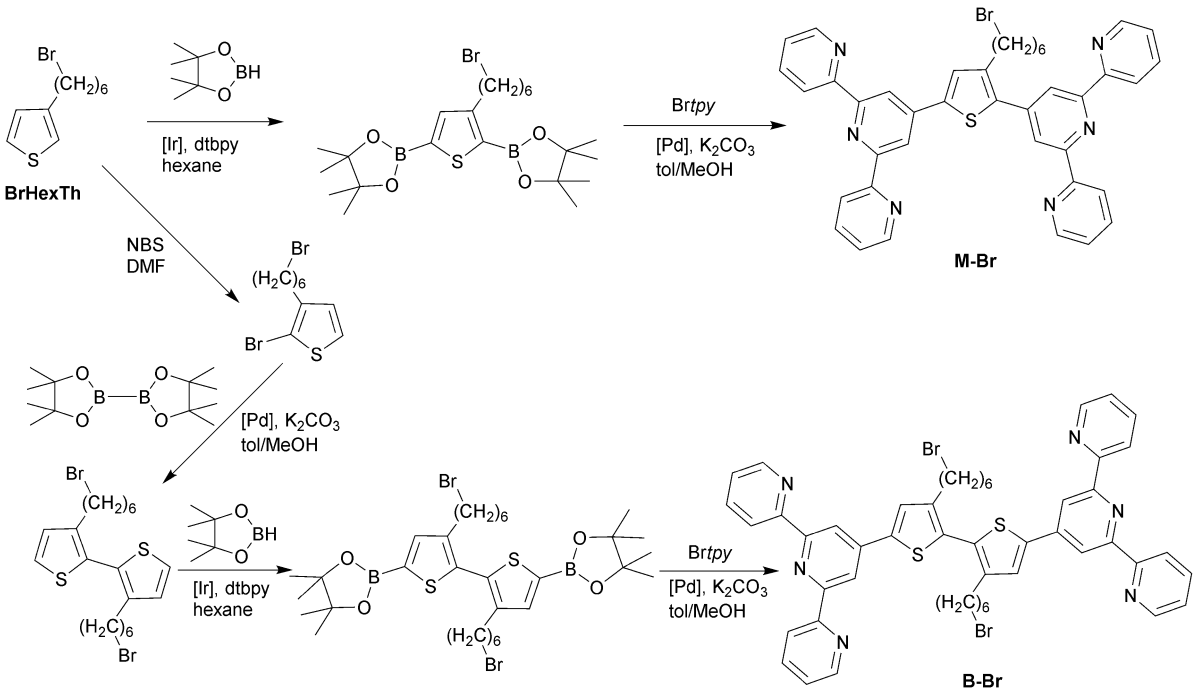

Scheme 1 Preparation of unimers **M-Br** and **B-Br** (precursors of ionic unimers).

Modification of bromohexyl to ionic unimers has surprisingly met serious difficulties. Originally we wanted to replace Br atoms with *N*-methylimidazolium groups – current cations of ionic liquids, since such modification took place easily with poly[3-(2-bromoethoxy)-4-methylthiophene],[31,32] poly(**BrHexTh**),[33] and also on **BrHexTh** even in the presence of free terpyridine in our preliminary experiments. However, in sharp contrast, the reaction of bromo-unimers with *N*-methylimidazole did not proceed at all at laboratory temperature and, at increased temperatures (about 50 °C or higher), significant elimination of HBr took place that gave a considerable fraction of unsaturated hex-5-en-1-yl side groups. The HBr elimination appeared even under the solvent-free conditions: in solutions of **M-Br** or **B-Br** in *N*-methylimidazole at 70 °C. Therefore, we decided to modify **M-Br** or **B-Br** with a stronger agent: trimethylamine (Me_3N), which has one important advantage: its stoichiometric excess is easy to remove by evaporation from the resulting reaction mixture.

The difficulties accompanying the ionization indicate that the reaction of bromohexyl unimers with *N*-methylimidazole is inhibited by *tpy* end-groups. The reason for it might be seen in the increased basicity of *tpy* end-groups due to donation of electrons from neighboring thiophene rings. Interactions between *tpy* and polar $-CH_2Br$ groups can be strong enough to keep these groups in close proximity. This suggests preferred macrocyclic conformations of **B-Br** and **M-Br** molecules since intramolecular cycles are much more resistant to the strain induced by thermal motion compared to linear supramolecular chains. Nevertheless, the intermolecular inhibition with *tpy* end-groups of other molecules is not excluded.

The ^{1}H NMR spectra evidenced the transformation of bromo- to trimethylammonium-unimers by disappearance of the signal of the CH_2(–Br) group (3.38 ppm for **M-Br**; 3.42 ppm for **B-Br**) and appearance of the signal of nine protons of the CH_3 group in Me_3N^+ groups (3.03 ppm for **M-N$^+$**; 3.07 ppm for **B-N$^+$**). The signal of the CH_2 unit linked to the $-N^+Me_3$ group was not seen being overlaid by the solvent signal (the spectrum taken in methanol). Neither the IR nor the off-resonance Raman spectra provided an additional clear evidence for modification of side groups since, as observed earlier,[24] the bands of thiophene rings and *tpy* end-groups unambiguously dominate in the spectra of unimers.

Metallo-supramolecular dynamers were simply prepared by mixing solutions of a given unimer and zinc(II) or iron(II) perchlorate in the stoichiometric ratio of 1 : 1 and subsequently evaporating the solvent. Bromohexyl unimers (**M-Br** and **B-Br**) were assembled in the acetonitrile/chloroform (1/1 by vol) mixed solvent while ionic unimers (**M-N$^+$** and **B-N$^+$**) in methanol. The ionic unimers as well as dynamers are well soluble in alcohols and sparingly soluble in water wherein, however, the dissolving is a long-lasting process accompanied by fractionation (see ESI,† Fig. S1). This process is the subject of further study.

Optical spectra of unimers and dynamers

The UV/vis absorption spectra of all unimers are very similar each showing a flat band at 280–284 nm, contributed with transitions in *tpy* end groups, and a band at wavelength λ_A = 336 nm (solutions) or 345 nm (films) belonging to transitions from HOMO that is spread over thiophene rings and central rings of *tpy* groups (Table 1 and ESI,† Fig. S2). The spectra are similar to the spectrum of **B-H** (unimer with unsubstituted hexyl side groups, λ_A = 339 nm).[24]

Close similarity of the UV/vis spectra of **Br**- and **N$^+$**-unimers is not surprising since the side end-groups are quite distant

Table 1 Spectroscopic characteristics of the prepared unimers and dynamers

	UV/vis absorption		Luminescence		Stokes shift	
	λ_A (nm)		λ_F (nm) (ϕ, %)		ν (cm^{-1})	
Sample	Solution	Film	Solution	Film	Solution	Film
Unimers						
M-Br	335	344	406 (3%)	543 (7%)	5200	10 650
M-N$^+$	334	347	404 (3%)	461 (7%)	5200	7150
B-Br	338	344	452 (5%)	561 (4%)	7450	11 250
B-N$^+$	337	346	450 (5%)	519 (3%)	7450	9650
B-H[a]	339	400–420 450_{sh}	450 (3%)	550	7280	~6000
Zn-dynamers						
P_{Zn}M-Br	380	407	440	460 (3%)	3600	2850
P_{Zn}M-N$^+$	370	393	444	473 (1%)	4500	4300
P_{Zn}B-Br	385	396	550	525 (4%)	7800	6200
P_{Zn}B-N$^+$	375	392	550	538 (3%)	8500	6900
P_{Zn}B-H[a]	390	391	535	545	6950	7230
			(λ_{MLCT})			(λ_{MLCT})
Fe-dynamers						
P_{Fe}M-Br			325, 373 (590)			394 (608)
P_{Fe}M-N$^+$			325, 370 (588)			388 (601)
P_{Fe}B-Br			322, 370 (594)			386 (598)
P_{Fe}B-N$^+$			320, 366 (591)			380 (598)

[a] Data for solutions measured in THF taken from ref. 24.

from main chains. On the other hand, close similarity of the absorption spectra of **M**- and **B**-unimers is not obvious regarding the different numbers of thiophene rings in their chains. The reason for it is a high dihedral angle (*ca.* 67°)[24] of the thiophene-to-thiophene bond in **B**-molecules (due to steric hindrances of side chains – see Chart 1), which greatly reduces the delocalization of electrons in **B** chains. Therefore, **B**-type molecules absorb light like two almost independent 4′-(thiophen-2-yl)terpyridine species.

The tiny difference (6 to 13 nm) between absorption maxima observed for solutions and films proves a negligible effect of the molecular packing on the light absorption by the studied unimers. Particularly interesting is the conformity of UV/vis spectra taken from solutions (~338 nm) and films (345 ± 1 nm) of **B-Br** and **B-N$^+$**. The parent unimer, **B-H**, namely shows considerable red shift when going from solution (339 nm) to film (410 nm with a shoulder at 450 nm), which proves substantial planarity of **B-H** molecules in the film.[24] Thus the conformity of the solution and solid-state absorption spectra proves to non-planar conformations of **B-Br** and **B-N$^+$** molecules in films. This can be explained by the above-proposed supramolecular macrocyclic conformations of polar and ionic **B**-type molecules, which stabilizes the crossing thiophene ring planes. As mentioned above, the disorder owing to analogous intermolecular interactions cannot be excluded. Anyway, these spectral features are consistent with the suggested explanation of the inhibitive effect of *tpy* end groups in ionization of bromo-precursors.

Unlike the UV/vis absorption, the luminescence emission of **B**-unimers (λ_F = 450 nm) in solutions is significantly red shifted compared to **M**-unimers (λ_F = 405 nm, ESI,† Table S1), obviously due to the transition of excited **B**-molecules to lowered-energy conformations with coplanar quinoidal rings and thus more delocalized π-electrons, from which the light emission takes place. The extent of the excited state relaxation of molecules in the solid state is higher than that observed for dissolved molecules as evidenced by the Stokes shift values (Table 1). The lowered extent of relaxation observed for the ionic **N$^+$**-type unimers can be attributed to limitations originating from more intense electrostatic interactions.

Absorption spectra of dynamers show the longest wavelength bands red shifted about 30 to 65 nm with respect to the corresponding free unimer, the shift being higher for **Br**-compared to **N$^+$**-dynamers and for Zn-compared to Fe-dynamers. Spectra of Fe-dynamers show an extra band at *ca.* 600 nm (wavelength λ_{MLCT}), which is typical of $(tpy)_2Fe^{2+}$ grouping[34] and is contributed by electronic transitions within the metal to ligand charge transfer (MLCT) complex. As usual, Zn-dynamers derived from $(tpy)_2$ oligomers show luminescence emission while Fe-dynamers do not. The absence of luminescence for Fe(II)-dynamers (complexes) is attributed to the fact that their lowest excited state is a d–d triplet state that is very close to the ground state.[35] As the potential d–d phosphorescence is spin forbidden, the d–d triplet state easy depletes the upper excited states and decays by unambiguously preferred non-radiative transitions in accord with the energy gap law.[36,37]

The luminescence emission bands of the solid **P_{Zn}M**-dynamers (467 ± 7 nm) are located close to each other as well as the bands of **P_{Zn}B**-dynamers (532 ± 7nm). Interestingly, the bands of dissolved dynamers: 442 ± 2 nm for **P_{Zn}M**- and 550 nm for **P_{Zn}B**-dynamers are not too distant from the bands of solid dynamers. This indicates that the conformational disorder of the dynamer chains in a film is comparable to their disorder in solution.

Raman spectra of dynamers

Because Fe-dynamers do not emit luminescence, it was possible to acquire their resonance as well as off-resonance Raman spectra using excitation wavelengths (λ_{ex}) across the whole visible region (λ_{ex} = 445, 532, 633 and 780 nm). In contrast, the spectra of Zn dynamers were measurable only in the off-resonance mode (λ_{ex} = 780 nm) since luminescence dominated the spectra collected with excitations at all other λ_{ex}.

Off-resonance Raman spectra of Zn-dynamers (Fig. 1) are similar to each other. Each shows a medium to low intensity band of coordinated *tpy* groups: (i) ring-stretching modes at 1610 to 1600 cm^{-1}, 1570 cm^{-1} and 1535 to 1548 cm^{-1}, (ii) in plane deformation mode at 1288 cm^{-1}, and (iii) asymmetric ring breathing mode at about 1025 cm^{-1}.[38,39] However, the strongest bands in these spectra are bands of thiophene-2,5-diyl units,[33,40–43] which appeared at 1484, 1450 and 1405 cm^{-1} for **P_{Zn}M**-type dynamers, and at 1484, 1457 and 1411 to 1417 cm^{-1} for **P_{Zn}B**-type dynamers. Different end-capping of hexyl-groups has very little impact on the spectral pattern. Thus it can be concluded that the spectral differences primarily stem from different numbers of thiophene rings in unimeric units.

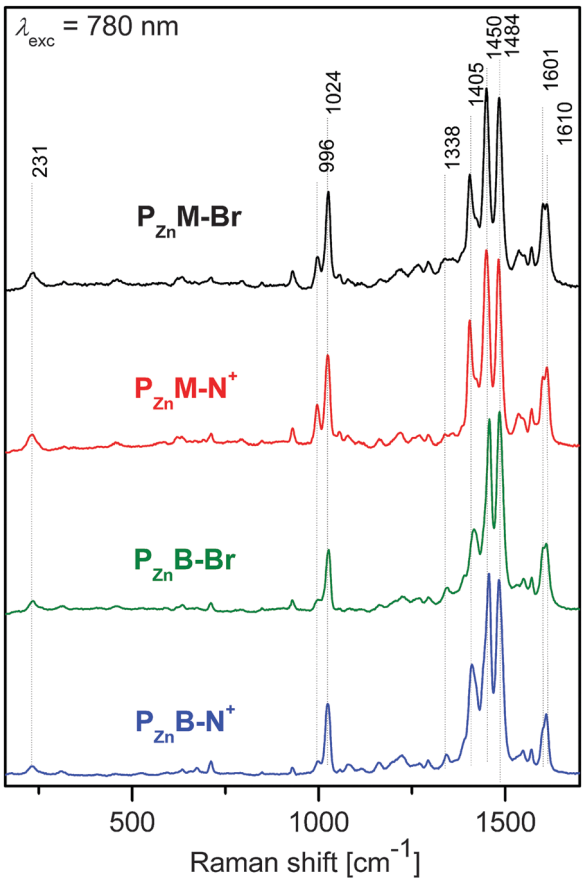

Fig. 1 Off-resonance Raman spectra of Zn-dynamers.

Compared to the spectra of Zn-dynamers, the off-resonance Raman spectra (λ_{ex} = 780 nm) of Fe-dynamers (Fig. 2) show a more intense (and not split into doublet) band of coordinated *tpy* groups at 1610 cm^{-1}, blue-shift of the *tpy* ring-breathing mode band to 1039 cm^{-1}, relatively strong band at 1288 cm^{-1} that should also be attributed to *tpy* groups[38] and somewhat different patterns of bands attributable to thiophene-rings (1478 to 1345 cm^{-1}). It should be mentioned here that the band at 1478 cm^{-1} is most probably also contributed with transitions in *tpy* groups coordinated to Fe^{2+} ions since Raman spectra of $[Fe(terpyridine)_2]^{2+}$ species show a strong band at 1472 cm^{-1}.[38] As can be seen, the spectral differences between $\mathbf{P_{Fe}M}$-type and $\mathbf{P_{Fe}B}$-type dynamers are more pronounced compared to differences between their Zn counterparts.

Raman spectra of Fe-dynamers taken with different λ_{ex} are compared in Fig. 2. The spectra of the given dynamer differ from each other because each excitation line selectively, resonantly enhances Raman bands of chromophore(s) absorbing at λ_{ex} (ESI,† Fig. S2). Thus the Raman spectra can help to identify chromophore(s) contributing to the respective absorption bands.

Raman spectra taken with λ_{ex} = 445 nm showed strong peaks typical of thiophene rings but weak peaks characteristic of *tpy* groups. Moreover, the intensity difference between the *tpy* and thiophene Raman bands of $\mathbf{P_{Fe}B}$-dynamers is much higher than in the case of $\mathbf{P_{Fe}B}$-dynamers, which obviously reflects a higher number of thiophene rings in the **B**-type repeating units. Hence it follows that the broad UV/vis band at about 400 nm is mainly contributed with electronic transitions between orbitals spread over the axis of a unimer unit that comprises thiophene ring(s).

The excitation at λ_{ex} = 532 nm matches the blue arm of the MLCT band (600 nm). Raman spectra of Fe-dynamers taken with this excitation are the only ones in which overtones and combination bands are observable in the region from 2200–3200 cm^{-1}. Peaks at 1610, 1562, 1537, 1470, 1347 and 1288 cm^{-1} unambiguously dominate the finger-print region of all these resonance Raman spectra, while bands typical of thiophene rings are weak (Fig. 2). Minor spectral differences between the **M**-type and **B**-type Fe-dynamers are seen in the position of a weak band at 1396 cm^{-1} (**M**-type) *vs.* 1408 cm^{-1} (**B**-type) and the presence of a triplet at 682, 673 and 652 cm^{-1} (**M**-type) but only a doublet at 681 and 653 cm^{-1} (**B**-type) in the corresponding spectra. Nevertheless, these differences are quite low and do not disturb the high similarity of spectral patterns. This extremely large consensus in the spectral patterns is in full concordance with the excitation into the MLCT band of *–tpy*-Fe^{2+}-*tpy*– linkages. However, these spectral patterns significantly differ from the spectral pattern of the resonance Raman spectrum of the $[Fe(terpyridine)_2]^{2+}$ complex taken with the same excitation: λ_{ex} = 532 nm.[35] This clearly proves that the MLCT state is localized not only on the directly coordinated *tpy* units but also on thiophene unit(s) that are more distant from the coordination centre.

Raman spectra taken with λ_{ex} = 633 nm, despite that this line well matches the red arm of the MLCT band, show similar spectral patterns as off-resonance spectra taken with λ_{ex} = 780 nm. Small differences are mainly (i) lowered intensity of the doublet (**M**-type) and triplet (**B**-type) in the range of 1345–1478 cm^{-1} and (ii) increased intensity of the bands at 345 cm^{-1} and in the region from 650 to 800 cm^{-1}. These spectra also differ in the intensity of the band of ring breathing mode (1039 cm^{-1}). However, this band shows rather exceptional trend for all excitations: continuous amplification with increasing λ_{ex}, the trend that has been reported for Raman spectra of various $[Ru^{II}(bpy)_3]^{2+}$ complexes (*bpy* is 2,2′-bipyridine)[38,44–46] and has remained unexplained.

Important observation is that overtones and combined bands are absent in the spectra excited at 633 nm and their spectral patterns substantially differ from the pattern of spectra excited at 532 nm (Fig. 2). Regarding that both these excitation lines match the MLCT band, one can conclude that the MLCT electronic absorption band of dynamers consists of several different electron transitions of different symmetry.

Assembly of unimers to metallo-supramolecular dynamers

Assembly of dynamers from unimers and metal ions (Mt^{2+}) in solutions (acetonitrile/chloroform 1/1 by vol. for **Br**-type and methanol for $\mathbf{N^+}$-type unimers and dynamers) was studied more in detail using the UV/vis and fluorescence spectroscopy, viscometry and size exclusion chromatography (SEC).

For spectroscopic studies, a set of solutions of the constant unimer concentration (2×10^{-5} M) and stepwise increasing of the ions-to-unimer mole ratio ($[Mt^{2+}]/[U] = r$ from 0 to 3) was prepared for each unimer – ions couple. The solutions were

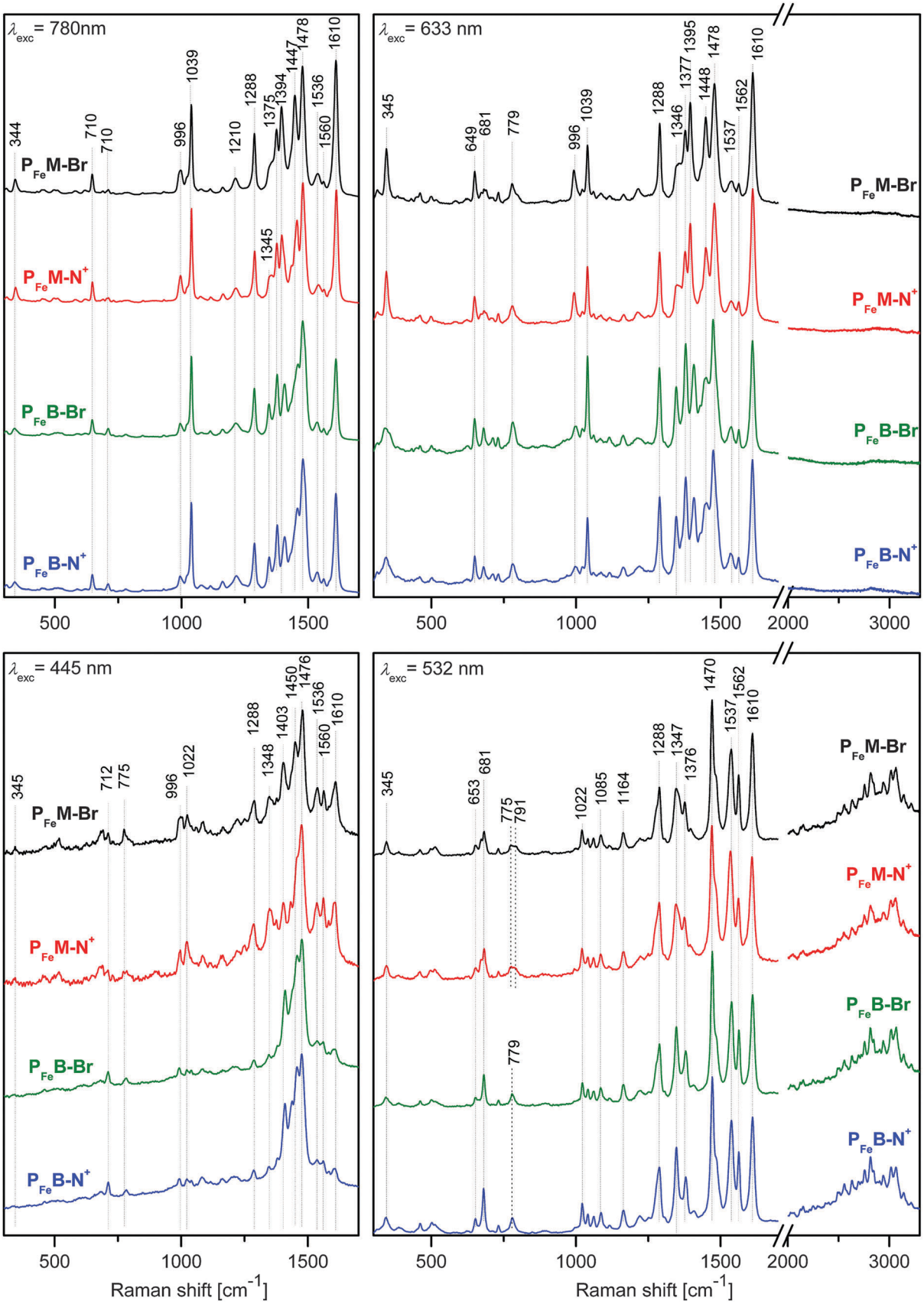

Fig. 2 Resonance and off-resonance Raman spectra of Fe-dynamers.

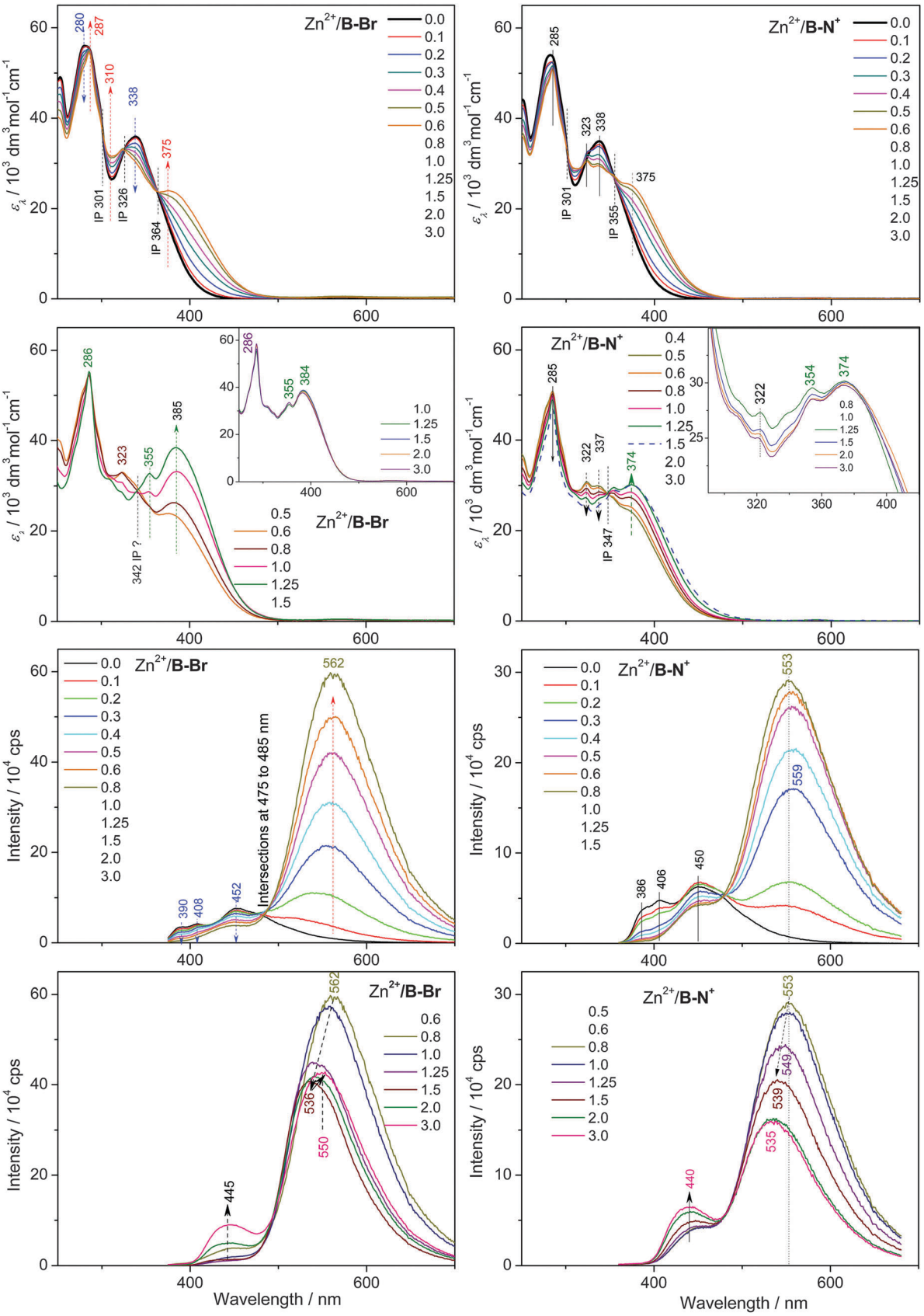

Fig. 3 Changes in UV/vis and photoluminescence spectra accompanying titration of **B-Br** (left) and **B-N$^+$** (right) unimers with Zn^{2+} ions. Initial unimer concentration 2×10^{-5} mol dm^{-3}; chloroform/acetonitrile (**Br**-unimers), methanol (**N$^+$**-unimers), room temperature.

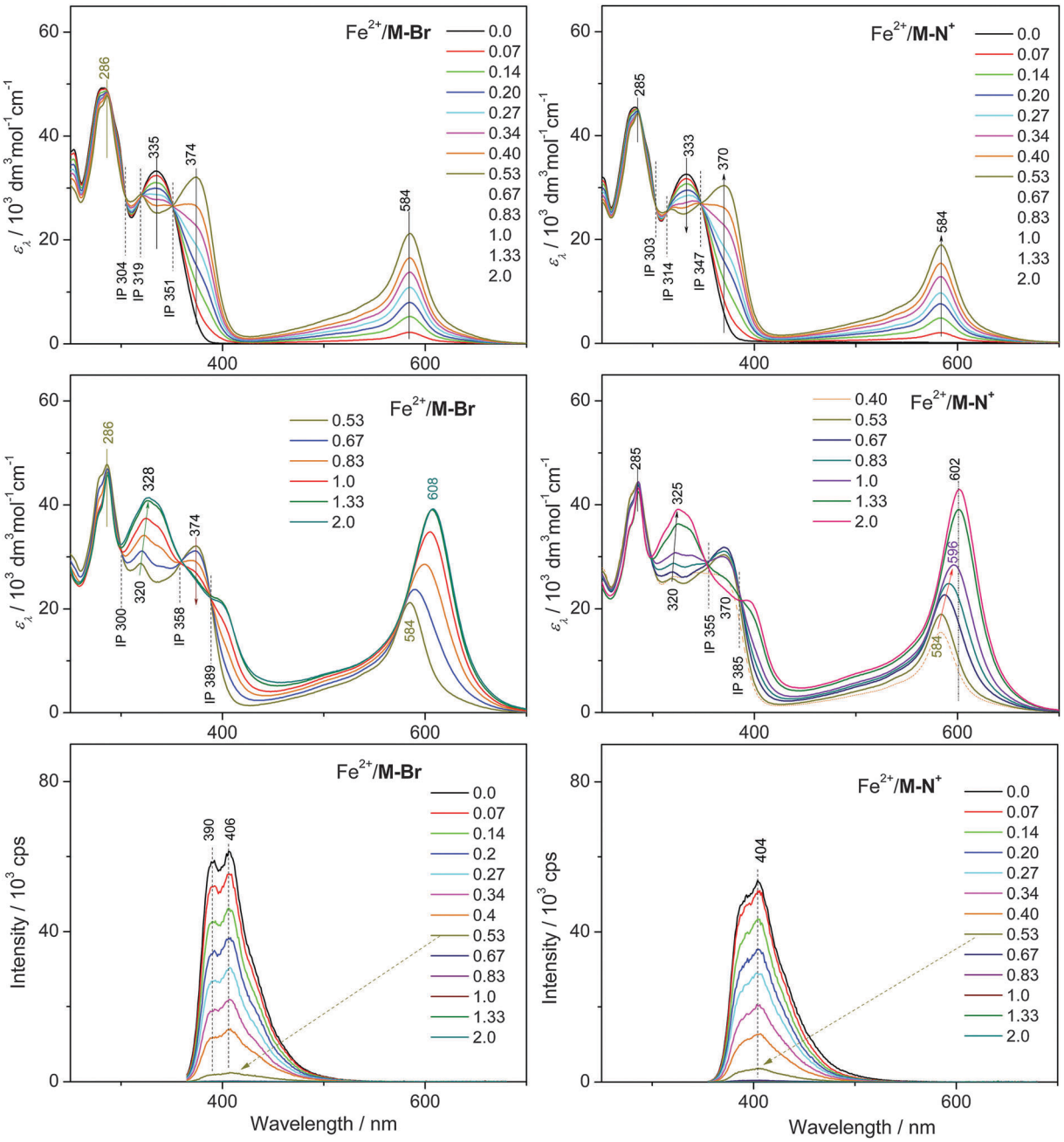

Fig. 4 Changes in UV/vis and photoluminescence spectra accompanying titration of **B-Br** (left) and **B-N$^+$** (right) unimers with Fe^{2+} ions. Initial unimer concentration 2×10^{-5} mol dm^{-3}; chloroform/acetonitrile (**Br**-unimers), methanol (**N$^+$**-unimers), room temperature.

allowed to equilibrate for 24 hours prior to measuring of their UV/vis and luminescence spectra. Changes in the spectra with the stepwise increasing composition ratio r are shown in Fig. 3 and 4 and ESI,† Fig. S5 and S6. The UV/vis and luminescence spectral sets are each presented in two figures (except for luminescence spectra of systems with Fe^{2+} ions) in order to show breaks in the development trend, which indicates existence of different stages of assembling. The first break in the trend appeared at r slightly above 0.5, the second one, if present, at $r > 1.0$.

The first stage of assembling (r from 0 to *ca.* 0.6) is reflected in the UV/vis spectra by: (i) a small change of the band shape at about 280 nm resulting in the shift of its apex to *ca.* 287 nm, (ii) the attenuating band at about 336 nm that is typical of the free unimer, and (iii) the appearance of a new band at 370–380 nm. The spectral set of each Mt^{2+}/U system shows two to three isosbestic points (IP), the presence of which indicates transformation of defined free unimer species into another defined species. The stoichiometry says that the newly formed species should be ''butterfly dimer'' species U–Mt^{2+}–U.

Complementary luminescence spectra of Zn^{2+}/U systems (r from 0 to *ca.* 0.6, Fig. 3, ESI,† Fig. S5) show a gradually attenuating band of free unimers and a simultaneously growing

new band of coordinated unimer species. Each spectral set shows one IP, thus supporting the idea on the prevailing formation of dimers. On the other hand, luminescence spectra of Fe^{2+}/U systems exhibit only gradually attenuated luminescence to its complete quenching at $r > 0.6$. However, it clearly demonstrates disappearance of free unimer species from solution at $r > 0.6$, and thus as well suggests their preferred conversion to butterfly dimers.

Electronic spectra monitored at r above 0.6, do not pass through IPs characteristic of the first stage, which indicates transition to the second stage of assembly where dynamer chains should grow. Unlike the first stage of assembly, the development of spectral patterns during the second stage is strongly influenced by the structure of unimers. Differences are mainly seen in: (i) the extent of amplification of the UV/vis band at 370–380 nm, (ii) the presence or absence of new IPs, and (iii) spectral patterns in the region from 300 to 400 nm. A direct correlation of the observed differences to the structure of dynamers is not apparent. Nevertheless, all these spectra show either a change in the development trend or almost conservation of the spectral pattern at ratios r above 1.25, which indicates occurrence of the third assembly stage (see Fig. 5 showing the dependence of λ_{MLCT} on r).

The third stage of assembly should consist of the end-capping of dynamer chains with Mt^{2+} ions and depolymerization of the chains to the shorter, also end-caped ones. The reaction of a bis(*tpy*)Zn^{2+} species with a free Zn^{2+} ion yielding two (*tpy*)Zn^{2+} species is well known.[47–49] A similar reaction of bis(*tpy*)Fe^{2+} species, particularly species with monotopic ligands, is not so obvious,[47,50] however, it was reported to take place in the case of metallo-supramolecular polymers.[48,51]

In order to examine whether this process takes place in solutions of our conjugated dynamers we carried out a viscometric study on the Fe^{2+}/**M-Br** system (see results in Fig. 6). As can be seen, the dependence of the relative viscosity (η_r) of **M-Br** solutions (0.5 mM) in $CHCl_3/CH_3CN$ (1 : 1) on the ratio r passes through maximum at $r = 1$ and then decreases. This indicates that the longest $\mathbf{P_{Fe}}$**M-Br** chains are obtained at $r = 1$ and that these chains most probably depolymerize at $r > 1$. Depolymerization should give the chains end-capped with Fe^{2+} ions.

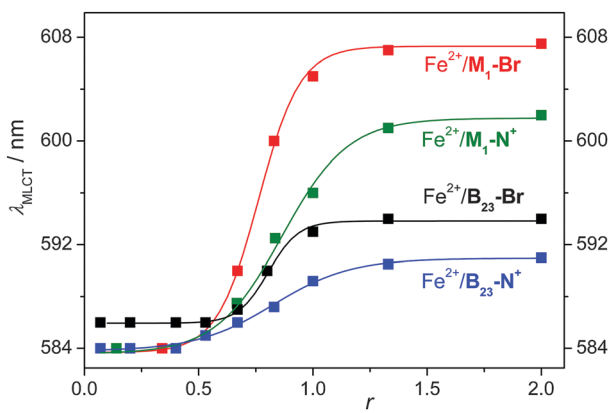

Fig. 5 The wavelength of MLCT bands of systems with Fe^{2+} ions as a function of the system composition.

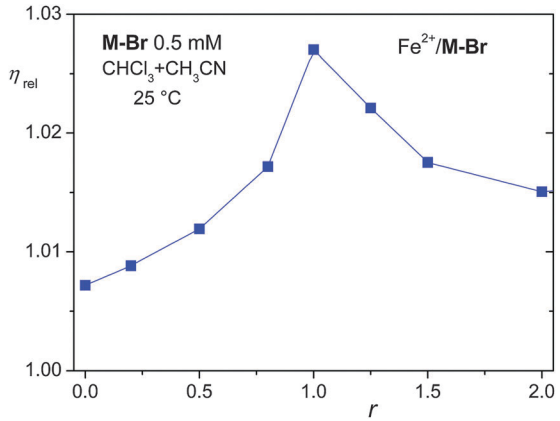

Fig. 6 Relative viscosity of solutions of the system Fe^{2+}/**M-Br** as a function of composition.

Assembling of unimers to dynamers was further studied using the SEC instrument equipped with a diode-array UV/vis detector (DAD). Mixed solutions of **M-Br** (0.5 mM) and Zn^{2+} or Fe^{2+} ions (r from 0 to 2.0) in $CHCl_3/CH_3CN$ (1 : 1) mixed solvent were allowed to equilibrate for one day and then injected into the SEC system. The same mixed solvent containing $Bu_4N^+PF_6^-$ (to suppress aggregation) was used as a mobile phase.

The SEC records of the Zn^{2+}/**M-Br** systems showed peaks of only free unimer **M-Br**, which proves a rapid complete dissociation of $\mathbf{P_{Zn}}$**M-Br** chains due to multifold dilution of the solution inside columns (injected 20 μL, elution volume of 37 mL). This proves that $\mathbf{P_{Zn}}$**M-Br** chains are supramolecular systems with rapid constitutional dynamics. In contrast, the Fe^{2+}/**M-Br** systems provided the SEC records typical of polymers, with the resolution decreasing with increasing ratio r (Fig. 7a). The DAD (*i.e.*, UV/vis) spectra of SEC fractions showed the dependence of the spectral patterns on the elution time (t_{el}): the patterns typical of long dynamer chains for short t_{el} and typical of butterfly dimers for long t_{el} (Fig. 7b). This proves that $\mathbf{P_{Fe}}$**M-Br** chains are the metallo-supramolecular systems with slow constitutional dynamics. As can be seen, well resolved SEC records were obtained only for systems with $r < 1$. The systems with $r \geq 1$ gave poorly resolved SEC records with the area below the elution curve decreasing with increasing value of r, which proves to retention of chains in SEC columns. The detained $\mathbf{P_{Fe}}$**M-Br** chains are obviously the chains end-capped with Fe^{2+} ions; they had to be additionally washed out with 2,2′-bipyridine.

The DAD spectra of SEC-fractions ($t_{el} = 1350$ s) of the systems with $r < 1$ (Fig. 8) are identical with the dilute solution (0.02 mM) spectrum of dimers. If this SEC peak is assigned to dimers, peak at 1273 s to trimers, *etc.* (Fig. 7a), the peak assignment provides linear semi-log dependence of the degree of polymerization (X) of $\mathbf{P_{Fe}}$**M-Br** chains on t_{el} for systems with $r < 1$ (ESI,† Fig. S7). Average values of X calculated from the SEC records using this calibration are listed in Table 2. The used peak assignment is supported by the DAD spectra of higher-X SEC-fractions, which correspond to dilute solution spectra of higher oligomers.

The presence of higher-X fractions in Fe^{2+}/**M-Br** solutions with fairly understoichiometric ratios, $r = 0.2$ and 0.5, should be

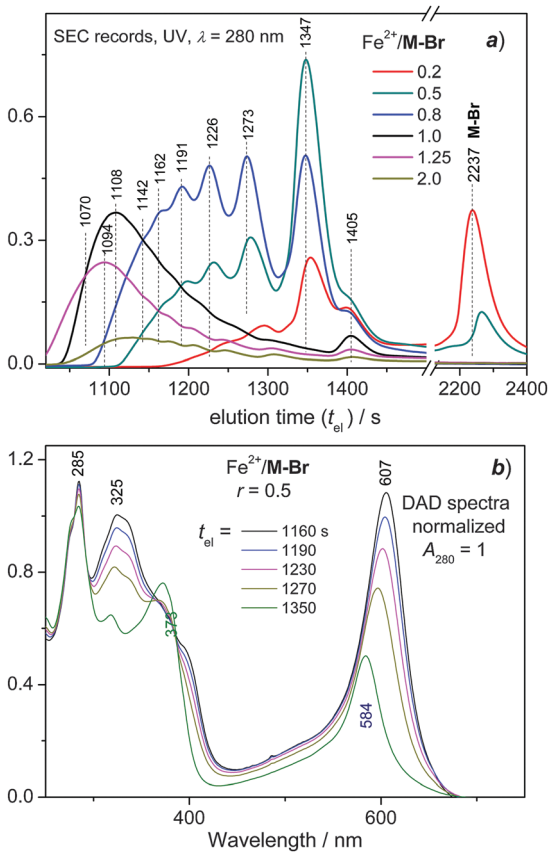

Fig. 7 The SEC records of Fe^{2+}/**M-Br** systems of different composition (a) and DAD spectra at different elution time t_{el} (b).

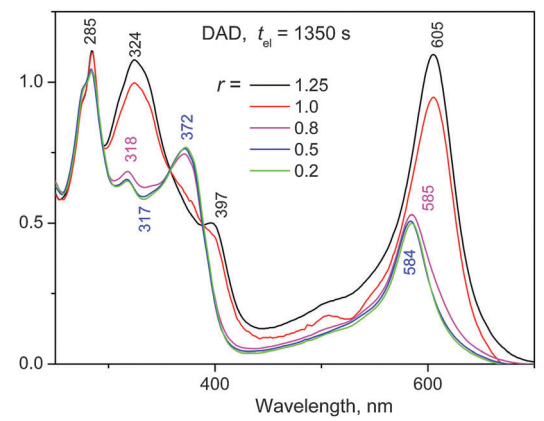

Fig. 8 The UV/vis spectra of SEC fractions (t_{el} = 1350 s) of Fe^{2+}/M-Br systems of different composition.

Table 2 Number-average (X_n) and weight-average (X_w) degrees of polymerization of $\mathbf{P_{Fe}M\text{-}Br}$ in solution calculated from SEC records

r	X_n	X_w	$Đ$
0.2	2.26	2.46	1.09
0.5	2.62	3.10	1.18
0.8	3.31	4.04	1.22
1	5.43	6.62	1.22
1.25	5.94	7.48	1.26

ascribed to the effect of transiently locally increased concentration during mixing of more concentrated solutions of **M-Br** and Fe^{2+} ions. Formation of dynamer chains is surely a kinetically controlled process which, when mixing twenty five times more concentrated solutions (0.5 mM instead 0.02 mM) should be *ca.* 625 times faster, thus giving rise to a high number of longer chains. As the constitutional dynamics of $\mathbf{P_{Fe}M\text{-}Br}$ is slow, the initially formed longer chains do not dissociate within one day. On the other hand, the dynamics slowness is lucky since it at all allows SEC analysis of Fe-dynamers (in contrast to Zn-dynamers).

Experimental section

Materials

n-Butyllithium (*n*-BuLi, 2.5 M in hexane), 3-bromothiophene, *N*-bromosuccinimide (NBS), bis(1,5-cyclooctadiene)di-μ-methoxy-diiridium(I) ([Ir(OMe)(COD)]$_2$), 4,4-di-*tert*-butyl-2,2-dipyridyl (dtbpy), 4,4,5,5-tetramethyl-1,3,2-dioxaborolane (HBpin), [1,3-bis(2,6-diisopropylphenyl)imidazol-2-ylidene](3-chloropyridyl)palladium(II) dichloride (Peppsi-IPr), bis(pinacolato)diboron (B_2pin_2), trimethylamine (4.2 M solution in ethanol), zinc perchlorate hexahydrate and iron(II) perchlorate hydrate (all Aldrich), K_2CO_3, $MgSO_4$ (Lachner) and 4-bromo-2,2:62-terpyridine (TCI) were used as received. Hexane (Lachner) was stored over a molecular sieve, tetrahydrofurane (Aldrich) was distilled from LiAlH before use, toluene (Lachner) was distilled from sodium/benzophenone before use, methanol (Aldrich) was bubbled with argon before use, dichloromethane, chloroform (Lachner) and acetonitrile were used as obtained.

Measurements

^{1}H and ^{13}C NMR spectra were recorded on a Varian ^{UNITY}INOVA 400 or Varian SYSTEM 300 instruments in d_8-THF, d_2-CD_2Cl_2, d-$CDCl_3$ or d_4-CD_3OD and referenced to the solvent signal: 7.25 ppm (d-$CDCl_3$), 5.32 ppm (d_2-CD_2Cl_2), 3.58 ppm (d_8-THF) or 3.31 ppm (d_4-CD_3OD) for ^{1}H and 77.0 ppm (d-$CDCl_3$), 53.84 ppm (d_2-CD_2Cl_2), 67.57 ppm (d_8-THF) or 49.15 ppm (d_4-CD_3OD) for ^{13}C spectra. Coupling constants, J (in Hz), were obtained by the first-order analysis. Infrared spectra were recorded on a Thermo Nicolet 7600 FTIR spectrometer equipped with a Spectra Tech InspectIR Plus microscopic accessory using KBr-diluted samples and a diffuse reflectance technique (DRIFT) (128 or more scans at resolution 4 cm^{-1}). Raman spectra of solid samples were recorded on a DXR Raman microscope (Thermo Scientific) using excitations across the whole visible region (λ_{ex} = 445, 532, 633 and 780 nm) and usual laser power at the sample from 0.1 to 0.4 mW. UV/VIS spectra were recorded on a Shimadzu UV-2401PC instrument and photoluminescence spectra on a Fluorolog 3-22 Jobin Yvon Spex instrument, using a four-window quartz cuvette (1 cm) for solutions and highly oriented pyrolytic graphite (NT-MDT Co., Russia) as substrate for films. The emission spectra were recorded with excitation wavelength, λ_{ex}, matching the absorption maximum of the measured compound. Quantum yields, ϕ_F, of photoluminescence were determined by means of a comparison of the integrated spectrum of the compound in

question with that of the standard: quinine sulfate diluted solution in 0.5 M H_2SO_4 (ϕ_F = 0.54; λ_{ex} = 380 nm). Absolute quantum yields for solid samples were measured using integration sphere Quanta-φ F-3029. Fluorescence decay was monitored using a FluoroHub single photon counting controller on a Fluorolog 3-22 Jobin Yvon Spex instrument with excitation at λ_{ex} = 378 nm for solutions and λ_{ex} = 472 nm for films. Viscometric measurements were done on a Lovis 2000 M/Me microviscometer (Anton Paar). SEC analyses were done on a Spectra Physics Analytical HPLC instrument fitted with two SEC columns Polymer Labs (Bristol, UK) Mixed-D, Mixed-E and THERMO UV6000 DAD detector. $CHCl_3$ + CH_3CN (1/1 by vol) (CHROMASOLV, Riedel-deHaen) containing $Bu_4N^+PF_6^-$ (0.05 mol dm^{-3}) was used as an eluent (0.7 mL min^{-1}).

Complexation experiments

In a typical complexation experiment a measured volume of a solution of Zn^{2+} or Fe^{2+} perchlorate (2×10^{-3} M) in $CHCl_3$ + CH_3CN (1/1 by vol) or MeOH was added into a solution of particular unimer in (2×10^{-5} M) in the same solvent. The metal to unimer (Mt^{2+}/U) composition ratio varied from 0 to 3. The UV/vis absorption and the photoluminescence emission spectra were measured for each solution at room temperature one day after preparing.

Syntheses of bisterpyridines

2,5-(3-(6-bromohexyl)thiophene-2,5-diyl)bis(4,4,5,5-tetramethyl-1,3,2-dioxaborolane). To a solution of 3-(6-bromohexyl)-thiophene (2.1 g; 8.45 mmol) in dry hexane (20 mL) $[Ir(OMe)(COD)]_2$ (42 mg, 0.06 mmol) and dtbpy (150 mg, 0.56 mmol) were added. The solution was bubbled with argon and HBpin (4 mL, 3.53 g, 27.6 mmol) was added. The reaction mixture was heated at 50 °C for 4 days. Then the mixture was diluted with water (20 mL). After an hour of stirring in an open vessel the solution was extracted with CH_2Cl_2 (3 × 50 mL). The organic layer were combined, dried with $MgSO_4$, filtered off and evaporated to get the product as a brownish oil. The product was used in following reaction as obtained without further purification. (2.3 g, 4.6 mmol, 55%).

^{1}H NMR (400 MHz, $CDCl_3$, δ/ppm): 7.50 (s, 1H, Th^4), 3.40 (t, J = 6.8, 2H, Hex^6), 2.87 (t, J = 7.5, 2H, Hex^1), 1.87–1.83 (m, 2H, Hex^5), 1.64–1.57 (m, 2H, Hex^2), 1.49–1.41 (m, 4H, Hex^3 + Hex^4), 1.37–1.32 (m, 32H, CH_3^-). ^{13}C NMR (101 MHz, $CDCl_3$, δ/ppm): 154.61, 139.46, 84.0, 83.56, 34.0, 32.69, 31.42, 29.67, 28.28, 27.92, 24.75. ^{11}B NMR (128.3 MHz, $CDCl_3$, δ/ppm): 22.24. FT-IR (cm^{-1}) 3427 (w), 2983 (s), 2940 (s), 2861 (s), 1537 (s), 1483 (s), 1469 (s), 1453 (m), 1396 (s), 1346 (m), 1297 (w), 1275 (w), 1214 (w), 1168 (s), 1152 (s), 1111 (w), 1048 (m), 963 (m), 925 (w), 860 (s), 828 (m), 786 (w), 728 (m), 688 (m), 671 (s), 647 (s), 577 (m), 562 (m), 520 (m), 427 (m). HRMS found m/z: 521.1673 $[M + Na]^+$, $C_{22}H_{37}O_4B_2BrNaS$ requires: 521. 1674.

2,5-Bis(2,2′:6′,2″-terpyridine-4′-yl)-3-(6-bromohexyl)thiophene, M-Br. 2,5-(3-(6-Bromohexyl)thiophene-2,5-diyl)bis(4,4,5,5-tetramethyl-1,3,2-dioxaborolane) (1.13 g, 2.26 mmol), Br*tpy* (1.47 g, 4.7 mmol), K_2CO_3 (1.9 g, 13.8 mmol) and Peppsi-IPr (100 mg, 0.15 mmol) were placed in the Schlenk tube and vacuum was applied. The tube was filled with argon and toluene (16 mL) and methanol (16 mL) were added. The reaction mixture was heated at 88 °C overnight. After cooling to room temperature the mixture was diluted with CH_2Cl_2 (50 mL) and washed with water (3 × 150 mL). The organic phase was dried with $MgSO_4$, filtered off and evaporated. Crude product was dissolved in the smallest amount of THF and hexane was added. After precipitation of white solid the mixture was filtered and the powder was collected. The residual solution was evaporated, dissolved in THF and precipitated again. White powder (0.46 g, 0.65 mmol, 29%).

^{1}H NMR (400 MHz, $CDCl_3$, δ/ppm): 8.79–8.68 (m, 12H, A^6 + A^3 + B^3), 7.94–7.89 (m, 4H, A^4), 7.79 (s, 1H, C^4), 7.42–7.37 (m, 4H, A^5), 3.38 (t, J = 6.9, 2H, Hex^6), 2.95–2.91 (m, 2H, Hex^1), 1.89–1.79 (m, 4H, Hex^2 + Hex^5), 1.49–1.46 (m, 2H, Hex^3 + Hex^4). ^{13}C NMR (101 MHz, $CDCl_3$, δ/ppm): 155.76, 149.14, 143.85, 143.12, 142.19, 141.02, 137.0, 128.98, 123.96, 121.33, 120.55, 117.05, 33.9, 32.70, 30.65, 29.22, 28.52, 27.92. FT-IR (cm^{-1}): 3056 (m), 3011 (m), 2932 (s), 2858 (m), 1597 (s), 1581 (s), 1565 (s), 1467 (s), 1441 (m), 1404 (s), 1310 (m), 1267 (m), 1124 (w), 1095 (w), 1073 (w), 1029 (w), 989 (m), 888 (m), 846 (w), 792 (s), 744 (s), 677 (m), 659 (m), 621 (m), 560 (w), 513 (m). HRMS found m/z: 709.1746 $[M + H]^+$, $C_{40}H_{34}N_6BrS$ requires: 709.1746.

3,3′-Bis(6-bromohexyl)-2,2′-bithiophene. 2-Bromo-3-(6-bromohexyl)thiophene (1 mL, 1.25 g, 3.84 mmol), B_2pin_2 (0.48 g, 1.9 mmol), K_2CO_3 (1.57 g, 11.4 mmol) and Peppsi-IPr (50 mg, 0.07 mmol) were placed into the Schlenk tube and vacuum was applied. After filling the tube with argon, toluene (15 mL) and methanol (15 mL) were added and the reaction mixture was heated at 90 °C for 18 hours. The mixture was cooled down and diluted with CH_2Cl_2 (50 mL). The solution was washed with water (3 × 150 mL), dried with $MgSO_4$, filtered off and evaporated. The crude product was purified on column chromatography (silica, CH_2Cl_2 + hexane 1/1). Yellowish oil (0.34 g, 0.69 mmol, 36%).

^{1}H NMR (400 MHz, $CDCl_3$, δ/ppm): 7.37 (d, J = 5.5, 2H, Th^4), 6.99 (d, J = 5.5, 2H, Th^5), 3.38 (t, J = 6.8, 4H, Hex^6), 2.52 (t, J = 7.8, 4H, Hex^1), 1.82–1.75 (m, 4H, Hex^5), 1.61–1.53 (m, 4H, Hex^2), 1.41–1.34 (m, 8H, Hex^3 + Hex^4). ^{13}C NMR (101 MHz, $CDCl_3$, δ/ppm): 143.04, 129.72, 129.45, 126.56, 34.38, 33.91, 32.71, 31.60, 28.99, 27.93. FT-IR (cm^{-1}): 3101 (w), 3059 (w), 3002 (w), 2932 (s), 2854 (s), 1519 (w), 1460 (m), 1437 (m), 1409 (w), 1371 (w), 1294 (w), 1257 (m), 1232 (m), 1090 (w), 1049 (w), 879 (w), 831 (m), 803 (w), 774 (w), 723 (m), 693 (m), 645 (m), 561 (m). HRMS found m/z: 491.0072 $[M + H]^+$, $C_{20}H_{29}Br_2S_2$ requires: 491.0072.

5,5′-(3,3′-Bis(6-bromohexyl)-2,2′-bithiophene-5,5′-diyl)bis-(4,4,5,5-tetramethyl-1,3,2-dioxaborolane). 3,3′-Bis(6-bromohexyl)-2,2′-bithiophene (0.34 g, 0.69 mmol), dtbpy (23 mg, 0.08 mmol) and $[Ir(OMe)(COD)]_2$ (30 mg, 0.04 mmol) were placed in the flask. The flask was flushed with argon and THF (7 mL) and hexane (7 mL) were added. HBpin (0.4 mL, 0.35 g, 2.76 mmol) was added through a septum and the reaction mixture was heated at 55 °C for 48 hours. The reaction mixture was diluted with water (20 mL) and stirred in an open vessel for an hour. Then the solution was extracted with CH_2Cl_2 (50 mL). The organic layer was dried with $MgSO_4$, filtered off and evaporated to get the product as a brownish oil. (0.48 g, 0.64 mmol, 93%).

^{1}H NMR (400 MHz, CD_2Cl_2, δ/ppm): 7.46 (s, 2H, Th^4), 3.37 (t, J = 7.0, 4H, Hex^6), 2.51 (m, 4H, Hex^1), 1.83–1.80 (m, 4H, Hex^5), 1.57–1.53 (m, 12H, Hex^2–Hex^4), 1.33 (s, 32H, CH_3–). ^{13}C NMR (101 MHz, CD_2Cl_2, δ/ppm): 144.06, 139.25, 84.73, 34.67, 33.30, 30.98, 28.96, 28.44, 26.14, 25.14. ^{11}B NMR (128 MHz, CD_2Cl_2, δ/ppm): 24.39. FT-IR (cm^{-1}): 3394 (m), 2976 (s), 2931 (s), 2856 (m), 1618 (w), 1530 (m), 1474 (s), 1379 (s), 1330 (s), 1298 (m), 1267 (m), 1214 (w), 1165 (m), 1142 (s), 1027 (m), 982 (m), 961 (w), 925 (w), 852 (s), 802 (m), 727 (w), 665 (m), 577 (w), 519 (w). HRMS found m/z: 765.1595 $[M + Na]^+$, $C_{32}H_{50}O_4B_2Br_2NaS_2$ requires: 765.1596.

5,5′-Bis(2,2′:6′,2″-terpyridine-4′-yl)-3,3′-di(6-bromohexyl)-2,2′-bithiophene, B-Br. 5,5′-(3,3′-Bis(6-bromohexyl)-2,2′-bithiophene-5,5′-diyl)bis(4,4,5,5-tetramethyl-1,3,2-dioxaborolane) (0.48 g, 0.64 mmol), Br*tpy* (0.43 g, 1.37 mmol), K_2CO_3 (0.52 g, 3.76 mmol) and Peppsi-IPr (26 mg, 0.04 mmol) were placed in the Schlenk flask and vacuum was applied. The flask was flushed with argon and toluene (15 mL) and methanol (15 mL) were added. The reaction mixture was heated at 90 °C for 18 hours. After cooling to room temperature the reaction mixture was diluted with CH_2Cl_2 (50 mL) and washed with water (3 × 100 mL), then dried with $MgSO_4$, filtered off and evaporated. The crude product was purified on column chromatography (aluminium oxide, hexane + THF 3/2). Yellow solid (0.12 g, 0.13 mmol, 20%).

^{1}H NMR (400 MHz, THF, δ/ppm): 8.83 (s, 4H, B^3), 8.72–8.70 (m, 8H, A^3 + A^6), 7.94–7.89 (m, 4H, A^4), 7.87 (s, 2H, C^4), 7.41–7.37 (m, 4H, A^5), 3.42 (t, J = 6.8, 4H, Hex^6), 2.77–2.74 (m, 4H, Hex^1), 1.89–1.79 (m, 8H, Hex^2 + Hex^5), 1.51–1.38 (m, 8H, Hex^3 + Hex^4). ^{13}C NMR (101 MHz, $CDCl_3$, δ/ppm): 156.08, 155.99, 149.12, 143.68, 143.09, 141.51, 136.84, 130.30, 127.45, 123.90, 121.32, 116.81, 33.88, 32.68, 30.49, 29.01, 28.51, 27.95. FT-IR (cm^{-1}): 3057 (w), 3010 (w), 2930 (m), 2854 (m), 1597 (m), 1581 (s), 1565 (s), 1528 (w), 1466 (m), 1443 (m), 1419 (w), 1403 (m), 1382 (w), 1360 (w), 1263 (m), 1209 (w), 1147 (w), 1123 (w), 1094 (m), 1072 (m), 1018 (m), 989 (m), 959 (w), 901 (w), 881 (m), 847 (m), 791 (s), 773 (m), 746 (m), 734 (m), 688 (w), 677 (w), 658 (m), 648 (w), 633 (w), 621 (m), 507 (w). HRMS found m/z: 953.1673 $[M + H]^+$, $C_{50}H_{47}N_6Br_2S_2$ requires: 953.1665.

Quarternization

A weighed amount of a given Br-unimer was dissolved in THF (conc. 4 × 10^{-3} M), trimethylamine was added (10 eq.) as ethanol solution (4.2 M) and the mixture was kept at 25 °C for four days. The precipitated product was isolated by centrifugation, washed with THF and dried under vacuum.

6-[2,5-Bis(2,2′:6′,2″-terpyridine-4′-yl)thiophene-3-yl]hexan-1-yl trimethylammonium bromide, M-N$^+$. Yellowish powder 37%. ^{1}H NMR (400 MHz, CD_3OD, δ/ppm): 8.70–8.69 (m, 4H, A^6), 8.64–8.60 (m, 6H, A^3 + B^3 or $B^{3\prime}$), 8.54 (s, 2H, $B^{3\prime}$ or B^3), 8.01–7.96 (m, 4H, A^4), 7.80 (s, 1H, C^4), 7.49–7.45 (m, 4H, A^5), 3.25–3.20 (m, 2H, Hex^6) 3.03 (s, 9H, N-$(CH_3)_3$), 2.98 (t, J = 7.6, 2H, Hex^1), 1.87–1.72 (m, 4H, Hex^5 + Hex^2), 1.54–1.50 (m, 2H, Hex^4), 1.42–1.38 (m, 2H, Hex^3). ^{13}C NMR (101 MHz, CD_3OD, δ/ppm): 157.74, 157.61, 157.20, 150.66, 145.41, 144.51, 139.06, 130.85, 126.0, 123.15, 121.48, 117.93, 68.14, 53.78, 31.73, 30.13, 27.47, 27.45, 24.20. FT-IR (cm^{-1}): 3412 (m), 3055 (m), 3012 (m), 2940 (s), 2861 (m), 1767 (w), 1722 (m), 1597 (s), 1582 (s), 1557 (s), 1468 (s), 1441 (m), 1403 (s), 1381 (m), 1266 (m), 1168 (w), 1126 (w), 1095 (w), 1073 (m), 1031 (m), 989 (m), 966 (w), 888 (m), 846 (w), 793 (s), 745 (s), 677 (m), 660 (m), 621 (m), 589 (w), 569 (w), 513 (m), 502 (w), 471 (w). HRMS found m/z: 688.3218 $[M + H]^+$, $C_{43}H_{42}N_7S$ requires: 688.3217.

6,6′-[5,5′-Bis(2,2′:6′,2″-terpyridine-4′-yl)-2,2′-bithiophene-3,3′-diyl]bis[hexan-1,1′-diyl trimethylammonium]bromide, B-N$^+$. Orange powder 41%. ^{1}H NMR (400 MHz, CD_3OD, δ/ppm): 8.72–8.71 (m, 4H, A^6), 8.62–8.59 (m, 4H, A^3), 8.56 (s, 4H, B^3), 8.01 (td, J = 7.7, J = 1.6, 4H, A^4), 7.8 (s, 2H, C^4), 7.53–7.50 (ddd, J = 7.4, J = 4.8, J = 1.3, 4H, A^5), 3.31–3.28 (m, 4H, Hex^6), 3.07 (s, 18H, N-$(CH_3)_3$), 2.74 (t, J = 7.7, 4H, Hex^1), 1.83–1.75 (m, 8H, Hex^5 + Hex^2), 1.53–1.30 (m, 8H, Hex^3 + Hex^4) ^{13}C NMR (101 MHz, CD_3OD δ/ppm): 157.82, 157.67, 157.22, 150.47, 144.68, 139.25, 139.14, 132.09, 129.53, 126.11, 123.30, 117.82, 68.19, 53.76, 31.78, 30.24, 27.49, 26.07, 24.25. FT-IR (cm^{-1}): 3404 (s), 3058 (m), 3015 (m), 2933 (s), 2858 (m), 1722 (s), 1674 (s), 1584 (s), 1567 (s), 1469 (s), 1402 (s), 1265 (m), 1210 (m), 1176 (w), 1124 (w), 1094 (w), 1072 (m), 1044 (w), 1018 (m), 991 (m), 971 (w), 907 (m), 886 (m), 846 (m), 792 (s), 743 (s), 659 (s), 622 (s), 586 (w), 573 (w), 529 (m), 507 (w), 490 (w), 457 (w), 430 (w). HRMS found m/z: 456.2343 $[M + H]^{2+}$, $C_{56}H_{64}N_8S_2$ requires: 456.2342.

Conclusions

The here exploited route to alcohol-soluble ionic unimers includes preparation of their ω-bromoalkyl precursors, which is not too easy but already well mastered procedure, and replacing terminal bromine atoms with ammonium type groups. An inverse approach, coupling of ionic thiophenes with Br*tpy*, is difficult owing to diverse solubility of reactants, the catalyst and the auxiliary base. Though the modification of bromo-unimers to the ionic ones seems trivial, it is inhibited by *tpy* end-groups and, therefore, is well feasible only with highly reactive amines.

A spectroscopic study of unimers' assembly with metal ions in dilute solutions provided the UV/vis and luminescence spectral patterns characteristic of the U-Mt^{2+}-U type dimers, dynamer chains with free *tpy* end-groups and dynamer chains capped with metal ions. Absorption spectra of SEC fractions of non-ionic Fe-dynamer $\mathbf{P_{Fe}M\text{-}Br}$ well agree with the dilute solution spectra of the systems with corresponding composition ratios r. The SEC study further proved that the constitutional dynamics of Zn-dynamers is fast while that of Fe-dynamers is slow. It also provided a good calibration dependence, which allowed determining the average values of the degree of polymerization of the dynamer in solutions; this characteristic of dynamers is otherwise almost not accessible and is the subject of the question after almost every conference presentation. Unfortunately, the ionic Fe-dynamers were not effectively separated in SEC columns due to the strong interference of the adsorption mode.

Relative stability of Fe-dynamer chains in solutions (changes lasting for two months are reported in the literature)[48] should be attributed to the MLCT within the *tpy*-Fe^{2+}-*tpy* linkages. The here presented UV/vis spectra as well as the spectra presented

earlier[47,50,52] confirm that the MLCT bands are contributed also with transitions within central blocks of unimeric units. The resonance Raman spectra obtained in this study indicate that the transitions within the central block significantly affect the longer-wavelength part of the MLCT band while its shorter-wavelength arm is mainly contributed with transitions within *tpy* end-groups.

Acknowledgements

Financial support of the Czech Science Foundation (P108/12/1143) and the Grant Agency of Charles University (project 64213) is greatly acknowledged.

References

1 J. Lehn, *Prog. Polym. Sci.*, 2005, **30**, 814.
2 J. W. Steed and J. L. Atwood, *Supramolecular chemistry*, John Wiley & Sons, Ltd, 2nd edn, 2009.
3 A. Ciferri, in *Supramolecular Polymers*, ed. A. Ciferri, CRC Press, 2nd edn, 2005.
4 M. Beley, D. Delabouglise, G. Houppy, J. Husson and J.-P. Petit, *Inorg. Chim. Acta*, 2005, **358**, 3075.
5 A. Wild, F. Schlütter, G. M. Pavlov, C. Friebe, G. Festag, A. Winter, M. D. Hager, V. Cimrová and U. S. Schubert, *Macromol. Rapid Commun.*, 2010, **31**, 868.
6 A. El-Ghayoury, A. P. H. J. Schenning and E. W. Meijer, *J. Polym. Sci., Part A: Polym. Chem.*, 2002, **40**, 4020.
7 A. Harriman, G. Izzet, S. Goeb, A. De Nicola and R. Ziessel, *Inorg. Chem.*, 2006, **45**, 9729.
8 S. C. Yu, C. C. Kwok, W. K. Chan and C. M. Che, *Adv. Mater.*, 2003, **15**, 1643.
9 P. R. Andres and U. S. Schubert, *Adv. Mater.*, 2004, **16**, 1043.
10 A. Barbieri, B. Ventura, F. Barigelletti, A. De Nicola, M. Quesada and R. Ziessel, *Inorg. Chem.*, 2004, **43**, 7359.
11 Q. Wu, J. Wang, H. Hu, Y. Shangguan, F. Fu, M. Yang, F. Dong and G. Xue, *Inorg. Chem. Commun.*, 2011, **14**, 484.
12 R. Siebert, A. Winter, M. Schmitt, J. Popp, U. S. Schubert and B. Dietzek, *Macromol. Rapid Commun.*, 2012, **33**, 481.
13 R. Dobrawa, M. Lysetska, P. Ballester, M. Grüne and F. Würthner, *Macromolecules*, 2005, **38**, 1315.
14 F. S. Han, M. Higuchi, Y. Akasaka, Y. Otsuka and D. G. Kurth, *Thin Solid Films*, 2008, **516**, 2469.
15 P. D. Vellis, J. A. Mikroyannidis, C. Lo and C. Hsu, *J. Polym. Sci., Part A: Polym. Chem.*, 2008, **46**, 7702.
16 Y. Chen and H. Lin, *J. Polym. Sci., Part A: Polym. Chem.*, 2007, **45**, 3243.
17 A. Winter, C. Friebe, M. Chiper, M. D. Hager and U. S. Schubert, *J. Polym. Sci., Part A: Polym. Chem.*, 2009, **3**, 4083.
18 F. Barigelletti and L. Flamigni, *Chem. Soc. Rev.*, 2000, **29**, 1.
19 M. Chiper, R. Hoogenboom and U. S. Schubert, *Macromol. Rapid Commun.*, 2009, **30**, 565.
20 A. Maier, K. Cheng, J. Savych and B. Tieke, *ACS Appl. Mater. Interfaces*, 2011, **3**, 2710.
21 A. Wild, A. Teichler, C.-L. Ho, X.-Z. Wang, H. Zhan, F. Schlütter, A. Winter, M. D. Hager, W.-Y. Wong and U. S. Schubert, *J. Mater. Chem. C*, 2013, **1**, 1812.
22 Y. Li, T. Ren and W.-J. Dong, *J. Photochem. Photobiol., A*, 2013, **251**, 1.
23 R. Siebert, Y. Tian, R. Camacho, A. Winter, A. Wild, A. Krieg, U. S. Schubert, J. Popp, I. G. Scheblykin and B. Dietzek, *J. Mater. Chem.*, 2012, **22**, 16041.
24 P. Bláhová, J. Zedník, I. Šloufová, J. Vohlídal and J. Svoboda, *Soft Mater.*, 2014, **12**, 214.
25 L. Fillaud, G. Trippé-Allard and J. C. Lacroix, *Org. Lett.*, 2013, **15**, 1028.
26 M. Barón, K.-H. Hellwich, M. Hess, K. Horie, A. D. Jenkins, R. G. Jones, J. Kahovec, P. Kratochvíl, W. V. Metanomski, W. Mormann, R. F. T. Stepto, J. Vohlídal and E. S. Wilks, *Pure Appl. Chem.*, 2009, **81**, 1131.
27 M. Hess, R. G. Jones, J. Kahovec, T. Kitayama, P. Kratochvil, P. Kubisa, W. Mormann, R. F. T. Stepto, D. Tabak, J. Vohlidal and E. S. Wilks, *Pure Appl. Chem.*, 2006, **78**, 2067.
28 J. Svoboda, P. Stenclova, F. Uhlík, J. Zedník and J. Vohlídal, *Tetrahedron*, 2011, **67**, 75.
29 G. a Chotana, V. a Kallepalli, R. E. Maleczka and M. R. Smith, *Tetrahedron*, 2008, **64**, 6103.
30 T. Ishiyama, Y. Nobuta, J. F. Hartwig and N. Miyaura, *Chem. Commun.*, 2003, 2924.
31 H. A. Ho and M. Leclerc, *J. Am. Chem. Soc.*, 2003, **125**, 4412.
32 F. Le Floch, H.-A. H. a. Ho, P. Harding-Lepage, M. Bédard, R. Neagu-Plesu and M. Leclerc, *Adv. Mater.*, 2005, **17**, 1251.
33 D. Bondarev, J. Zedník, I. Šloufová, A. Sharf, M. Procházka, J. Pfleger and J. Vohlídal, *J. Polym. Sci., Part A: Polym. Chem.*, 2010, **48**, 3073.
34 U. S. Schubert, H. Hofmeier and G. R. Newkome, *Modern Terpyridine Chemistry*, Wiley-VCH Verlag GmbH, Weinheim, 2006.
35 J. N. Demas and B. A. DeGraft, in *Topics in Fluorescence Spectroscopy: Volume 4: Probe Design and Chemical Sensing*, ed. J. R. Lakowicz, Springer Science & Business Media, 1994, ch. 4.5, p. 81.
36 R. Englman and J. Jortner, *Mol. Phys.*, 1970, **18**, 145.
37 R. Siebert, A. Winter, M. Schmitt, J. Popp, U. S. Schubert and B. Dietzek, *Macromol. Rapid Commun.*, 2012, **33**, 481.
38 I. Šloufová, B. Vlčková, M. Procházka, J. Svoboda and J. Vohlídal, *J. Raman Spectrosc.*, 2014, **45**, 338.
39 R. Horvath, J. Lombard, J.-C. Leprêtre, M.-N. Collomb, A. Deronzier, J. Chauvin and K. C. Gordon, *Dalton Trans.*, 2013, **42**, 16527.
40 S. Kazim, J. Pfleger, K. Halašová, M. Procházka, D. Bondarev and J. Vohlídal, *Eur. Phys. J.: Appl. Phys.*, 2011, **55**, 23905.
41 S. Kazim, J. Pfleger, M. Procházka, D. Bondarev and J. Vohlídal, *J. Colloid Interface Sci.*, 2011, **354**, 611.
42 E. A. Bazzaoui, M. Bazzaoui, J. Aubard, J. S. Lomas, N. Félidj and G. Lévi, *Synth. Met.*, 2001, **123**, 299.
43 K. Mukherjee, D. Bhattacharjee and T. Misra, *J. Colloid Interface Sci.*, 1999, **213**, 46.
44 I. Srnova-Šloufová, B. Vlčková, T. L. Snoeck, D. J. Stufkens and P. Matjka, *Inorg. Chem.*, 2000, **39**, 3551.

45 P. K. Mallick, G. D. Danzer, D. P. Strommen and R. Kincaid James, *J. Phys. Chem.*, 1988, **92**, 5628.
46 D. P. Strommen, P. K. Mallick, G. D. Danzer, R. S. Lumpkin and R. Kincaid James, *J. Phys. Chem.*, 1990, **94**, 1358.
47 T. Vitvarová, J. Zedník, M. Bláha, J. Vohlídal and J. Svoboda, *Eur. J. Inorg. Chem.*, 2012, 3866.
48 G. Schwarz, I. Haßlauer and D. G. Kurth, *Adv. Colloid Interface Sci.*, 2014, **207**, 107.
49 V. Stepanenko, M. Stocker, P. Müller, M. Büchner and F. Würthner, *J. Mater. Chem.*, 2009, **19**, 6816.
50 R. A. Dobrawa, PhD thesis, Bayerischer Julius-Maximilians-Universität Würzburg, 2004.
51 G. Schwarz, Y. Bodenthin, T. Geue, J. Koetz and D. G. Kurth, *Macromolecules*, 2010, **43**, 494.
52 R. Dobrawa and F. Würthner, *J. Polym. Sci., Part A: Polym. Chem.*, 2005, **43**, 4981.

Electronic supplementary information

Alcohol-soluble bis(*tpy*)oligothiophenes: new building units for constitutional dynamic conjugated polyelectrolytes

Pavla Bláhová, Jan Svoboda,* Ivana Šloufová, Jiří Vohlídal*

Charles University in Prague, Faculty of Science, Department of Physical and Macromolecular Chemistry, Hlavova 2030, CZ-128 40, Prague 2, Czech Republic.
Fax:+420 224919752; Tel:+420 221951310;
E-mail: jan.svoboda@natur.cuni.cz (J. Svoboda)
jiri.vohlidal@natur.cuni.cz (J. Vohlídal)

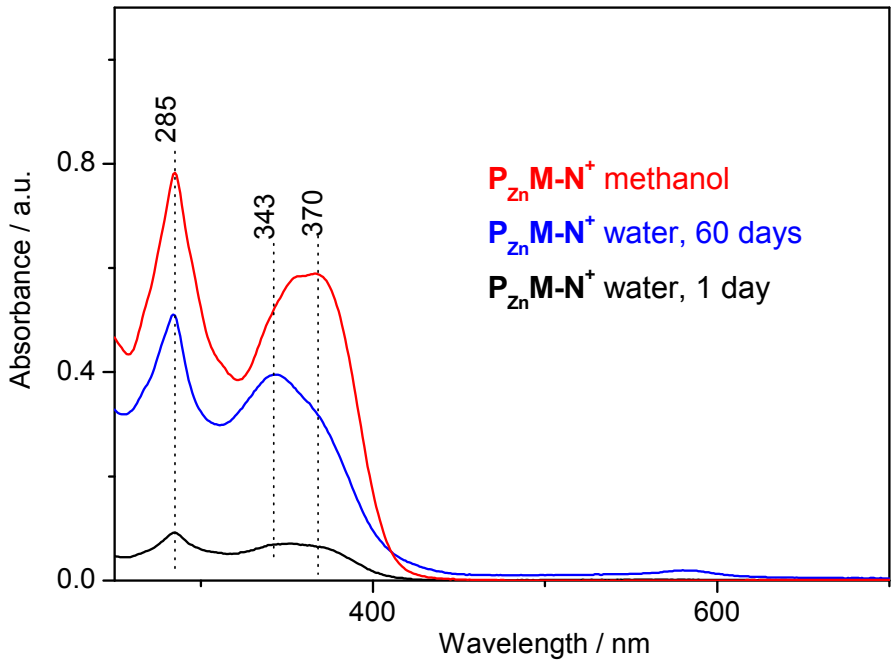

Figure S1: Absorption spectra of $\mathbf{P_{Zn}M\text{-}N^+}$ in methanol and in water after 1 and 60 days of dissolving.

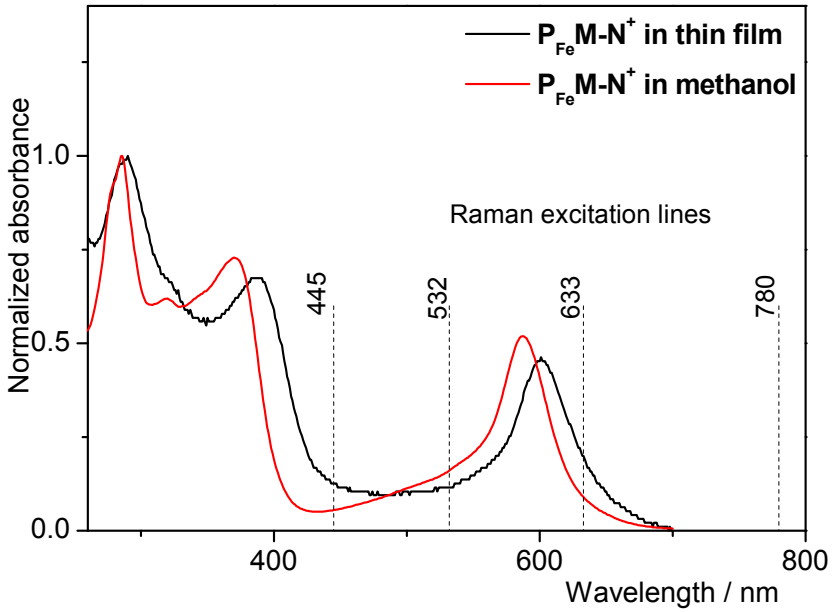

Figure S2: Normalized absorption spectra of $\mathbf{P_{Fe}M\text{-}N^+}$ in solution and in thin film and position of Raman excitation lines.

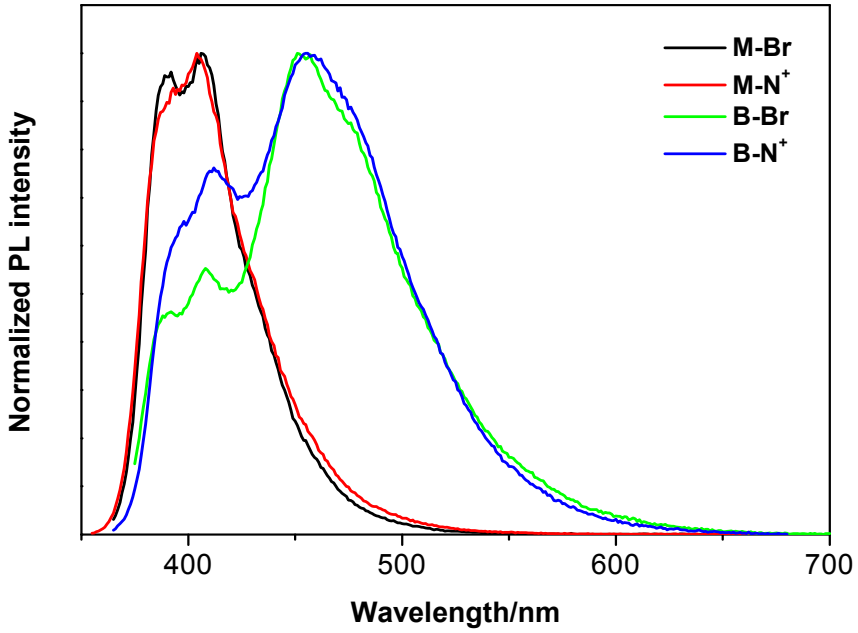

Figure S3: Normalized photoluminescence spectra of unimers in solution.

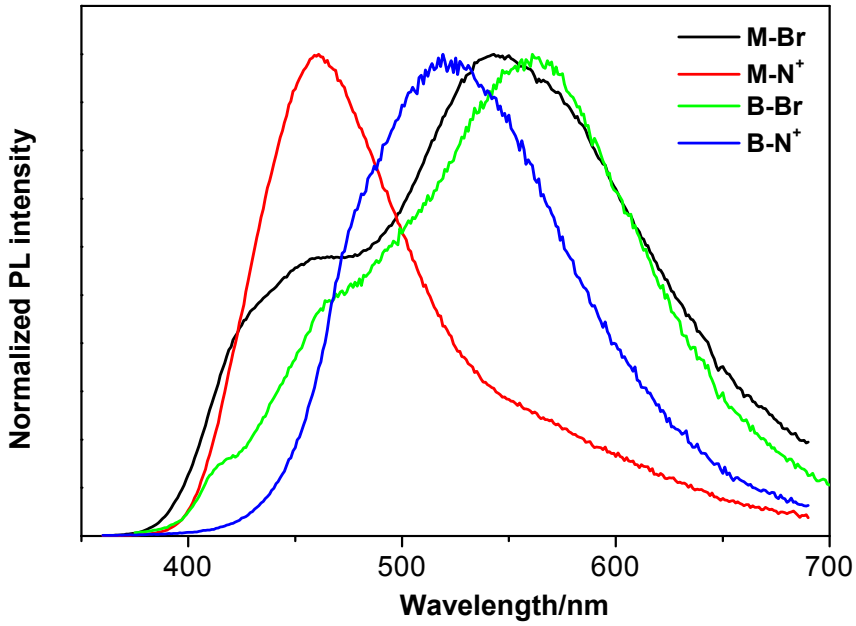

Figure S4: Normalized photoluminescence spectra of unimers in thin film.

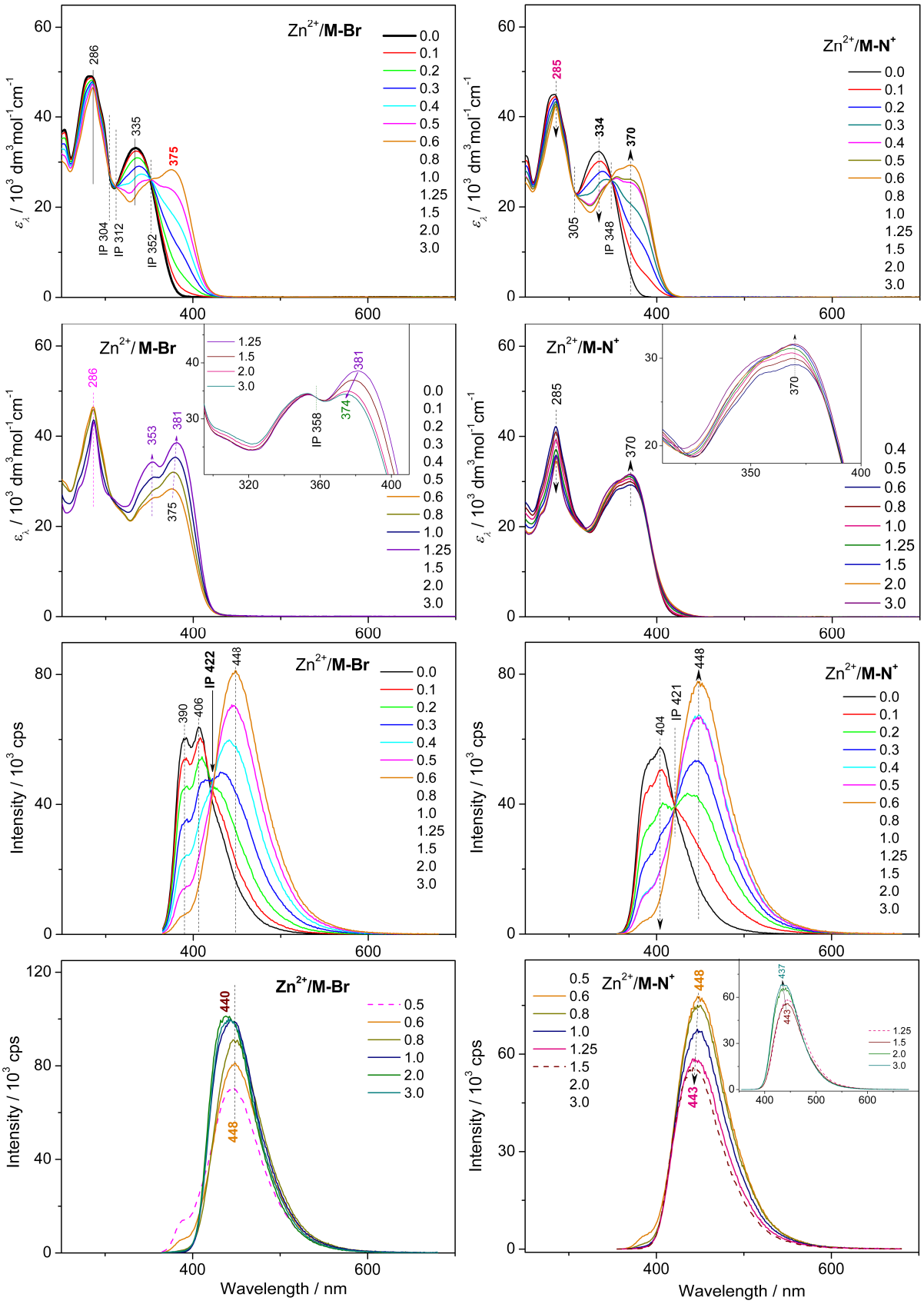

Figure S5: Changes in UV/vis and photoluminescence spectra accompanied titrations of **M-Br** (left) and **M-N**$^+$ (right) unimers with Zn^{2+} ions. Initial unimer concentration $2 \cdot 10^{-5}$ mol·dm^{-3}; chloroform/acetonitrile (**Br**-unimers), methanol (**N**$^+$-unimers), room temperature.

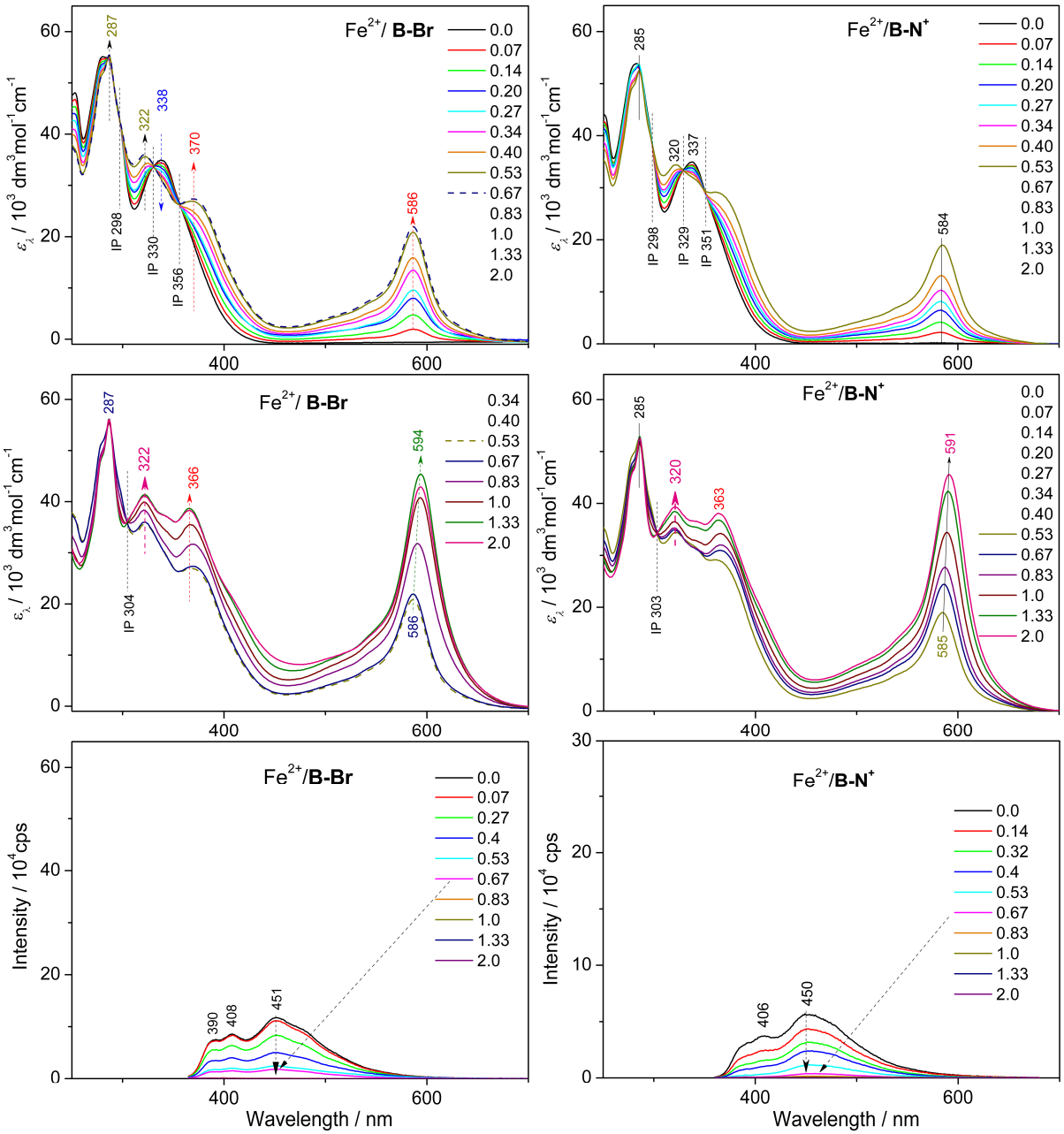

Figure S6: Changes in UV/vis and photoluminescence spectra accompanied titrations of **B-Br** (left) and **B-N**$^+$ (right) unimers with Fe^{2+} ions. Initial unimer concentration $2 \cdot 10^{-5}$ mol·dm^{-3}; chloroform/acetonitrile (**Br**-unimers), methanol (**N**$^+$-unimers), room temperature.

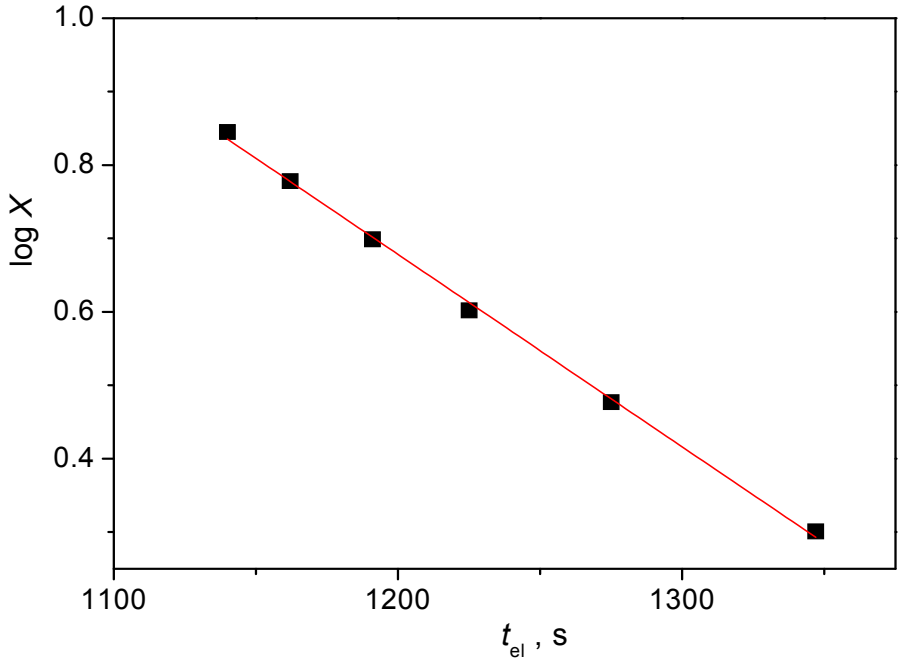

Figure S7: Dependence of the degree of polymerization, *X*, of **P_{Fe}M-Br** on the elution time, t_{el}.

Table S1: The photoluminescence maxima, λ_F, in solution and in thin film, photoluminescence quantum yield, ϕ, and lifetime of excited states, τ.

Sample	Luminescence			
	λ_F , nm (ϕ, %)		τ , ps	
	solution	film	solution	film
Unimers				
M-Br	406 (3 %)	543 (7 %)	186 (6%) 593 (94%)	777 (55%) 136 (27%) 3520 (18%)
M-N$^+$	404 (5 %)	461 (4 %)	122 (6%) 581 (6%)	450 (22%) 1550 (57%) 3780 (21%)
B-Br	452 (5 %)	561 (3 %)	428 (20%) 51 (71%) 965 (9%)	1800 (60%) 426 (16%) 5050 (24%)
B-N$^+$	450 (5 %)	519 (3 %)	390 (19%) 35(71%) 886 (10%)	912 (50%) 218 (32%) 3280 (18%)
Zn-dynamers				
P$_{Zn}$M-Br	440	460 (1 %)		119 (47%) 542 (42%) 1950 (11%)
P$_{Zn}$M-N$^+$	444	473 (4 %)		481 (33%) 82 (54%) 1660 (13%)
P$_{Zn}$B-Br	550	525 (3 %)		866 (54%) 195 (33%) 3380 (13%)
P$_{Zn}$B-N$^+$	550	538 (3 %)		192 (55%) 616 (49%) 2310 (6%)

ATTACHEMENT D

Štenclová P., Šichová K., Šloufová I., Zedník J., Svoboda J. Vohlídal J.: Alcohol- and water-soluble bis(*tpy*)quaterthiophenes with phosphonium side groups: new conjugated units for metallo-supramolecular polymers;
Dalton Trans. 2015, DOI: 10.1039/C5DT04133C.

Journal Name

ARTICLE

Alcohol- and water-soluble bis(*tpy*)quaterthiophenes with phosphonium side groups: new conjugated units for metallo-supramolecular polymers

Received 00th January 20xx,
Accepted 00th January 20xx

P. Štenclová, K. Šichová, I. Šloufová, J. Zedník, J. Vohlídal* and J. Svoboda*

DOI: 10.1039/x0xx00000x

www.rsc.org/

Bis(*tpy*)quaterthiophenes with symmetrically distributed two and four 6-bromohexyl side groups are prepared and modified by the reaction with triethylphosphine to give corresponding ionic species. Both ionic and non-ionic bis(*tpy*)quaterthiophenes (unimers) are assembled with Zn^{2+} and Fe^{2+} ions to conjugated metallo-supramolecular polymers (MSPs), of which the ionic ones are soluble in alcohols and those derived from tetrasubstituted unimers even in water. Differences in assembling are specified between systems with (i) ionic and non-ionic unimers; (ii) Zn^{2+} and Fe^{2+} ion couplers, and (iii) methanol and water solvents. A substantial decrease in the stability of Fe-MSPs and surprisingly high red shift of the luminescence band of Zn-MSPs are observed when going from methanol to aqueous solutions.

Introduction

Conjugated metallo-supramolecular polymers (MSPs) derived from α,ω-bis(*tpy*)oligoarylenes (*tpy* stands for 2,2':6',2''-terpyridine-4'-yl end-group) are of interest as potential materials for devices with applications based on the light/electricity inter-conversion and non-linear optical phenomena (light-emitting devices, photovoltaic cells, etc.).[1–16] However, overwhelming majority of these MSPs suffers from low solubility, which makes their processing difficult. For example, MSPs derived from α,ω-bis(*tpy*)oligophenylenes have been processed from acids[17,18] that surely are not optimum solvents.

Chains of conjugated MSPs of this type are composed of molecules of a bisterpyridines that are linked via facial and meridian coordination of their *tpy* end-groups to metal ions such as Ru^{2+}, Fe^{2+}, Zn^{2+} and Co^{2+} (generally Mt^{2+}) ions. The *tpy*–Mt^{2+}–*tpy* linkages are strictly linear and rigid.[11,19–27] The enchained unimers are also quite rigid due to the delocalization of π-electrons. Rigidity of both of these constitutional units together with electrostatic repulsions of the main-chain Mt^{2+} cations favor extended conformations of MSPs chains that are favorable for the inter-chain attraction. Thus the above structure features can be regarded as the main reason for low solubility of MSPs derived from α,ω-bis(*tpy*)oligoarylenes.

Department of Physical and Macromolecular Chemistry, Charles University in Prague, Faculty of Science, Hlavova 2030, Prague 2, CZ-128 40, Czech Republic
Fax:+420 224919752; Tel:+420 221951310
E-mail: jiri.vohlidal@natur.cuni.cz (Prof. J. Vohlídal)
jan.svoboda@natur.cuni.cz (Dr. J. Svoboda)

Electronic Supplementary Information (ESI) available: [details of any supplementary information available should be included here]. See DOI: 10.1039/x0xx00000x

An increase in solubility of the discussed conjugated MSPs has been achieved by introducing pendant alkyl groups to unimer units. However, this increase is insufficient.[28] Further improvement in solubility of MSPs can be achieved by introducing cationic pendant groups onto unimer building blocks. Markedly cationic character of MSPs chains should reduce the inter-chain attraction and thus make MSPs more soluble mainly in polar solvents such as alcohols or even in water. Such solvents are perhaps most desired for processing of conjugated MSPs.

The above approach has been recently examined on thiophene and bithiophene with *tpy* end-groups.[29] In the present paper, we report the preparation and basic properties α,ω- bis(*tpy*)quaterthiophenes with cationic side groups and related conjugated MSPs with Zn^{2+} and Fe^{2+} ion couplers. Since the studied MSPs show constitutional dynamics[30,31] they exist in solutions as short oligomeric chains composed of starting unimers. The term unimer proposed by Ciferri[32] is used in further text for a building block of MSPs.

Results and Discussion

Prepared ionic as well as non-ionic unimers and their abbreviations are shown in **Chart 1** together with the numbering of the central block positions and marking of rings used in assignments of NMR spectra. The letter **Q** denotes the unimers with quaterthiophene central block and numbers behind it indicate the positions occupied by hexyl groups (suffix **-H**), or by hexyl groups capped with: 4-methoxyphenoxy group (suffix **-A**); or bromine atom (suffix **-Br**); or triethylphosphonium group (suffix **-P^+**). MSPs are marked with the prefix **P_{Zn}** (polymers with Zn^{2+} ion couplers) or **P_{Fe}** (Fe^{2+} ion couplers) before the unimer label: for example, **P_{Zn}Q27-Br**

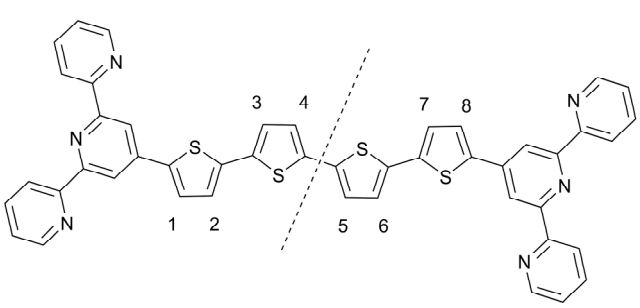

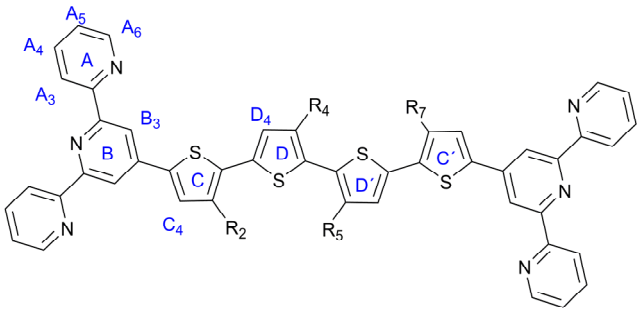

positions 1, 3, 6, 8 are occupied by hydrogen atoms in all structures

Q	$R_2, R_4, R_5, R_7 = H$	**Q45-A**	$R_2, R_7 = H$ $R_4, R_5 = (CH_2)_6OC_6H_6OCH_3$
Q27-H	$R_2, R_7 = (CH_2)_5CH_3$ $R_4, R_5 = H$	**Q45-Br**	$R_2, R_7 = H$ $R_4, R_5 = (CH_2)_6Br$
Q27-A	$R_2, R_7 = (CH_2)_6OC_6H_6OCH_3$ $R_2, R_5 = H$	**Q45-P$^+$**	$R_2, R_7 = H$ $R_4, R_5 = (CH_2)_6P^+Et_3Br^-$
Q27-Br	$R_2, R_7 = (CH_2)_6Br$ $R_4, R_5 = H$	**Q2457-A**	$R_2, R_4, R_5, R_7 = (CH_2)_6OC_6H_6OCH_3$
Q27-P$^+$	$R_2, R_7 = (CH_2)_6P^+Et_3Br^-$ $R_4, R_5 = H$	**Q2457-Br**	$R_2, R_4, R_5, R_7 = (CH_2)_6Br$
		Q2457-P$^+$	$R_2, R_4, R_5, R_7 = (CH_2)_6P^+Et_3Br^-$

Chart 1. Structures and codes of prepared unimers.

denotes the MSPs formed by assembly of Zn^{2+} ions and unimer **Q27-Br** which contains 6-bromohexyl groups attached to the quaterthiophene central block at positions 2 and 7; **P_{Fe}Q45-P$^+$** stands for the MSPs formed from Fe^{2+} ions and unimer **Q45-P$^+$** that contains two 6-(triethylphosphonium)hexyl groups attached to positions 4 and 5 of the central block, etc.

Synthesis and characterization of unimers and polymers

The reference unimers **Q** and **Q27-H** were prepared using the Suzuki-Miyaura coupling strategy (**Scheme 1**) and conditions applied earlier.[28,29,33] **Br**-unimers were prepared using the strategy shown in **Schemes 1** and **2*a***. Starting monomer 3-[6-(4-methoxyphenoxy)hexyl]thiophene was prepared using the procedure described elsewhere.[34] The procedure starting from 3-(6-bromohexyl)thiophene used for the synthesis of ionic unimers with mono- (**M**) and bithiophene (**B**) central blocks[29] was not too effective owing to low efficiency of purification of unimers with bromohexyl groups. Connecting of *tpy* end-groups by Suzuki coupling (**Scheme 1*c***) was namely accompanied by partial dehydrobromination of bromohexyl side groups promoted with *tpy* end-groups.[29] Purification of short unimers could be done easily (for **M**) or feasibly (for **B**), but purification of bis(*tpy*)quaterthiophenes was almost impossible.

The use of new starting monomer avoided the above difficulties and, in addition, made isolation of all intermediates as well as **A**-unimers much easier. The **A**-unimers were then allowed to react with BBr_3 (**Scheme 2*a***) to give corresponding **Br**-unimers with bromohexyl side groups (yield 85 – 95 %), which were finally treated with triethylphosphine to give corresponding ionic **P$^+$**-unimers (**Scheme 2*b***). The excess PEt_3 was easy removed by vacuum distillation and its oxide ($POEt_3$) washed away by toluene and ether. Solid products were isolated by centrifugation (yield of ionization step was from 75 to 95 %).

Solubility in methanol was the first evidence of successful transformation of the **Br-** into **P$^+$**-unimers. NMR spectra of modified unimers accordingly showed a ^{31}P signal of **P$^+$**-groups at around 39 ppm (38.93 for **Q27-P$^+$**, 38.44 for **Q45-P$^+$**, 39.99 for **Q2457-P$^+$**), ^1H signals of ethyl groups (part of **P$^+$**) but not signal at 3.4 ppm that is typical of CH_2-Br groups. Weak ^1H signals at 5.93 ppm and 5.55 – 5.45 ppm were also observed indicating that some side chains contain terminal double bond formed by dehydrobromination accompanying quaternization of **Br**-unimers. Complete removal of imperfect molecules from **P$^+$**-unimers was not successful since they are soluble in alcohols.

TGA analyses of **Br**-unimers and **P$^+$**-unimers showed thermal stability up to 205°C.

Metallo-supramolecular polymers were simply prepared by mixing solutions of a given unimer and zinc(II) or iron(II) perchlorate in the metal ions to unimer mole ratio r = 1 (r = $[Mt^{2+}]/[unimer]$). **Br**-unimers were assembled in the acetonitrile/chloroform mixed solvent (1/1 by vol.) while **P$^+$**-unimers in methanol.

Solubility of prepared unimers and polymers depends on the substitution of the unimer central block. Unsubstituted unimer **Q** is soluble in dichloromethane but poorly soluble in chloroform. **Br**-unimers are well-soluble in solvents such as THF, $CHCl_3$, CH_2Cl_2, DMSO and acetonitrile/chloroform mixture, which facilitates their isolation and purification. Unimers with two ionic groups are well-soluble in polar solvents such as methanol, ethanol and DMSO and sparingly soluble in water (complete dissolving to a colloidal solution takes a few weeks). Unimer **Q2457-P$^+$** carrying four ionic groups is easily soluble in water, which is quite unusual for this type of conjugated structures. Nevertheless, complete dissolution of **Q2457-P$^+$** to the molecular level takes time on a day scale as can be seen from the time development of the UV/vis spectrum of its aqueous solution shown in (**Figure S1**, ESI). MSPs show similar solubility as corresponding unimers.

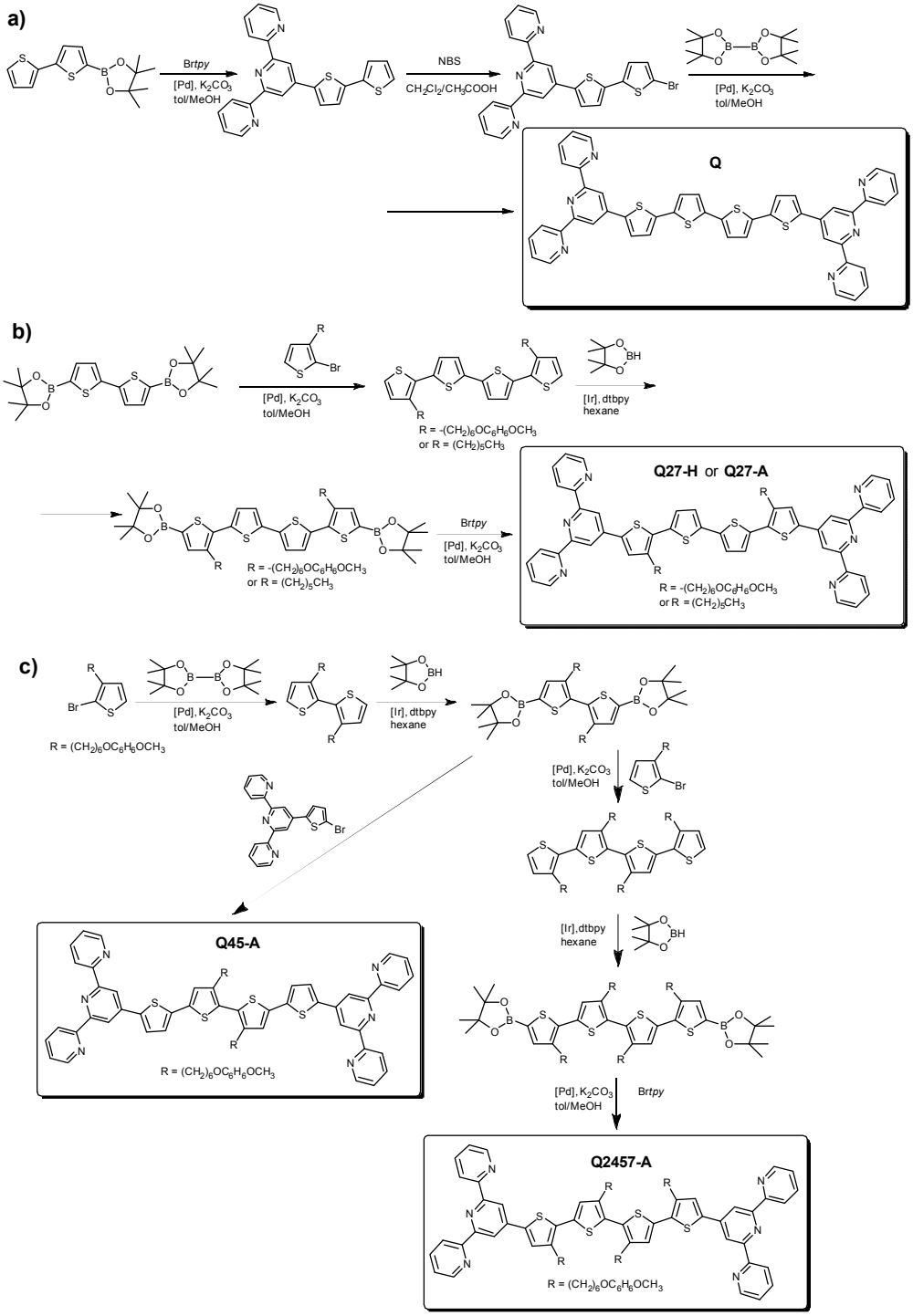

Scheme 1. Synthesis pathways to the reference unimers Q and Q27-H and A-unimers.

Vibrational spectra of unimers and polymers

The IR spectra of unimers show each the bands of stretching modes (ν_{CC}, ν_{CN}) of *tpy* end-groups (1500 – 1620 cm^{-1}), quaterthiophene central block (1370 – 1500 cm^{-1}), aromatic ν_{CH} modes (3000 – 3100 cm^{-1}) and main out-of-plane modes (ρ_{CH}) of aromatic moieties (790 and 658 cm^{-1}) at nearly identical positions (**Figure S2**, ESI). Differences due to different substitution of the central blocks are mainly seen in the fingerprint region from 850 to 1350 cm^{-1}. The presence of hexyl chains is mainly observable in the C-H stretching region (2800 – 3000 cm^{-1}). The most intensive bands characteristic of vibrations of hexyl groups in the fingerprint region (1466 and 1379 cm^{-1}) are overlapped by the ring stretching modes of the quaterthiophene central blocks. As to differences in IR spectra of unimers with and without linked hexyl groups (e.g. **Q** vs. **Q27-H**) only a small shift of the band maximum from 1459 cm^{-1} (for **Q**) to 1466 cm^{-1} (for **Q27-H)** and a new shoulder at 1384 cm^{-1} for **Q27-H** are observable. Broad spectral band at 3400 cm^{-1} observed for all **P^+**-unimers is due to the presence of hydrogen bonded water molecules in these unimers.

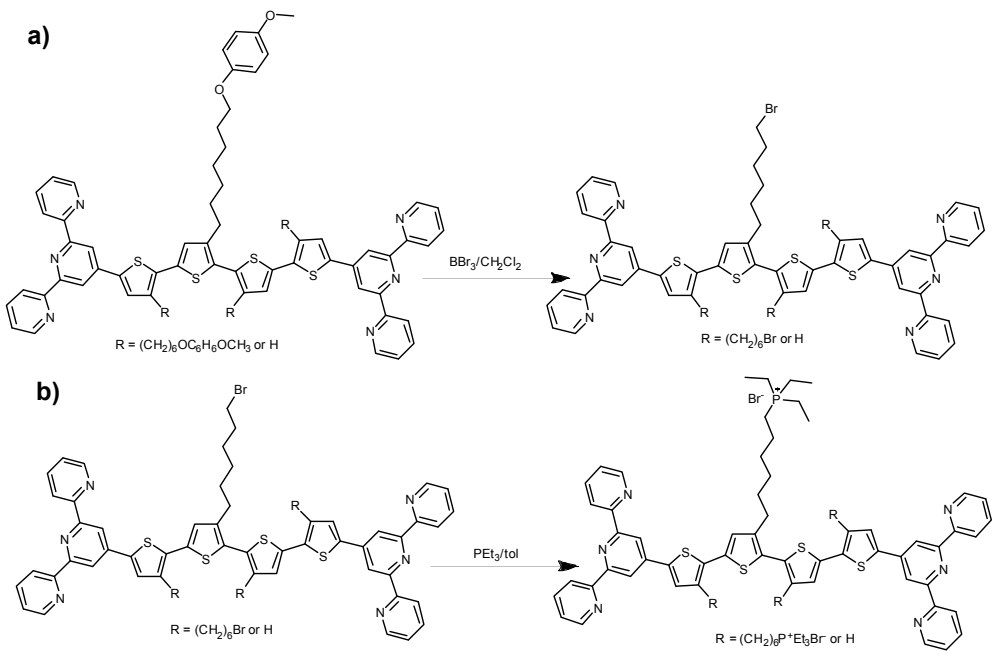

Scheme 2. Transformation of the type **A-**unimers into the type **Br-** (a) and type **P^+-**unimers (b).

The off-resonance Raman spectra of unimers show strong stretching bands of quaterthiophene blocks but weak bands of *tpy* end-groups. Their spectral patterns reflect differences in the substitution of quaterthiophene blocks (**Figure S3**, ESI). Raman spectra of Zn-polymers were disturbed by strong fluorescence but spectra of non-fluorescent Fe-polymers were well measurable. The bands characteristic of *tpy* groups[35] occur at 1610 cm^{-1} (ν_s), 1290 cm^{-1} (δ_{ip}) and 1038 cm^{-1} (breathing mode) while the bands of quaterthiophene blocks[36–38] in the region 1380 - 1520 cm^{-1} (**Figure S4a-S7a**, ESI). Deconvolution of the latter band using the OMNIC software gave robust result showing that this band is composed of at least five bands (**Figure S4b-S7b**, ESI) whose intensities depend on positions of side groups. The band at 1472 cm^{-1} should be also contributed with transitions *tpy* groups.[35]

Optical spectra of unimers and polymers

The solution UV/vis absorption spectra of unimers (ESI, **Figure S8*a***) show: *(i)* flat band at 280-284 nm mainly contributed with transitions in *tpy* end groups, and *(ii)* band with apex at a wavelength λ_A from 381 nm (**Q2457-P^+**) to 441 nm (**Q**) belonging to transitions from HOMO that is spread over thiophene rings and central rings of *tpy* groups.[28,33] The value of λ_A (see **Table 1**) decreases *(i)* with increasing distortion of the quaterthiophene central block (see **Table 2**), and *(ii)* when going from the non-ionic (**-Br**, **-H**) to ionic unimer (**-P^+**) of the same type. Absorption maximum in spectra of unimer thin films (ESI, **Figure S8*b***) are not in such good correlation with the chain distortion, which reflects the importance of the molecular packing effect or electronic effect of substituents. Exceptionally high λ_A of **Q2457-Br** thin film (500 ± 10 nm) was obtained. The fact that the **Q2457-P^+** shows much lower λ_A can be ascribed to bulkiness of P^+Et_3 groups and the effect of bromine counterions.

In the spectra of Zn-polymers, the absorption band of transitions involving quaterthiophene blocks is red shifted about 35 - 65 nm compared to its position λ_A for unimer in the solution spectra and about 20 – 75 nm in thin film (**Table 1**). The only but great exception is the spectrum of **P_{Zn}Q2457-Br** thin film that surprisingly shows a blue shift of λ_A about -70 nm, which obviously is due to exceptionally high value of λ_A of the unimer **Q2457-Br**.

The spectra of Fe-polymers contain a new band belonging to transitions in the metal-to-ligand charge transfer (MLCT) complex which is typical of *tpy*-Fe-*tpy* linkages[35,39] (see **Table 1** and **Figures S8*c*** and ***d*** in the ESI). In Fe-polymers, this band is significantly contributed with transitions involving neighboring oligothiophene block.[29]

Luminescence spectra of unimers in solutions (ESI, **Figure S9*a***) show higher similarity than their UV/vis spectra (λ_F around 550 nm; lowered values about 535 nm are actually given by different band shapes). This is obviously due to the fast transition of excited unimer molecules to nearly coplanar conformations with quinoidal rings, from which the light emission takes place.[36] Minor differences are nevertheless seen: unimers with less distorted chains (**Q**, **Q27-H**, **Q27-Br** and **Q27-P^+**) show better resolved vibrational structure than unimers with more distorted chains (**Q45-Br**, **Q45-P^+**, **Q2457-Br** and **Q2457-P^+**). Luminescence spectra of unimer and Zn-polymer thin films are shown in (ESI, **Figures S9*b*-*d***) and the band wavelengths are summarized in **Table 1**, the luminescence lifetimes are presented in ESI, **Table S1**. Fe-polymers do not show luminescence.[28,29,36]

Table 1. UV/vis and luminescence spectral characteristics of prepared unimers and polymers; solvent: methanol for ionic unimers and polymers (suffix **-P$^+$**); acetonitrile/chloroform (1/1 by vol.) for all the other unimers and polymers. λ_A – apex of absorbance maxima; λ_F – apex of emission maxima; υ -stokes shift; λ_{MLCT} – apex of the MLCT band; Φ – absolute luminescence quantum yield.

	UV/vis absorption λ_A, nm		Luminescence λ_F , nm (ϕ, %)		Stokes Shift υ, cm^{-1}	
Sample	solution	film	solution	film	solution	film
Q	441	425	514,546 (30%)	645 (<1%)	4350	7450
Q27-H	425	460	554 (26%)	630 (1%)	5500	5300
Q27-Br	425	455	554 (31%)	630 (1%)	5500	6000
Q27-P$^+$	419	455	550 (18%)	~650 (<1%)	5700	7300
Q45-Br	397	425	530 (14%)	610 (1%)	6300	7000
Q45-P$^+$	393	410	536 (11%)	550 (1%)	6800	6200
Q2457-Br	386	500	536 (14%)	560,603(3%)	7250	3600
Q2457-P$^+$	381	410	536 (10%)	560 (1%)	7600	6400
Q2457-P$^+$[a]	400		555		6980	
Zn polymers						
P$_{Zn}$Q	486	500	656	~690 (1%)	5350	5050
P$_{Zn}$Q27-H	468	490	673	~640 (2%)	6500	5250
P$_{Zn}$Q27-Br	470	510	675	~710 (1%)	6450	5450
P$_{Zn}$Q27-P$^+$	483	500	550	~705 (<1%)	2500	570
P$_{Zn}$Q45-Br	447	455	673	585 (3%)	7500	4850
P$_{Zn}$Q45-P$^+$	426	430	536	660 (1%)	4800	8050
P$_{Zn}$Q2457-Br	432	430	668	590 (3%)	8200	5800
P$_{Zn}$Q2457-P$^+$	439	440	552	625 (1%)	4650	6450
P$_{Zn}$Q2457-P$^+$	462[a]		720[a]		7750[a]	

Fe polymers	UV/vis absorption λ_A, nm, (λ_{MLCT}, nm)	
	solution	film
P$_{Fe}$Q	395, 471 (603)	475 (621)
P$_{Fe}$Q27-H	437 (601)	460 (622)
P$_{Fe}$Q27-Br	387, 452 (601)	465 (621)
P$_{Fe}$Q27-P$^+$	386, 436 (593)	465 (611)
P$_{Fe}$Q45-Br	405 (598)	410 (613)
P$_{Fe}$Q45-P$^+$	399 (593)	410 (609)
P$_{Fe}$Q2457-Br	384, 423sh, (594)	395[b] (609)
P$_{Fe}$Q2457-P$^+$	384 (591)	395[b] (604)
P$_{Fe}$Q2457-P$^+$	400 (607)[a]	

[a] data from aqueous solution, [b] shoulder

Table 2. Calculated geometry of the unimers; $\delta_{BC}...\delta_{C'B'}$ are dihedral angles between planes of neighbouring main-chain rings given in the subscript (for ring labels see **Chart 1.**)

	Ground State			Excited State		
	δ_{BC}	δ_{CD}	$\delta_{DD'}$	δ_{BC}	δ_{CD}	$\delta_{DD'}$
Q	15.8	12.5	0.7	0.0	0.0	0.0
Q27-H	17.3	28.6	1.0	0.0	0.0	0.0
Q27-Br	13.9	22.8	1.0	0.5	3.2	1.3
Q27-P$^+$ Br$^-$	17.3	32.4	16.3	*	*	*
Q45-Br	14.6	18.5	58.9	1.4	3.1	23.7
Q45-P$^+$Br$^-$	18.0	15.4	63.5	*	*	*
Q2457-Br	19.6	40.8	97.5	*	*	*
Q2457-P$^+$ Br$^-$	15.8	27.4	124.4	*	*	*

* values are not available during the first 720 hours

Assembly of unimers to metallo-supramolecular polymers in solutions

Assembling in solutions was monitored by the UV/vis and luminescence spectroscopy, viscometry and size exclusion chromatography (SEC). Chloroform/acetonitrile mixed solvent (1/1 by volume) was used for **Br-**unimers while methanol and water for **P$^+$-**unimers. For spectroscopic studies, a set of solutions of the constant unimer concentration ($2\cdot10^{-5}$ M) and stepwise increasing the metal ions to unimer mole ratio (r from 0 to 3) was prepared for each Mt^{2+}/unimer system and solutions were allowed to equilibrate for 24 hours before monitoring the spectra. The SEC and viscometric measurements were done with solutions of the concentration of $5\cdot10^{-4}$ M.

Spectral changes accompanying assembling of unimers with Mt^{2+} ions showed three stages differing in the development trend, similarly as recently studied related systems.[21,25,28,29,40] The UV/vis spectra obtained for the systems of the composition ratios r from 0 to ca 0.5 (first stage of assembling) showed up to three isosbestic points (see examples in **Figures 1*a*** and **2*a*** and complete set of the spectra in ESI, **Figures S10** and **S11**), which indicates transformation of unimer species into another well-defined species. Regarding the stoichiometry, the new species should be dimer species unimer-Mt^{2+}-unimer.

The spectra obtained for systems with ratios r from ca 0.6 to 1 also show isosbestic points but at different wavelengths (**Figures 1*b*** and **2*b***). This indicates that systems entered the second stage of assembling in which longer polymer chains are formed. As can be seen from ESI, **Figures S10** and **S11**, the absorption bands characteristic of free unimer and dimers disappear while the band of enchained unimer units fully develops in the case of systems with non-ionic **Br-**unimers. These systems then enter the third stage of assembling (r > 1), where spectral changes are quite low and can be attributed to the end-capping of polymer chains with the metal ions and partial depolymerization of the polymer chains to the shorter also end-capped ones (**Figures 1*c*** and **2*c***). The reaction of $(tpy)_2Zn^{2+}$ species with Zn^{2+} ions giving two $(tpy)Zn^{2+}$ species has been reported for mono- as well as bis(tpy) species.[18,29,41,42] The reaction of $(tpy)_2Fe^{2+}$ species with Fe^{2+} ions two giving $(tpy)Fe^{2+}$ species was reported only for metallo-supramolecular polymers.[18,29,43]

Spectral changes in the second stage of assembling of ionic **P$^+$-**unimers are less progressive than in the case of **Br**-unimers or even incomplete, which indicates lowered thermodynamic stability (i.e., stability constants) of ionic polymers in methanol. The lowered stability of ionic Fe-polymers is also seen from changes in the position and intensity of the MLCT band (at around 595 nm) that is not fully developed at the ratios $r \cong 1$ (**Figure 2*b***). The UV/vis spectral patterns indicate that the ionic polymers acquire their maximum length at the ratios r about 1.5 or higher in methanol solutions.

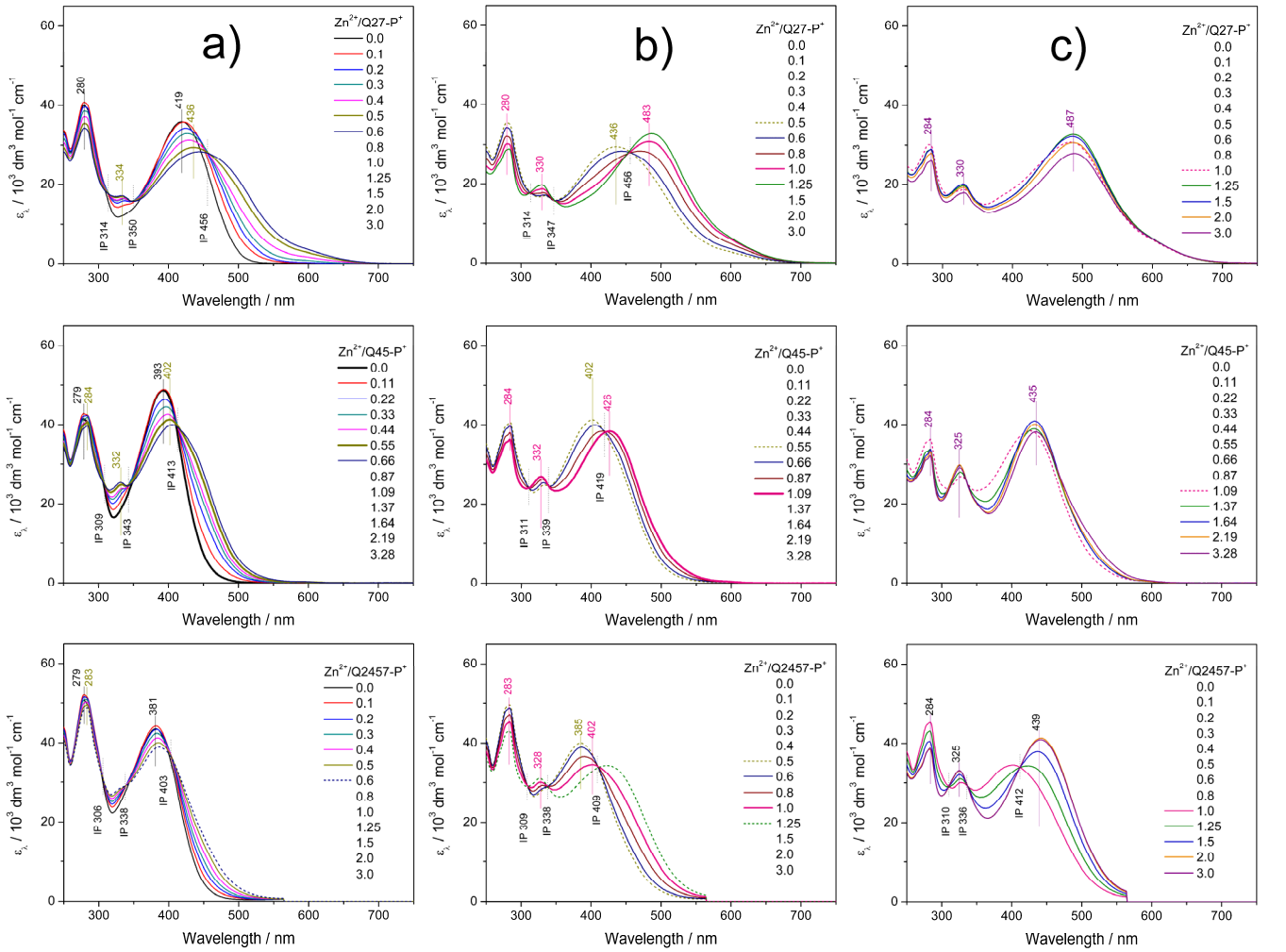

Figure 1. Changes in UV/vis spectra accompanying titration of ionic unimers with Zn^{2+} ions. Initial unimer concentration $2 \cdot 10^{-5}$M in methanol, room temperature. Column a) shows the first stage of assembling, column b) shows the second stage and column c) shows the third stage; see text.

Changes in luminescence spectra accompanying assembly of ionic unimers with Zn^{2+} ions are shown in **Figure 3**. The complexation is manifested by the disappearance of the unimer emission band and creation of a new band red shifted of about 130 nm. Unlike the case of shorter ionic polymers derived from bis(*tpy*) mono- and bithiophenes,[29] the new emission band is significantly less intense than the band of free unimer. Similar luminescence attenuation exhibit also systems with non-ionic polymers. This shows that the prolongation of the unimer central oligothiophene block increases the efficiency of non-radiative paths of the decay of excited states in Zn-polymers.

Unlike the systems with Zn^{2+} ions, those with Fe^{2+} ions show monotonous luminescence quenching with increasing ratio *r* up to ca 0.6, at which the luminescence disappears (for example see ESI, **Figure S12**). This behaviour, which exhibit other systems with bis(*tpy*)Fe^{2+} species, is attributed to the fact that the lowest excited state of bis(*tpy*)Fe^{2+} species, the d-d triplet state, is close to the ground state.[44] As the d-d triplet state easily depletes upper excited states and potential phosphorescence from the d-d state is spin forbidden, its decay by non-radiative transitions is unambiguously preferred in accord with the energy gap law.[8,45]

Molar mass distribution of **Br**-polymers in $CHCl_3/CH_3CN$ (1:1) solutions was examined using an SEC system equipped with a diode-array UV/vis detector (DAD). (Analysis of ionic polymers failed owing to the strong adsorption of their chains inside SEC columns.) Mixed solutions of a **Br**-unimer (0.5 mM) and Zn^{2+} or Fe^{2+} ions (*r* from 0 to 2.0) equilibrated for one day were injected into the SEC system. The SEC records of systems with Zn^{2+} ions showed nothing but the peak of free unimer, which proves rapid dissociation of the Zn-polymer chains upon multifold dilution of their solution inside SEC columns. In contrast, the systems with Fe^{2+} ions provided SEC records typical of covalent polymers (**Figures 4** and ESI, **S13**), which demonstrates very slow constitutional dynamics of Fe-polymers in used solvent. Similar results were recently obtained for MSPs of shorter bis(*tpy*)thiophenes.[29]

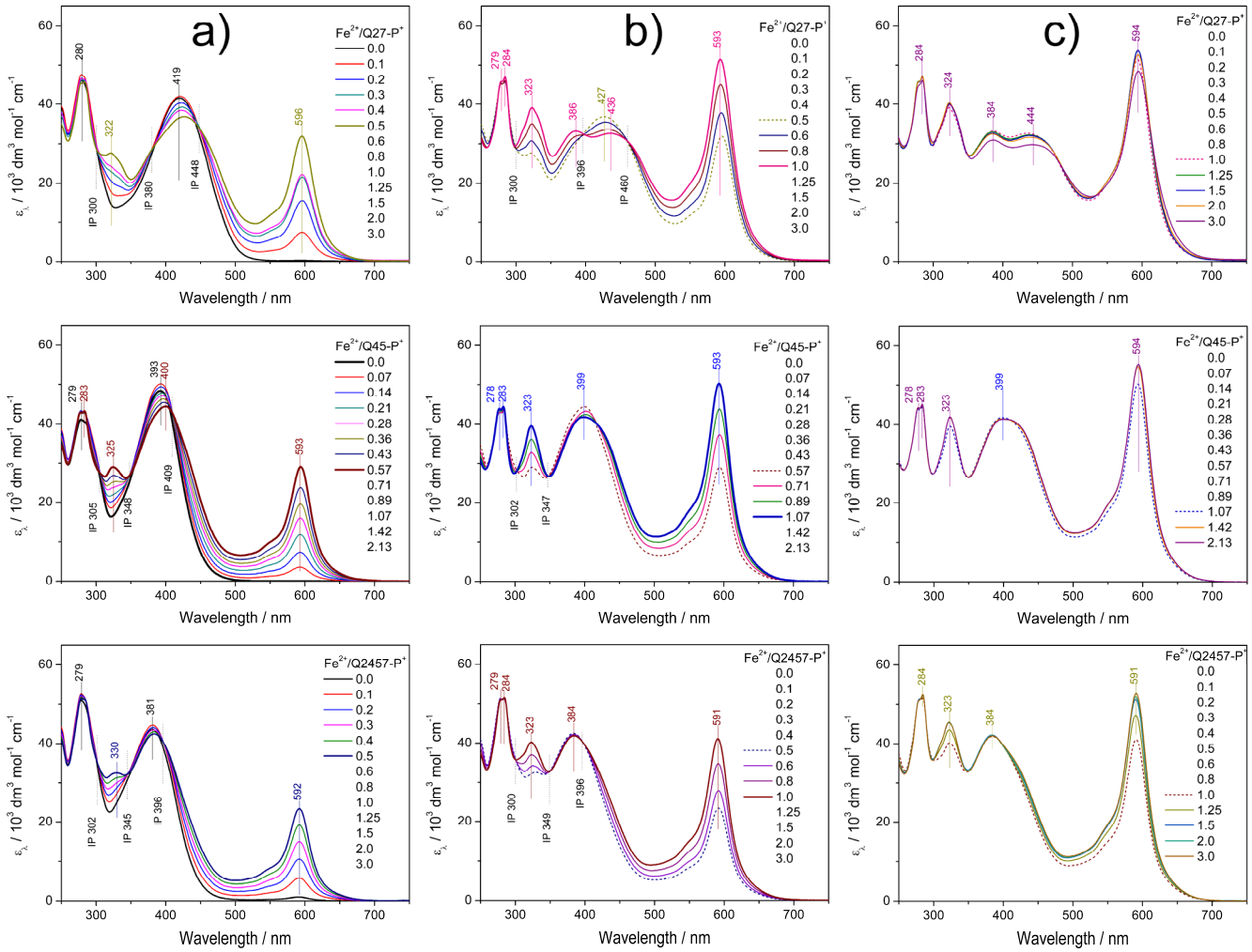

Figure 2. Changes in UV/vis spectra accompanying titration of ionic unimers with Fe^{2+} ions. Initial unimer concentration $2 \cdot 10^{-5}$M in methanol, room temperature. Column a) shows the first stage of assembling, column b) shows the second stage and column c) shows the third stage; see text.

Well resolved SEC records were obtained only for systems with composition ratio $r < 1$ (**Figure 4**). Systems with $r \geq 1$ gave poorly resolved SEC records, in which the area under elution peak decreased with increasing value of r. This indicates retention of longer chains in SEC columns. The detained polymer chains, obviously end-capped with Fe^{2+} ions, had to be additionally washed out of the columns with 2,2'-bipyridine. The UV/vis spectral pattern of SEC fractions showed a perfect development with the elution time (t_{el}): a pattern typical of long polymer chains was observed for first eluted SEC fractions while that one typical of the dimers for the last fraction (**Figure 5*a*** and ESI, **Figure S14*a***). Differences are also seen when comparing the spectra of fractions of dimers formed in systems of different composition (**Figure 5*b*** and ESI, **Figure S14*b***). These differences can be attributed to the end-capping of their molecules with Fe^{2+} ions. However, these differences are substantially smaller than those observed for the Fe-polymers formed from unimers with mono- and bithiophene central blocks.[29]

The presence of higher fractions in solutions containing a stoichiometric lack of Fe^{2+} ions (r = 0.2 and 0.5) can be explained by the transiently locally increased concentration of the ions and unimer during mixing their solutions. Formation of polymer chains is most likely a kinetically controlled process which, when mixing twenty five times more concentrated solutions (0.5 mM instead 0.02 mM), shall be ca 625 times accelerated. Thus it can give rise to a significant number of longer chains that do not dissociate during the SEC analysis thanks to their slow constitutional dynamics. Thus the degree of polymerization, X, of Fe-polymer chains in solution could be estimated. If the peak eluted at t_{el} = 1460 s (see **Figure 4**) is ascribed to dimers, peak with t_{el} = 1305 s to trimers, and so on, one can still resolve the peak of heptamers at t_{el} = 1114 s. Calculation based on this peak assignment provides the weight-average degree of polymerization equal to ca 7 for Fe-polymer in the solution with $r \cong 1$ (**Table 3**). In addition, it is seen from **Figure 4** that the stoichiometric excess of Fe^{2+} ions in solution results in the formation of shorter chains. The last is supported by the results of viscometric measurements, which also indicate shortening of the polymer chains in the presence of excess Fe^{2+} ions (ESI, **Figure S15**).

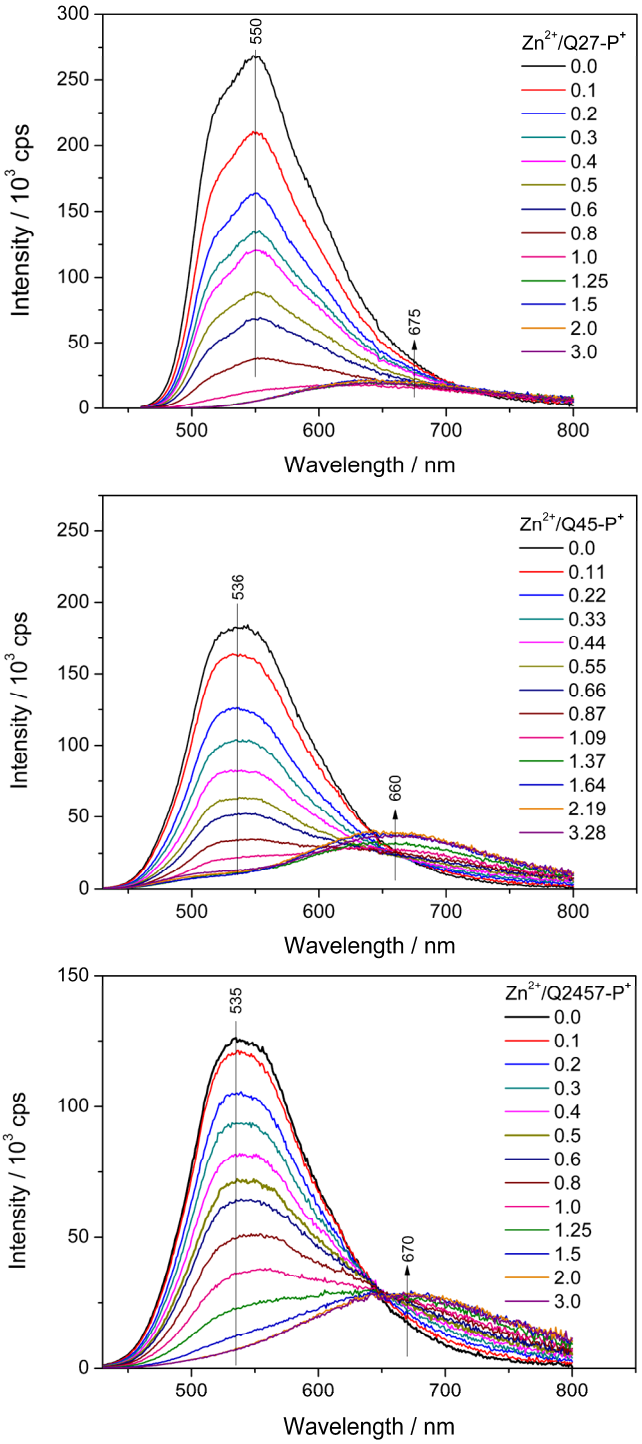

Figure 3. Changes in photoluminescence spectra accompanying titration of ionic unimers with Zn^{2+} ions. Initial unimer concentration $2 \cdot 10^{-5}$M in methanol, room temperature.

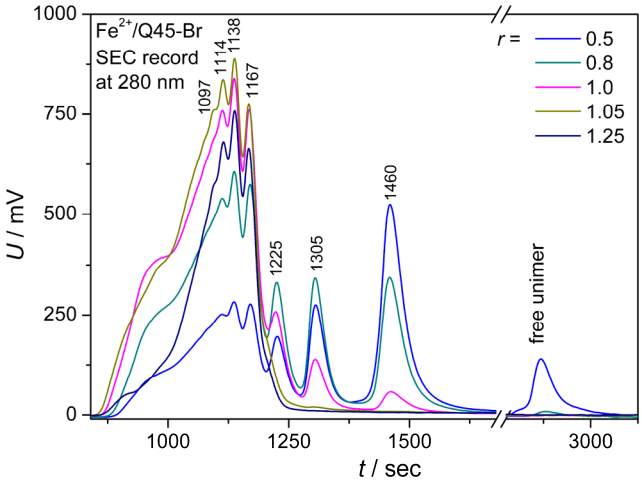

Figure 4. The SEC records of the Fe^{2+} / **Q45-Br** systems of different composition.

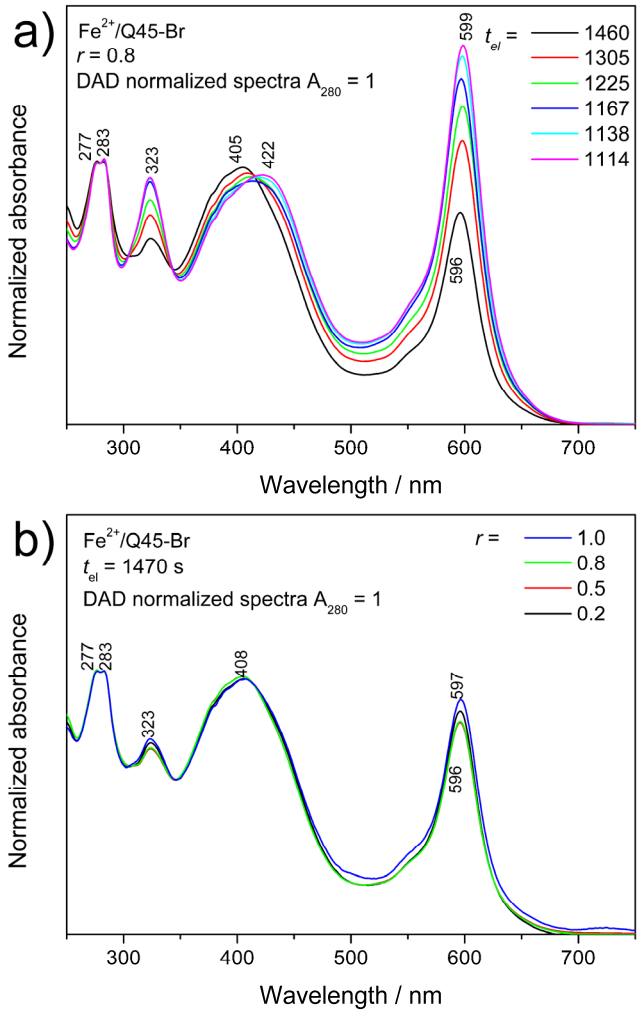

Figure 5. The UV/vis DAD spectra of SEC fractions of the Fe^{2+}/**Q45-Br** system (r = 0.8) eluted at different elution times t_{el} (*a*) and comparison of the spectra of the last fraction (dimers; t_{el} = 1470 s) of systems of the composition r from 0.2 to 1.0 (*b*).

Table 3. Number-average (X_n) and weight-average (X_w) degrees of polymerization and dispersity index ($Đ$) of **P_{Fe}Q45-Br** in solution calculated from SEC records.

r	X_n	X_w	$Đ$
0.2	3.07	4.23	1.36
0.5	3.24	4.77	1.47
0.8	4.43	6.02	1.36
1.0	6.13	7.23	1.18
1.05	6.79	7.62	1.12
1.25	6.26	6.84	1.09

Assembling of Q2457-P$^+$ in water

The water-soluble unimer **Q2457-P$^+$** has been assembled with metal ions also in aqueous solutions. Since molecular dissolving of this unimer in water takes a long time a month-old solution of **Q2457-P$^+$** was used in these experiments. As can be seen from **Figure 6**, the optical spectral changes accompanying the assembly in water substantially differ from those observed for assembling in methanol.

(i) The absorption maxima of **Q2457-P$^+$** (λ_A = 400 nm) and its Zn-polymer (r = 2, λ_A = 462 nm) as well as the luminescence maximum of the unimer (λ_F = 555 nm) are red shifted about ca 20 nm compared to their positions in methanol solutions, which indicates that the free as well as enchained unimer species acquire more planar conformations in water than in methanol. This can be attributed to the substantial increase in the solvent permittivity, which, in accord with the Coulomb law, reduces repulsive ionic interactions among neighbouring P^+Et_3 groups as well as their attractive interactions with counterions.

(ii) The luminescence emission band observed for Zn-polymer (λ_F = 720 nm) is enormously red shifted (about 168 nm) compared to the band for methanol solution. Stokes shift for **P_{Zn}Q2457-P$^+$** in water (7 750 cm^{-1}) is much higher than the shift in methanol (4 650 cm^{-1}, **Table 1**), which proves much higher extent of conformational relaxation of excited states in aqueous compared to methanol solutions.

(iii) The UV/vis spectra for assembling of **Q2457-P$^+$** with Zn^{2+} ions show a single set of isosbestic points and fluent course of changes up to r = 2. Luminescence spectra indicate the presence of free unimer in solution up to r equal to at least 1.5. These features consistently indicate a lowered stability and increased constitutional dynamics of **P_{Zn}Q2457-P$^+$** in aqueous solutions.

(iv) Surprisingly, but in accord with the last mentioned observations, the UV/vis spectra for assembling of **Q2457-P$^+$** with Fe^{2+} ions show small changes and weak MLCT band

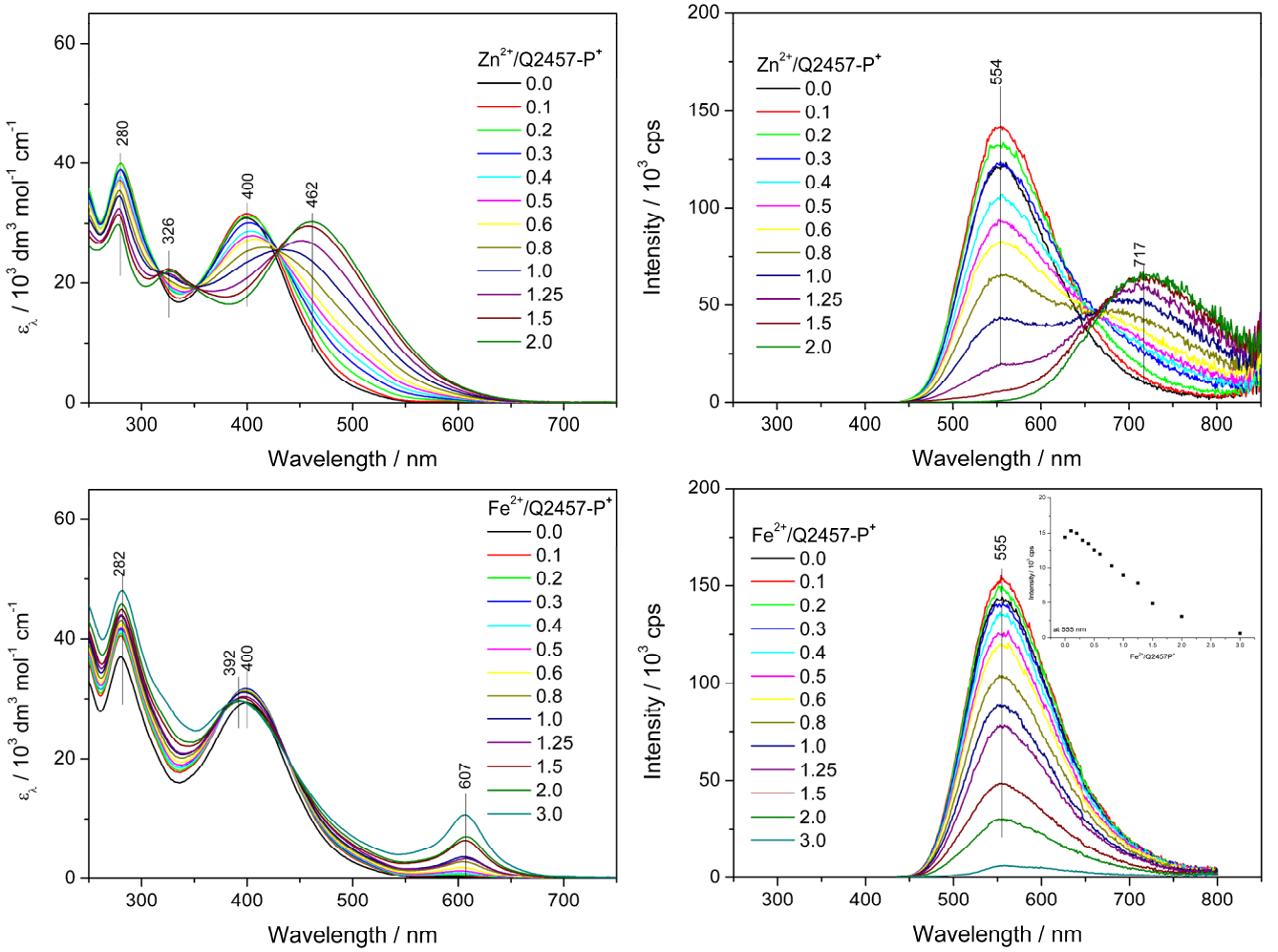

Figure 6. Changes in UV/vis (left column) and photoluminescence (right column) spectra accompanying titration of ionic unimers with Zn^{2+} or Fe^{2+} ions. Initial unimer concentration 2·10^{-5}M in water, room temperature.

and the luminescence spectra show emission even at the composition ratio r = 3. It should be stressed here that no new emission band occurs, only reluctant luminescence quenching with increasing *r* is observed. The observed spectral changes indicate that the chains of highly ionic Fe-polymer are in aqueous solution less stable than the chains of its Zn- counterpart. This observation represents a flip in the stability of Fe- and Zn- polymers derived from bis(*tpy*)quaterthiophenes compared to perhaps all so far reported data.[41,46–49] Reduced stability of the ionic Fe-polymer in water is obviously associated with the inhibition of the MLCT process by water. Solvent dependence of the MLCT is well known.[50,51]

Conclusions

The synthesis strategy developed here enables preparing bis(*tpy*)quaterthiophenes with two or four side groups symmetrically distributed along the quaterthiophene central block. The modification of side groups enabled preparation of ionic unimers that are soluble in green solvents such as alcohols or even in water.

Optical spectral patterns of dissolved unimers and corresponding polymers depend primarily on the distribution of side groups along quaterthiophene central block and only secondarily on the nature of side-chain-capping groups. The effect of the latter is more apparent in the solid state spectra since the capping groups significantly influence molecular packing.

During the assembling of unimers with metal ions the developments of UV/vis spectra with increasing ratio *r* conclusively indicate that the **P**$^{+}$-unimers assemble with metal ions less readily than the **Br**-unimers. Besides in water, **Q2457-P**$^{+}$ assembles with Zn^{2+} ions considerably less progressively (with rising *r*) than in methanol and, with Fe^{2+} ions, still much less readily showing only a very weak MLCT band but significant luminescence of the free unimer even at ratio *r* = 3. Solvation effect is thus obvious. The red shift of the luminescence band of **P$_{Zn}$Q2457-P**$^{+}$ about ca 170 nm when going from methanol into aqueous solution is observed. Such a big shift indicates much higher conformational freedom of **P$_{Zn}$Q2457-P**$^{+}$ chains in aqueous compared to methanol solutions.

The SEC study of the non-ionic polymers proved that the constitutional dynamics of Zn-polymers is fast and that of Fe-polymers very slow in the chloroform/acetonitrile mixed solvent, which is in accord with observations of other authors on related systems. However, the results obtained here on assembling of the ionic unimers in aqueous solutions anticipate faster constitutional dynamics of Fe-polymers compared to Zn-polymers.

Experimental Section

Materials

2,2′–Bithiophene-5-boronic acid pinacol ester, 2,2′-bithiophene-5,5′-diboronic acid bis(pinacol) ester, thiophene-2-boronic acid pinacol ester, 3,3‴-dihexyl-2,2′:5′,2″:5″,2‴-quaterthiophene, bis(pinacolato)diboron (B_2pin_2), 4,4,5,5-tetramethyl-1,3,2-dioxaborolane (HBpin), 4,4′-di-tert-butyl-2,2'-dipyridyl (dtbpy), bis(1,5-cyclooctadiene)di-μ-methoxydiiridium(I) ([Ir(OMe)(COD)]$_2$), boron tribromide (BBr_3), triethylphosphine (PEt_3, 1.0M in THF), *N*-bromosuccinimide (NBS), [1,3-bis(2,6-diisopropylphenyl)imidazol-2-ylidene](3-chloropyridyl)palladium(II) dichloride (PEPPSI-IPr), zinc perchlorate hexahydrate, iron(II) perchlorate hydrate and tetrabutylammonium hexafluorophosphate (all Aldrich), K_2CO_3, $MgSO_4$, acetic acid (Lachner) and 4′-bromo-2,2′:6′2″-terpyridine (TCI) were used as recieved. Hexane (Lachner) was stored over molecular sieve, tetrahydrofurane (Aldrich) was distilled from $LiAlH_4$ before use, toluene (Lachner) was distilled from sodium/benzophenone before use, methanol (Aldrich) was bubbled with argon before use, diethylether, dichloromethane, chloroform (Lachner) and acetonitrile (ACN) were used as obtained.

Measurements

^{1}H and ^{13}C NMR spectra were recorded on a Varian ^{UNITY}INOVA 400 or Varian SYSTEM 300 instruments in d_8-THF, d_2-CD_2Cl_2, *d*-$CDCl_3$, d_6-DMSO or d_4-CD_3OD and referenced to the solvent signal: 7.25 ppm (*d*-$CDCl_3$), 5.32 ppm (d_2-CD_2Cl_2), 3.58 ppm (d_8-THF), 2.50 ppm (d_6-DMSO) or 3.31 ppm (d_4-CD_3OD) for ^{1}H and 77.0 ppm (*d*-$CDCl_3$), 53.84 ppm (d_2-CD_2Cl_2), 67.57 ppm (d_8-THF) or 49.15 ppm (d_4-CD_3OD) for ^{13}C spectra. Coupling constants, *J* (in Hz), were obtained by the first-order analysis. Infrared spectra were recorded on a Thermo Nicolet 7600 FTIR spectrometer equipped with a Spectra Tech InspectIR Plus microscopic accessory using KBr-diluted samples and diffuse reflectance technique (DRIFT) (128 or more scans at resolution 4 cm^{-1}). Raman spectra of solid samples were recorded on a DXR Raman microscope (Thermo Scientific) using excitations across the whole visible region (λ_{ex} = 445, 532, 633 and 780 nm) and usual laser power at the sample 0.1 to 0.4 mW. UV/VIS spectra were recorded on a Shimadzu UV-2401PC instrument or SPECORD instrument measured in methanol or $CHCl_3$/ACN (1/1, v/v), solid samples were coated on surface of quartz cuvette. Photoluminescence spectra were measured on a Fluorolog 3-22 Jobin Yvon Spex instrument, using four-window quartz cuvette (1 cm) for solutions and using quartz glass for films. The emission spectra were recorded with excitation wavelength, λ_{ex}, matching the absorption maximum of measured compound. Quantum yields, λ_F, of photoluminescence were measured using integration sphere Quanta-φ F-3029. Fluorescence decay was monitored with a FluoroHub single photon counting controller on a Fluorolog 3-22 Jobin Yvon Spex instrument using excitation at λ_{ex} = 378 nm for solutions and λ_{ex} = 472 nm for films. Viscosimetric measurements were determined at Microviscometer Lovis

2000 M/Me (Anton Paar). SEC records were obtained on a Spectra Physics Analytical HPLC pump P1000 with two SEC columns Polymer Labs (Bristol, USA) Mixed-D, Mixed-E. System was equipped with THERMO UV6000 DAD detector. 0.05M tetrabutylammonium hexafluorophosphate in $CHCl_3$/ACN (1/1, v/v, CHROMASOLV, Riedel-deHaen) was used as an eluent (0.7 mL/min).

5-(2,2′:6′,2″-Terpyridine-4′-yl)-2,2′-bithiophene

2,2′–Bithiophene-5-boronic acid pinacol ester (0.509 g, 1.74 mmol), Br*tpy* (0.439 g, 1.41 mmol), K_2CO_3 (0.59 g, 4.26 mmol) and PEPPSI-IPr (50 mg) were placed in the Schlenk tube. Vacuum – argon cycles were applied several times and toluene (10 mL) and methanol (10 mL) were added through septum. The reaction mixture was heated at 90°C overnight. After cooling to room temperature the reaction mixture was diluted with dichloromethane (50 ml) and washed with water (3×200 mL). The organic layer was dried with $MgSO_4$, filtered and evaporated to get the crude product. The crude product was contaminated by bithiophene, which was washed off with hexane to get the pure product as the yellow powder. (0.53 g, 95 %) ^{1}H NMR (400 MHz, d_2-CD_2Cl_2) δ ppm 8.74 – 8.72 (m, 2H, A^6), 8.70 (s, 2H, B^3), 8.67 – 8.65 (m, 2H, A^3), 7.90 (td, 2H, J_1 = 7.7, J_2 = 1.7, A^4), 7.73 – 7.71 (m, 1H, C^4), 7.40 – 7.37 (m, 2H, A^5), 7.33 – 7.31 (m, 2H, C^3 + D^5), 7.29 (d, J = 3.8, 1H, D^3), 7.10 – 7.08 (m, 1H, D^4). ^{13}C NMR (101 MHz, d_2-CD_2Cl_2) δ ppm 156.49, 156.10, 149.48, 143.11, 141.15, 140.61, 139.30, 137.15, 128.39, 126.89, 125.53, 125.10, 124.69, 124.32, 121.36, 116.71. IR (DRIFT), cm^{-1} 3086 (m), 3066 (m), 3013 (m), 2988 (w), 2965 (w), 2922 (m), 2871 (w), 2856 (w), 1598 (s), 1583 s), 1565 (s), 1553 (m), 1541 (m), 1509 (m), 1464 (s), 1435 (m), 1422 (m), 1399 (s), 1366 (w), 1353 (w), 1323 (w), 1306 (w), 1290 (w), 1267 (m), 1253 (w), 1239 (m), 1232 (m), 1227 (m), 1209 (w), 1184 (w), 1162 (w), 1146 (w), 1124 (m), 1092 (m), 1077 (w), 1064 (m), 1051 (m), 1044 (m), 1010 (m), 988 (m), 961 (w), 954 (w), 915 (w), 898 (w), 885 (m), 878 (m), 838 (m), 789 (s), 773 (m), 746 (m), 741 (m), 730 m), 717 (s), 690 (m), 683 (m), 668 (m), 658 (m), 643 (w), 632 (m), 622 (m), 587 (w), 565 (w), 523 (m), 489 (m), 466 (m), 447 (w), 418 (w), 402 (m). HRMS found *m/z*: 420.05998 $[M^+Na]^+$, $C_{23}H_{15}N_3NaS_2$ requires: 420.05996.

5-Bromo-5′-(2,2′:6′,2″-terpyridine-4′-yl)-2,2′-bithiophene

5-(2,2′:6′,2″-Terpyridine-4′-yl)-2,2′-bithiophene (0.52 g, 1.31 mmol) was dissolved in dichloromethane (20 mL) and acetic acid (20 mL) and NBS (0 .26 g, 1.46 mmol) was added in dark and the reaction mixture was stirred overnight. Then the acidic mixture was slightly neutralized by saturated solution of K_2CO_3 in water, diluted with dichloromethane (40 mL) and washed with water (3×250 mL). The organic layer was dried with $MgSO_4$, filtered and evaporated to get the product as the yellow solid. (0.52 g, 83 %) ^{1}H NMR (400 MHz, d_2-CD_2Cl_2) δ ppm 8.74 – 8.72 (m, 2H, A^6), 8.68 – 8.65 (m, 4H, A^3 + B^3), 7.90 (td, J_1 = 7.8, J_2 = 1.8, 2H, A^4), 7.71 (d, J = 3.8, 1H, C^4), 7.38 (ddd, J_1 = 7.5, J_2 = 4.8, J_3 = 1.2, 2H, A^5), 7.23 (d, J = 3.8, C^3), 7.07 – 7.05 (m, 2H, D^3 + D^4). ^{13}C NMR (101 MHz, d_2-CD_2Cl_2) δ ppm 156.80, 156.30, 149.77, 143.19, 139.04, 138.35, 137.46, 133.99, 131.67, 128.78, 127.18, 125.01, 124.60, 121.67, 121.62, 117.06. IR (DRIFT), cm^{-1} 3091 (m), 3072 (m), 3061 (m), 3051 (m), 3013 (m), 2990 (w), 2962 (m), 2926 (m), 2855 (m), 1735 (w), 1600 (m), 1584 (s), 1566 (s), 1553 (w), 1547 (m), 1515 (m), 1477 (m), 1467 (s), 1438 (w), 1428 (m), 1399 (s), 1369 (w), 1340 (w), 1265 (m), 1237 (m), 1223 (w), 1206 (w), 1196 (w), 1148 (m), 1127 m), 1100 (m), 1079 (w), 1067 (m), 1042 (m), 1010 (m), 987 (m), 973 (m), 958 (w), 906 (w), 889 (w), 880 (s), 874 (s), 849 (w), 785 (s), 773 (m), 752 (m), 743 (m), 729 (m), 690 (m), 669 (m), 659 (m), 632 (m), 622 (m), 581 (w), 556 (w), 526 (m), 495 (m), 474 (m), 455 (m), 439 (w), 414 (m), 406 (m). HRMS found *m/z*: 475.98846 $[M^+H]^+$, $C_{23}H_{15}N_3BrS_2$ requires: 475.98853.

5,5‴-Bis(2,2′:6′,2″-terpyridine-4′-yl)-2,2′:5′,2″:5″,2‴-quaterthiophene Q

5-Bromo-5′-(2,2′:6′,2″-terpyridine-4′-yl)-2,2′-bithiophene (0.372 g, 0.78 mmol), B_2pin_2 (0.168 g, 0.66 mmol), K_2CO_3 (0.34 g, 2.46 mmol) and PEPPSI-IPr (25 mg) were placed in the Schlenk tube and vacuum – argon cycles were applied. Ten toluene (15 mL) and methanol (15 mL) were added through septum and the reaction mixture was heated at 90 °C overnight. After cooling to room temperature the product precipitated. The suspension was filtered, washed with toluene, water and hexane and dried in vacuo. Orange powder (0.18 g, 58 %) ^{1}H NMR (400 MHz, d_2-CD_2Cl_2) δ ppm 8.75 – 8.74 (m, 4H, A^6), 8.71 – 8.66 (m, 8H, A^3 + B^3), 7.91 (td, J_1 = 7.7, J_2 = 1.8, 4H, A^4), 7.75 (d, J = 3.9, 2H, C^4), 7.41 – 7.38 (m, 4H, A^5), 7.35 (d, J = 4.3, 2H, C^3), 7.32 – 7.21 (m, 4H, D^3 + D^4). Due to low solubility of this compound we were not able to get ^{13}C NMR spectrum in a sufficient quality. IR (DRIFT), cm^{-1} 3064 (m), 3012 (m), 2991 (w), 2937 (w), 1718 (w), 1599 (s), 1582 (s), 1567 (s), 1551 (s), 1508 (w), 1476 (m), 1466 (m), 1459 (m), 1438 (m), 1400 (m), 1365 (w), 1327 (w), 1308 (w), 1292 (w), 1266 (w), 1251 (w), 1237 (w), 1208 (w), 1126 (m), 1094 (m), 1079 (w), 1065 (m), 1042 (m), 1011 (m), 988 (m), 963 (w), 919 (w), 898 (w), 872 (m), 855 (w), 849 (w), 786 (s), 742 (s), 732 (m), 726 (m), 690 (m), 683 (m), 667 (m), 660 (m), 640 (m), 633 (m), 621 (m), 564 (w), 518 (w), 493 (m), 485 (w), 466 (m), 408 (m). HRMS found *m/z*: 793.13281 $[M^+H]^+$, $C_{46}H_{29}N_6S_4$ requires: 793.13310.

3,3‴-Dihexyl-(2,2′:5′,2″:5″,2‴-quaterthiophene-5,5‴-diyl)-bis(4,4,5,5-tetramethyl-1,3,2-dioxaborolane)

3,3‴-Dihexyl-2,2′:5′,2″:5″,2‴-quaterthiophene (0.6 g, 1.2 mmol), dtbpy (15 mg, 0.0056 mmol) and ([Ir(OMe)(COD)]$_2$) (18 mg, 0.00271 mmol) were placed in the Schlenk tube and vacuum-argon cycles were applied. Tetrahydrofurane (20 mL) and hexane (20 mL) and the HBpin (0.7 mL, 0.62 g, 4.9 mmol) were added and the reaction mixture was heated to 45 ° overnight. Then the reaction mixture was poured into water and extracted with dichloromethane. The organic fraction was collected, dried with $MgSO_4$, filtered and evaporated to get the product as brownish oil. The product was used without further purification. ^{1}H NMR (300 MHz, *d*-$CDCl_3$) δ ppm 7.47 (s, 2H, C^4), 7.15 (d, J = 3.9, 2H, D^3 or D^4), 7.10 (d, J = 3.9, 2H, D^4 or D^3), 2.79 (t, J = 7.8, 4H, Hex^1), 1.72 – 1.59 (m, 8H, Hex^2 + Hex^3), 1.40 –

1.25 (m, 32H, Hex^4 + Hex^5 + $–CH_3$ pinacol ester), 0.92 – 0.87 (m, 4H, Hex^6). ^{13}C NMR (101 MHz, d_8-THF) δ ppm 141.79, 141.15, 138.20, 138.04, 136.54, 127.89, 125.34, 84.92, 32.80, 31.70, 30.32, 30.16, 25.24, 23.66, 14.6. ^{11}B NMR (128,3 MHz, d_8-THF) δ ppm 24.19. IR (DRIFT), cm^{-1} 3062 (w), 2976 (m), 2956 (m), 2925 (s), 2871 (m), 2855 (m), 1777 (w), 1730 (w), 1549 (m), 1521 (m), 1460 (s), 1429 (s), 1381 (s), 1372 (s), 1329 (s), 1297 (s), 1269 (s), 1214 (m), 1194 (m), 1166 (m), 1143 (s), 1112 (m), 1060 (w), 1050 (w), 1027 (m), 1002 (w), 983 (w), 961 (m), 927 (w), 853 (s), 830 (w), 781 (s), 741 (w), 725 (w), 704 (w), 686 (m), 664 (s), 607 (w), 579 (w), 522 (w), 437 (w). HRMS found *m/z*: 773.31403 $[M^+Na]^+$, $C_{40}H_{56}O_4B_2NaS_4$ requires: 773.31398.

3,3‴-Dihexyl-5,5‴-bis(2,2′:6′,2″-terpyridine-4′-yl)-2,2′:5′,2″:5″,2‴-quaterthiophene Q27-H

3,3‴-Dihexyl-(2,2′:5′,2″:5″,2‴-quaterthiophene-5,5‴-diyl)-bis(4,4,5,5-tetramethyl-1,3,2-dioxaborolane) (0.58 g, 0.77 mmol), B*rtpy* (0.488 g, 1.56 mmol), K_2CO_3 (0.34 g, 2.46 mmol) and PEPPSI-IPr (36 mg) were placed in the Schlenk tube and vacuum – argon cycles were applied. Toluene (15 mL) and methanol (15 mL) were added through septum and the reaction mixture was heated to 90 °C overnight. After cooling to room temperature the mixture was diluted with dichloromethane (30 mL) and washed with water (3×200 mL). The organic layer was dried with $MgSO_4$, filtered and evaporated to get the crude product. The product was purified by column chromatography (Al_2O_3, Hexane/THF, 3:2). Orange powder (0.12 g, 17%) ^1H NMR (400 MHz, *d*-$CDCl_3$) δ ppm 8.78 – 8.76 (m, 4H, A^6), 8.68 (s, 4H, B^3), 8.65 (m, 4H, A^3), 7.89 (td, J_1 = 7.7, J_2 = 1.7, 4H, A^4), 7.66 (s, 2H, C^4), 7.38 (ddd, J_1 = 7.5, J_2 = 4.7, J_3 = 1.3, 4H, A^5), 7.21 (d, *J* = 3.9, 2H, D^3 or D^4), 7.17 (d, *J* = 3.9, D^4 or D^3), 2.87 (t, *J* = 3.9, 4H, Hex^1), 1.82 – 1.72 (m, 4H, Hex^2), 1.50 – 1.36 (m, 12H, Hex^3 – Hex^5), 0.97 – 0.89 (m, 4H, Hex^6). ^{13}C NMR (101 MHz, *d*-$CDCl_3$) δ ppm 156.05, 149.14, 142.96, 140.96, 139.17, 137.10, 136.87, 135.09, 132.42, 128.91, 126.85, 124.17, 123.92, 121.35, 116.59, 31.69, 30.57, 29.73, 29.73, 22.64, 14.13. IR (DRIFT), cm^{-1} 3063 (m), 3013 (w), 2957 (m), 2925 (s), 2852 (m), 1974 (w), 1955 (w), 1724 (m), 1599 (s), 1583 (s), 1567 (s), 1544 (m), 1468 (s), 1458 (s), 1434 (m), 1403 (s), 1386 (m), 1361 (m), 1340 (w), 1298 (w), 1265 (m), 1254 (m), 1210 (m), 1195 (w), 1177 (w), 1146 (w), 1124 (m), 1093 (m), 1070 (m), 1037 (m), 1021 (m), 990 (m), 970 (w), 918 (w), 897 (w), 879 (m), 848 (m), 839 (m), 789 (s), 776 (s), 742 (s), 728 (m), 715 (w), 693 (w), 682 (m), 663 (m), 658 (m), 642 (m), 631 (m), 622 (m), 585 (w), 566 (w), 524 (w), 501 (m), 461 (w), 403 (m). HRMS found *m/z*: 961.32106 $[M^+H]^+$, $C_{58}H_{33}N_6S_4$ requires: 961.32090.

3,3‴-Bis(6-(4-methoxyphenoxy)hexyl)-2,2′:5′,2″:5″,2‴-quaterthiophene

2-Bromo-3-(6-(4-methoxyphenoxy)hexyl)thiophene (3.5 g, 9.5 mmol), 5,5′-bis(4,4,5,5-tetramethyl-1,3,2-dioxaborolan-2-yl)-2,2′-bithiophene (1.4 g, 4.8 mmol), K_2CO_3 (3.94 g, 28.5 mmol), PEPPSI-IPr (150 mg) were introduced to the pre-dried Schlenk tube with magnetic stirring bar and vacuum-argon cycles were applied. Mixed solvent (toluene/methanol, 1:1) was added and reaction mixture was heated at 90°C for 24 hours. After cooling to room temperature the reaction mixture was extracted with dichloromethane, the organic phase was dried with $MgSO_4$, filtered off and evaporated. The crude product was purified by precipitation from concentrated THF solution by hexane. Orange powder (3.4 g, 97 %) ^1H NMR (400 MHz, *d*-$CDCl_3$) δ ppm 7.19 (d, *J* = 5.2, 2H, C^4 or C^5), 7.12 (d, *J* = 3.8, 2H, D^3 or D^4), 7.01 (d, *J* = 3.8, 2H, D^4 or D^3), 6.95 (d, *J* = 5.2, 2H, C^5 or C^4), 6.81 – 6.83 (m, 8H, –Ph), 3.90 (t, *J* = 6.6, 4H, Hex^6), 3.76 (s, 6H, $–OCH_3$), 2.81 (t, *J* = 7.9, 4H, Hex^1), 1.65 – 1.81 (m, 8H, Hex^2 + Hex^5), 1.41 – 1.51 (m, 8H, Hex^3 + Hex^4). ^{13}C NMR (101 MHz, *d*-$CDCl_3$) δ ppm 160.43, 153.65, 153.24, 150.09, 144.13, 139.65, 135.24, 130.39, 126.60, 123.86, 115.41, 114.60, 69.10, 68.54, 30.53, 29.31, 29.18, 27.14, 25.87. IR (DRIFT), cm^{-1} 3096 (m), 3070 (m), 3056 (m), 3042 (w), 3001 (m), 2937 (s), 2928 (s), 2855 (s), 2834 (m), 2067 (w), 1857 (w), 1750 (m), 1615 (w), 1591 (m), 1539 (w), 1508 (s), 1495 (m), 1467 (m), 1456 (m), 1442 (m), 1422 (m), 1389 (m), 1378 (w), 1347 (w), 1322 (m), 1308 (m), 1294 (m), 1231 (s), 1193 (s), 1176 (m), 1154 (w), 1146 (w), 1108 (m), 1090 (m), 1071 (s), 1056 (m), 1038 (s), 1005 (w), 989 (s), 958 (w), 940 (m), 929 (m), 919 (m), 906 (w), 889 (w), 876 (m), 855 (m), 826 (s), 805 (s), 792 (s), 757 (m), 742 (s), 722 (m), 699 (m), 687 (m), 669 (m), 654 (m), 638 (w), 631 (w), 599 (w), 586 (w), 566 (w), 521 (s), 506 (m), 472 (w), 462 (m), 426 (w). HRMS found *m/z*: 765.21732 $[M^+Na]^+$, $C_{42}H_{46}O_4NaS_4$ requires: 765.21711.

5,5‴-(3,3‴-Bis(6-(4-methoxyphenoxy)hexyl-2,2′:5′,2″:5″,2‴-quaterthiophene-5,5‴-diyl)bis(4,4,5,5-tetramethyl-1,3,2-dioxaborolane)

3,3‴-Bis(6-(4-methoxyphenoxy)hexyl)-2,2′:5′,2″:5″,2‴-quaterthiophene (0.6 g, 0.8 mmol), dtbpy (9 mg, 0.03 mmol) and ($[Ir(OMe)(COD)]_2$) (9 mg, 0.01 mmol) were placed in a tube and vacuum-argon cycles were applied. Tetrahydrofurane (12 mL) and hexane (12 mL) and HBpin (0.24 mL, 0.21 g, 2.1 mmol) were added. The tube was heated at 50°C for 24 hours. After opening the tube, water was added and the mixture was stirred for an hour. Then the reaction mixture was extracted with dichloromethane, the organic phase was dried with $MgSO_4$, filtered off and evaporated to get the product (0.76 g, 95 %). The product was used as obtained for following synthesis without purification. ^1H NMR (400 MHz, *d*-$CDCl_3$) δ ppm 7.47 (s, 2H, C^4), 7.13 (d, *J* = 3.9, 2H, D^3 or D^4), 7.07 (d, *J* = 3.9, 2H, D^4 or D^3), 6.82 (s, 8H, –Ph), 3.89 (t, *J* = 6.6, 4H, Hex^6), 3.76 (s, 6H, $–OCH_3$), 2.81 (t, *J* = 7.4, 4H, Hex^1), 1.80 – 1.69 (m, 8H, Hex^2 + Hex^5), 1.52 – 1.44 (m, 8H, Hex^3 + Hex^4), 1.36 (s, 24H, $–CH_3$pinacol ester). ^{13}C NMR (101 MHz, *d*-$CDCl_3$) δ ppm 153.64, 153.25, 140.70, 140.09, 137.53, 137.07, 135.30, 126.85, 124.10, 115.41, 114.59, 84.18, 68.56, 55.71, 30.44, 29.29, 29.26, 29.12, 25.88, 24.75, 24.59. ^{11}B NMR (128,3 MHz, *d*-$CDCl_3$) δ ppm 22.50. IR (DRIFT), cm^{-1} 3092 (w), 2975 (m), 2936 (m), 2861 (m), 2833 (w), 1752 (w), 1617 (w), 1593 (w), 1544 (w), 1508 (s), 1471 (m), 1456 (m), 1380 (m), 1372 (m), 1334 (m), 1306 (m), 1266 (m), 1231 (s), 1180 (m), 1167 (m), 1143 (m), 1107 (m), 1073 (m), 1039 (m), 1009 (m), 983 (m), 967 (w), 926 (w), 902 (w), 851 (m), 825 (m), 793 m), 743 (m), 721 (m),

700 (m), 674 (m), 606 (w), 578 (w), 522 (m). HRMS found *m/z*: 1017.38703 $[M^+Na]^+$, $C_{54}H_{68}O_8B_2NaS_4$ requires: 1017.38753.

3,3‴-bis(6-(4-methoxyphenoxy)hexyl)-5,5‴-bis(2,2′:6′,2″-terpyridin-4′-yl)- 2,2′:5′,2″:5″,2‴-quaterthiophene Q27-A

Br*tpy* (0.33 g, 1.03 mmol), K_2CO_3 (0.20 g, 1.47 mmol) and PEPPSI-IPr (20 mg) were placed into the pre-dried Schlenk tube and three vacuum - argon cycles were applied. 5,5‴-(3,3‴-Bis(6-(4-methoxyphenoxy)hexyl-2,2′:5′,2″:5″,2‴-quaterthiophene-5,5‴-diyl)-bis(4,4,5,5-tetramethyl-1,3,2-dioxaborolane) (0.47 g, 0.47 mmol) was dissolved in toluene (15 mL) and added to the tube. Methanol (15 mL) was added and the reaction mixture was heated at 90°C for 24 hours. After cooling to room temperature the mixture was extracted with dichloromethane, the organic phase was dried with $MgSO_4$, filtered off and evaporated. The crude product was purified on column chromatography (Al_2O_3, hexane/THF, 3:2) to get the product as an orange solid (0.18 g, 32 %). ^{1}H NMR (400 MHz, *d*-$CDCl_3$) δ ppm 8.75 – 8.78 (m, 4H, A^6), 8.68 – 8.65 (m, 8H, B^3 + A^3), 7.89 (td, J_1 = 8.0, J_2 = 1.8, 4H, A^4), 7.66 (s, 2H, C^4), 7.38 (ddd, J_1 = 7.6, J_2 = 4.9, J_2 = 1.5, 4H, A^5), 7.19 (d, J = 3.8, 2H, D^3 or D^4), 7.14 (d, J = 4.10, 2H, D^4 or D^3), 6.79 – 6.86 (m, 8H, –Ph), 3.93 (t, J = 6.3, 4H, Hex^6), 3.75 (s, 6H, –O*C*H_3), 2.88 (t, J = 7.9, 4H, Hex^1), 1.76 – 1.86 (m, 8H, Hex^2 + Hex^5), 1.52 – 1.59 (m, 8H, Hex^3 + Hex^4). ^{13}C NMR (101 MHz, *d*-$CDCl_3$) δ ppm 156.07, 156.03, 153.65, 153.27, 149.14, 142.91, 140.72, 139.27, 137.10, 136.86, 135.00, 132.48, 128.84, 126.93, 124.22, 123.92, 121.33, 116.53, 115.44, 114.59, 68.56, 55.72, 30.47, 29.57, 29.34, 29.32, 25.94. IR (DRIFT), cm^{-1} 3060 (m), 3050 (m), 3011 (w), 2930 (s), 2858 (m), 1601 (s), 1584 (s), 1568 (s), 1545 (m), 1508 (s), 1466 (s), 1441 (m), 1401 (s), 1384 (w), 1334 (w), 1303 (w), 1289 (w), 1263 (m), 1231 (s), 1181 (m), 1146 (w), 1123 (m), 1105 (m), 1095 (m), 1071 (m), 1039 (m), 1019 (m), 990 (m), 882 (m), 831 (m), 823 (m), 787 (s), 774 (m), 740 (m), 726 (m), 706 (w), 670 (w), 660 (m), 630 (m), 622 (m), 567 (w), 525 (w), 498 (w), 468 (w), 425 (w), 400 (m). HRMS found *m/z*: 1205.39458 $[M^+H]^+$, $C_{72}H_{65}O_4N_6S_4$ requires: 1205.39446.

3,3′-Bis(6-(4-methoxyphenoxy)hexyl-2,2′-bithiophene

2-Bromo-3-(6-(4-methoxyphenoxy)hexyl)thiophene (1.66 g, 4.5 mmol), B_2pin_2 (0.71 g, 2.8 mmol), K_2CO_3 (1.8 g, 13 mmol) and PEPPSI-IPr (112 mg) were placed to the Schlenk tube and vacuum – argon cycles were applied. Toluene (16 mL) and methanol (16 mL) were added and the reaction mixture was heated at 90°C for 24 hours. After cooling to room temperature the reaction mixture was extracted with dichloromethane, the organic phase was dried with $MgSO_4$, filtered off and evaporated. The crude product was purified on column chromatography (SiO_2, hexane/CH_2Cl_2, 1:1) to get the pure product (0.62 g, 48 %). ^{1}H NMR (300 MHz, *d*-$CDCl_3$) δ ppm 7.29 (d, J = 5.4, 2H, D^4 or D^5), 6.96 (d, J = 5.1, 2H, D^5 or D^4), 6.82 (s, 8H, –Ph), 3.84 (t, J = 6.5, 4H, Hex^6), 3.77 (s, 6H, –O*C*H_3), 2.52 (t, J = 7.7, 4H, Hex^1), 1.74 – 1.67 (m, 4H, Hex^5), 1.63 – 1.56 (m, 4H, Hex^2), 1.44 – 1.29 (m, 8H, Hex^3 + Hex^4). ^{13}C NMR (101 MHz, *d*-$CDCl_3$) δ ppm 153.32, 152.93, 141.80, 128.43, 128.19, 125.0, 115.08, 114.27, 68.21, 55.43, 30.29, 28.94, 28.77, 28.34, 25.49. IR (DRIFT), cm^{-1} 3107 (m), 3064 (m), 3046 (m), 3011 (m), 2932 (s), 2854 (s), 2836 (m), 1510 (s), 1476 (m), 1466 (m), 1442 (m), 1395 (m), 1379 (w), 1349 (w), 1335 (w), 1291 (s), 1269 (m), 1239 (s), 1179 (m), 1154 (w), 1130 (w), 1109 (m), 1090 (m), 1073 (w), 1038 (s), 1016 (m), 1001 (m), 943 (w), 932 (m), 915 (m), 894 m), 884 (m), 826 (s), 789 (w), 767 (w), 742 (s), 732 (m), 717 (s), 695 (m), 686 (m), 663 (m), 629 (m), 602 (w), 571 (w), 531 (m), 521 (m), 509 (m), 490 (w), 436 (w), 422 (w). HRMS found *m/z*: 579.25984 $[M^+H]^+$, $C_{34}H_{43}O_4S_2$ requires: 579.25973.

5,5′-(3,3′-Bis(6-(4-methoxyphenoxy)hexyl-2,2′-bithiophene-5,5′-diyl)bis(4,4,5,5-tetramethyl-1,3,2-dioxaborolane)

3,3′-Bis(6-(4-methoxyphenoxy)hexyl-2,2′-bithiophene (0.6 g, 1.0 mmol), dtbpy (46 mg, 0.17 mmol) and ($[Ir(OMe)(COD)]_2$) (48 mg, 0.07 mmol) were placed in a tube and vacuum – argon cycles were applied. Tetrahydrofurane (15 mL) and hexane (15 mL) and HBpin (0.6 mL, 0.53 g, 4.2 mmol) were added through septum. The tube was heated at 50°C for 4 days. After opening the tube water was added and the solution was stirred for an hour. Then the reaction mixture was extracted with dichloromethane, the organic phase was dried with $MgSO_4$, filtered off and evaporated to get the product (0.88 g, 100 %). The product was used as obtained for following synthesis without purification. ^{1}H NMR (300 MHz, *d*-$CDCl_3$) δ ppm 7.52 (s, 2H, D^4), 6.82 (s, 8H, –Ph), 3.85 (t, J = 6.5, 4H, Hex^6), 3.77 (s, 6H, –O*C*H_3), 2.53 (t, J = 7.7, 4H, Hex^1), 1.88 – 1.84 (m, 4H, Hex^5), 1.72 – 1.68 (m, 4H, Hex^2), 1.60 – 1.54 (m, 4H, Hex^3), 1.42 – 1.30 (m, 28H, Hex^4 + –CH_3 pinacol ester). ^{13}C NMR (101 MHz, *d*-$CDCl_3$) δ ppm 153.59, 153.25, 143.42, 138.71, 136.29, 128.71, 115.41, 114.58, 84.10, 68.55, 55.74, 30.56, 29.24, 29.10, 28.57, 25.82, 24.76. ^{11}B NMR (128,3 MHz, *d*-$CDCl_3$) δ ppm 22.48. IR (DRIFT), cm^{-1} 3045 (w), 2977 (s), 2934 (s), 2857 (s), 2833 (m), 1615 (w), 1591 (m), 1532 (m), 1508 (s), 1470 (m), 1456 (m), 1435 (m), 1380 (m), 1373 (m), 1329 (m), 1296 (m), 1268 (m), 1232 (s), 1180 (w), 1167 (w), 1142 (s), 1107 (m), 1074 (w), 1039 (m), 984 (w), 961 (m), 925 (w), 853 (m), 825 (m), 802 (m), 773 (w), 742 (m), 723 (m), 686 (m), 665 (s), 605 (w), 578 (m), 523 (m), 436 (w). HRMS found *m/z*: 853.41211 $[M^+Na]^+$, $C_{46}H_{64}O_8B_2NaS_2$ requires: 853.41209.

4′,3″-Bis(6-(4-methoxyphenoxy)hexyl-5,5‴-bis(2,2':6',2''-terpyridine-4'-yl)-2,2′:5′,2″:5″,2‴-quaterthiophene Q45-A

4′-(5-Bromothiophene-2-yl)-2,2′:6′2″-terpyridine (0.6 g, 1.62 mmol), K_2CO_3 (0.78 g, 5.6 mmol) and PEPPSI (54 mg) were placed in the Schlenk tube and vacuum-argon cycles were applied. 5,5′-(3,3′-Bis(6-(4-methoxyphenoxy)hexyl-2,2′-bithiophene-5,5′-diyl)bis(4,4,5,5-tetramethyl-1,3,2-dioxaborolane) (0.68 g, 0.8 mmol) was dissolved in toluene (16 mL) and added to the tube. Methanol (16 mL) was added and the reaction mixture was heated at 95°C for 20 hours. After cooling to room temperature the mixture was extracted with dichloromethane, the organic phase was dried with $MgSO_4$, filtered off and evaporated. The crude product was purified on column chromatography (Al_2O_3, hexane/THF 3:2) to get the product as an orange solid (0.28 g, 28 %). ^{1}H NMR (400 MHz, *d*-$CDCl_3$) δ ppm 8.77 – 8.75 (m, 4H, A^6), 8.70 (s, 4H, B^3), 8.67 (dt,

J_1 = 8.0, J_2 = 1.1, 4H, A^3), 7.89 (td, J_1 = 7.8, J_2 = 1.8, 4H, A^4), 7.71 (d, J = 7.3, 2H, C^4), 7.38 (ddd, J_1 = 7.4, J_2 = 4.8, J_3 = 1.4, 4H, A^5), 7.24 (d, J = 3.6, 2H, C^3), 7.19 (s, 2H, D^4), 6.8 (s, 4H, –Ph), 6.79 (s, 4H, –Ph), 3.89 (t, J = 6.5, 4H, Hex^6), 3.71 (s, 6H, –OMe), 2.61 (t, J = 7.6, 4H, Hex^1), 1.80 – 1.73 (m, 4H, Hex^5), 1.70 – 1.64 (m, 4H, Hex^2), 1.50 – 1.40 (m, 8H, Hex^3 + Hex^4). ^{13}C NMR (101 MHz, *d*-$CDCl_3$) δ ppm 156.12, 155.99, 153.60, 153.26, 149.16, 143.53, 142.98, 140.34, 138.88, 136.86, 136.23, 127.99, 126.64, 125.88, 124.62, 123.92, 121.30, 116.66, 115.38, 114.57, 68.54, 55.66, 30.52, 29.28, 29.06, 28.89, 25.84. IR (DRIFT), cm^{-1} 3064 (m), 3049 (m), 3004 (m), 2936 (s), 2859 (m), 2831 (w), 1599 (m), 1582 (s), 1566 (m), 1552 (m), 1507 (s), 1466 (s), 1446 (m), 1399 (m), 1382 (w), 1362 (w), 1303 (w), 1290 (w), 1265 (m), 1231 (s), 1181 (m), 1152 (w), 1146 (w), 1125 (w), 1107 (m), 1095 (m), 1085 (w), 1065 (m), 1038 (m), 1011 (m), 990 (m), 946 (w), 919 (w), 907 (w), 882 (m), 878 (m), 862 (w), 848 (w), 825 (s), 789 (s), 773 (m), 743 (m), 729 (m), 720 (m), 701 (w), 680 (m), 658 (m), 633 (m), 622 (m), 584 (w), 565 (w), 535 (w), 523 (m), 506 (w), 494 (w), 468 (w), 456 (w), 418 (w), 403 (m). HRMS found *m/z*: 1205.39479 $[M^+H]^+$, $C_{72}H_{65}O_4N_6S_4$ requires: 1205.39446.

3,4′,3″,3‴-Tetra(6-(4-methoxyphenoxy)hexyl)-2,2′:5′,2″:5″,2‴-quaterthiophene

5,5′-(3,3′-Bis(6-(4-methoxyphenoxy)hexyl-2,2′-bithiophene-5,5′-diyl)bis(4,4,5,5-tetramethyl-1,3,2-dioxaborolane) (1.04 g, 1.25 mmol), 2-bromo-3-(6-(4-methoxyphenoxy)hexyl)thiophene (0.991 g, 2.68 mmol), K_2CO_3 (1.16 g, 8.4 mmol) and PEPPSI-IPr (94 mg) were placed in a Schlenk tube and vacuum – argon cycles were applied. Toluene (15 mL) and methanol (15 mL) were added through septum and the reaction mixture was heated at 90 °C overnight. After cooling to room temperature the reaction mixture was diluted with dichloromethane (25 mL) and washed with water. The organic layer was dried with $MgSO_4$, filtered and evaporated. The crude product was purified on column chromatography (Al_2O_3, Hexane/THF, 4:1). (0.42 g, 30 %) ^{1}H NMR (400 MHz, d_2-CD_2Cl_2) δ ppm 7.18 (d, J = 5.1, 2H, E^5), 7.02 (s, 2H, F^3), 6.95 (d, J = 5.5, 2H, E^4), 6.78 (s, 8H, –Ph), 6.76 (s, 8H, –Ph), 3.87 – 3.81 (m, 8H, Hex^6), 3.72 (s, 12H, –OCH_3), 2.80 (t, J = 7.8, 4H, Hex^1), 2.59 (t, J = 7.8, 4H, Hex^1), 1.75 – 1.61 (m, 16H, Hex^2 + Hex^5), 1.46 – 1.39 (m, 16H, Hex^3 + Hex^4). ^{13}C NMR (101 MHz, d_2-CD_2Cl_2) δ ppm 154.25, 153.85, 143.37, 140.11, 136.57, 131.12, 130.77, 128.76, 128.00, 124.20, 115.82, 115.04, 69.04, 56.13, 32.16, 31.20, 29.84, 29.72,.26.44. IR (DRIFT), cm^{-1} 3105 (w), 3074 (w), 3047 (w), 2997 (w), 2935 (s), 2858 (s), 1512 (s), 1466 (m), 1439 (w), 1389 (w), 1288 (m), 1242 (s), 1215 (s), 1180 (m), 1157 (w), 1111 (m), 1068 (m), 1041 (s), 987 (w), 941 (w), 922 (w), 825 (s), 741 (m), 721 (m), 687 (w), 652 (w), 525 (m). HRMS found *m/z*: 1155.49656 $[M^+H]^+$, $C_{68}H_{83}O_8S_4$ requires: 1155.49653.

5,5‴-(3,4′,3″,3‴-Tetra(6-(4-methoxyphenoxy)hexyl)-2,2′:5′,2″:5″,2‴-quaterthiophene-5,5‴-diyl)bis(4,4,5,5-tetramethyl-1,3,2-dioxaborolane)

3,4′,3″,3‴-Tetra(6-(4-methoxyphenoxy)hexyl)-2,2′:5′,2″:5″,2‴-quaterthiophene (0.42 g, 0.36 mmol), dtbpy (13 mg) and ([Ir(OMe)(COD)]$_2$) (15 mg) were placed in the tube and vacuum – argon cycles were applied. Tetrahydrofurane (10 mL), hexane (10 mL) and HBpin (0.2 mL, 0.176 g, 1.38 mmol) and the reaction mixture was heated at 50 °C for 2 days. After opening the vessel the reaction mixture was diluted with water and stirred for an hour. Then the product was extracted with dichloromethane, dried with $MgSO_4$, filtered and evaporated. The product was used in following synthesis without purification. (0.48 g, 94 %) 1H NMR (400 MHz, d_2-CD_2Cl_2) δ ppm 7.43 (s, 2H, C^4), 7.09 (s, 2H, D^3), 6.78 (s, 8H, –Ph), 6.76 (s, 8H, –Ph), 3.87 – 3.81 (m, 8H, Hex^6), 3.72 (s, 12H, –OCH_3), 2.81 (t, J = 8.0, 4H, Hex^1), 2.60 (t, J = 7.6, 4H, Hex^1), 1.75 – 1.60 (m, 16H, Hex^2 + Hex^5), 1.48 – 1.40 (m, 16H, Hex^3 + Hex^4), 1.34 (s, 24H, –CH_3pinacol ester). ^{13}C NMR (101 MHz, d_2-CD_2Cl_2) δ ppm 154.22, 153.86, 143.53, 141.23, 138.16, 136.51, 131.09, 129.23, 128.37, 115.83, 115.04, 84.74, 68.32, 56.13, 30.92, 29.89, 26.42, 26.15, 25.14, 24.93. ^{11}B NMR (128,3 MHz, d_2-CD_2Cl_2) δ ppm 22.39.

3,4′,3″,3‴-Tetra(6-(4-methoxyphenoxy)hexyl)-5,5‴-bis(2,2′:6′,2″-terpyridin-4′-yl)-2,2′:5′,2″:5″,2‴-quaterthiophene Q2457-A

5,5‴-(3,4′,3″,3‴-Tetra(6-(4-methoxyphenoxy)hexyl)-2,2′:5′,2″:5″,2‴-quaterthiophene-5,5‴-diyl)bis(4,4,5,5-tetramethyl-1,3,2-dioxaborolane) (0.45 g, 0.32 mmol), Br*tpy* (0.215 g, 0.69 mmol), K_2CO_3 (0.40 g, 2.89 mmol) and PEPPSI-IPr (32 mg) were placed in the Schlenk tube and vacuum and three vacuum-argon cycles were applied. The reaction mixture was heated to 90 °C overnight. After cooling to room temperature the mixture was diluted with dichloromethane (40 mL)and washed with water (3×200 mL). The organic layer was dried with $MgSO_4$, filtered and evaporated to get the crude product. The product was purified on column chromatography (Al_2O_3, Hexane/THF, 3:2). Orange solid (0.17 g, 33 %) ^{1}H NMR (400 MHz, d_2-CD_2Cl_2) δ ppm 8.74 (m, 4H, A^6), 8.70 (s, 4H, B^3), 8.67 (m, 4H, A^3), 7.91 (td, J_1 = 7.7, J_2 = 2.1, 4H, A^4), 7.67 (s, 2H, C^4), 7.40 – 7.37 (m, 4H, A^5), 7.19 (s, 2H, D^4), 6.80 – 6.72 (m, 16H, –Ph), 3.90 – 3.83 (m, 8H, Hex^6), 3.69 (s, 6H, –OCH_3), 3.66 (s, 6H, –OCH_3), 2.89 (t, J = 7.8, 4H, Hex^1), 2.66 (t, J = 7.8, 4H, Hex^1), 1.80 – 1.69 (m, 16H, Hex^2 + Hex^5), 1.45 – 1.38 (m, 16H, Hex^3 + Hex^4). ^{13}C NMR (101 MHz, d_2-CD_2Cl_2) δ ppm 156.71, 156.41, 154.23, 153.85, 149.74, 143.72, 143.37, 141.35, 139.47, 137.42, 136.23, 133.28, 129.58, 129.34, 128.46, 124.58, 121.62, 116.88, 115.83, 115.03, 69.06, 56.09, 31.06, 29.92, 29.70, 26.50, 26.42. IR (DRIFT), cm^{-1} 3063 (w), 3009 (w), 2935 (s), 2854 (m), 1601 (m), 1581 (s), 1566 (s), 1508 (s), 1462 (s), 1400 (w), 1288 (w), 1238 (w), 1180 (w), 1149 (w), 1107 (m), 1072 (w), 1038 (s), 991 (w), 883 (w), 825 (m), 795 (m), 744 (m), 679 (w), 656 (m), 633 (w), 621 (w), 525 (w). HRMS found *m/z*: 1617.65658 $[M^+H]^+$, $C_{98}H_{101}O_8N_6S_4$ requires: 1617,65582.

General procedure for bromination of A-unimers. A unimer was dissolved in dichloromethane (to concentration ca. 0.02 M), the solution was then cooled in an ice bath and the BBr_3 was added (excess). After 4 hours of stirring the cooling bath was removed and the solution was poured into water. The

mixture was carefully neutralized with saturated solution of K_2CO_3. Then the product was extracted with dichloromethane, dried with $MgSO_4$, filtered off and evaporated to get the desired product.

3,3‴-Di(6-bromohexyl)-5,5‴-bis(2,2′:6′,2″-terpyridin-4′-yl)-2,2′:5′,2″:5″,2‴-quaterthiophene Q27-Br

Red solid (90 %). ^{1}H NMR (300 MHz, *d*-$CDCl_3$) δ ppm 8.75 – 8.79 (m, 4H, A^6), 8.64 – 8.69 (m, 8H, A^3 + B^3), 7.89 (td, J_1 = 7.8, J_2 = 1.7, 4H, A^4), 7.65 (s, 2H, C^4), 7.38 (ddd, J_1 = 7.8, J_2 = 4.5, J_3 = 1.3, 4H, A^5), 7.21 (d, *J* = 3.6, 2H, D^3 or D^4), 7.16 (d, *J* = 3.9, 2H, D^4 or D^3), 3.45 (t, *J* = 6.9, 4H, Hex^6), 2.88 (t, *J* = 7.9, 4H, Hex^1), 1.99 – 1.73 (m, 12 H, Hex^2 + Hex^4 + Hex^5), 1.57 – 1.45 (m, 4 H, Hex^3). ^{13}C NMR (101 MHz, *d*-$CDCl_3$) δ ppm 155.97, 155.94, 149.08, 142.88, 140.52, 139.25, 137.08, 136.93, 134.97, 132.53, 128.82, 126.91, 124.22, 123.94, 121.37, 116.59, 33.92, 32.71, 30.32, 29.51, 28.69, 28.03. IR (DRIFT), cm^{-1} 3063 (m), 3012 (w), 2931 (m), 2858 (m), 1601 (s), 1585 (s), 1566 (s), 1543 (m), 1466 (s), 1404 (s), 1385 (m), 1265 (w), 1122 (w), 1095 (w), 1072 (w), 1045 (w), 1018 (w), 991 (w), 883 (m), 845 (m), 791 (s), 741 (m), 660 (w), 621 (w). HRMS found *m/z*: 1117.14218 $[M^+H]^+$, $C_{58}H_{51}N_6Br_2S_4$ requires: 1117.14193

4′,3″-Di(6-bromohexyl-5,5‴-bis(2,2':6',2''-terpyridine-4'-yl)-2,2′:5′,2″:5″,2‴-quaterthiophene Q45-Br

Orange solid (87%). 1H NMR (400 MHz, *d*-$CDCl_3$) δ ppm 8.76 (dd, J_1 = 5.2, J_2 = 1.2, 4H, A^3), 8.70 (s, 4H, B^3), 8.67 (d, *J* = 7.9, 4H, A^6), 7.89 (td, J_1 = 7.8, J_2 = 1.8, 4H, A^4), 7.73 (d, *J* = 3.9, 2H, C^4), 7.38 (m, 4H, A^5), 7.17 (s, 2H, D^4), 3.41 (t, *J* = 6.9, 4H, Hex^6), 2.60 (t, *J* = 7.3, 4H, Hex^1), 1.72 – 1.61 (m, 8H, Hex^2 + Hex^5), 1.49 – 1.36 (m, 8H, Hex^3 + Hex^4). ^{13}C NMR (101 MHz, *d*-$CDCl_3$) δ ppm 156.11, 155.97, 149.14, 143.35, 142.97, 140.41, 138.80, 136.87, 127.96, 126.65, 125.81, 124.66, 123.94, 123.37, 121.32, 116.67, 33.91, 32.70, 30.44, 28.90, 28.49, 27.98. IR (DRIFT), cm^{-1} 3063 (m), 3011 (m), 2932 (s), 2856 (m), 1775 (w), 1655 (w), 1599 (s), 1582 (s), 1567 (s), 1551 (s), 1509 (w), 1466 (s), 1438 (m), 1400 (s), 1378 (w), 1362 (m), 1301 (w), 1292 (w), 1266 (m), 1235 (m), 1182 (w), 1148 (w), 1126 (m), 1096 (m), 1065 (m), 1042 (m), 1011 (s), 989 (m), 903 (w), 877 (m), 860 (m), 848 (m), 825 (m), 791 (s), 772 (s), 745 (s), 732 (s), 680 (m), 659 (m), 633 (m), 622 (m), 584 (w), 564 (m), 537 (m), 497 (m), 468 (m), 452 (w), 439 (w), 404 (m). HRMS found *m/z*: 1117.14240 $[M^+H]^+$, $C_{58}H_{51}N_6Br_2S_4$ requires: 1117.14193.

3,4′,3″,3‴-Tetra(6-bromohexyl)-5,5‴-bis(2,2′:6′,2″-terpyridin-4′-yl)-2,2′:5′,2″:5″,2‴-quaterthiophene Q2457-Br

Red solid (95 %). ^{1}H NMR (400 MHz, d_2-CD_2Cl_2) δ ppm 8.74 (m, 4H, A^6), 8.71 (s, 4H, B^3), 8.68 (m, 4H, A^3), 7.92 (td, *J* = 7.8, *J* = 7.8, *J* = 1.8, 4H, A^4), 7.69 (s, 2H, C^4), 7.40 (ddd, *J* = 7.8, *J* = 4.6, 4H, A^5), 7.19 (s, 2H, D^4), 3.46 – 3.41 (m, 8H, Hex^6), 2.90 (m, 4H, Hex^1), 2.66 (m, 4H, Hex^1), 1.92 – 1.69 (m, 16H, Hex^2 + Hex^5), 1.55 – 1.47 (m, 16H, Hex^3 + Hex^4). ^{13}C NMR (101 MHz, d_2-CD_2Cl_2) δ ppm 156.29, 155.97, 149.32, 143.22, 142.97, 140.85, 139.19, 137.0, 135.89, 132.87, 129.14, 128.95, 128.06, 124.22, 121.29, 116.53, 34.32, 33.00, 30.55, 29.71, 28.75, 28.22. IR (DRIFT), cm^{-1} 3062 (m), 3012 (m), 2930 (s), 2855 (s), 1731 (w), 1656 (w), 1598 (s), 1582 (s), 1567 (s), 1543 (m), 1466 (s), 1453 (s), 1437 (m), 1401 (s), 1382 (m), 1335 (w), 1278 (w), 1265 (m), 1236 (w), 1204 (w), 1192 (w), 1145 (w), 1124 (w), 1094 (m), 1071 (m), 1042 (m), 1014 (m), 990 (m), 971 (w), 936 (w), 883 (m), 865 (w), 847 (m), 837 (m), 820 (m), 791 (s), 773 (m), 743 (s), 730 (s), 712 (w), 676 (w), 660 (s), 633 (m), 622 (m), 564 (m), 540 (w), 500 (m), 467 (w), 403 (m). HRMS found *m/z*: 1441.15190 $[M^+H]^+$, $C_{70}H_{73}N_6Br_4S_4$ requires: 1441.15076.

General procedure for quaternization of Br-unimers. A unimer was dissolved in toluene (to concentration ca. 6.5mM) and the flask was flushed with argon. Triethylphosphine (PEt_3) was added as 1M solution in THF (ca. 20 eq.) and the reaction was heated to 110°C for 4 days during these the quaternized product has been precipitated from the solution. After cooling to room temperature the product was filtered and washed with toluene and diethylether. The desired product was dried in vacuo.

6,6′-[5,5‴-bis(2,2′:6′,2″-terpyridine-4′-yl)-(2,2′:5′,2″:5″,2‴-quaterthiophen-3,3‴-diyl)]-bis(hexan-1,1′-diyl triethylphosphonium) bromide Q27-P$^+$

Dark red solid (74 %). ^{1}H NMR (400 MHz, d_4-CD_3OD) δ ppm 8.60 (dd, *J* = 5.0, *J* = 1.4, 4H, A^6), 8.44 (d, *J* = 7.9, 4H, A^3), 8.29 (s, 4 H, B^3), 7.89 (td, J_1 = 7.7, J_2 = 1.8, 4H, A^4), 7.47 (s, 2H, C^4), 7.39 – 7.45 (m, 4H, A^5), 7.12 (d, *J* = 3.6, 2H, D^3 or D^4), 7.08 (d, *J* = 3.9, 2H, D^4 or D^3), 2.78 – 2.87 (m, 4H, Hex^1), 2.09 – 2.35 (m, 20H, P–CH_2 + Hex^5 + Hex^6), 1.69 – 1.83 (m, 8H, Hex^2 + Hex^3), 1.10 – 1.34 (m, 22H, P–CH_3 + Hex^4). Due to low solubility of this compound we were not able to get ^{13}C NMR spectrum in a sufficient quality. ^{31}P NMR (121.42 MHz, d_4-CD_3OD) δ ppm 38.93. IR (DRIFT), cm^{-1} 3061 (m), 3012 (w), 2976 (m), 2933 (m), 2861 (m), 1599 (m), 1582 (s), 1567 (m), 1545 (m), 1535 (w), 1466 (m), 1454 (m), 1402 (m), 1387 (w), 1292 (w), 1267 (w), 1200 (w), 1146 (w), 1125 (m), 1096 (m), 1072 (m), 1048 (m), 1016 (m), 989 (m), 969 (w), 882 (m), 837 (w), 791 (s), 743 (s), 731 (m), 680 (m), 660 (s), 622 (m), 567 (m), 553 (m), 491 (m), 468 (m), 407 (m). HRMS found *m/z*: 597.23970 $[M^+H]^{2+}$, $C_{70}H_{80}N_6P_2S_4$ *z=2* requires: 597.23958.

6,6′-[5,5‴-bis(2,2′:6′,2″-terpyridine-4′-yl)-(2,2′:5′,2″:5″,2‴-quaterthiophen-4′,3″-diyl)]-bis(hexan-1,1′-diyl triethylphosphonium) bromide Q45-P$^+$

Red solid (95 %). ^{1}H NMR (400 MHz, d_4-CD_3OD) δ ppm 8.55 – 8.60 (m, 4H, A^3), 8.43 (dd, J_1 = 7.9, J_2 = 1.1, 4H, A^6), 8.33 (s, 4H, B^3), 7.85 – 7.91 (m, 4H, A^4), 7.55 (d, *J* = 3.8, 2H, C^4), 7.39 (ddd, J_1 = 7.5, J_2 = 4.7, J_3 = 1.4, 4H, A^5), 7.23 (s, 2H, D^4), 7.13 - 7.16 (m, 2H, C^3), 2.56 – 2.64 (m, 4H, Hex^1), 2.07 – 2.21 (m, 20H, P–CH_2 + Hex^5 + Hex^6), 1.60 – 1.72 (m, 8H, Hex^2 + Hex^3), 1.07 – 1.20 (m, 22H, P–CH_3 + Hex^4). ^{13}C NMR (101 MHz, d_4-CD_3OD) δ ppm 156.81, 156.46, 149.98, 144.93, 144.07, 141.29, 140.29, 139.01, 138.11, 129.48, 128.51, 127.55, 126.29, 125.77, 122.94, 117.29, 31.88, 31.67, 30.26, 29.96, 22.47 (d, *J* = 4.4), 18.5 (d, *J* = 47.9), 12.44 (d, *J* = 49.4), 5.92 (d, *J* = 5.3). ^{31}P NMR (121.42 MHz, d_4-CD_3OD) δ ppm 38.44. IR (DRIFT), cm^{-1} 3062 (m), 3011 (m), 2975 (m), 2930 (s), 2858 (s), 1600 (s), 1583 (s), 1567 (s), 1551 (m), 1535 m), 1466 (s), 1439 (m), 1400 (s), 1363 (w), 1324 (w), 1292 (w), 1267 (m), 1234 (m), 1179 (w), 1147

(w), 1125 (m), 1096 (m), 1062 (m), 1046 (m), 1011 (m), 990 (m), 969 (w), 880 (m), 861 (w), 847 (w), 791 (s), 773 (s), 742 (m), 726 (m), 682 (m), 660 (m), 623 (m), 580 (w), 539 (w), 497 (m), 470 (m), 463 (w), 405 (m). HRMS found *m/z*: 597.23959 $[M^+H]^{2+}$, $C_{70}H_{80}N_6P_2S_4$ *z=2* requires: 597.23958.

6,6′,6″,6‴-[5,5‴-bis(2,2′:6′,2″-terpyridine-4′-yl)-(2,2′:5′,2″:5″,2‴-quaterthiophen-3,4′,3″,3‴-tetrayl)]tetra(hexan-1,1′,1″,1‴-tetrayl triethylphosphonium) bromide Q2457-P$^+$

Red solid (92 %). ^{1}H NMR (400 MHz, d_4-CD_3OD) δ ppm 8.67 – 8.41 (m, 12H, A^6 + A^3 + B^3), 7.99 – 7.90 (m, 4H, A^4), 7.67 (s, 2H, C^4), 7.49 – 7.43 (m, 4H, A^5), 7.23 (s, 2H, D^4), 2.90 – 2.84 (m, 4H, Hex^1), 2.70 – 2.84 (m, 4H, Hex^1), 2.31 – 2.15 (m, 40H, P–CH_2 + Hex^5 + Hex^6), 1.84 – 1.79 (m, 16H, Hex^2 + Hex^3), 1.31 – 1.10(m, 44H, P–CH_3 + Hex^4). ^{13}C NMR (101 MHz, d_4-CD_3OD) δ ppm 157.03, 156.58, 150.25, 144.59, 144.04, 142.02, 139.94, 138.92, 137.23, 134.15, 130.61, 129.97, 129.05, 125.69, 122.83, 117.39, 31.91, 31.31, 30.15, 22.55, 18.61 (d, *J* = 46.4), 13.94 (d, *J* = 50.8), 12.56 (d, *J* = 48.6), 6.03 (m). ^{31}P NMR (161.92 MHz, d_4-CD_3OD) δ ppm 39.99. IR (DRIFT), cm^{-1} 3444 (m), 3055 (w), 2978 (m), 2931 (s), 2854 (m), 1597 (m), 1581 (s), 1566 (m), 1466 (s), 1404 (m), 1269 (w), 1246 (w), 1200 (w), 1122 (w), 1095 (w), 1049 (m), 1018 (w), 991 (w), 887 (w), 845 (w), 795 (m), 744 (m), 660 (m), 621 (w), 509 (w), 471 (w), 455 (w). HRMS found *m/z*: 399.20815 $[M^+H]^{4+}$, $C_{94}H_{132}N_6P_4S_4$ *z=4* requires: 399.20812.

Acknowledgements

This work was supported by the Czech Science Foundation (P108/12/1143), the Grant Agency of Charles University (project 64213) and the COST Action CM1302 (SIPS) European Network on Smart Inorganic Polymers.

References

1 E. Figgemeier, V. Aranyos, E. C. Constable, R. W. Handel, C. E. Housecroft, C. Risinger, A. Hagfeldt and E. Mukhtar, *Inorg. Chem. Commun.*, 2004, **7**, 117–121.
2 C. Houarner, E. Blart, P. Buvat and F. Odobel, *Photochem. Photobiol. Sci.*, 2005, **4**, 200–204.
3 C. Houarner-Rassin, E. Blart, P. Buvat and F. Odobel, *J. Photochem. Photobiol. A Chem.*, 2007, **186**, 135–142.
4 S. Caramori, J. Husson, M. Beley, C. a. Bignozzi, R. Argazzi and P. C. Gros, *Chem. - A Eur. J.*, 2010, **16**, 2611–2618.
5 K. W. Cheng, C. S. C. Mak, W. K. Chan, A. M. Ching NG and A. B. Djurišič, *J. Polym. Sci. Part A Polym. Chem.*, 2008, **46**, 1305–1317.
6 V. Duprez and F. C. Krebs, *Tetrahedron Lett.*, 2006, **47**, 3785–3789.
7 A. Wild, F. Schlütter, G. M. Pavlov, C. Friebe, G. Festag, A. Winter, M. D. Hager, V. Cimrová, U. S. Schubert, V. Cimrova and U. S. Schubert, *Macromol. Rapid Commun.*, 2010, **31**, 868–874.
8 R. Siebert, A. Winter, M. Schmitt, J. Popp, U. S. Schubert and B. Dietzek, *Macromol. Rapid Commun.*, 2012, **33**, 481–497.
9 P. D. Vellis, J. A. Mikroyannidis, C. Lo and C. Hsu, *J. Polym. Sci. Part A Polym. Chem.*, 2008, **46**, 7702–7712.
10 X. Chen, Q. Zhou, Y. Cheng, Y. Geng, D. Ma, Z. Xie and L. Wang, *J. Lumin.*, 2007, **126**, 81–90.
11 X. Chen, L. Ma, Y. Cheng, Z. Xie and L. Wang, *Polym. Int.*, 2007, **56**, 648–654.
12 R. Siebert, A. Winter, B. Dietzek, U. S. Schubert and J. Popp, *Macromol. Rapid Commun.*, 2010, **31**, 883–888.
13 S. Etienne and M. Beley, *Inorg. Chem. Commun.*, 2006, **9**, 68–71.
14 L. D. Carlos, R. a S. Ferreira, V. De Zea Bermudez and S. J. L. Ribeiro, *Adv. Mater.*, 2009, **21**, 509–534.
15 M. Barboiu, Y.-M. Legrand, L. Prodi, M. Montalti, N. Zaccheroni, G. Vaughan, A. van der Lee, E. Petit and J.-M. Lehn, *Eur. J. Inorg. Chem.*, 2009, **2009**, 2621–2628.
16 S. Encinas, L. Flamigni, F. Barigelletti, E. C. Constable, C. E. Housecroft, E. R. Schofield, E. Figgemeier, D. Fenske, M. Neuburger, J. G. Vos and M. Zehnder, *Chem. Eur. J.*, 2002, **8**, 137–150.
17 T. K. Sievers, A. Vergin, H. Möhwald, D. G. Kurth, A. Verging, H. Möhwald and D. G. Kurth, *Langmuir*, 2007, **23**, 12179–12184.
18 G. Schwarz, I. Haßlauer and D. G. Kurth, *Adv. Colloid Interface Sci.*, 2014, **207**, 107–120.
19 F. S. Han, M. Higuchi and D. G. Kurth, *Adv. Mater.*, 2007, **19**, 3928–3931.
20 Y. Y. Chen, Y.-T. Tao and H.-C. Lin, *Macromolecules*, 2006, **39**, 8559–8566.
21 A. Winter, C. Friebe, M. Chiper, M. D. Hager and U. S. Schubert, *J. Polym. Sci. Part A Polym. Chem.*, 2009, **3**, 4083–4098.
22 A. Wild, A. Teichler, C.-L. Ho, X.-Z. Wang, H. Zhan, F. Schlütter, A. Winter, M. D. Hager, W.-Y. Wong and U. S. Schubert, *J. Mater. Chem. C*, 2013, **1**, 1812–1822.
23 R. Siebert, Y. Tian, R. Camacho, A. Winter, A. Wild, A. Krieg, U. S. Schubert, J. Popp, I. G. Scheblykin and B. Dietzek, *J. Mater. Chem.*, 2012, **22**, 16041–16050.
24 Y. Y. Chen and H. C. Lin, *J. Polym. Sci. Part A-Polymer Chem.*, 2007, **45**, 3243–3255.
25 R. Dobrawa, M. Lysetska, P. Ballester, M. Grüne and F. Würthner, *Macromolecules*, 2005, **38**, 1315–1325.
26 C. Ringenbach, A. De Nicola and R. Ziessel, *J. Org. Chem.*, 2003, **68**, 4708–4719.
27 S. C. Yu, C. C. Kwok, W. K. Chan and C. M. Che, *Adv. Mater.*, 2003, **15**, 1643–1647.
28 P. Bláhová, J. Zedník, I. Šloufová, J. Vohlídal and J. Svoboda, *Soft Mater.*, 2014, **12**, 214–229.
29 P. Štenclová-Bláhová, J. Svoboda, I. Šloufová and J. Vohlídal, *Phys. Chem. Chem. Phys.*, 2015, **17**, 13743–13756.
30 J. Lehn, *Prog. Polym. Sci.*, 2005, **30**, 814–831.
31 J. W. Steed and J. L. Atwood, *Supramolecular chemistry, 2nd edition ed.*, John Wiley & Sons, Ltd., 2009.
32 A. Ciferri, *Macromol. Rapid Commun.*, 2002, **23**, 511–529.
33 J. Svoboda, P. Stenclova, F. Uhlík, J. Zedník and J. Vohlídal, *Tetrahedron*, 2011, **67**, 75–79.
34 D. Bondarev, J. Zedník, I. Šloufová, A. Sharf, M. Procházka, J. Pfleger and J. Vohlídal, *J. Polym. Sci. Part a-Polymer Chem.*, 2010, **48**, 3073 – 3081.
35 C. G. Bochet, C. Piguet and A. F. Williams, *Helv. Chim. Acta*, 1993, **76**, 372–384.
36 D. Rais, M. Menšík, P. Štenclová-Bláhová, J. Svoboda, J. Vohlídal and J. Pfleger, *J. Phys. Chem. A*, 2015, **119**, 6203–6214.
37 I. Šloufová, B. Vlčková, M. Procházka, J. Svoboda and J. Vohlídal, *J. Raman Spectrosc.*, 2014, **45**, 338 – 348.
38 S. Kazim, J. Pfleger, K. Halašová, M. Procházka, D. Bondarev and J. Vohlídal, *Eur. Phys. J. Appl. Phys.*, 2011, **55**, 23905.
39 P. S. Braterman, J.-I. Song and R. D. Peacock, *Inorg. Chem.*, 1992, **31**, 555–559.

40 F. Schlütter, A. Wild, A. Winter, M. D. Hager, A. Baumgaertel, C. Friebe and U. S. Schubert, *Macromolecules*, 2010, **43**, 2759–2771.
41 T. Vitvarová, J. Zedník, M. Bláha, J. Vohlídal and J. Svoboda, *Eur. J. Inorg. Chem.*, 2012, **2012**, 3866–3874.
42 V. Stepanenko, M. Stocker, P. Müller, M. Büchner and F. Würthner, *J. Mater. Chem.*, 2009, **19**, 6816–6826.
43 R. A. Dobrawa, Bayerischer Julius-Maximilians-Universität Würzburg, 2004.
44 J. N. Demas and B. A. DeGraft, *Topics in Fluorescence Spectroscopy: Volume 4: Probe Design and Chemical Sensing*, 1994.
45 R. Englman and J. Jortner, *Mol. Phys.*, 1970, **18**, 145–164.
46 R. Dobrawa and F. Würthner, *J. Polym. Sci. Part A Polym. Chem.*, 2005, **43**, 4981–4995.
47 U. S. Schubert, H. Hofmeier and G. R. Newkome, *Modern Terpyridine Chemistry*, Wiley-VCH Verlag GmbH, Weinheim, 2006.
48 R. Hogg and R. G. Wilkins, *J. Chem. Soc.*, 1962, 341–350.
49 R. H. Holyer, C. D. Hubbard, S. F. A. Kettle and R. G. Wilkins, *Inorg. Chem.*, 1966, **5**, 622–625.
50 J. R. Winkler, C. Creutz and N. Sutin, *J. Am. Chem. Soc.*, 1987, **109**, 3470–3471.
51 J. Burgess, S. Radulović and F. Sánchez, *Transit. Met. Chem.*, 1987, **12**, 529–536.

Electronic supplementary information

Alcohol- and water-soluble bis(*tpy*)quaterthiophenes with phosphonium side groups: new conjugated units for metallo-supramolecular polymers

Pavla Štenclová, Kristýna Šichová, Ivana Šloufová, Jiří Zedník, Jiří Vohlídal* and Jan Svoboda *

Charles University in Prague, Faculty of Science, Department of Physical and Macromolecular Chemistry, Hlavova 2030, CZ-128 40, Prague 2, Czech Republic.
Fax:+420 224919752; Tel:+420 221951310;

E-mail: jan.svoboda@natur.cuni.cz (J. Svoboda)
jiri.vohlidal@natur.cuni.cz (J. Vohlídal)

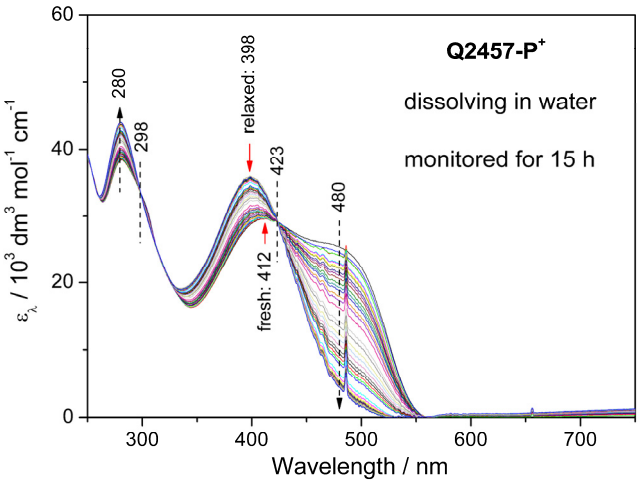

Figure S1. Time-development of the UV/vis spectra during the dissolution of **Q2457-P$^+$** in water. Room temperature, $2 \cdot 10^{-5}$M

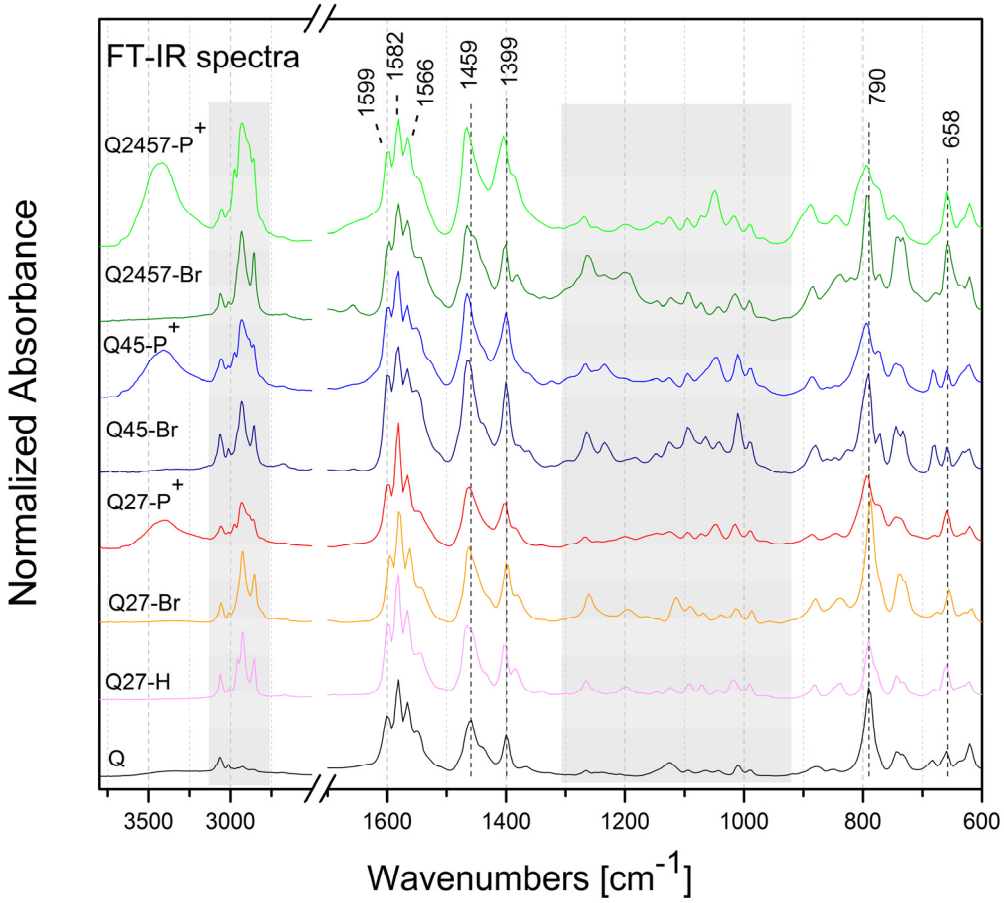

Figure S2. Infrared spectra of prepared unimers.

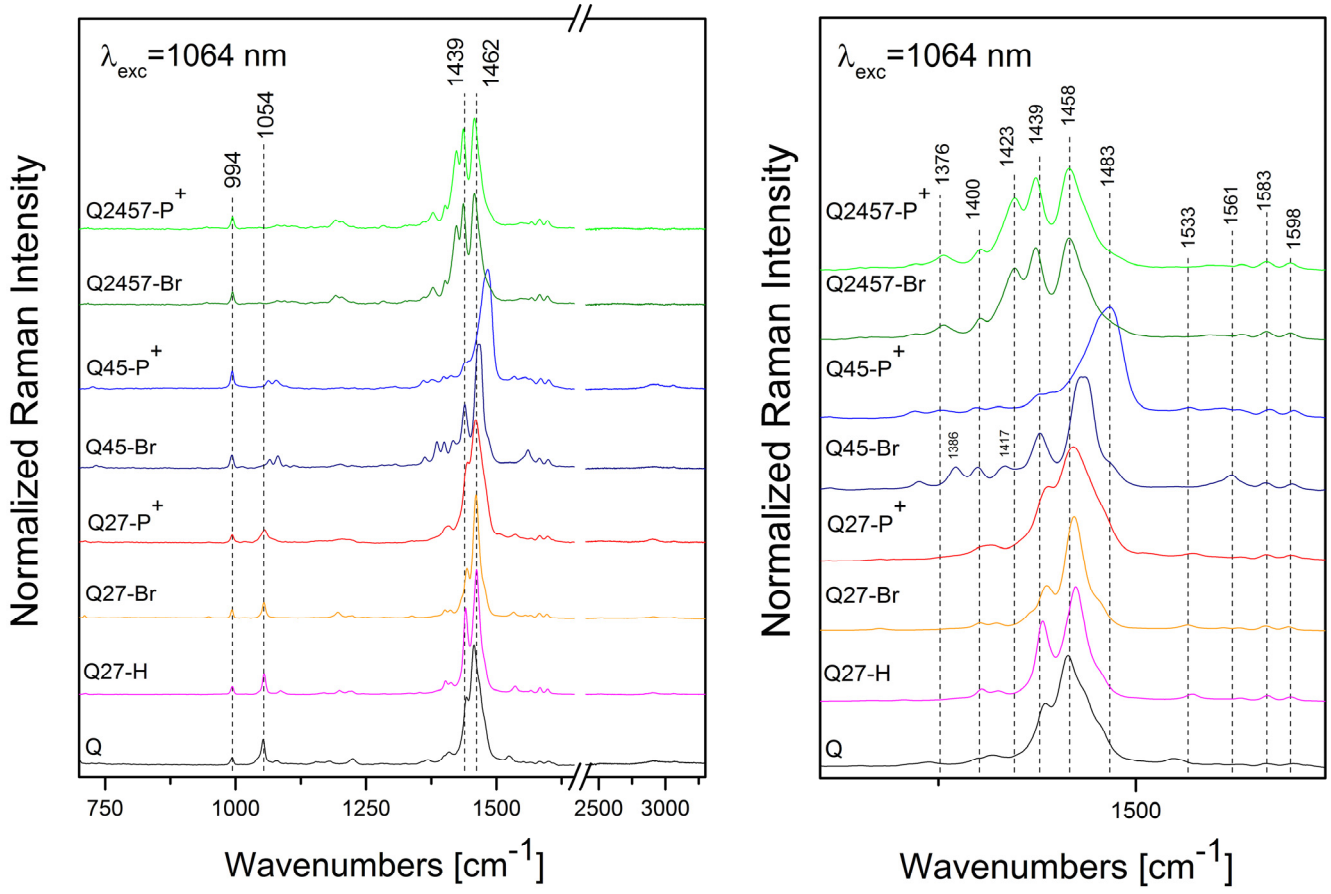

Figure S3. Off-resonance Raman spectra of prepared unimers (λ_{exc} = 1064 nm).

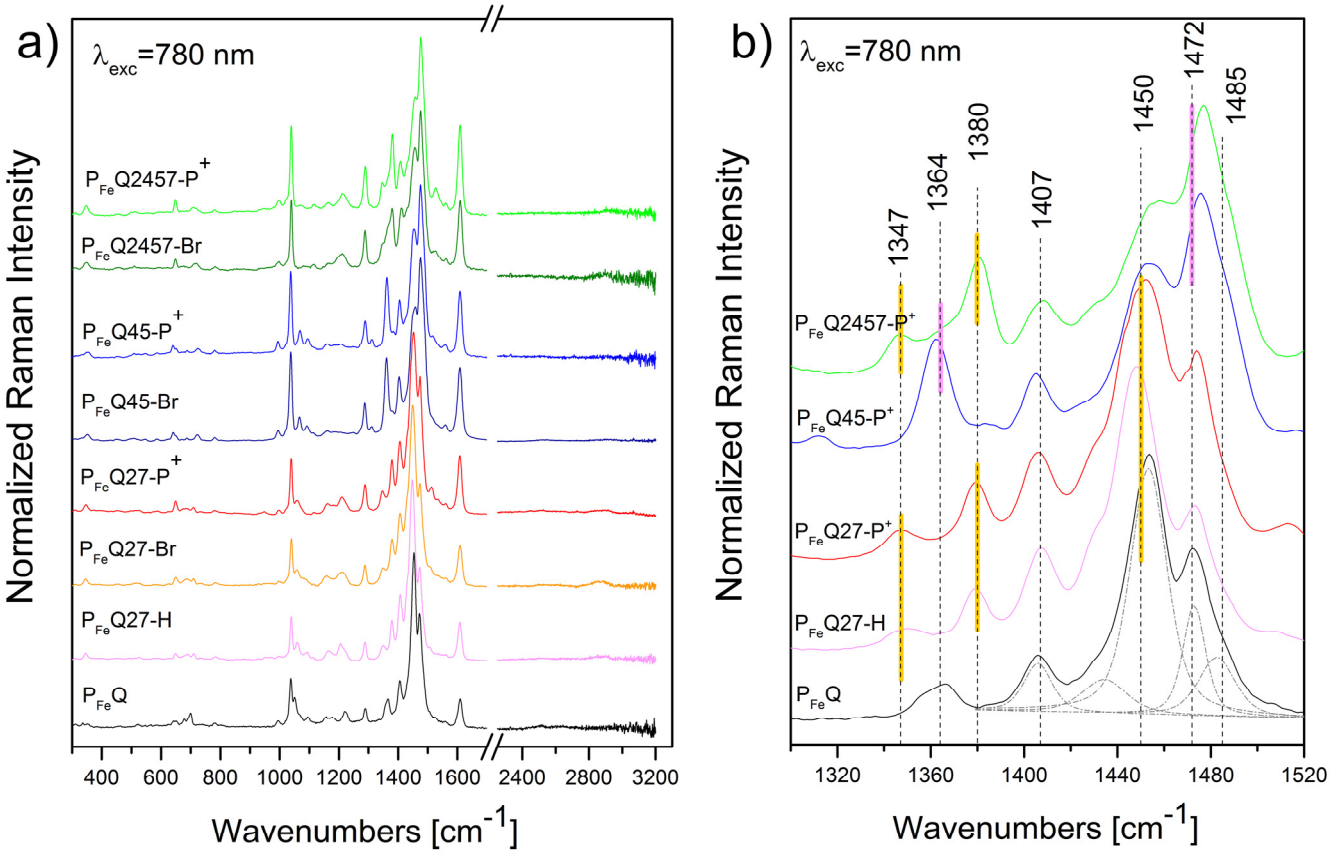

Figure S4. Off-resonance Raman spectra of Fe-polymers at λ_{exc} = 780 nm (a) and deconvolution of spectra (b).

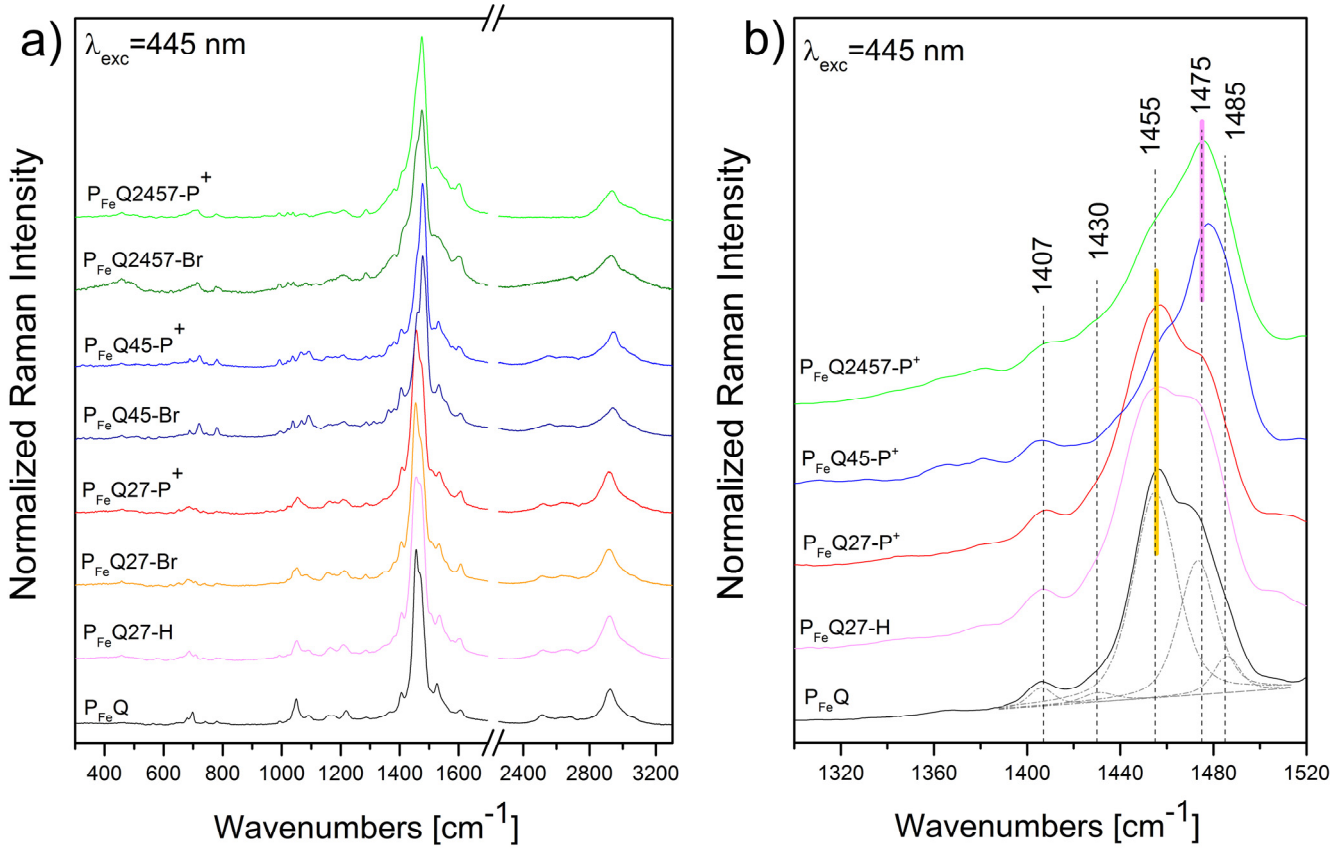

Figure S5. Off-resonance Raman spectra of Fe-polymers at λ_{exc} = 445 nm (a) and deconvolution of spectra (b).

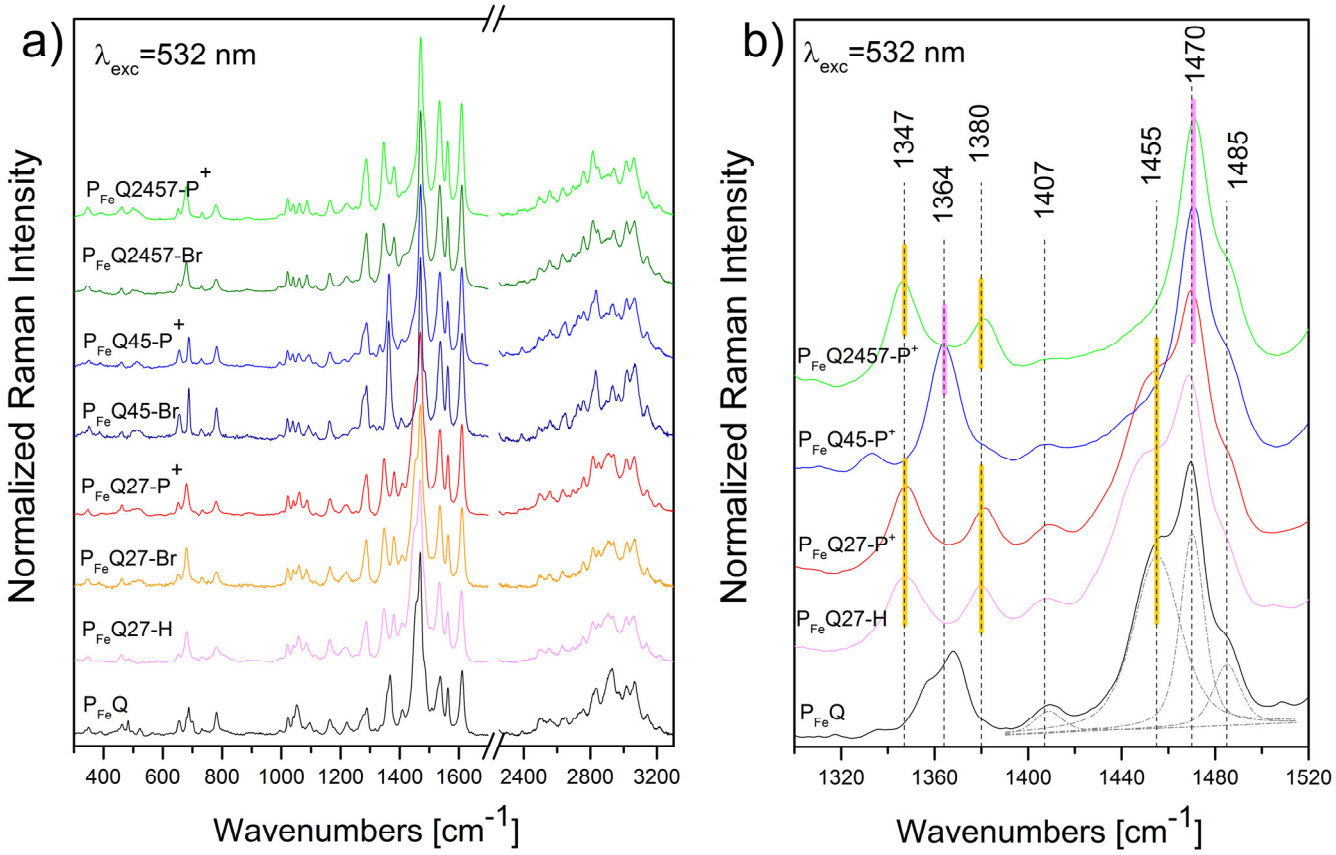

Figure S6. Off-resonance Raman spectra of Fe-polymers at λ_{exc} = 532 nm (a) and deconvolution of spectra (b).

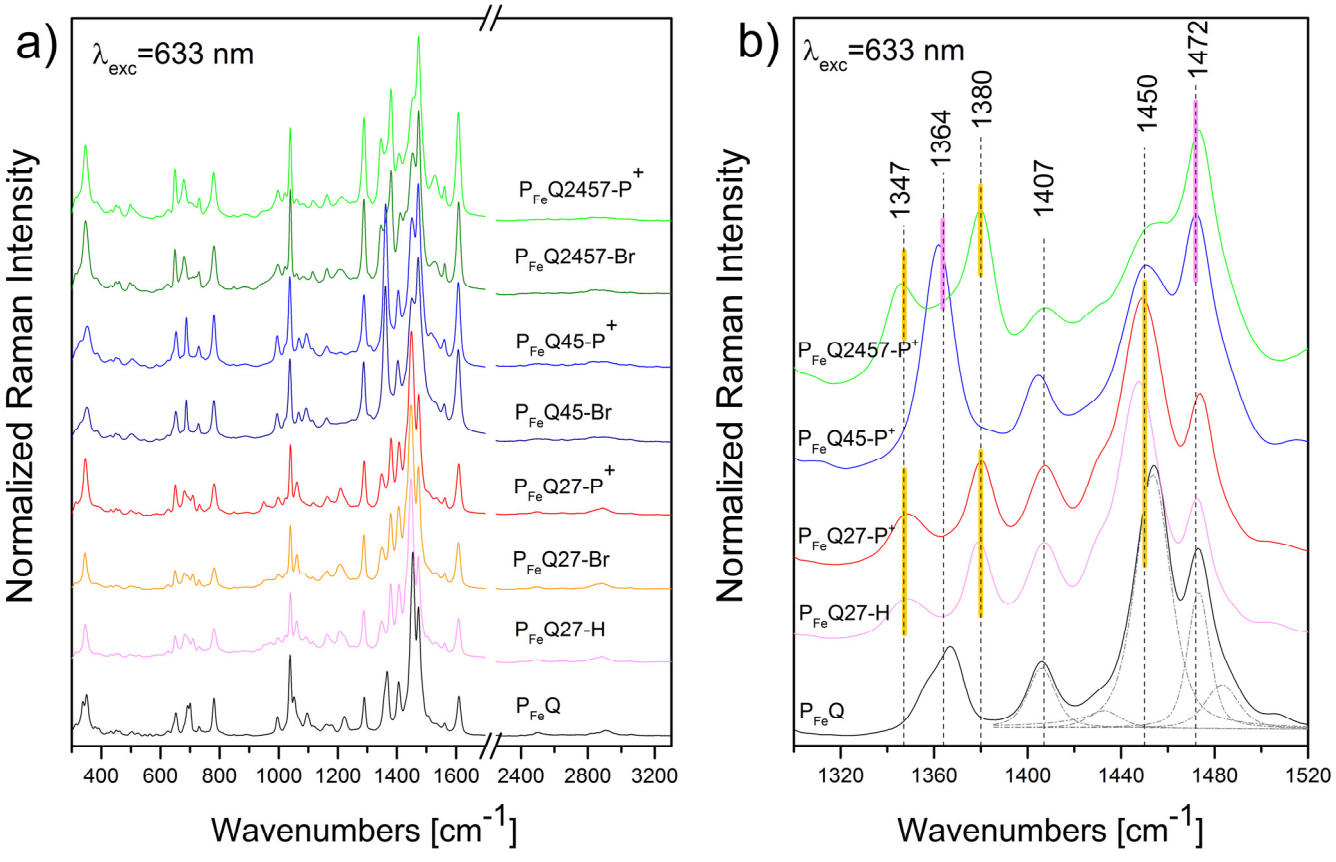

Figure S7. Off-resonance Raman spectra of Fe-polymers at λ_{exc} = 633 nm (a) and deconvolution of spectra (b).

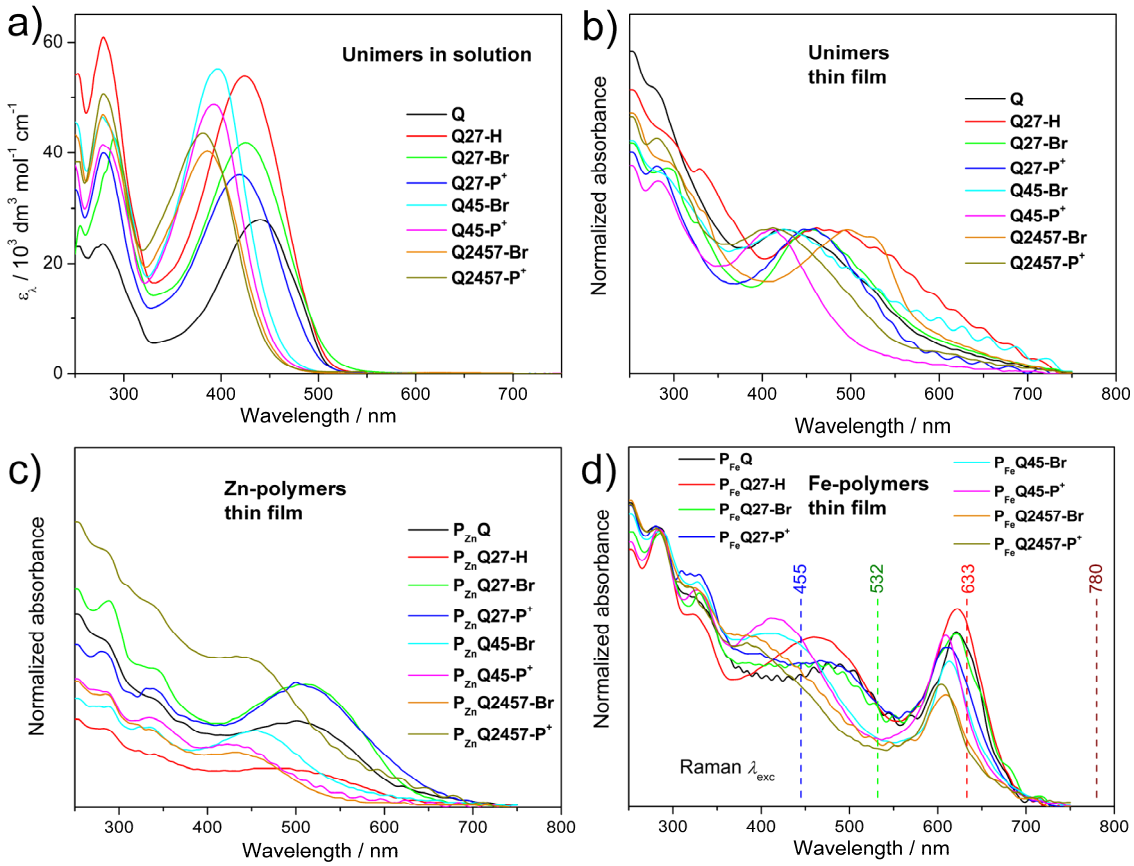

Figure S8. UV/vis spectra of prepared unimers and polymers.

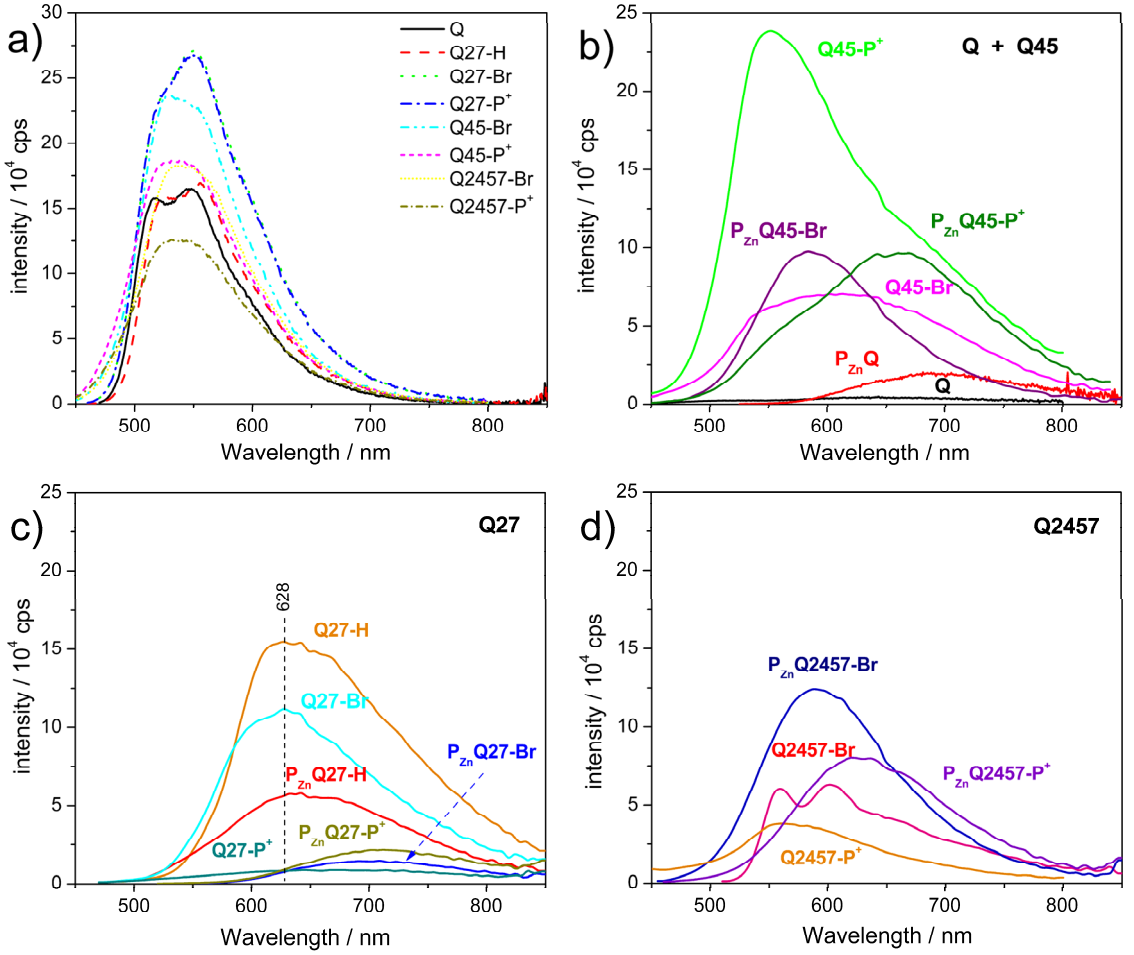

Figure S9. Luminescence spectra of prepared unimers in solution (a) and unimers and Zn-polymers in thin film (b-d).

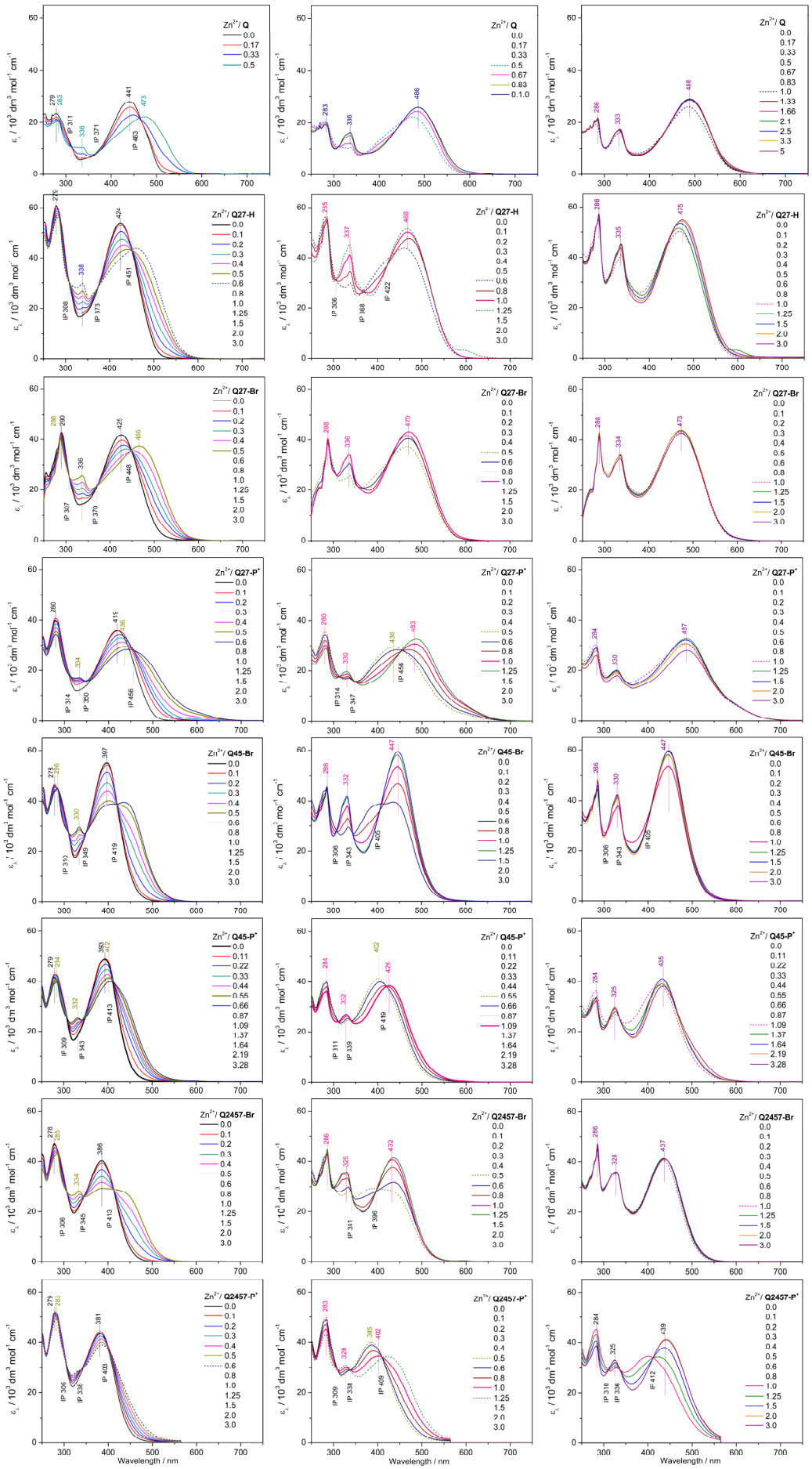

Figure S10. Complete set of UV/vis spectra accompanying the titration of non-ionic and ionic unimers with Zn^{2+} ions. Initial unimer concentration $2 \cdot 10^{-5}$M in chloroform/acetonitrile (non-ionic species) or methanol (ionic unimers), room temperature. Each column depicts the particular stage of assembling.

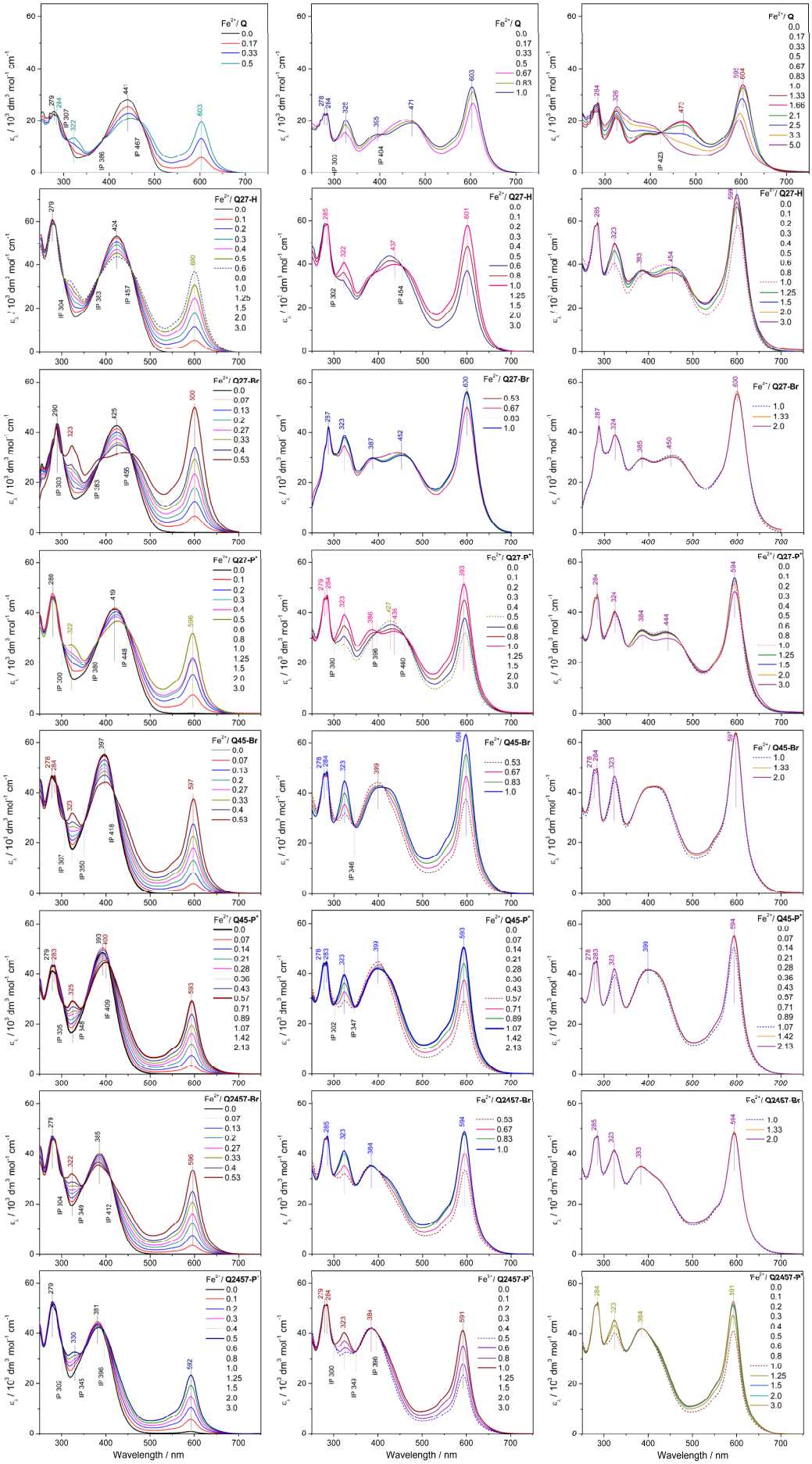

Figure S11. Complete set of UV/vis spectra accompanying the titration of non-ionic and ionic unimers with Fe^{2+} ions. Initial unimer concentration $2 \cdot 10^{-5}$M in chloroform/acetonitrile (non-ionic species) or methanol (ionic unimers), room temperature. Each column depicts the particular stage of assembling.

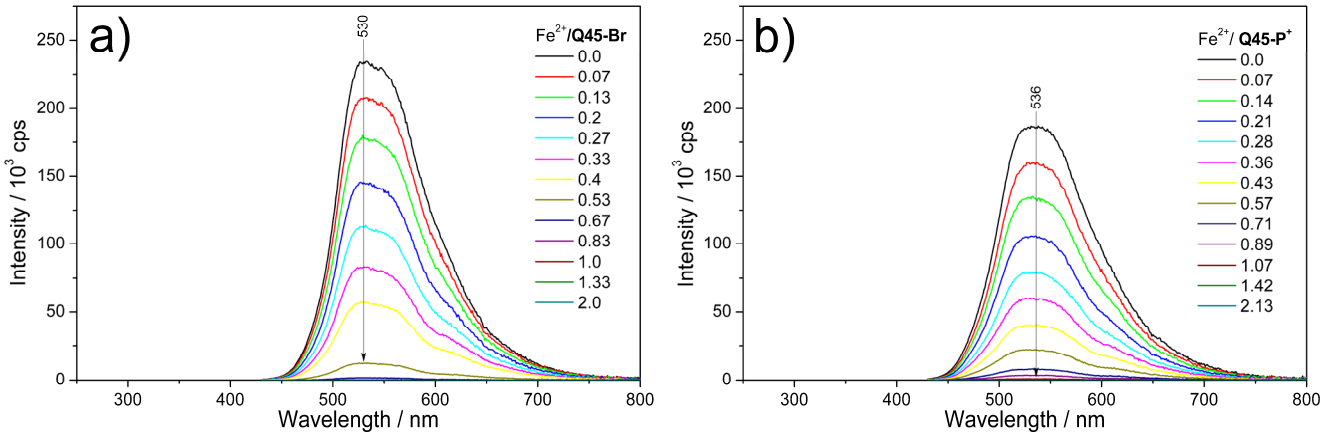

Figure S12. Changes in photoluminescence spectra accompanying titration of unimers **Q45-Br** (a) and **Q45-P$^+$** (b) with Fe^{2+} in chloroform/acetonitrile (a) or methanol (b).

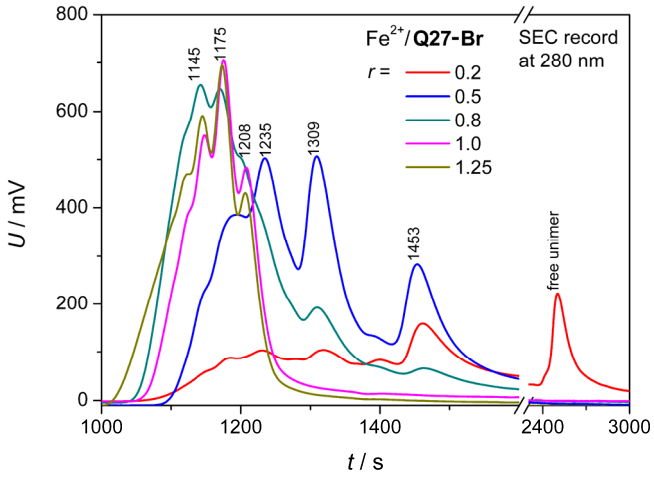

Figure S13. The SEC records of the Fe^{2+}/**Q27-Br** systems of different composition.

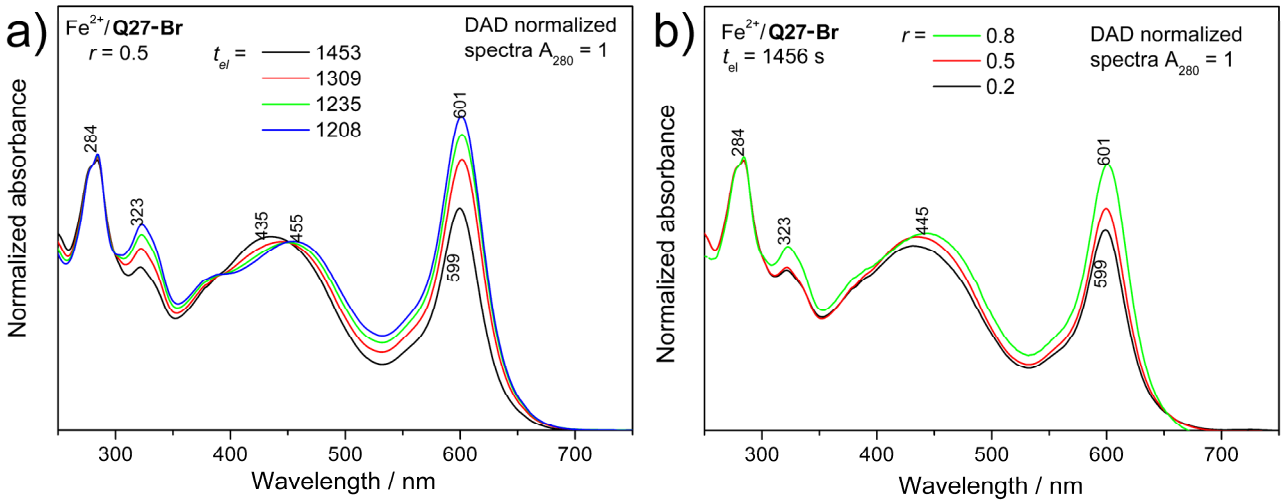

Figure S14. The DAD spectra at different elution time t_{el} (a) and the UV/vis spectra of SEC fractions (t_{el} = 1456 s) of Fe^{2+} / **Q27-Br** systems of different composition (b).

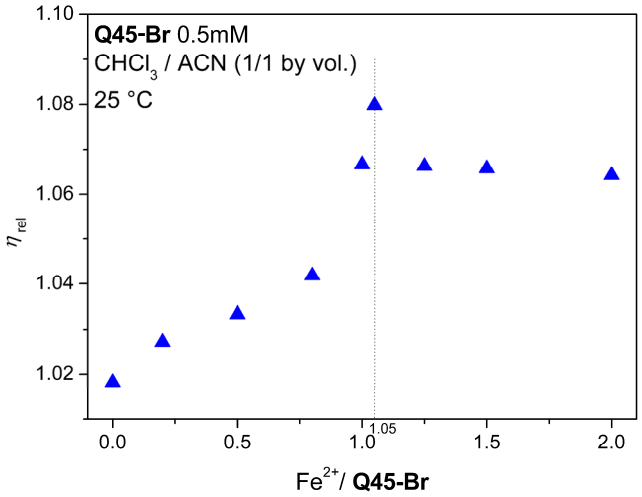

Figure S15. Relative viscosity of solution of the system Fe^{2+}/**Q45-Br** as a function of composition.

Table S1. The photoluminescence maxima, $\lambda_{F,}$ in solution and in thin film, photoluminescence quantum yield, Φ, and lifetime of excited states, τ. Solvent: methanol for ionic unimers and polymers (suffix **-P$^+$**); acetonitrile/chloroform (1/1 by vol.) for all the other unimers and polymers.

	λ_F , nm (ϕ, %)		τ, ns	
Sample	solution	film	solution	film
		Unimers		
Q	514,546 (30%)	645 (<1%)	0.79 (100%)	0.24 (35%) 0.98 (49%) 3.71 (16%)
Q27-H	554 (26%)	630 (1%)	0.62 (94%) 1.53 (6%)	0.15 (56%) 0.51 (38%) 1.84 (6%)
Q27-Br	554 (31%)	630 (1%)	0.57 (85%) 1.20 (15%)	0.13 (54%) 0.50 (36%) 1.98 (10%)
Q27-P$^+$	550 (18%)	~650 (<1%)	0.69 (100%)	0.15 (35%) 0.83 (43%) 2.54 (22%)
Q45-Br	530 (14%)	610 (1%)	0.43 (9%) 0.55 (91%)	0.18 (51%) 0.75 (39%) 3.82 (10%)
Q45-P$^+$	536 (11%)	550 (1%)	0.31 (33%) 0.57 (67%)	0.08 (62%) 0.40 (30%) 2.27 (8%)
Q2457-Br	536 (14%)	560,603 (3%)	0.37 (44%) 0.50 (56%)	0.07 (79%) 0.42 (16%) 1.84 (5%)
Q2457-P$^+$	536 (10%)	560 (1%)	0.39 (57%) 0.56 (43%)	0.07 (74%) 0.39 (22%) 1.84 (4%)
		Zn-polymers		
P$_{Zn}$Q	656	~690 (1%)		0.27 (53%) 0.92 (34%) 2.51 (13%)
P$_{Zn}$Q27-H	673	~640 (2%)		0.18 (41%) 0.91 (44%) 3.54 (15%)
P$_{Zn}$Q27-Br	675	~710 (1%)		0.16 (57%) 0.72 (36%) 3.05 (7%)
P$_{Zn}$Q27-P$^+$	550	~705 (<1%)		0.11 (47%) 0.54 (42%) 1.92 (11%)
P$_{Zn}$Q45-Br	673	585 (3%)		0.21 (45%) 0.98 (39%) 3.63 (16%)
P$_{Zn}$Q45-P$^+$	536	660 (1%)		0.06 (79%) 0.29 (17%) 1.98 (4%)
P$_{Zn}$Q2457-Br	668	590 (3%)		0.15 (43%) 0.71 (42%) 3.24 (15%)
P$_{Zn}$Q2457-P$^+$	552	625 (1%)		0.15 (56%) 0.56 (36%) 2.05 (8%)